AN EXPERIMENTAL INVESTIGATION INTO THE EFFECTIVENESS OF STEEL FIBRE-REINFORCED CONCRETE RELATIVE TO CONVENTIONAL MESH-REINFORCED CONCRETE IN THIN SHELL CONSTRUCTION

by

Michael J E Neumann, B.Sc. (Civil) Engineering, Cape Town

A thesis submitted in partial fulfilment of the requirements for the degree Master of Science in Engineering

Department of Civil Engineering

University of Cape Town

February 1988

DECLARATION OF CANDIDATE

I, Michael J E Neumann, hereby declare that this thesis is my own work and that it has not been submitted for a degree at another university.

Signed by candidate

M Neumann

February 1988

SYNOPSIS

This report presents the results of an investigation into the suitability of steel-fibre reinforced concrete (SFRC) as a building material. The performance of the SFRC is gauged relative to conventional steel mesh-reinforced concrete.

The report begins with the historical background of fibre-reinforcing, its development and diversity in modern times. The theoretical principles governing the strength of SFRC are formulated, followed by an extensive review of factors influencing the fibre's potential and its subsequent effect on the mechanical properties of a concrete matrix.

The experimental program is thereafter detailed in two stages : the "Efficiency and Proving Phase" followed by the "Application Phase". The former involves a series of tests to determine the most promising fibre of the five types available, while the latter compares the strength properties of slabs and arches reinforced with this fibre to those reinforced with wire mesh.

The test results obtained from the two phases are evaluated and discussed in the succeeding two sections and the report ends with the conclusions drawn and recommendations regarding the effectiveness of SFRC relative to mesh-reinforced concrete.

ACKNOWLEDGEMENTS

The author wishes to thank the following :

Mr R D Kratz, Department of Civil Engineering, U.C.T., thesis supervisor, for his guidance and encouragement. I am especially indebted to Professor M O de Kock for his help over the last six months.

The Council for Scientific and Industrial Research for the award of a post-graduate grant which made this research possible.

Messrs G Bertuzzi, D J Botha and R Edge of the Civil Engineering Workshop, U.C.T., for their assistance with the fabrication of experimental apparatus.

Mr R Allan of Allans Meshco for cutting the binding wire fibres at no charge.

Messrs J Lemmetjies, D S Swartz and J J Williams of the Department of Civil Engineering, U.C.T., for the assistance and encouragement throughout the thesis.

Mrs Shirley Breed for her patience and efficient typing of this thesis.

TABLE OF CONTENTS

LIST OF FIGURES

LIST OF TABLES

LIST OF PHOTOGRAPHIC PLATES

GLOSSARY

COMPOSITE	a combination of materials. In this instance in the form concrete and steel fibres
CRITICAL FIBRE VOLUME	The volume of fibres which, after matrix cracking, will carry the load which the composite sustained before cracking
FIRST CRACK STRENGTH	The load at which matrix/composite cracking occurs
FULLY REINFORCED	The inclusion of steel fibres into a matrix over the full depth of the test specimen
PARTIALLY REINFORCED	The inclusion of steel fibres into a matrix over only a partial thickness of the test specimen
PROPORTIONAL LIMIT	That range over which the elastic deformation of a concrete beam subjecgted to increasing loads remains linear
RELATIVE STRENGTH INCREASE/DECREASE	Comparison of the strength of a composite specimen relative to a control (i.e. unreinforced) specimen, expressed as a percentage
SFRC	Steel fibre-reinforced concrete
STRENGTH INCREASE/ DECREASE	Direct comparison between two sets of data
ULTIMATE STRENGTH	The maximum load which the test specimen can support

LIST OF SYMBOLS

Symbol		Units
A	area	m^2
D	diameter of steel fibre	m
f_{cf}	compressive strength of a 100 x 100 x 100mm fibre reinforced cube	MPa
f_{cu}	compressive strength of a 100 x 100 x 100mm unreinforced cube	MPa
F	axially applied force	kN
ℓ	length of steel fibre	m
ℓ_c	fibre critical length	m
ℓ_{eff}	effective length of steel fibre	m
ℓ/D	Aspect Ratio of steel fibre	
MOR	Modulus of Rupture	MPa
r_o	fibre radius	m
S	distance between the centroids of fibres in a matrix i.e. fibre spacing	m
S_c	effective fibre spacing	m
V_c	volume occupied by the composite	m^3
V_f	volume occupied by the steel fibres	m^3
V_{fCRIT}	critical fibre volume	m^3
V_{fe}	effective volume of fibres in the direction of stress	m^3
ϵ	strain	
η_ℓ	fibre length efficiency factor	
η_o	fibre orientation factor	

η	total efficiency factor incorporating both orientation and length factors	
τ_{AV}	average bond stress	MPa
τ_u	ultimate bond stress	μpa
σ_{cb}	Modulus of Rupture of the composite	MPa
σ_{ft}	tensile stress in fibre subjected to tensile load	MPa
σ_{fu}	ultimate strength of fibre	MPa
σ_{mb}	Modulus of Rupture of matrix	MPa
σ_{mt}	direct tensile strength of matrix	MPa

Subscripts

AV	denotes average
b	denotes bending, i.e. flexural
c	denotes composite
eff	denotes effective
f	denotes fibre
m	denotes matrix i.e. concrete only
o	denotes orientation
t	denotes tensile
u	denotes ultimate

CHAPTER 1

INTRODUCTION

The idea of adding steel fibres to a concrete matrix to improve its strength was first reported on in the early 1900's. The first research work on SFRC was carried out in 1963, and by 1971 the material was being evaluated seriously for commerical products and applications throughout the United States and Western Europe.
Extensive testing on SFR concretes revealed that the steel fibres improved substantially the engineering properties of a plain concrete matrix. SFR concretes have thus been used extensively to provide a "thin skin" of reinforcement for such applications as pavements, overlays, patching, tunnel linings, thin shells and precast products. The last two applications formed the basis of this study.

In South Africa the problem of providing adequate housing for the many thousands is a very real problem. It is thought that SFRC may be a contribution. The objectives of this report are :

1. To set out the findings of an investigation into the effectiveness of SFRC in thin shell construction relative to the conventional mesh-reinforced shells.
2. To draw conclusions from the findings on the possible application of SFRC for housing and industrial roofing.

The investigation was restricted to testing large slabs and arches, possible applications seen as walls and roofing in buildings.

CHAPTER 2

THE DEVELOPMENT OF FIBRE REINFORCED CONCRETE

2.1 GENERAL

The practice of using fibres to reinforce brittle materials goes back to ancient times. Early civilizations quickly realised the benefits of adding straw to mud and clay to get strong sun-dried bricks. The bricks proved to have a greater cracking resistance, and did not fall apart once cracking became visible. It is no surprise therefore that, with the development of portland cement and its gradual increased use as a building material, attemps were made to add fibres to concrete in order to improve its behaviour.

2.2 HISTORICAL BACKGROUND

In 1847 Joseph Lambot developed a new building material by adding continuous fibres in the form of wires or wire meshes to concrete. This led to the development of ferrocement and reinforced concrete as it is known today[1]. However, the cost, careful placement and skills required to use these continuous wires prompted engineers to look for a more versatile, easily placeable reinforcing. The idea of using strong discontinuous fibres as reinforcement to concrete, which could simply be added to the mix like sand or stone, was first patented in 1874 by A Bernard from California. He suggested the use of granular waste iron in a concrete to create an artificial stone.

A French patent dated 1918 by H Alfsen shows the first cognisance of fibre shape optimization - Alfsen describes the process of adding small longitudinal fibres of iron, wood or other materials to concrete, thereby improving the tensile strength. He also suggested that the surface of these be rough or roughened with the ends bent to provide better adherence to the concrete.

In 1912, R Weakly obtained a patent for using a steel wire strip made out of two wires and containing loops to enable a durable bond with concrete (see Figure 2.1 below)[2].

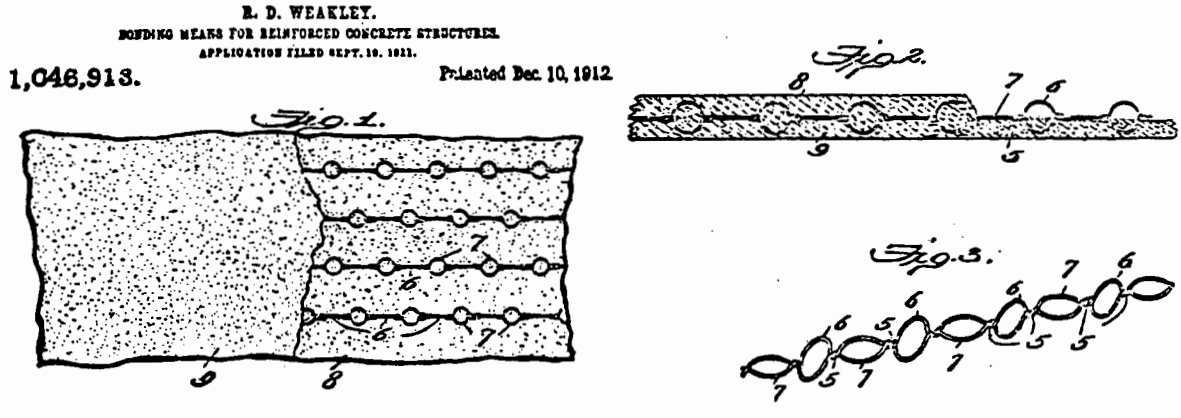

Figure 2.1 : The Weakly patent on fibre for concrete

The idea of changing the shape of the fibre itself was put forward shortly thereafter by G Martin and W Meischke-Smith in 1927. Martin's patent describes the use of plain or crimped pieces of steel wire mixed with concrete to strengthen concrete pipes. Meischke-Smith's patent proposed the use of flat, twisted pieces of wire as fibre reinforcement for concrete mixtures. Both patents are shown in Figure 2.2. below.

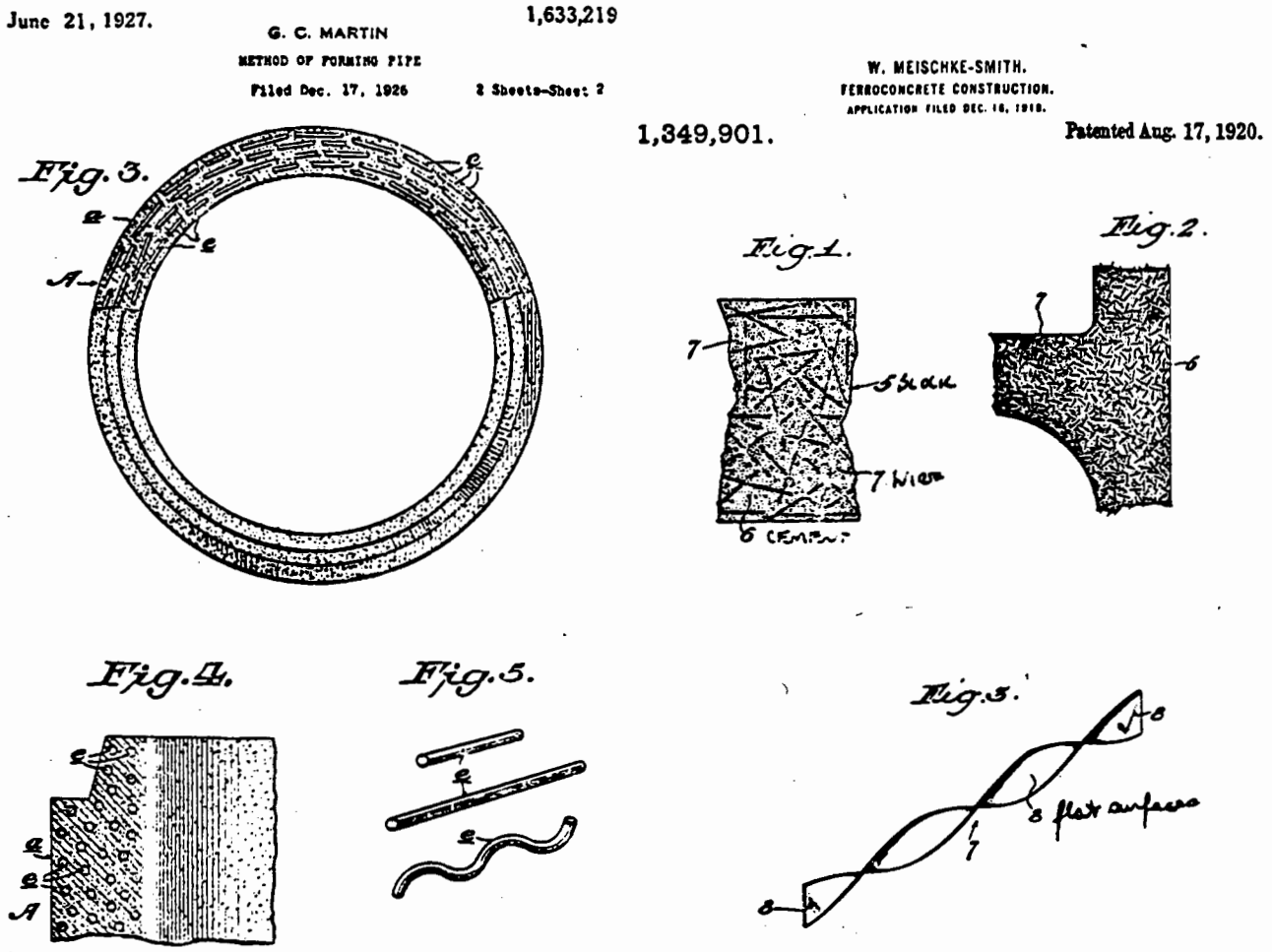

Figure 2.2 : Additional fibre patents. Left is Martin's patent and right is that awarded to Meischke-Smith

Capitalising on this idea, Etheridge (1933) proposed adding "annuli fibres" of varying sizes and diameters to improve the crack resistance and fatigue of concrete for use in railway ties. He wrote :

> "The object that I have in view is the prevention of local cracks and fractures and I accomplish such object by mixing with the plastic concrete a mass a metal annuli insufficient to effect coupling of what I may term the "stitching" together of the adjacent masses of concrete ....."

June 13, 1933. H. ETHERIDGE 1,913,707

CONCRETE CONSTRUCTION

Filed June 1, 1931

Fig. 1

Fig. 2

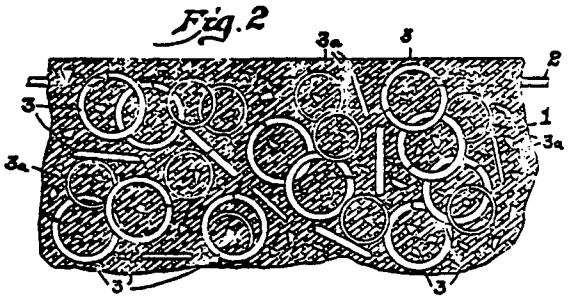

Fig. 3

Figure 2.3 : Etheridge's "annuli fibres"

Additional patents were granted worldwide in subsequent years but one which particularly stands out is that of G Constantinesco whose patent was granted in England in 1943 and subsequently in 1954 in the U.S.A. His patent describes the use of coiled or helical type steel fibres in order to increase the crack resistance and energy absorption of concrete masses. He went so far as to recommend certain parameters relating to the fibre geometry, which are quite similar to those used today in steel-fibre reinforced concrete (SFRC). Suggested applications included army tanks, air raid shelters and machinery foundations. Figure 2.4 below gives an impression of the remarkable diversity of Constantinesco's patent.

The pace of developments thus far, i.e. prior to the 1960's, can be viewed as a slow pioneering with almost no applications.

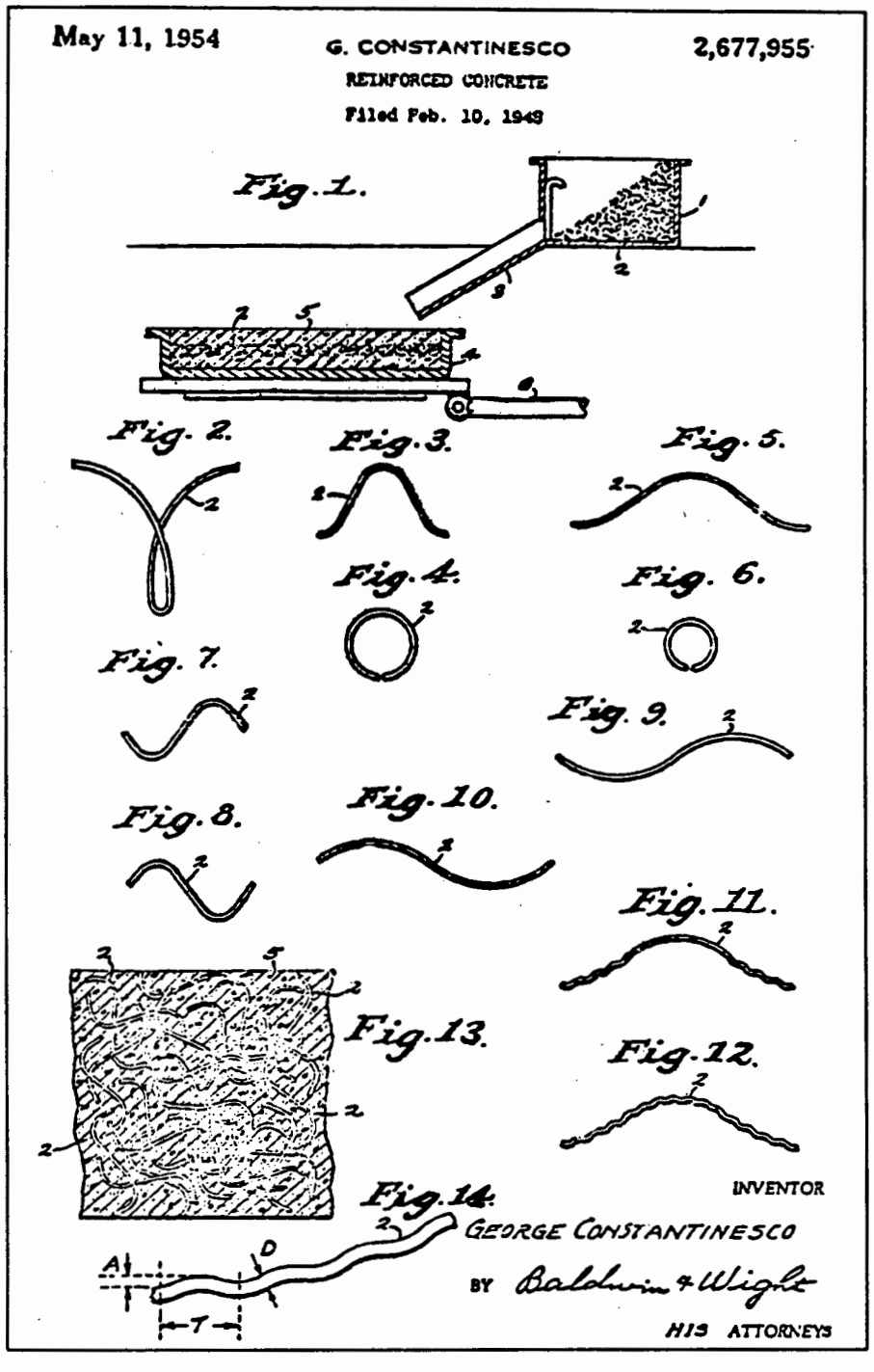

Figure 2.4 : Constantinesco's patent. Note geometry parameters at bottom left.

However, commencing from the early 1960's, rapid, modern development with increasing applications saw the discovery of a wide spectrum of fibre types.

2.3 MODERN DEVELOPMENTS

Beginning in the early 1960's a multitude of fibres and fibre materials were introduced and are being continuously introduced in the market as new applications are identified.

2.3.1 Steel Fibres

Manufacturers of steel wire fibre have attempted to improve the mechanical bond in a variety of ways, resulting in various configurations as shown in Figure 2.5 below[3].

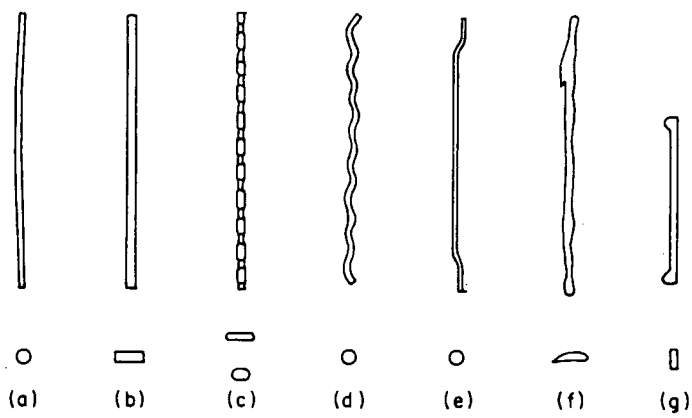

Figure 2.5 : Shapes of commercial steel fibres

Round steel-fibres (a) are produced by normal wire-drawing techniques (i.e. by cutting or chopping wire), typically having diameters between 0.25 - 0.76 mm. However, this technique is relatively expensive which has led to production methods utilising unprocessed, i.e. "raw" materials. One production method utilises

slit sheets resulting in rectangular cross-section fibres (b) which may be produced cheaply when supplies of scrap metal are readily available. Typical cross-sections range from 0.15 - 0.41 mm in thickness by 0.25 - 0.90 mm in widths.

Another economic technique is the "melt-extracts" process, patented by the Batelle Development Corporation and developed in the U.K. by Johnson and Nephew Ltd. This method uses a rotating wheel that touches a molten metal surface, lifts off liquid metal and rapidly freezes it into fibres which are subsequently thrown off by the centrifugal force. The fibres have an irregular surface and a crescent shaped cross section (see Figure 2.5, fibre (f)).
Crimped and deformed steel fibres have been produced both full-length (c) and (d) and crimped or bent at the ends only (e), or alternatively the ends are enlarged (g).

Before looking at non-steel fibres, special mention should be made of a patent granted to A G Naaman in 1974, who developed a tri-dimensional steel fibre made with four wires forming a frame, like two successive footballs (see Figure 2.6 below)[4].

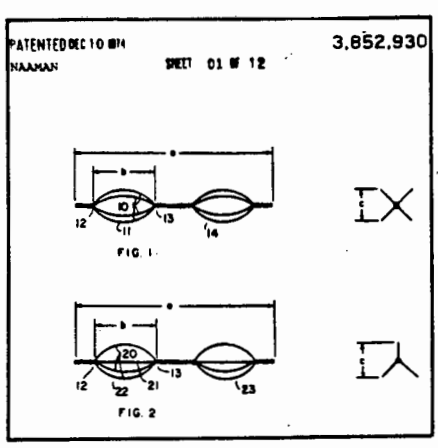

Figure 2.6 : Tri-dimensional steel fibres

2.3.2 Glass Fibres

Glass wool with fibre lengths up to 150 mm can be produced by blowing compressed air or steam at a stream of molten glass, and similar but longer fibres can be manufactured by centrifuging molten glass. However, although these fibres are cheap, they are not very suitable for mixing with cement and therefore mechanically drawn fibres are used for this purpose.

Mechanical production of continuous fibres consists of drawing filaments from the bottom of a heated platinum brushing or tank containing several hundred holes. The glass fibres are collected in strands of about 200 filaments on a rotating drum and their final diameter depends on the speed of rotation of the drum, the viscosity of the melt and the size of the holes in the brushing. It should be noted that before reaching the drum the strand is coated with a SIZE, which holds the filaments together in a lens-shaped form, as shown in Figure 2.7 below[5].

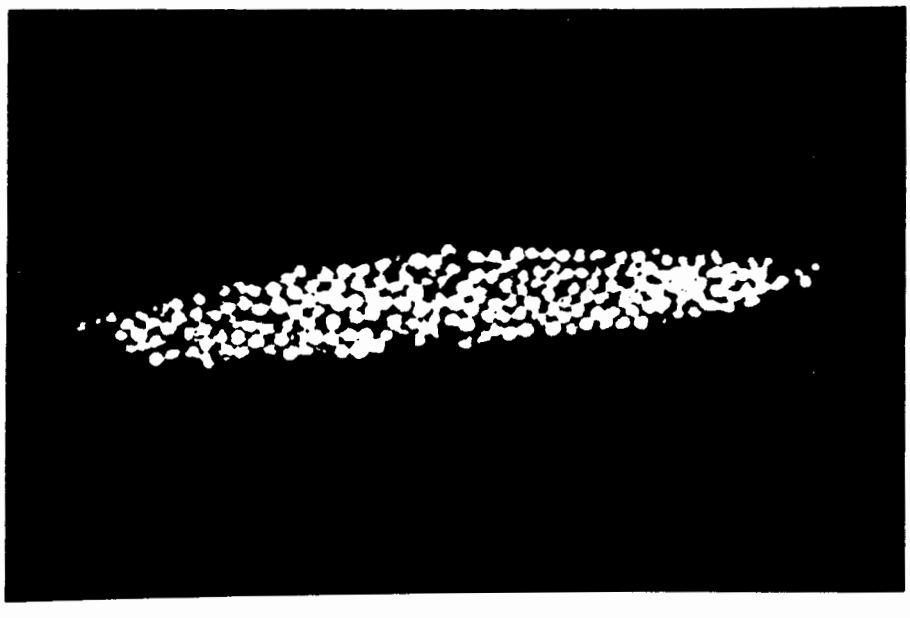

Figure 2.7 : View of a glass fibre strand composed of 214 filaments

Several strands may be lightly bonded to form a ROVING, which may be wound as a cheese. This roving is then unwound on location and chopped into the required lengths for their use in concrete, or for the production of choped fibre-matts. Typically the glass fibres have diameters of 0.005 - 0.015 mm but, as mentioned above, these fibres may be bonded together to produce fibre elements with diameters of 0.013 - 1.3 mm. Mechanically drawn glass fibres are available in three groups :

- soda-lime-silica (A glass)
- Borosilicate glass (E glass)
- Zirconia glass

Of the three types Zirconia glass is the most resistant to attack by the highly alkaline ordinary Portland cements commonly used in Europe and America. Figure 2.8(a) below shows some typical precut glass fibre 25 mm (1 inch) long, and (b) shows the fracture surface of a glass reinforced cement[6,7].

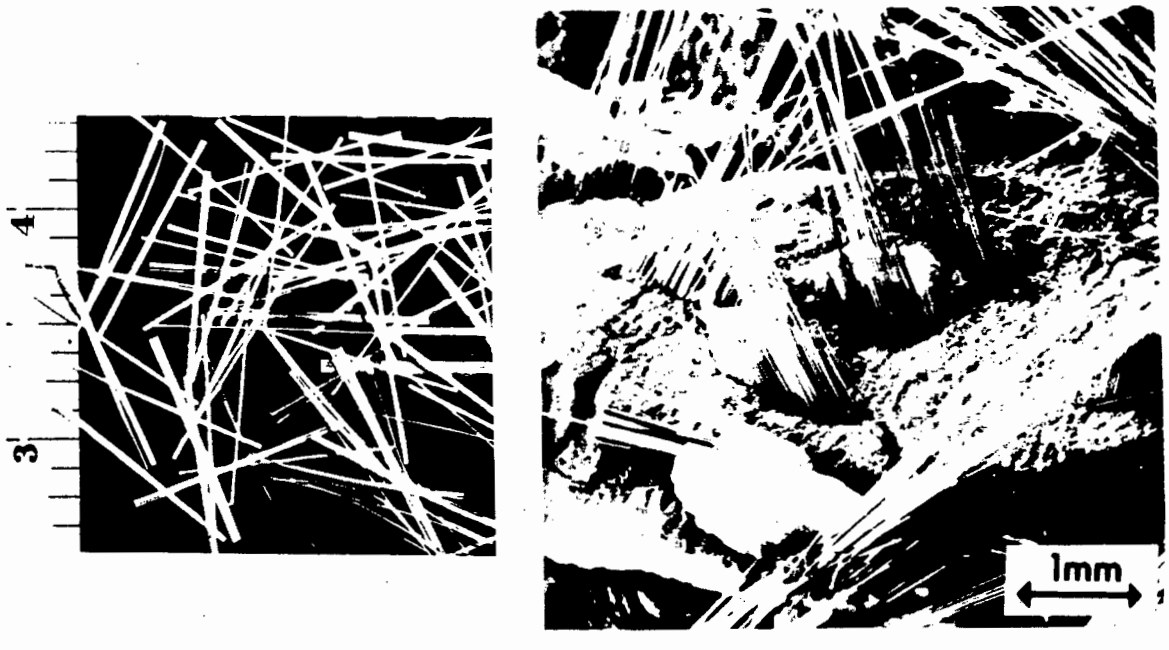

Figure 2.8 : Glass fibres are shown on left; fracture surface on right

2.3.3 Carbon Fibres

Although carbon fibres are very expensive compared to other fibres, their qualities of high stiffness and tensile strength combined with their relative inertness to alkaline attack in cement paste have encouraged extensive laboratory testing, especially in Japan.

Carbon fibres are available in the continuous form or as short staples. They are produced by carbonizing suitable organic materials at high temperatures, and then aligning the resultant graphite crystallites by "hot-stretching". The strength and stiffness of the fibre is therefore dependant on the source material and the extent of hot-stretching. By employing temperatures as high as 2750^{o} during stretching, fibres with Young's Modulus in excess of 700 GN/m^2 have been produced. These high modulus fibres are commonly referred to as TYPE I, while high strength fibres are referred to as TYPE II. The fibres have a fibrillar structure similar to that of asbestos, as shown by Figure 2.9 below. Figure 2.9(b) shows some smaller carbon fibre[8,9].

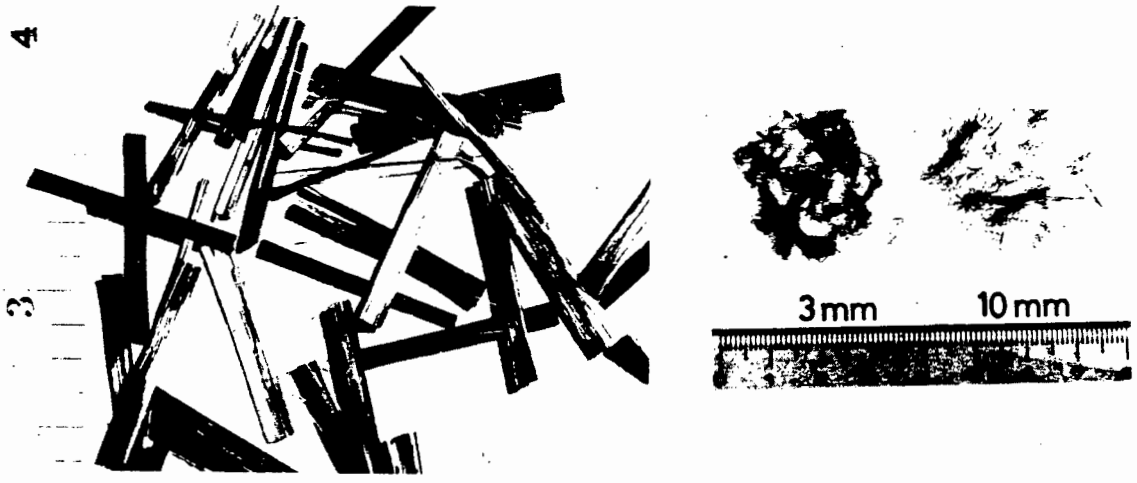

Figure 2.9 : One inch staples of carbon fibre (left), small 3 and 10mm long carbon fibres (right)

Carbon fibres may be made from textiles, such as polyacrylonitile or rayon, yielding high quality fibres. Those made from pitch and some types of agricultural waste have created a lot of interest on economic grounds[10]. In recent years, inexpensive carbon fibres (low modulus) made from coal and petroleum pitches have been developed in Japan, and the applications of short carbon fibres as reinforcement for cement materials are being used there in the construction industry[11].

2.3.4 Polypropylene Fibres

Early in the 1960's polypropylene fibres became available in two forms - MONOFILAMENT (or spinneret) and FILM fibres. The extrusion of synthetic polymers into fibres by spinneret has long been the conventional method for rayon and nylon production, and this technique is used to produce polypropylene fibres which are normally circular in cross section. The new process of film extrusion is more economical and particularly suited for the processing of isostatic polypropylene. The extruder is fitted with a die to produce a tubular or flat film which is then slit into tapes, and monoaxially stretched. A molecular orientation results from the stretching which accounts for the high tensile strength of polypropylene fibres. Once the required properties of the film are reached, the film is fibrillated - this is the generation of longitudinal splits. This can be achieved by rubbing the film together, or by the use of a carefully designed pin system of rollers over which the stretched films are led. Figure 2.10(a) shows a fibrillated yarn which has been split by rubbing resulting in random lengths over which the film is torn.[12]. Figure 2.10(b)

shows the regular pattern of a pinned yarn[13]. Fibrillated films which have been twisted into fibres are softer and easier to handle than monofilament (spinneret) fibres.

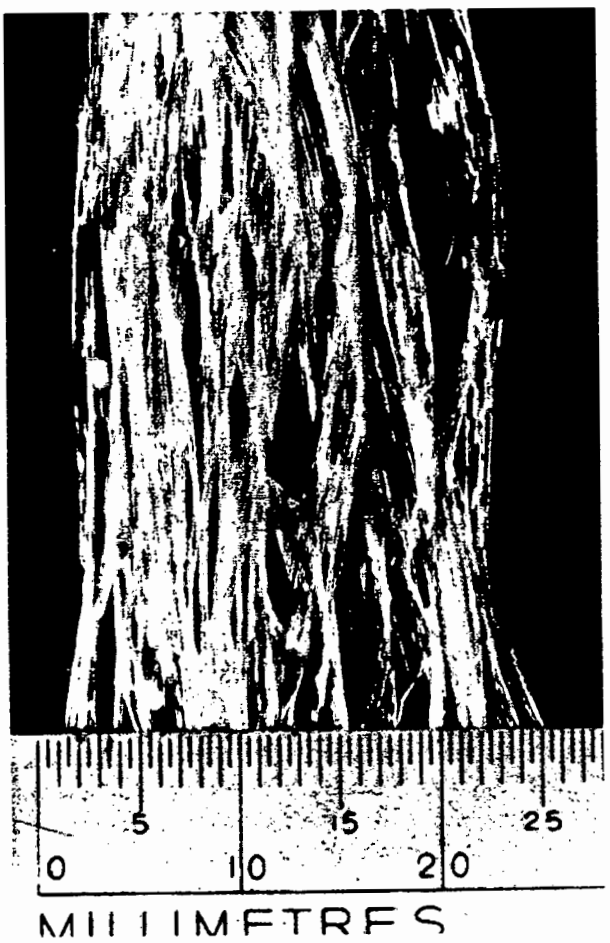

(a)

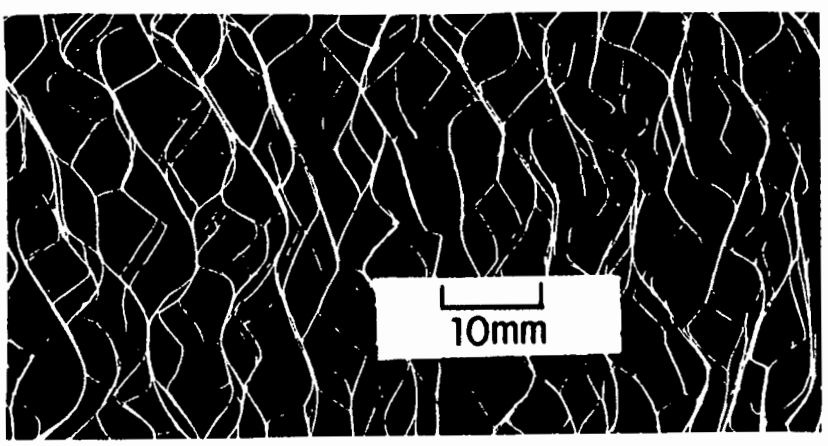

(b)

Figure 2.10 : Yarn split by rubbing (a) and by pin system (b)

Two outstanding properties of polypropylene fibres are :

(i) the fibre is inert making it resistant to attack from most chemicals. On contact with more aggressive chemicals the concrete will always be the first to deteriorate;

(ii) the hydrophobic surface helps to prevent chopped fibres from balling up during mixing. Stated in another way, the fibres are not wetted by a cement paste because their water demand is nil.

Unlike glass and steel fibres, polypropylene fibre is supplied in a spool for cutting on site or on request are chopped by the manufacturer into lengths between 25 to 75mm. The advantages of purchasing the fibre in spools and cutting to the required lengths are that it is cheaper, it is easier to transport the spools, and the spools take up less space. The benefit of these considerations are obvious relative to precast works.

2.3.5 Asbestos Fibres

Asbestos is a naturally occurring crystalline fibrous silicate material, the two main groups being the Serpentines and the Amphiboles. The most abundant material is CHRYSOTILE (or White Asbestos), which is the sole member of the Serpentine group. Figure 2.11 shows an enlarged view of Chrysotile fibres[14].

Figure 2.11 : Scanning electron microscope view of Chrysotile asbestos fibres

Chrysotile constitutes more than 90% of the world asbestos reserves and is used to a large extent in the manufacture of asbestos cement. Asbestos cement has been used as a fibre-cement composite since the early 1900's. The proportion by weight of asbestos fibre is normally between;

9 - 12% for flat or corrugated sheet

11 - 14% for pressure pipes

20 - 30% for fire-resistant boards.

The binder used is normally a portland cement. However, before the asbestos fibres can be mixed with cement they undergo heavy pre-treatment to break up the blocks of fibres into thin fibre units of

an effective diameter of 1 μm or less. Edge runners or hammer mills are then used to split the fibres into even thinner sections or into cohesive bundles of parallel fibres. The fibres can then be easily disposed of in a water and cement suspension by continuous dilution and mechanical stirring. One of the advantages of asbestos fibres over other fibres is that it has an affinity for portland cement which settles on the surface of the fibres and remains there even under high dilution or water extraction. This enables a reduction in water content from about 90% to 20% without segregation of the cement, which leads to a well distributed and bonded fibre composition[15]. Although the tensile strength of chrysotile is very high (up to 3000 MPa has been reported), it should be noted that the strength of the fibre bundles in the composite is much lower. Ranges such as 560 - 750 MPa, 300 - 1800 MPa and 550 - 970 MPa are considered.

Despite the wide usage of asbestos fibres as a reinforcing fibre, it should be noted that prolonged exposure to asbestos fibre has been shown to be injurious to health. It is this factor which has led to a reduction in the usage of asbestos fibres, and the search for alternative fibre types, both manufactured and synthetic or naturally occurring.

2.3.6 Synthetic Fibres

KEVLAR FIBRES - This is the name given to a group of high modulus organic fibres, examples of which are PRD 49 and PRD 29 (typical properties are given in Table 2.1, section 2.4). Their high strength and stiffness make them an attractive reinforcement of cement. Tests carried out by Majunder with 2% by volume of fibres,

yielded modulus of rupture of the composite in the range 40 - 50 MPa and ultimate tensile strengths between 14 - 16 MPa, despite unsatisfactory distribution of the fibres[16]. However the one problem with Kevlar fibres is that they are known to lose all of their room temperature strength at 300°C and the rate of creep increases with temperature, which limits their application in environments where high temperatures are encountered.

NYLON FIBRES - Nylon was one of the first polymer fibres to be included in cement and concrete, but due to its high cost compared to polypropylene, its commercial usage is limited. Using 5.5% by volume of fibres greatly enhances the impact resistance of composites. Watar and Majunder achieved moduli of rupture up to 11 MPa using 4% by weight (about 7% by volume) of 25 mm long nylon monofilament fibres, and large increases in impact strength were observed[17]. It should be noted though that the flexural strength of concrete is reduced by the inclusion of small volumes of short nylon monofilaments.

POLYETHYLENE - This fibre has not been used to any extent in cement composites because of its low modulus of elasticity. However, the development of high modulus polyethylenes with E up to 70 000 MPa has enabled the production of relatively cheap fibres - these should enable considerable strengthening of cement based composites, but so far no test results have been published.

2.3.7 Natural Organic and Mineral Fibres

The relatively high cost of man-made fibres and wire meshes for use in fibre-reinforced concrete and ferrocement induced researchers to

experiment with natural fibres as possible substitutes. This is particularly relevant in terms of low-cost housing applications in underdeveloped and backward countries, where the cost of the reinforcement and, more importantly its availability, have precluded its use. Some of the more common fibres available which have been investigated, are briefly outlined below :

CELLULOSE FIBRES - Studies undertaken by Krenchel show that cellulose fibres may be used in cement composites, but volumes in the region of 15 - 20% are required to provide adequate strengthening of the composite. However, their disadvantages are :

- they are hygroscopic
- the fibre dispersion varies with moisture content
- the fibres rot if kept for prolonged periods in moist conditions, and
- they cannot tolerate heating beyond 100 - 120^{o}C.

It is therefore unlikely that cellulose fibres will be solely used as reinforcement, but rather in conjunction with other fibres (e.g. asbestos).

COCONUT FIBRES - These fibres are very durable under natural weathering conditions and attempts have been made to include them in cement-based composites. However, like most vegetable fibres their modulus of elasticity is low and they are sensitive to moisture variations.

SISAL - Studies undertaken by the Building Research Institute showed that sisal fibres tended to clump in the mix, and setting of

cement was retarded by bleaching or organic impurities from the presoaked cuttings. Concrete beams were produced with sisal up to 5% by weight of cement, but unfortunately no additional strength was observed[16]. More promising results have been obtained by Swift at the Kenyatta University College (Kenya), who has produced effective corrugated sheeting using a combination of long and short sisal fibres[17].

The most comprehensive studies conducted on the AGAVE family (of which sisal is the most common fibre) have been undertaken by Castro and Naaman[18]. They conducted tests on two other species of agave plants, Lechuguilla and Maguey. Their tests showed that water absorption occurred rapidly, which tended to render the mix very harsh and occasionally led to fibre balling. This was overcome by the use of a superplasticizer and preliminary tests were conducted with fibre volumes less than 5%. The results were often erratic with large variability being encountered, so fibre volumes exceeding 5% were used. Subsequent tests showed elasto-plastic behaviour in flexure and multiple matrix cracking for volume fractions greater than 7%. Tests on the fibres themselves yielded average tensile strengths of 330 MPa. Again, however, the fibre strength deteriorated at elevated temperatures and moisture conditions, a general problem associated with organic fibres.

2.4 COMPARING FIBRES

From this chapter one will have reached an insight into the vast volume of research which has been conducted on a wide spectrum of fibre types, be they processed, synthetic or naturally occurring.

Steel, polypropylene, glass and asbestos fibres are commercially produced and used today, the aim being production of high strength fibres at lowest possible cost. In order to gain an overall picture of the different fibre properties and typical volumes of these fibres which are required to strengthen a cement based composite, Table 2.1 is presented below (19-21). The fibres can be classified into two categories :

1. those with a high modulus of elasticity e.g. glass, asbestos, steel and carbon (marked †) and
2. those with a low modulus of elasticity such as natural, synthetic and organic fibres (marked #).

Even though carbon and kevlar fibres are very expensive, they have been included for completeness.

The blue file accompanying this report contains several different types of fibres which are used commercially today. The text accompanying each sample gives an indication of the geographical spread of fibre use.

Table 2.1 : Some Typical Fibre Properties

Type	Diameter (μm)	Length (mm)	Density 10^3kg/m^3	Young's Modulus GPa	Tensile Strength GPa	Elongation at break %	Typical volume in composites %
† Chrysotile Asbestos (white)	0.02-30	≤ 40	2.55	164	0.2-1.8 bundles	2-3	10
Crocidolite Asbestos (blue)	0.1-20	-	3.37	196	3.5-4.5	2-3	-
‡ Carbon, type 1 high modulus	14.5 8	3-10 10-cont.	1.63 1.90	386 380	0.0083 1.800	~0.5	1-5 2-12
Carbon, type 2 † high strength	9	"	1.90	230	2.6	~1.0	"
# Cellulose			1.2	10	0.3-0.5		
† Glass E " CEM-FIL f'mt " 201 filament strand	8-10 12.5 110x650	 10-50 10-50	2.54 2.7	72 80 70	3.5 2.5 1.250	4.8 3.6	2-8
‡ Kevlar PRD 49 PRD 29	 10 12	 6-65 6-65	 1.45 1.44	 133 69	 2.9 2.9	 2.1 4.0	 < 2
Nylon,Type 242 Perlon Polypropylene monofilament fibrillated	> 4 13 100-200 500-4000	5-50 6 5-50 20-75	1.44 0.9 0.9	Rate dep. up to 4 " " Rate dep. up to 8	0.75-0.9 0.011 0.4 0.4	13.5 18 8	0.1-6 8-9 0.1-6 0.2-1.2
Polycristalline Alumina	500-770		3.9	245	0.65		
# Sisal	10-50	200-500	1.5	14-28	0.2-0.8	~3.0	> 5
† Steel High tensile Stainless	 100-600 10-330	 10-60 10-60	 7.86	 200 160	 0.700-2.000 2.100	 3.5 3	 0.5-2.0

‡ high cost
† high modulus of elasticity
# low modulus of elasticity

CHAPTER 3

THEORETICAL PRINCIPLES OF FIBRE REINFORCEMENT

3.1 GENERAL

So far a general overview of different fibre types and their relevant properties has been presented. At this point the investigation is narrowed down to dealing with steel fibres only. The use of ductile steel fibres as reinforcement of a basically brittle, non-ductile cement matrix has been widely researched and documented. The concept of fibre reinforcement is to use the deformation of the matrix under stress to transfer load to the fibre. Depending on the strength of the fibres and the degree to which they are stressed, substantial improvements in the static and dynamic strength properties of the concrete are attainable.

For SFRC several different approaches to design are available. Some approaches are based on conventional design methods which have been modified to incorporate fibre contribution, some are empirical and may apply only to special applications. In this investigation the "Law of Mixtures" theory is outlined and its applicability in direct tensile and flexure testing presented. This is succeeded by an alternative approach to the theoretical prediction of the cracking stress, known as the Fibre Spacing Concept. The former mechanism relates the strength to the volume, orientation and aspect ratio of the fibres while the latter mechanism relates the "first-crack strength" to the spacing of the fibre reinforcement.

Initially, a brief explanation on the action of the fibres in the matrix and their behaviour when the composite is stressed, is given. This will facilitate the ensuing derivation of the Law of Mixtures and Spacing Concept, regarding the fibres' contribution towards composite strength.

3.2 THE ROLE OF FIBRES AS CRACK ARRESTORS

When a plain concrete beam is subjected to increasing loads, the strain in the tensile zone will also increase until a certain point is reached, which is commonly referred to as the Proportional Limit. This proportional limit is defined as that load below which the matrix is essentially linearly elastic, i.e. an examination of a plotted load vs deflection curve would show a more or less linear line up to the proportional limit. Increasing the load above this point results in the matrix cracking strain being reached. Additional loading (a very small increment) will lead to cracking of the tensile zone and subsequent immediate failure of the beam. The aggregates in concrete do exert an influence on crack propagation, but once cracking has commenced, its propagation is very rapid in unreinforced matrices. The load at which matrix cracking occurs is thus referred to as the "first-crack strength" of the concrete.

For fibre reinforced concrete, the proportional limit is defined the same as above. It is assumed that both the plain concrete and fibre behave elastically up to the proportional limit. The first crack in the composite will occur when the composite strain exceeds the cracking strain of the concrete matrix.

When the matrix cracks, the load previously supported by the matrix in the crack area is carried by any fibres bridging the crack. This load carried by the fibres is transferred back into the matrix along the fibre-matrix interface causing shear stress. If the bond strength is small compared with the matrix strength, failure occurs as soon as the bond is broken[22]. In composites where the fibre-matrix shear strength is high, failure occurs only after the matrix fails. This failure manifests itself in the form of yielding of the fibres themselves or most commonly bond failure at the fibre-matrix interface. The factor that determines whether failure by yielding or bond failure occurs is the fibre length, but as will be shown in Chapter 4, a number of factors must be considered collectively.

3.3 LAW OF MIXTURES THEORY FOR SFRC

The following theory makes a number of assumptions :

(i) the fibres are aligned in the direction of stress

(ii) before cracking, the fibres are fully bonded to the matrix (i.e. equal strains in fibre and matrix), and

(iii) the Poisson's ratio in fibre and matrix is equal to zero.

Assumption (i) is valid in the idealized state only - in actual fact the fibres are randomly orientated and this consideration in combination with a host of other variables will have a marked affect on the strength of a SFRC composite. However, the law of mixtures provides for a basic formulae which can be modified later to account for these variables. Figure 3.1 should be read in conjunction with the development of the theory.

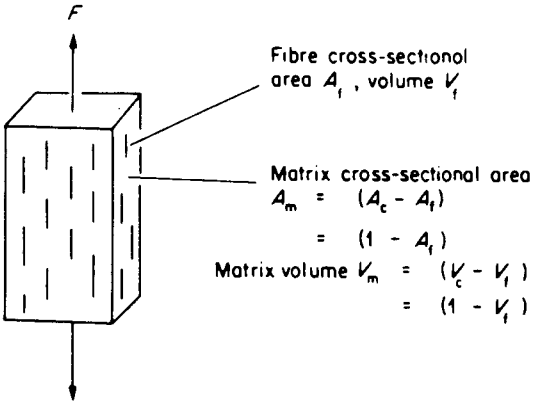

Figure 3.1 : Uniaxial tension applied to a unit volume of SFRC[23]

The volume of the composite is taken as unity

$$V_c = 1 \quad .$$

The fibre volume can then be expressed as a fraction of the composite volume

$$\frac{V_f}{V_c} = \frac{V_f}{1} = V_f \quad .$$

From assumption (ii), for equal strains in the fibre and matrix before cracking

$$\epsilon_c = \epsilon_f = \epsilon_m = \frac{\sigma_{ct}}{E_c} = \frac{\sigma_{ft}}{E_f} = \frac{\sigma_{mt}}{E_m}$$

subscripts (c,f) and (m) referring to the composite, fibre and matrix and (t) to direct tensile respectively. The axially applied force (F) will be distributed among the matrix and the fibre as follows :

$$F = \sigma_{ct} A_c = \sigma_{ft} A_f + \sigma_{mt} A_m \quad .$$

For a unit llength composite $V_c = A_c = 1$ and $A_f = V_f$

$$\therefore \quad \sigma_{ct} = \sigma_{ft} V_f + \sigma_{mt} (1 - V_f) \quad . \qquad (3.1)$$

Equation (3.1) is dependent only on the properties and volume fractions of the constituents. Although until now the theory has been applied to a direct tensile stress situation, it has been suggested that there would be no loss of generality if the equation was modified to apply to a bending tensile stress field[24]. Indeed, the difficulty of applying a direct tensional force free of eccentricity and the variability of the secondary stresses induced by the grips in the tension test, make it preferable to measure the tensile strength by subjecting a concrete beam to flexure[25]. One merely has to look at the many methods used/proposed for the single fibre pull-out test to appreciate the difficulty of developing a test set-up which closely approximates the stresses and strains encountered in a fibre composite[26-29].

Although there is no unique relationship which can be drawn up between the direct tensile strength and flexural tensile strength for <u>all</u> types of mix proportions and aggregate types, there does exist a relationship for a specific matrix[30] (see Figure 3.2). The following theory is taken from work by Swamy *et al*[31].

The modulus of rupture of the matrix (σ_{mb}) is thus related to the direct tensile strength of the form :

$$\sigma_{mb} = \beta \sigma_{mt} \qquad (3.2)$$

where β is a factor incorporating all the parameters which generally influence concrete strength, and varies from 1.3 - 1.5.

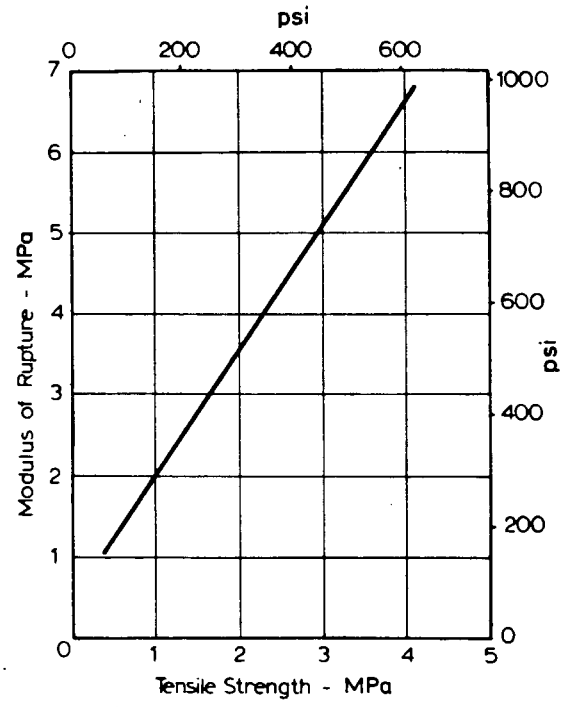

Figure 3.2 : Relation between modulus of rupture and strength in direct tension

The modulus of rupture of the matrix (σ_{mb}) is thus related to the direct tensile strength in the form :

$$\sigma_{mb} = \beta \sigma_{mt} \tag{3.2}$$

where β is a factor incorporating all the parameters which generally influence concrete strength, and varies from 1.3 - 1.5.

If failure occurs by fibre pull-out, then the average tensile stress in the fibre is related to the average bond stress (τ_{AV}) by

$$\sigma_{ft} = 2 \tau_{AV} \ell/D \tag{3.3}$$

substituting equations (3.2) and (3.3) into equation (3.1) yields

$$\sigma_{ct} = \frac{\sigma_{mb}}{\beta} V_m + 2 \tau_{AV} V_f \ell/D \quad . \tag{3.4}$$

The modulus of rupture of the composite is a more difficult consideration. In plain concrete a linear stress distribution is assumed up to failure. If this were true for fibrous composites, the modulus of rupture σ_{cb} is related to the section modulus Z by

$$M = \sigma_{cb} Z \qquad (3.5)$$

where M is the applied moment.

However, it has been shown by various authors that there is no stress linearity even where failure occurs by fibre pull-out, this nonlinearity occuring in both the tension and compression zones[32,33,34]. The nonlinear flexural stress distribution is related to the direct tensile strength as follows

$$M = \sigma_{ct}(\alpha Z) \qquad (3.6)$$

where (α Z) is analogous to plastic modulus.

From equations (3.5) and (3.6)

$$\sigma_{cb}(Z) = \sigma_{ct}(\alpha Z)$$

and substituting this relationship into equation (3.4)

$$\sigma_{cb} = \left(\frac{\alpha}{\beta}\right) \sigma_{mb} V_m + 2\alpha \tau_{AV} V_f \ell/D$$

which can be rewritten as :

$$\boxed{\sigma_{cb} = A \sigma_{mb} V_m + B \tau_{AV} V_f \ell/D \quad .} \qquad (3.7)$$

The values A and B in equation (3.7) can be determined statistically from experimental results, (see Chapter 7).

At the outset of the theoretical formulation a number of assumptions were made for the purpose of simplifying the former. In practice none of these assumptions are likely to occur, because many different variables are instrumental in determining the strength of a SFRC, be it in bending, tension or compression.

3.4 FIBRE SPACING CONCEPT

The spacing concept is based on the assumption that concrete is a notch sensitive medium in which the critical flaw size can be calculated[35]. The approach taken by Romauldi and Batson for increasing the tensile strength was to reduce the stress intensity at internal flaws or at the tip of cracks by using closely spaced wires as crack arrestors. The ability of the fibres to act as crack arrestors depends on the extent to which a crack can propagate before encountering a fibre, i.e. the "spacing" of the fibres determines crack growth. Romauldi *et al* reasoned that for a fixed volume of fibres of constant length, a reduction in the fibre diameter would lead to an increasing number of fibres. Consequently, the fibres would be more densely packed such that the "spacing" of the fibre centroids decreases leading to an increase in the tensile strength of the SFRC. Figure 3.3 shows the theoretical results linking first-crack propagation stress to wire spacing[36]. Results of tests conducted by Romualdi and Mandel are shown in Figure 3.4, which compares the strength ratio of SFRC at first-crack to that of plain concrete as a function of the fibre spacing[37].

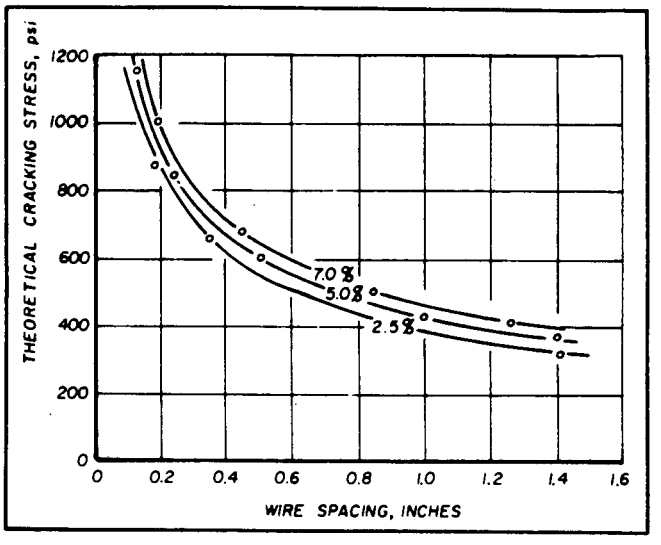

Figure 3.3 : Theoretical tensile cracking stress vs wire spacing

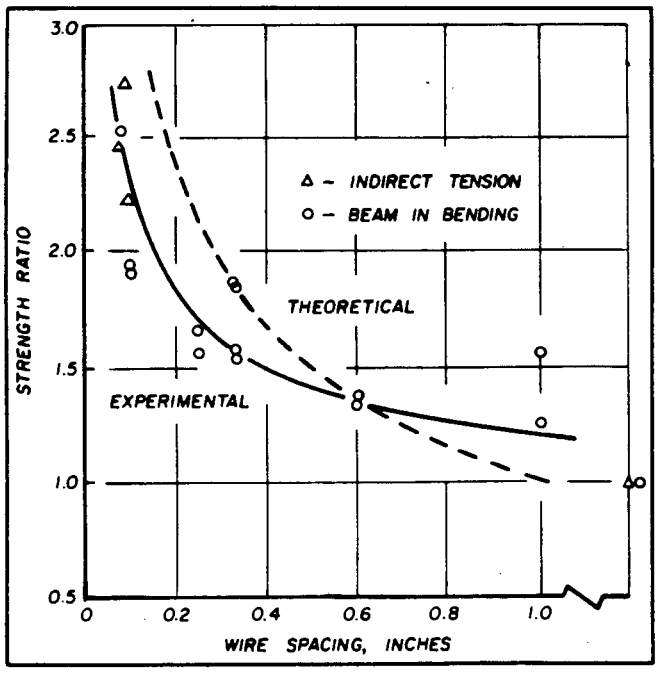

Figure 3.4 : Theoretical and experimental strength ratio as a function of fibre spacing

The expression derived by Romualdi and Mandel for the average fibre spacing reads as follows :

$$S = 1.38 \frac{d}{\sqrt{V_f}} \quad . \qquad (3.8)$$

Since their initial investigation, various authors have questioned the accuracy and assumptions made by Romauldi regarding the effects of fibre spacing on composite strength as well as the correct method of calculating the fibre spacing. Spacing equations have been formulated using either the distance between the centroids of separate fibres or from the number of fibres intersecting a unit area of a given plane section through the composite.

The former case has been investigated by Swamy *et al*, which takes into account the following considerations

(i) the fibre transfer length

(ii) the fibre-matrix bond, and

(iii) the orientation of the fibres in the composite.

The effective spacings (S_c) for the first crack modulus of rupture is given by;

$$S_c = 27\sqrt{\frac{d}{p\,\ell}} \qquad (3.9)$$

and for the ultimate modulus of rupture;

$$S_c = 25\sqrt{\frac{d}{p\,\ell}} \qquad (3.10)$$

where p is the volume percentage of fibres in the matrix, d and ℓ the fibre diameter and length respectively[38].

McKee has derived an equation for fibre spacing similar to that proposed by Romauldi and Batson in equation (3.8). His spacing equation is given by $S = 3\sqrt{\frac{V}{p}}$ where V is the volume of a single fibre and p the volume fraction of the fibre in the mortar[39].

The plane section case has been examined by Krenchel and the spacing equations given below are applicable to cylindrical fibres[40]

1-D ALL fibres parallel, plane section perpendicular to the direction of orientation

$$S_{1.0} = \frac{\sqrt{\pi}}{2} \frac{d}{\sqrt{V_f}} \approx 0.885 \frac{d}{\sqrt{V_f}} \qquad (3.11)$$

2-D Random fibre orientation, plane section perpendicular to the plane in which the fibres lie

$$S_{2.0} = \frac{\pi}{2\sqrt{2}} \frac{d}{\sqrt{V_f}} \approx 1.11 \frac{d}{\sqrt{V_f}} \qquad (3.12)$$

3-D Random fibre orientation

$$S_{3.0} = \sqrt{\frac{\pi}{2}} \frac{d}{\sqrt{V_f}} \approx 1.25 \frac{d}{\sqrt{V_f}} \quad . \qquad (3.13)$$

It is generally agreed that the ultimate strength of a steel-fibre reinforced concrete (SFRC) is relatively insensitive to fibre spacing, and depends primarily on the volume, aspect ratio and bond characteristics of the fibres. The ultimate strength of a SFRC specimen is thus determined from equation (3.1) for a direct tensile stress test or from equation (3.7) where the composite is tested in flexure. Since the "Law of Mixtures" theory is derived for an idealised situation, an extensive review of factors which affect the strength of SFRC is given in the ensuing chapter.

CHAPTER 4

FACTORS AFFECTING THE STRENGTH OF SFRC

4.1 GENERAL

The strength of a fibre composite depends primarily on the strength of the fibres and the degree to which all the fibres within the matrix are stressed. If the fibres are weak, then they will have a weakening influence on the composite. If the fibres are strong but are not effectively loaded in the matrix, the composite will still be weak. If the fibres are strong and effectively loaded in the matrix, then substantial increase in static and dynamic strengths is possible.

In practice, there are a number of other parameters which have to be considered when determining the influence which steel fibres will have on a concrete matrix.

4.2 PARAMETERS INFLUENCING COMPOSITE STRENGTH

Table 4.1 lists most of the factors which will affect the strength of a composite. These factors can be divided into two categories, namely, those contributing to the fibre strength and those contributing to the loading of the fibres in the matrix[41].

Table 4.1 : Factors contributing to the strength of a fibre composite

A FIBRE CONTRIBUTIONS

1. ULTIMATE STRENGTH OF THE INDIVIDUAL FIBRES
2. COLLECTIVE (i.e. bundle) STRENGTH OF THE FIBRES
3. VOLUME FRACTION IN THE COMPOSITE
4. STRENGTH vs FIBRE DIAMETER OR LENGTH
5. STRENGTH vs TEMPERATURE
6. FRACTURE STRAIN (brittle vs ductile fibres).

B. TRANSFER OF LOAD FROM MATRIX TO FIBRES
(This relates to average stress of the fibres in the matrix)

1. STRESS-STRAIN CURVES OF THE CONSTITUENTS
2. FIBRE VOLUME FRACTION
3. MATRIX SHEAR STRENGTH AND SHEAR MODULUS
4. INTERFACIAL BOND STRENGTH
5. FIBRE CRITICAL LENGTH
6. FIBRE ASPECT RATIO
7. FIBRE DISTRIBUTION
8. FIBRE ORIENTATION
9. COMPOSITE FAILURE MODE AND STATISTICS OF FIBRE FRACTURE

Some of the more important factors, namely A3, B4, B5, B8 and B9 are discussed in greater detail below.

4.2.1 Volume Fraction in the Composite

It has been shown that while the inclusion of steel fibres in concrete matrices increases the cracking stress (between 35-80% as the fibre volume varies from 1.25-2.50%), the greater advantage lies in the load carrying ability of the fibres after matrix

cracking[42]. The cracked composite may experience a lower or greater load after cracking than the uncracked composite as shown by Figure 4.1 below. σ_{mb} represents the load at which the unreinforced concrete cracks and cases (i) to (iv) show the result of increasing the fibre volume in the composite (assuming a fibre of adequate length is used throughout).

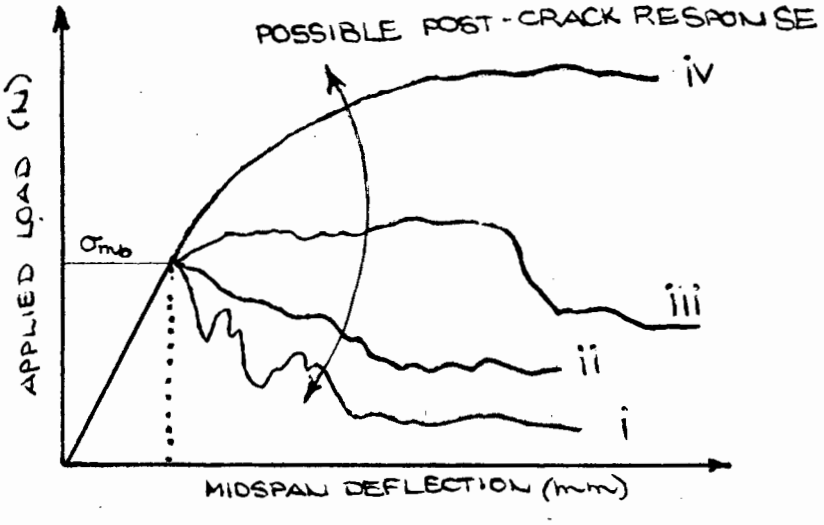

Figure 4.1 : Typical load deflection plots for SFRC beams in flexure

All four cases show greater energy absorption than plain concrete, although multiple cracking of the composite is likely to occur in cases (iii) and (iv) endowing the composite with a much greater ductility. In order for the curve to follow that of cases (iii) and (iv) the quantity of fibres added must exceed the CRITICAL FIBRE VOLUME (V_{fCRIT}) . This critical volume is defined as the volume of fibres which, after matrix cracking, will carry the load which the composite sustained before cracking. Hannant gives the following formulae to calculate the minimum fibre volume necessary to achieve flexural strengthening[43]

$$1\ D \quad V_{f(MIN)} = 0.41 \frac{\sigma_{mb}}{\tau} \frac{1}{\ell/D}$$

$$2\ D \quad V_{f(MIN)} = 0.64 \frac{\sigma_{mb}}{\tau} \frac{1}{\ell/D}$$

$$3\ D \quad V_{f(MIN)} = 0.82 \frac{\sigma_{mb}}{\tau} \frac{1}{\ell/D}$$

where σ_{mb} is the matrix cracking strength, τ_{AV} the average interfacial bond strength and ℓ/D the aspect ratio.

Where the SFRC specimens are subjected to uniaxial direct tension, the determination of the critical fibre volume is far easier. A graphical representation of the critical fibre volume is shown in Figure 4.2. It can be seen that the slope of the line $\sigma_{fu}\ V_f$ affects the intersection at which the critical fibre volume is reached. The strength of the composite reinforced with fibre volumes in excess of $V_{f(CRIT)}$ is given by $\sigma_{fu}\ V_f$ where σ_{fu} is the fracture stress or pull-out stress of the fibres. Thus, for fibres which generally pull-out at failure the bond strength is the controlling influence on $V_{f(CRIT)}$.

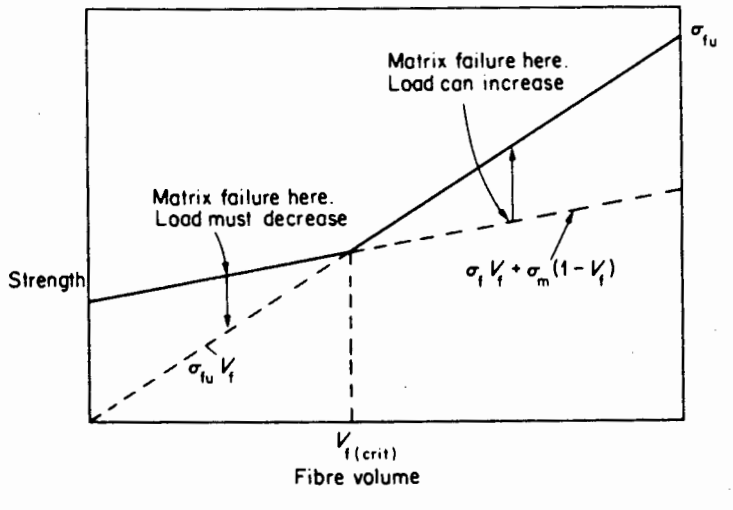

Figure 4.2 : Graphical plot of critical fibre volume position, as determined by equation (3.1) (Chapter 3)

It should be noted though that if the bond strength is small compared with the matrix strength, failure occurs as soon as the bond is broken.

4.2.2 Fibre Critical Length

In SFRC an important design parameter is the length of the fibre which should be such that the maximum strength of the fibre can be utilised. This length is commonly refered to as the CRITICAL LENGTH (ℓ_c) , and is defined as the minimum length required to cause fibre failure in a pull-out test. Usually, if the fibre length is smaller than the critical length composite failure will occur by fibre pull-out, whereas for fibre lengths greater or equal to the critical length the fibres themselves will yield at ultimate failure of the composite.

The critical fibre length can be determined from the relationship[46]

$$\ell_c = \sigma_{fu} \frac{d}{2\tau_{AV}}$$

where σ_{fu} is the ultimate strength of the fibre, d the fibre diameter and τ_{AV} the average interfacial bond stress. Argon and Shack have theorised that for fibres to have any effect at all on the first-crack strength of a concrete composite, they must have a minimum effective length of

$$\ell_m = 2 r_o \frac{E_f}{\tau_{AV}} \epsilon_c$$

where r_o is the fibre radius, ϵ_c the strain in the extreme tensile layer and the other symbols having their usual meaning[47]. If the fibres are longer than this minimum, then for the composite to have

any post-cracking behaviour the fibres would then have to support that portion of the stress previously carried by the matrix prior to cracking. This defines a minimum effective length for post-cracking behaviour :

$$\ell_{m\ post} = 2\, r_o \frac{\epsilon_c\, E_c}{\tau_b\, V_f} \quad .$$

Finally, if $\frac{\ell}{4} > \frac{r_o}{2} \frac{f_f}{\tau_b}$ the fibres should yield in failure instead of being pulled out at composite failure. The fibre strength f_f has the same value as σ_{fu} , the symbol designated merely differing between authors. Upon reflection, the last formulae proposed by Argon and Shack is of the same form as that given by Kelly for ℓ_c .

4.2.3 Interfacial Bond Strength

The tensile stress and the bond stress distribution along an elastic fibre length ($\ell < \ell_c$) embedded in a non-ductile matrix are shown in Figure 4.3 below. This shows that the bond stress is linear along most of the fibre's length, nonlinearity being confined to the ends of the fibre only.

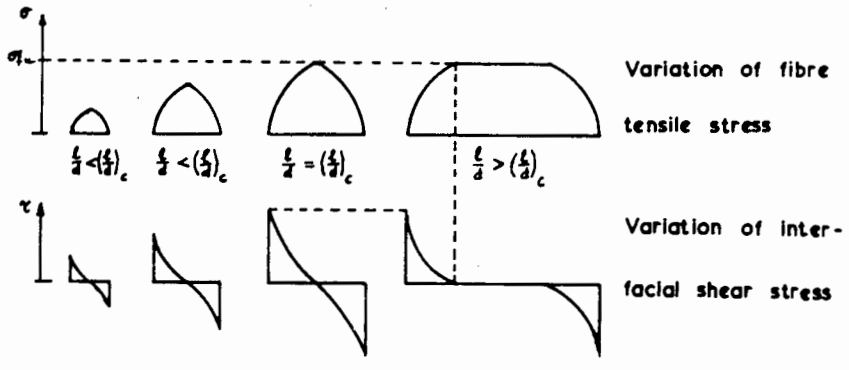

Figure 4.3 : Assumed interfacial bond stress distribution and the fibre tensile stress distribution

To simplify calculations it is assumed that the bond stress distribution is linear throughout. It should be noted that considerable differences of opinion exist on the validity of this assumption[48,49], however, there is general agreement that if failure occurs through fibre pull-out then the bond stress remains linear over the whole length of the fibre beyond the crack.

The determination of the bond stress is usually achieved by conducting bond tests. A typical bond stress vs displacement diagram for a SFRC specimen is shown in Figure 4.4. P is the maximum load which can be carried by the composite beyond which fibre pull-out occurs, which is seen by the drop in load carrying capacity. The load carried beyond point P results from the frictional interfacial stress between the fibre and the surrounding matrix.

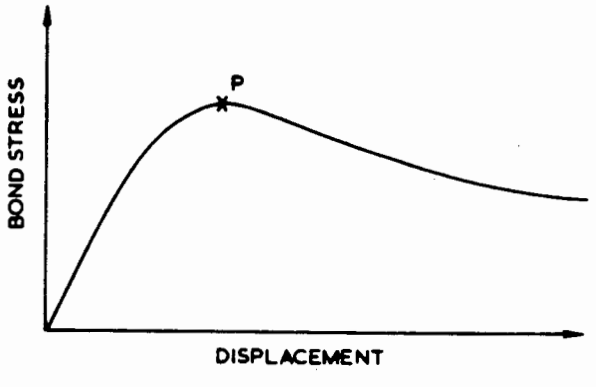

Figure 4.4 : Typical bond stress-displacement diagram for SFRC

A somewhat different method of determining the bond stress has been submitted by Swamy and Mangat, which utilises the test results of several authors applied to a theoretical determination of the bond stress. This method is actually used in Chapter 7.

4.2.4 Fibre Orientation

A substantial amount of analytical work has been reported to evaluate the effect of fibre orientation on the concrete matrix. Most of the investigations have assumed that the matrix and the fibre behave elastically and that there is no relative slip between the fibres and the matrix. This assumption is valid only up to the point immediately prior to cracking of the matrix, because only after matrix cracking does the contribution of the fibres become apparent. As such the fibre reinforcing is expected to exert a very small influence on composite behaviour within the limits of elastic deformations.

In the region before matrix failure strain is reached, Laws considers that a length efficiency factor for an aligned short fibre's composite with frictional bond at the fibre interface is given by[50]

$$\eta_\ell = 1 - \frac{\ell_c}{2\ell}\frac{\epsilon_{mu}}{\epsilon_{fu}}$$

Since the ultimate strain of steel fibres ϵ_{fu} is much higher than that of concrete, the length efficiency factor will unlikely be less than 0.98 , i.e. nearly unity. Allan, however, considers that for thin laminates a fibre orientation factor should be applied in addition to the length efficiency factor[51]

$$\ell \leq \ell_c \qquad \eta_\ell = \frac{\ell}{2\,\ell_c}$$

$$\ell \geq \ell_c \qquad \eta_\ell = 1 - \frac{\ell_c}{2\,\ell} \quad .$$

It can be seen from his length efficiency factors that when the length of the aligned, discontinuous fibres in the composite is critical, the composite is only 50% efficient compared to one with long, aligned fibres.

The orientation of the fibres relative to the direction of stress (for the composite in the uncracked state) can be allowed for by multiplying the fibre volume (V_f) by orientation factors (η_o) , some typical values of which are given in Table 4.2.

Fibre orientation		η_o according to Cox	Krenchel
1-D	aligned	1	1
2-D	random in plane	$\frac{1}{3}$	$\frac{3}{8}$
3-D	random	$\frac{1}{6}$	$\frac{1}{5}$

Table 4.2 : Factor (η_o) for a given fibre orientation relative to the direction of stress

In practice, however, it seems irrelevant to try and accurately quantify values for (η_ℓ) and (η_o) . This is because the fibres have marginal influence on the composite in the uncracked state as mentioned and because the variability of concrete occurring even within the same mix would nullify any precise factors which are applied.

The situation changes drastically, however, once the composite has cracked. The following parameters now become of influence in determining the ultimate strength of the cracked composite :

(i) the orientation of the fibre

(ii) the length of the fibre, and

(iii) the sliding frictional bond.

The length efficiency factors previously given now increase because as the crack opens the fibres tend to pull into line with the maximum stress, as shown by Figure 4.5.

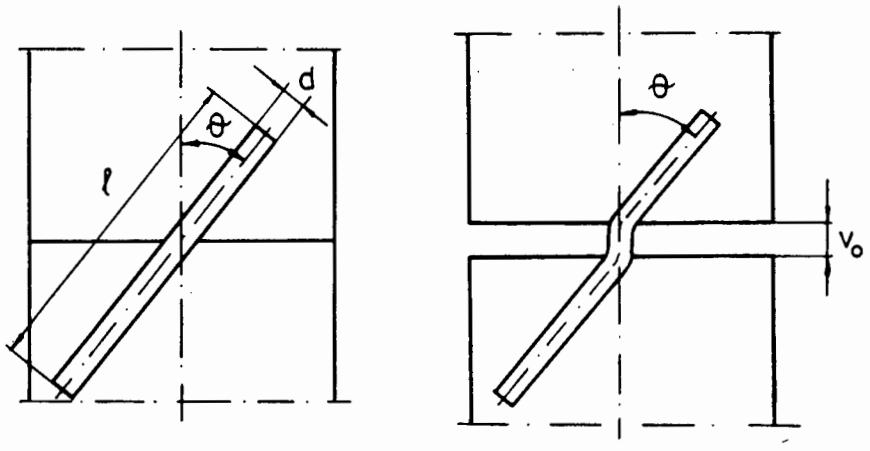

Figure 4.5 : Realignment of fibres due to crack opening

The variation of strength with the orientation has been widely studied[52,53] perhaps the most conclusive being those reported by Naaman[54]. He experimentally determined that for fibre orientations less than or equal to 45^{o} to the direction of stress, the peak load on pull-out was of the same order as for fibres which were aligned parallel to the direction of maximum stress. Beyond orientations of 60^{o} to the maximum stress, the pull-out load decreased drastically due to disruption of the concrete wedges at the root of the fibre. Brandt has calculated the optimal values of orientation relative to the axis of maximum stress, and has shown that the total fracture energy of the composite is at its maximum when the orientation of the fibres is at 35^{o} maximum[55]. These findings show that orientation factors applicable to pre-cracked composites cannot be used to determine or explain post-cracking behaviour. An interesting approach by Laws involves the combination of the orientation and length efficiency factors to arrive at a TOTAL efficiency factor. Table 4.3 below shows the total efficiency

factor proposed by Laws, which is derived from considerations of the fibre orientation, length and bond stress (static interfacial τ_s and sliding frictional τ_α)[56].

Table 4.3 : Efficiency factors for post-cracking strength calculations

ORIENTATION	EFFICIENCY FACTOR (continuous fibres)	EFFICIENCY FACTOR (short fibres)	
ALIGNED	1	$\frac{\ell}{4\,\ell_c}$	$\ell \leq 2\,\ell_c$
		$1 - \frac{\ell_c}{\ell}$	$\ell \geq 2\,\ell_c$
RANDOM 2-D	$\frac{3}{8}$	$\frac{9}{80}\left[\frac{\ell}{\ell_c}\right]$	$\ell \leq \frac{5}{3}\,\ell_c$
		$\frac{3}{8}\left[1 - \frac{5}{6}\frac{\ell_c}{\ell}\right]$	$\ell \geq \frac{5}{3}\,\ell_c$
RANDOM 3-D	$\frac{1}{5}$	$\frac{7\,\ell}{100\ell_c}$	$\ell \leq \frac{10}{7}\,\ell_c$
		$\frac{1}{5}\left[1 - \frac{5}{7}\frac{\ell_c}{\ell}\right]$	$\ell \geq \frac{10}{7}\,\ell_c$

All the efficiency factors in Table 4.3 above relate to the case where no sliding frictional bond stress occurs once the fibre starts to slip, pull-out. However, in order to take account of the sliding or ploughing frictional bond stress (τ_α), the term

$$\ell_c' = \frac{\ell_c}{2}\left[2 - \frac{\tau_\alpha}{\tau_s}\right]$$

is simply substituted for ℓ_c in Table 4.3.

The total efficiency factor can be conveniently read off from Figure 4.6 where the solid lines represent $\tau_\alpha = 0$, the dashed lines $\tau_\alpha = \tau_s$, (for values $\tau_\alpha \leq \tau_s$ simply interpolate).

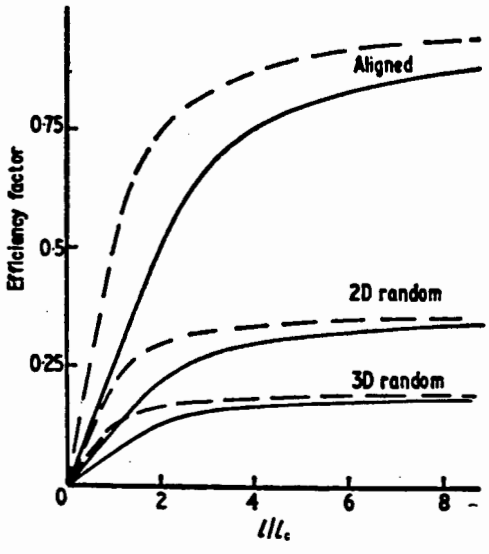

Figure 4.6 : The total efficiency factor η as a function of the ratio of fibre length to critical fibre length

So far little attention has been given to the role of the sliding frictional force during fibre pull-out on the strength of SFRC, and no measurements have been reported. From Laws' deduction above, it would appear to be an important point warranting further experimental work.

A different approach is used by Schnutgen, whereby various efficiency factors are applied to a derived strength equation;

$$\sigma_{cb} = \sigma_{mb}[1 + \eta_\ell \, \eta_o \, V_f(n - 1)] + 2 \, \tau_{ULT} \, \frac{\ell}{D} \, \eta \, V_f$$

the symbols having their usual meanings. Factor η_ℓ is the factor for the fibre aspect ratio which can be determined from Figure 4.7. Factor η_o is the orientation factor which is read off Figure 4.8[57].

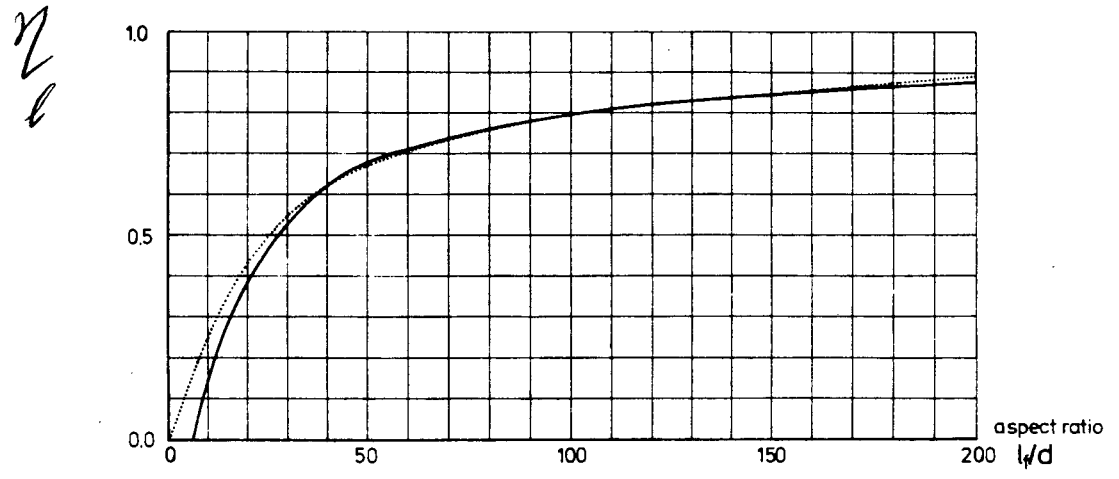

Figure 4.7 : Factor for fibre aspect ratio

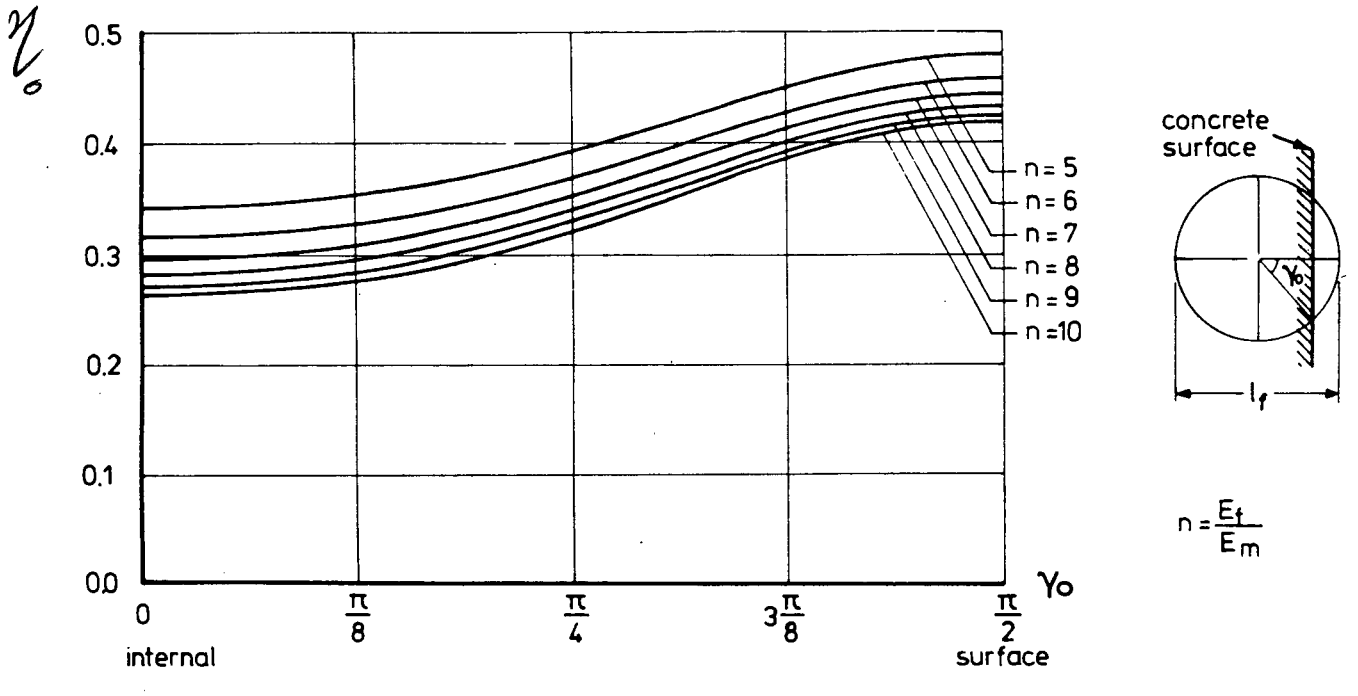

Figure 4.8 : Factor for fibre orientation near the concrete surface

Factor η is given by : $\eta = \eta_{\ell u}\, \eta_\alpha\, \eta_d$.

If the composite fails by fibre pull-out, it has been shown that the mean pull-out length is $(\ell/4)$[58]. If the pull-out length was equal either side of the crack, $\eta_{\ell u}$ would equal unity, and thus for a pull out length of $(\ell/4)$ Schnütgen assigns $\eta_{\ell u}$ a value of 0.5. The value of η_{α} has to be determined experimentally; η_{α} takes into account the fact that fibres are forced to align in the direction of major stress once cracking has occurred, producing additional frictional force between the fibre and the matrix. This agrees with the findings of Naaman and Brandt, mentioned previously. Unfortunately Schnütgen only makes reference to factor η_{d} which accounts for the random orientation of small length steel fibres, without giving usable values.

Perhaps the most simple though widely used efficiency factor is that proposed by Romualdi and Mandel; they showed that the effective length of N number of fibres in the direction of principal stress is[59];

$$\ell_{EFFECTIVE} = 0.41 \times \ell \quad .$$

Therefore the effective volume of the fibres in the direction of stress is;

$$V_{fe} = \frac{\pi d^2}{4} \times 0.41 \times \ell \times N \quad .$$

Since the total volume of fibres

$$V_f = \frac{\pi d^2}{4} \times \ell \times N$$

one obtains

$$V_{fe} = 0.41\ V_f \quad .$$

Some of the factors reviewed are derived purely theoretically, others have been obtained from theory made to fit experimental results. Additionally, since most research work is conducted with differing fibres and mixes, it is difficult to correlate results to determine fibre behaviour. On this account the choice of factors should be made carefully, with testing conditions approximating those in the derivation of such factors.

4.2.5 Composite Failure Mode

When a fibre reinforced concrete specimen is tested in tension up to failure, various failure mechanisms can develop. These mechanisms include single or multiple cracking of the matrix, fibre pull-out, fibre debonding over a limited zone on either side of the crack and fibre straining to failure, as represented by Figure 4.9.

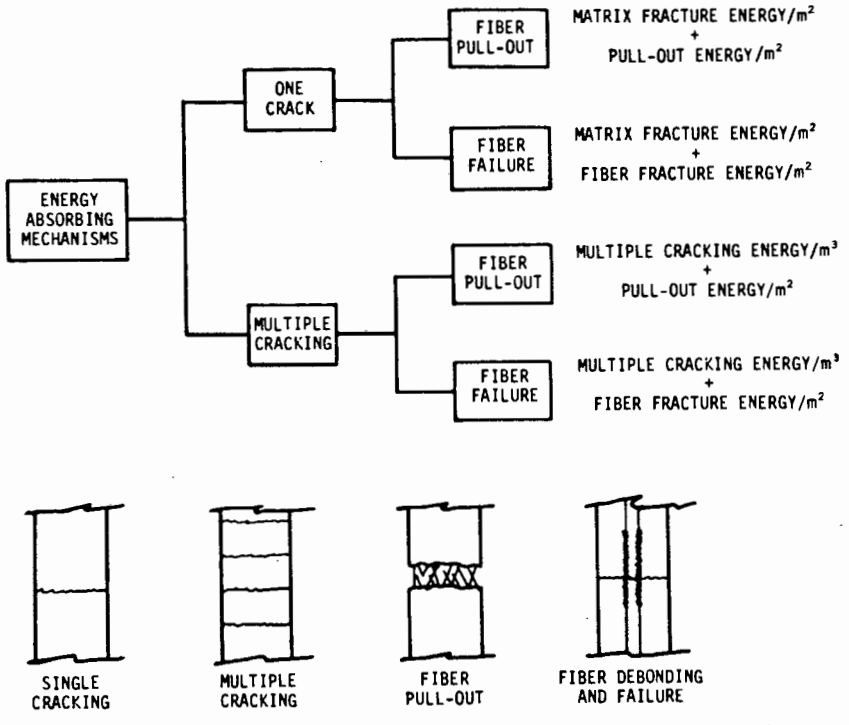

Figure 4.9 : Composite failure mechanisms

These failure mechanisms will also manifest themselves in flexure and compression testing in which tension forces determine composite behaviour. The occurrence of one mechanism or another depends on the fibre reinforcing parameters, the fibre-matrix interfacial bond and the rate of loading. Generally SFRC with discontinuous fibres exhibit a single macrocrack at failure while composites with continuous fibres typically fail by multiple cracking in the matrix, fibre debonding on either side of the cracks and fibre straining to failure.

FAILURE MODE FOR $\ell < \ell_c$ In SFRC in which the randomly oriented fibres are of short lengths, fibre pull-out invariably occurs at the failure of the composite since the effective length of each fibre in the direction of stress is less than the critical length (ℓ_c) . When the composite cracks, those fibres bridging the crack take on the load previously supported by the matrix. At this stage the bond stress corresponds to the average bond stress (τ_{AV}) and bond slip begins. Upon further loading, progressive debonding of the fibres occurs in tandem with slow crack propagation. Multiple cracking may occur, but only if the surface geometry of the steel fibres is such as to involve considerable bond resistance (e.g. Dramix fibres).

Ultimate failure occurs when the interfacial shear stress reaches the ultimate bond strength (τ_u) between the fibre and its surrounding concrete matrix. This stage is signified by unstable crack propagation and failure by fibre pull-out. It should be noted that the ultimate shear stress (τ_u) at failure differs from the average interfacial shear stress (τ_{AV}) in the initial phase of fibre debonding (see section 4.2.3, Figure 4.4).

Since ultimate failure occurs by fibre pull-out, it is obvious that the tensile strength of the fibre is not fully utilised. While most fibres are made of high tensile steel it would be sufficient to use mild steel. Provided that the steel fibres are sufficiently long enough to get a good bond grip and/or have some form of end anchorage, there should be no reason why fibres made of mild steel should not provide greater strengthening than plain round, high strength fibres.

FAILURE MODE FOR $\ell > \ell_c$ When pull-out of the steel fibres succeeds cracking for a direct tension test, the ultimate strength can be approximated by the "rule of mixtures" theory as given in section 3.3, equation (3.1). In the case of a composite with supercritical length fibres (i.e. $\ell > \ell_c$) , it has been shown that the strength of a composite in direct tension is equal to that of the fibre only. Thus, in the case where the composite fails due to fibre fracture, the "rule of mixtures" is inapplicable in predicting the ultimate strength[60].

After cracking of the matrix has occurred that portion of the stress previously carried by the matrix is transmitted to the fibres bridging the cracked zone. The subsequent behaviour of the composite will depend on whether the fibres can withstand the additional load, i.e.

$$\sigma_{fu} V_f > \sigma_{mt}(1 - V_f) .$$

If they can, the load is transferred back into the matrix over a transfer length (x') and the matrix will upon further loading be

broken down into a series of blocks of length between x' and 2 x' . This theoretical approach is described in reference (43). Various authors have theorised that the ultimate strength will be given by $\sigma_{fu}\ V_f$. Hannant, however, has shown that the ultimate strength will be less than this, because a portion of the fibres will have one end within a distance of $(\ell_c/2)$ of a crack and will therefore pull out instead of fracture. He gives the following equation for determining the ultimate failure stress;

$$\sigma_{ct} = \left[1 - \frac{\ell_c}{2\,\ell}\right] \sigma_{fu}\ V_f \quad .$$

For SFRC beams tested in flexure, the same condition will apply. Additionally, the fibres bridging a crack are not all subjected to the same stress as would be the case in a direct uniaxial tension test, the extreme fibres experiencing higher stresses than those within the specimen depth. This is demonstrated in Figure 4.10.

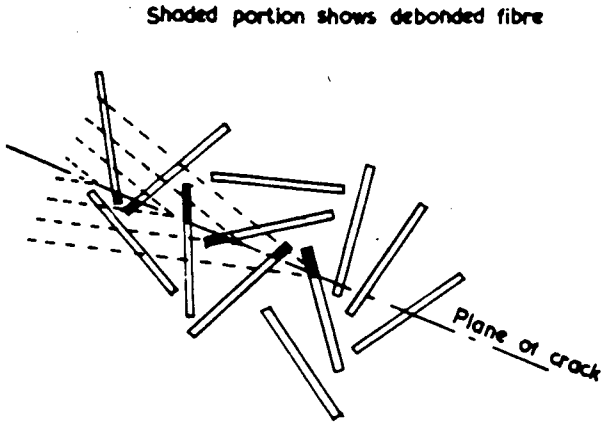

Figure 4.10 : Sketch showing the progressive debonding of fibres during which slow crack propagation occurs

4.2.6 Which factor counts most?

The answer to such a question would most probably be based along the following line of reasoning :

> "If I get a very strong fibre, make it long enough so that it yields rather than pulling out at failure (or shape the fibre cross-section such as to obtain the highest possible bond strength resulting in fibre-yielding) and place these fibres in the direction of maximum stress, then the resulting composite strength will improve substantially. Since the composite strength increases with increasing volume of fibres, the more fibres I put in, the stronger it will be".

Each of the reasons given to justify the choice of fibre length, shape, orientation or quantity is correct when viewed on its own. But, when all the factors are considered collectively, a rather narrower selective margin is defined. The following "discussion" refers extensively to Table 4.1, factors given therein being designated in parenthesis, e.g. fibre volume fraction is referred to as (B2).

The use of high strength fibres (A1) would be expected to have a substantial effect on the composite strength. Since the bond (B4) increases with increasing length and diameter of the fibre (B6), it follows that the longer the fibre, the greater the effect of the fibre on composite strength. Along this line of reasoning, it would appear desirable to have a sufficient fibre length (B5) so as to cause failure of the fibre (B9). In practice however, for fibres with an aspect ratio in excess of 100, there is a limit to the volume of fibres which can be added to the mix (A3), because beyond 2% (for some mixes even 1%) the fibres begin to bundle up resulting in non-uniform fibre distribution (B7) or inadequate workability of the concrete mix.

Assuming that a fibre of adequate strength (i.e. one which preferably yields gradually (A6) is chosen with particular dimensions, it must then be ascertained what volume needs to be added (B2) to bring about the required strengthening of the matrix.

Fortunately, the choice of steel fibres is facilitated by the use of guides and reports for specific applications, published by research institutions[60] or companies producing fibres. These reports discuss the type and volume of fibre, mix proportions, placing and curing conditions best suited for different applications. Most will comment upon the influence which the fibres exert on the composite material properties.

4.3 INFLUENCE OF STEEL FIBRES ON MECHANICAL PROPERTIES

4.3.1 Compression

The effect of steel fibres on the compressive strength of concrete is variable and it has been established that strength increases are generally less than 25% for concrete at a fibre volume (V_f) of 1.2 - 2%. Tests carried out on SFRC at different strain rates (one constant and one variable rate) however, yielded increases varying from 15% to 40% respectively[61]. Inexplicably there appears to be no increase in compressive strength for mortar mixes. A survey conducted by Johnston showed similar low findings, which illustrates that steel fibres should not be included in concrete purely to increase its compressive strength[61].

Research has shown however, that the addition of fibres to the concrete leads to a marked change in the stress-strain response of specimens subjected to compression. The volume and aspect ratio (ℓ/D) greatly influence the peak strain and descending portion of the stress-strain curve; as shown in Figure 4.11(a) and (b)[63]. A significant increase in ductility is imparted to the compression specimen, which is not apparent in plain concrete. This toughness in compression will help prevent sudden and explosive compressive failure, under static or dynamic loading.

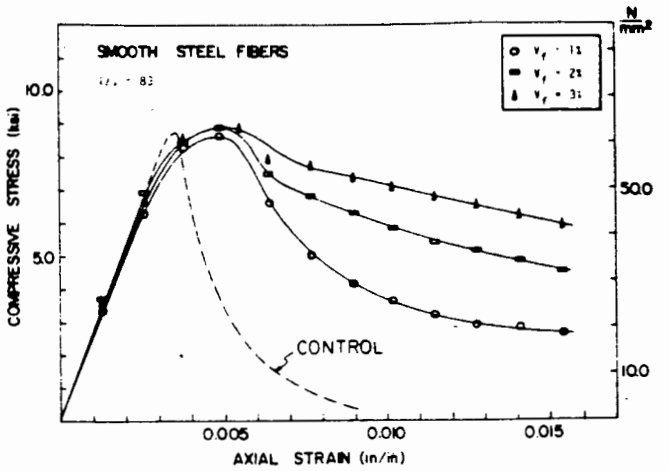

(a)

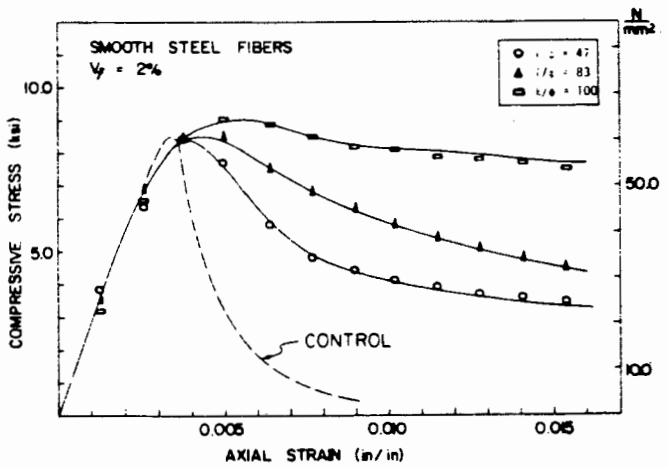

(b)

Figure 4.11 : Influence of the volume fraction V_f(a) and the aspect ratio ℓ/D of the fibres (b) on the compressive stress-strain curve

It should be noted that smaller test specimens (especially cylinders) tend to give different strengths for the same concrete, and steel fibres may exaggerate these differences. Additionally, since fibres tend to align in planes at right angles to the direction of vibration[64], these differences will be magnified when comparing cylinders and cubes. Because cubes are rotated 90 degrees before testing, the fibres will lie more parallel to the line of applied stress, compared to cylinders where the fibres lie more perpendicular to the applied force. This increase in lateral reinforcing will render the cylinders noticeably stronger. The size of the compression specimen should therefore be reported together with test results before comparisons with other experimental test data can be made.

4.3.2 Direct Tension

The stress-strain behaviour of a SFRC specimen subjected to uniaxial tension is shown in Figure 4.12 below[65]. The plot shows a sudden drop after an initial peak, signifying where failure of the matrix occurred. Thereafter a decreasing residual tension stress remains due to the frictional forces between the fibre and the matrix. The descending portion may also be attributed to successive fibre failure with corresponding drops in stress.

It has been confirmed that at fibre volumes up to 3% by volume, the maximum tensile strength increase is 30% and the maximum strengths rarely reach 5 MPa. Evaluation of results illustrated that the maximum tensile strength depends chiefly on the aspect ratio (ℓ/D) and the fibre volume (V_f). Because of the usually small volume of

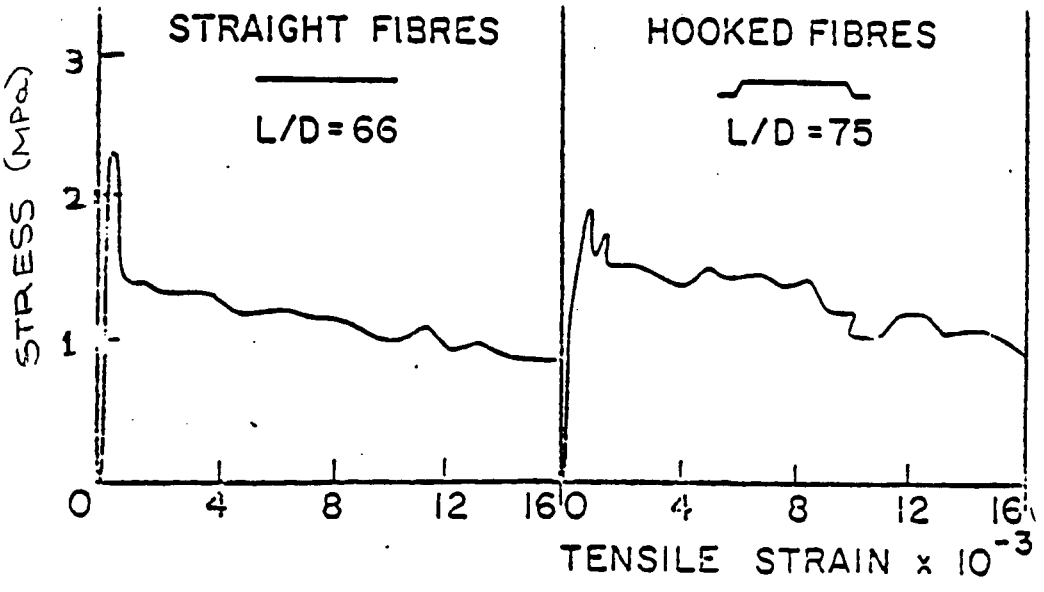

Figure 4.12 : Stress-strain curves for SFRC in tension (V_f = 1.73%)

fibres used, the resulting tensile strength increase is also small, and does not justify the additional fibre costs.

4.3.3 Flexure

The flexural (or bend) test has been used extensively to measure the strengths of SFR concretes. The simplicity of the test procedure makes it an ideal test whereby the results from different authors can be compared.

The test can be conducted in one of two standard ways (see Chapter 5);

(i) the Third-Point Loading Test, or

(ii) the Centre-Point Loading Test.

Each method has its advantages and disadvantages, although various arguments have been forwarded concerning the reliability of the centre-point loading test[66].

From the various surveys and extensive experimental work which has been conducted on SFRC beams, two important design parameters have emerged which have a major influence on the flexural strength; these are the fibre volume (V_f) and the aspect ratio (ℓ/D); an increase in either resulting in higher flexural strengths. Although section 4.2 exemplified the large number of factors which influence the strength of SFRC, there is general agreement between authors that the flexural strength increases evenly with the volume and aspect ratio of the fibres[67-69].

The addition of steel fibres to concrete unmistakeably delays the onset of flexural cracking of the concrete matrix; increases in cracking strength varying between 35% to 80% as the fibre volume varied between 1.25% to 2.50%[70]. Steel fibres up to about 4% by volume were found to increase the first-crack flexural strength of the composite up to 2½ times the strength of the unreinforced matrix[71], which seems to be in agreement with other reported results[72,73].

The greatest influence of the fibres though, is on the ultimate flexural strength. For fibre volumes of 1.25% to 2.50% the ultimate flexural strength may increase between 70% to 200%! Moduli of rupture (MOR) up to 10-15 MPa are possible although common values average around 7 MPa, compared to the flexural strength of 4 to 4.5 MPa for plain concrete. Extensive testing by Hughes and Fattuni, using a variety of fibre types and shapes, showed a maximum ultimate flexural strength increase of 98% for hocked and Duoform steel fibres[74]. Results obtained by Edgington support Hughes' findings

that the ultimate flexural strength increased significantly with increasing aspect ratio and fibre anchorage (in the form of surface deformation)[75]. Figure 4.13 shows the results obtained from Edgington for mortars and concretes reinforced with fibres of various (ℓ/D) ratios and wire strengths.

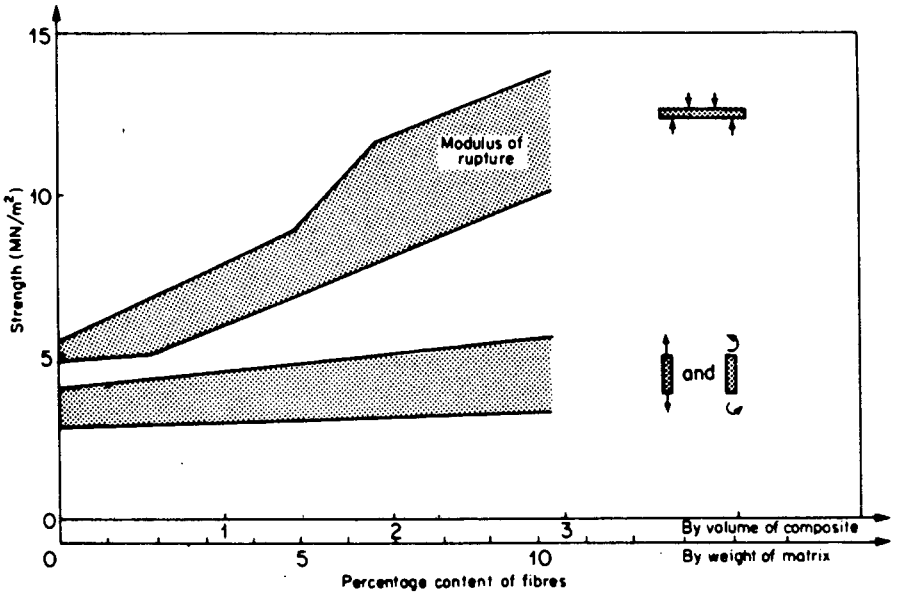

Figure 4.13 : Flexural, direct tensile and torsional strengths of SFRC

4.3.4 Toughness

If the load-deflection plots of two beamlets, one plain and one reinforced with fibre, are compared, two observations become apparent :

(i) the plot for the unreinforced beamlet will show a near vertical drop in load capacity almost immediately after cracking has occurred, i.e. ultimate flexural load has been reached;

(ii) the fibre reinforced specimen plot may have a higher ultimate strength and in most cases there is a gradual or erratic drop in load capacity after the peak load has been reached.

Figure 4.14 is a schematic representation showing how the plain concrete load-deflection plot differs from that of a steel fibre reinforced concrete specimen.

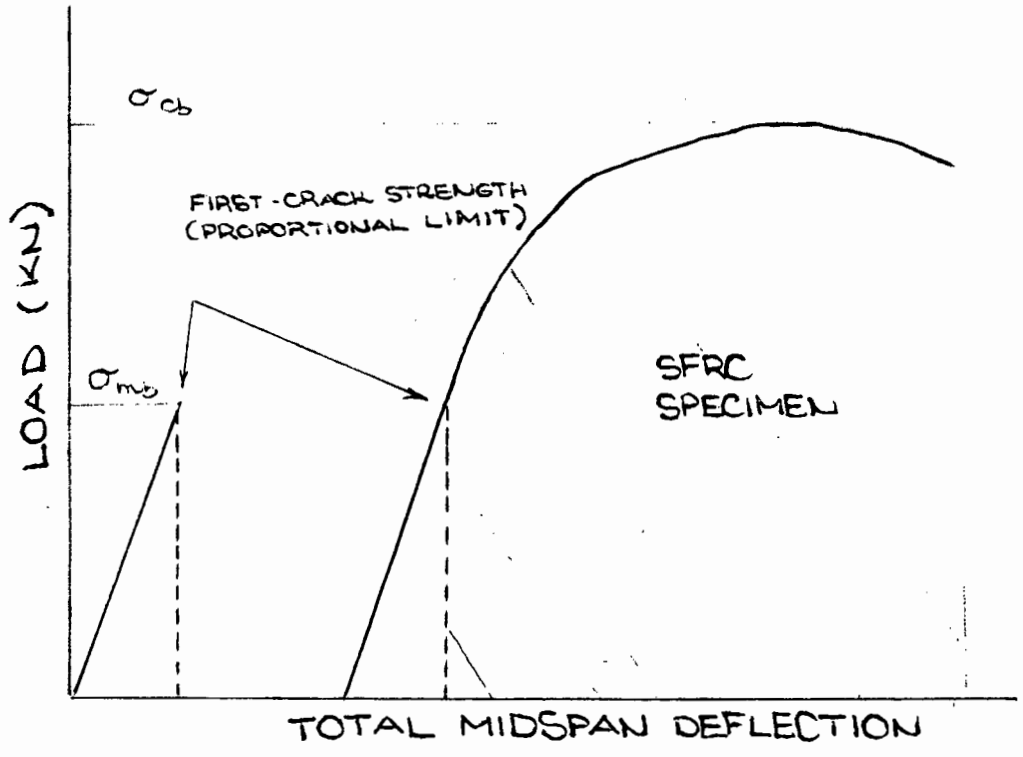

Figure 4.14 : Load-deflection curves for plain concrete and steel-fibre concrete

Greater energy is required to crack the SFRC beamlet and more importantly, to cause these cracks to widen until ultimate failure occurs. This energy absorption characteristic of SFRC over reinforced concrete is commonly referred to as toughness, post-cracking ductility or energy absorbing capability. Under static loading the toughness can be evaluated by calculating the area under the load-deflection curve up to a predicted deflection. In order for different mixes and fibres to be comparable, the Toughness Index

has been proposed[76];

$$\text{TOUGHNESS INDEX (TI)} = \frac{\text{AREA UNDER LOAD-DEFLECTION CURVE UP TO 1.9MM DEFLECTION}}{\text{AREA UNDER LOAD-DEFLECTION CURVE UP TO FIRST-CRACK}}$$

Shah and Rangan, and Blood were the first researchers to measure toughness, but unfortunately their index numerator incorporated the whole load-deflection curve[77]. Their indexes were thus very high and most probably encompassed situations where the crack(s) were unacceptably wide in terms of serviceability regulations. Various modifications to the Toughness Index are used today which take into account the serviceability static limits as regarding the degree of cracking and crack widths.

Extensive testing by Henager revealed total energy absorption ranges from 113 J to about 452 J (for total deflection of 1.9mm) while the energy to first crack centred around the 11 to 14 J. The Toughness Index thus varied between 12 and 45[78]. An increase of over 20 times in the toughness of concrete was reported by Hughes, using 0.64 x 59mm ordinary Duform fibres[79].

At present no documented correlation between the Index and the actual performance of SFRC in the field is available. This should be investigated enabling the Index to measure a meaningful property instead of a statistical comparison between plain and fibre concretes.

4.3.5 Dynamic Strength

The effect of steel fibres on the compressive, tensile, flexural and toughness properties of SFRC is that a considerable amount of energy

is required to cause failure. This improvement is most marked when a SFRC specimen is subjected to dynamic loading. The increased impact strength and the resistance to spalling and fragmentation of SFRC has attracted its use in pavements, airport runways, explosion shelters and structures in regions of earthquake activity.

Several methods for testing the impact resistance of a SFRC have been developed; such as the swinging pendulum, the falling ball, the Charpy and the Izod tests on beams to name a few. Improvements in impact resistance of 3-10 times and greater for SFRC compared to plain concrete have been reported. A series of tests carried out by Verhagen on most of the current impact test methods revealed however that no correlation between these tests was apparent[80]. Consideration of the variability of the impacting mass, velocity, size, support rigidity and even definition of failure between tests tends to support Verhagen's findings.

One impact test which appears to be used increasingly worldwide involves the use of a 10 pound hammer which is dropped from a set height onto a steel ball, which rests on a cylindrical SFRC specimen. For SFRC concretes the number of blows to failure may be several hundred, compared to the 30-50 blows required to fail plain concrete specimens[81]. This test is described in Chapter 5, section 5.4.5.

4.3.6 Creep

Since the volume of fibres which are incorporated in fibre-reinforced concrete is usually small, the creep behaviour is unlikely to be influenced by their presence. Compressive creep data

on tests performed by Edgington *et al* over a period of 12 months revealed no significant reductions of creep strains of the composite[82]. Unfortunately, this is the only data available on the effect of steel fibres on concrete creep.

4.3.7 Fatigue Strength

For a given type of fibre, significant increase in fatigue strength occurs with increasing volume of steel fibres. The mix proportions and fibre type will also affect the behaviour of SFRC under fatigue loading. Surveys of experimental data from various researchers using different concretes and conditions, revealed that a linear relationship between the relative strength rating and the number of load cycles to failure existed. The relative strength rating is defined as the ratio of the maximum fatigue stress applied to the matrix cracking strength. Previous authors used the cracking strength of SFRC as the denominator and since the first-crack strength of SFRC was usually higher than that of the unreinforced, plain matrix, the fatigue strengths of SFRC were mostly underrated.

Figure 4.15 contains flexural fatigue data (Landers and Bailey's) which has been rectified to remove this inconsistency.

The bottom line refers to the Portland Cement Association's (PCA) design curve for airport pavements. All the modified data is seen to lie above the PCA design curve, even for fully reversed loading. About half the points lie above the stress ratio of units, emphasizing the enhanced fatigue strength while the steel fibres impart on plain concrete.

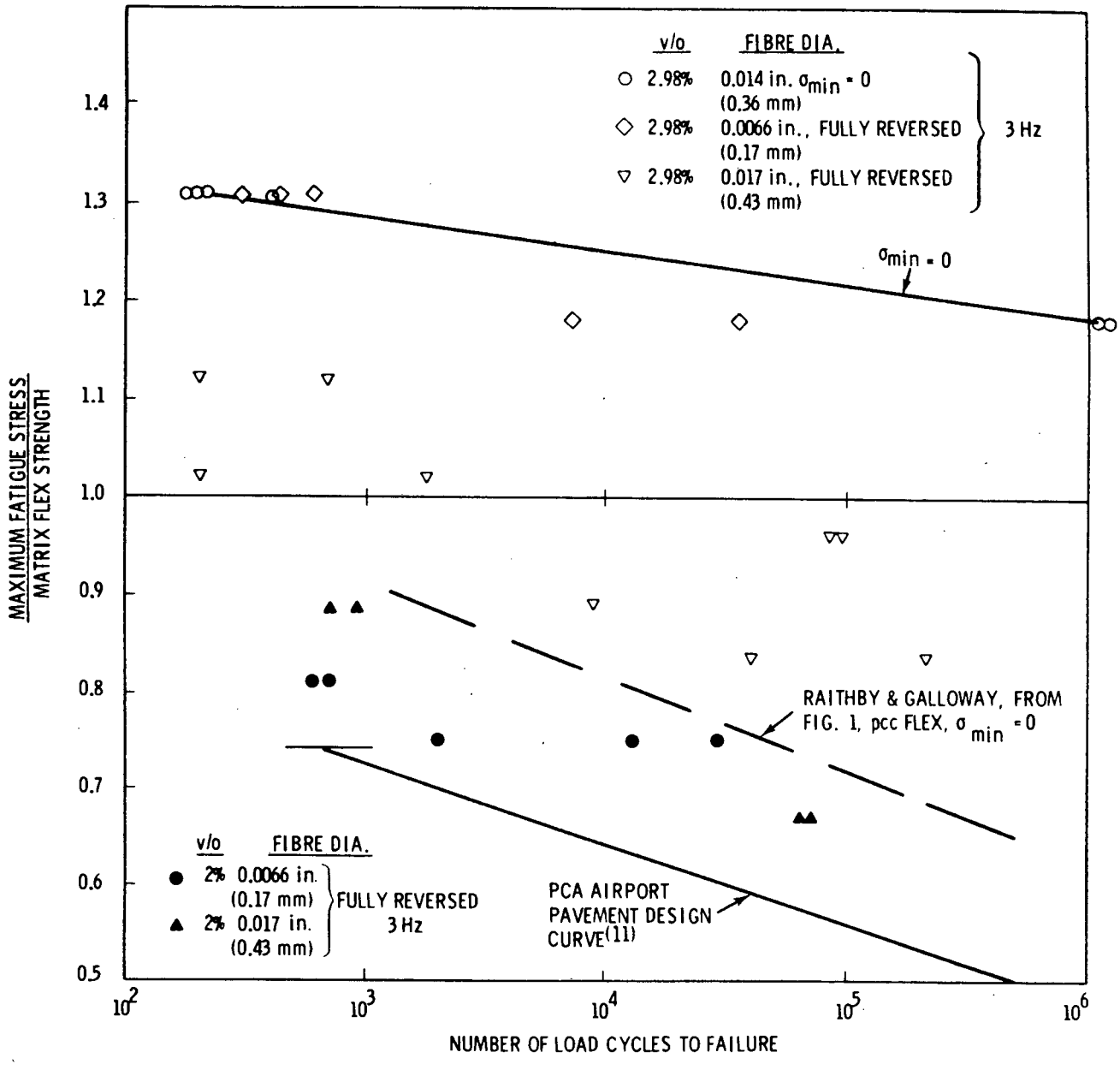

Figure 4.15 : Performance of SFRC subjected to cyclical flexural fatigue loading[83]

In general, a properly designed SFRC will sustain about 90% of the static strength at 2 x 10^6 cycles when non-reversed loading is used. When full-reversal of load is used, fatigue strength of about 70% of the static strength can be expected[84].

4.3.8 Durability

Before addition of the steel fibres to the concrete mix, their surfaces will have corroded slightly forming an insoluble oxide film. During the hardening phase of concrete made with OPC, the calcium silicate and tricalcium aluminate hydrate forming a highly alkaline material, i.e. of high pH. This will protect the fibre from additional corrosion, provided the film is not broken. This may occur, however, when the concrete cracks thereby exposing the fibres in the crack to atmospheric attack, or where carbonation lowers the pH of the concrete rendering the fibres open to attack if oxygen and moisture are present. Carbonation is a chemical process whereby Carbon Dioxide (CO_2) present in the atmosphere reacts, in the presence of moisture, with hydration products. This neutralizes the alkaline condition of concrete, the pH dropping from over 12 to about 8[85].

UNCRACKED CONCRETE - tests involving standard 152mm diameter x 300mm cylinders placed in environments of mild exposure, marine conditions and polluted industrial atmosphere showed :

(i) slight rusting of surface fibres after 7 months, and slight surface deteriorations, even after 57 months for the most corroded set of specimens;

(ii) small differences in carbonation depths between sites. Carbonation depth was less than 5mm after 5 years in dense concrete. Occasional rusting occurs at 6mm depth for those specimens subjected to marine environments[86].

Another study on cement mortar reinforced with 2% volume of steel fibres, showed insignificant corrosion by salt water, with no change

in flexural strength for specimens which had been repeatedly immersed and removed from saturated salt water for 90 days. In long term tests on SFRC at the Batelle Laboratories, Ohio, minimal fibre corrosion and no adverse effect on the flexural strength after 7 years exposure to de-icing salts was observed, corrosion of steel fibres occurring at or near the concrete surface only. Additional testing by the Batelle Development Corporation on the compressive strength of steel fibre reinforced mortar continuously immersed in seawater for 10 years, showed only a 15% loss in strength[87].

CRACKED CONCRETE - because of the toughness of SFRC under flexural loading, its applications will most likely involve situations where it is in the cracked condition. Unfortunately, these cracks enable carbonation to occur deeper within the matrix than would be possible in the uncracked state.

Hannant and Edgington conducted tests on cracked beams which had been subjected to marine environments for 11 months, and found greatly increased carbonation and fibre corrosion local to the crack when compared with uncracked beams. The depth of carbonation varied according to the crack width, with 45mm, 30mm and 15mm depths resulting from 0.4mm, 0.3mm and 0.1mm wide cracks respectively. Two types of fibre were used (0.25mm diameter x 25mm and 0.50mm diameter x 50mm) to investigate the effect of rusting on the strength of the composite. Although severe rusting had occurred after 11 months in those specimens with wider cracks, there was a general increase in load capacity! The authors attributed this behaviour to improved fibre-cement bond and autogeneous healing of the cracks[86].

It is well known that most failures in SFRC occur due to fibre pull-out, resulting in the fibres not being stressed to their ultimate strength. A slight degree of rusting should therefore have no adverse effect on the fibres and their strengthening of a concrete matrix. The results of Hannant and Edgington should be used carefully however, because increased and prolonged exposure to aggressive environments will eventually reduce the fibres' cross-sectional area such that the composite may exhibit brittle failure characteristics.

CHAPTER 5

EXPERIMENTAL PROGRAM

(EFFICIENCY AND PROVING PHASE)

5.1 GENERAL

Steel Fibre Reinforced Concrete has found widespread popularity and is used in numerous applications in Europe and America. In South Africa, SFRC is still in its infancy mostly due to the conservative attitudes prevailing in the building industry. Some encouraging work has been conducted on fibre-reinforced concrete at the University of Stellenbosch by Mr G Maritz. However, a major problem encountered during this research was that of firms discontinued the production of steel fibres due to the lack of demand. Indeed, one of the companies which was supplying the author with two different steel fibre types actually stopped production of the one type during the initial stage of the experimental programme.

5.2 OBJECTIVES OF THE STUDY

The first step of the programme was therefore to find out what types of steel fibres were available, whether produced locally or imported. Five different fibre types were obtained, the details of which are given in section 5.3. These fibres were then subjected to a series of tests to determine their influence on the mechanical properties of a concrete matrix. These tests formed the "Efficiency and Proving Phase" of the programme :

The galvanised mild steel fibres of aspect ratio 100 were produced by cutting up 50 kg spools of "Galvanised Process Wire" which was obtained from Consolidated Wire Industries, Cape Town Branch. The spools were cut into fibres at Allan's Meschco in Cape Town. This wire is commonly used as binding wire for fencing applications.

Plate 5.1 shows bundles of binding wire, ME430(35), ME430(25) wire and Shreddic fibres from left to right, with single fibres descending in the same order.

Plate 5.1 : The five steel fibre types tested

The results of tensile tests conducted on some Binding Wire fibres are given in Appendix B.1.

STEEL MESH - The wire mesh used as reinforcing in the Application Phase testing is commonly referred to as "gunite or swimming pool reinforcing". The wire diameter of 3.15mm was the same both ways, the spacing of the wires being 50 x 50mm. This spacing resulted in a cross-sectional area of 156mm^2 per metre length of mesh.

Tensile tests carried out on several small lengths cut from the mesh sheets yielded an average tensile strength of 500 MPa (see Appendix B.2 for test results).

CONCRETE - All specimens had the same concrete composition, the basic constituents being Ordinary Portland Cement (OPC), Klipheuwel well graded sand and crushed Malmesbury hornfels aggregate with a maximum size of 13mm. All the sand used was air-dried prior to mixing, by spreading a thin layer on concrete floors and allowing the sand to reach a consistent moisture content less than 1%. This facilitated quicker production of the required concrete workability.

The mix proportions cement:sand:stone by weight were 1:2.53:2.53 with a water/cement ratio of 0.52. The mix design was chosen so as to have a workable mix after fibre addition, the slump of the unreinforced mix being 90mm. The mix yielded a concrete strength of approximately 30 MPa after 7 days curing, after which all the specimens were tested. Table 5.2 gives the mix proportions per cubic metre and also the weight of fibres added for various fibre concentrations.

Table 5.2 : Mix design

STONE	937.30 kg
SAND	937.30 kg
CEMENT	370.67 kg
WATER	192.75 ℓ (kg)
FIBRE (% by volume)	
0.75%	54.86 kg
1.50%	109.71 kg
2.25%	164.57 kg

5.4 EFFICIENCY AND PROVING PHASE

Five separate groups of test specimens were tested, group A,B,C,D and E representing concrete reinforced with Shreddic, Wirand, ME430(25), ME430(25) and Binding Wire respectively. Within each fibre group, 3 sets of specimens were made and tested, the first set reinforced with 0.75%, the second set with 1.50% and the third set with 2.25% fibres by volume.

Generally, the shorter the steel fibre, the greater the quantity that can be mixed with and distributed throughout the concrete matrix. The addition of increasing concentrations of fibre to the mix would therefore serve a dual purpose;

(i) to determine the maximum degree of reinforcement (as a function of the length or aspect ratio of the fibres) which could be added to the mix, the limiting volume fraction

being that where workability problems due to fibre-balling occurred;

(ii) to examine the effect of different fibre shapes, aspect ratios and fibre concentrations on composite strength.

The standard Modulus of Rupture (MOR) test was performed on each set of specimens. This test was chosen because of the simplicity of the test setup and ease of operation. More importantly, the results obtained could then be compared with other documented research results, many of which haved used the MOR test. Shear strength tests were then conducted, utilising the fractured prisms from the flexure testing.

A flow chart of the efficiency and proving phase tests is shown in Figure 5.1.

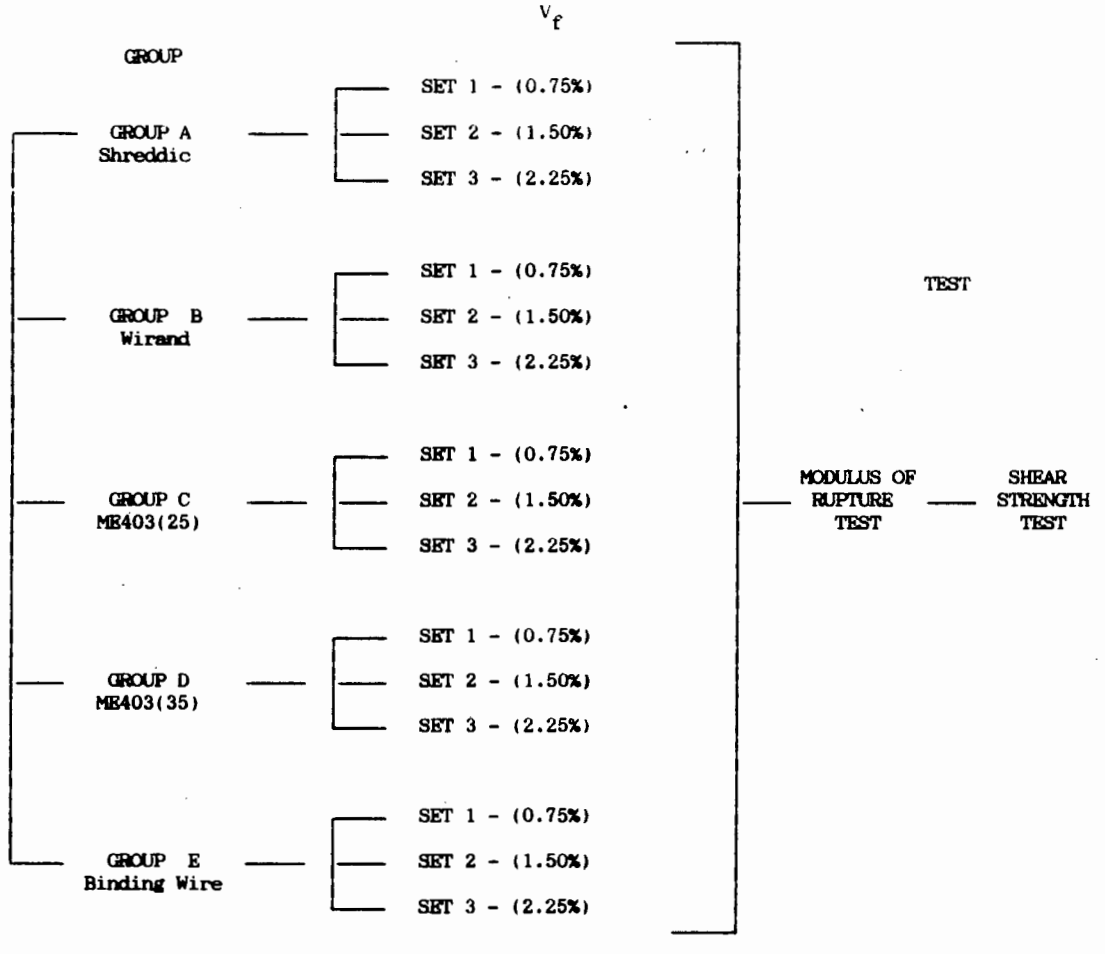

Figure 5.1 : Flow chart of the experimental programme

5.4.1 Flexural Strength Testing

APPARATUS - A 'Denison' Universal Testing Machine with a load capacity of 500 kN was used to determine the flexural strength of the five different groups of fibre-concrete, using a simple beam with third-point loading (Plate 5.2).

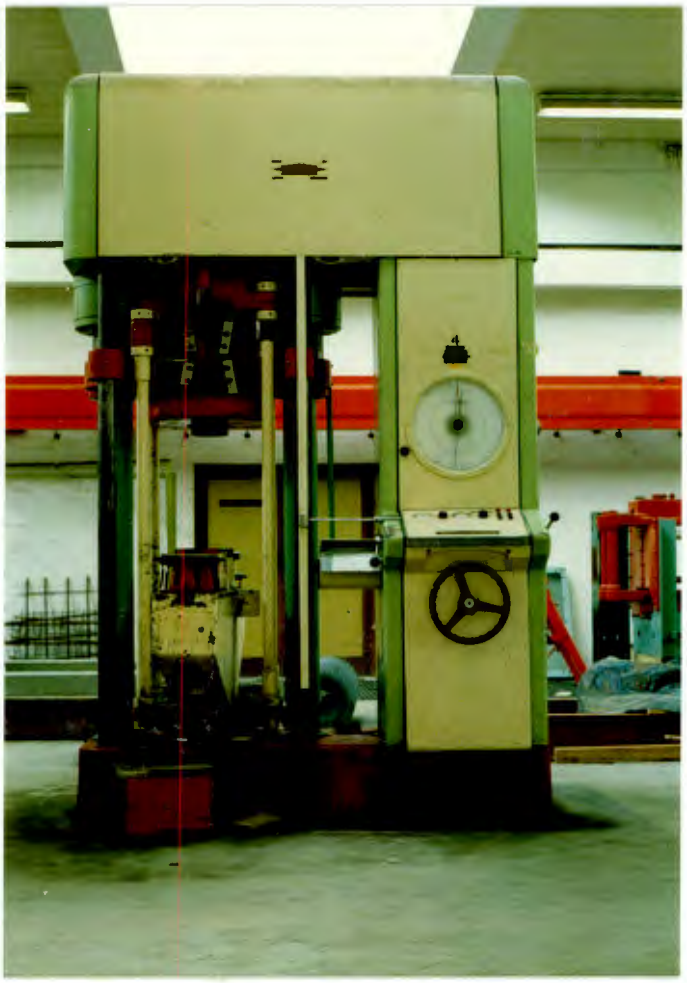

Plate 5.2 : The 'Denison' Universal Testing Machine as viewed from the front

SPECIMEN PREPARATION - The volume of concrete mixed for each set of specimens was chosen so as to make nine 100mm wide x 60mm deep x 500mm prisms and eighteen 100 x 100 x 100mm cubes.

The stone, sand and cement were first placed in a pan mixer and dry mixed for roughly 1 minute. The required water was then slowly added and mixing continued for about 3 minutes. The slump of the fresh mix was measured and adjustments made, if required. Mixing was continued for 1 minute, then stopped and three 100 x 60 x 500mm prisms and nine 100 x 100 x 100mm cubes cast, the test specimens being compacted on a vibrating table. While the cubes and prisms were cast, the mix in the pan mixer was reworked once or twice with a trowel to prevent segregation. A precalculated mass of the plain concrete mixture was weighed off in a steel bucket, covered with plastic sheeting to prevent any moisture loss and set aside.

The mixer was restarted and a selected mass of steel fibre slowly added to the remaining mix by manually shaking handfuls of fibres into the pan. Protective leather gloves of the type worn in welding workshops were used to handle the fibres, because of the ease with which the thinner fibres pierced any exposed skin. The fibre addition period varied between 4-6 minutes, depending on the volume percentage of fibres added. The next three prisms were cast, the 60mm depth being made up of two layers. Each layer was firmly compacted with a tamper having a 98mm x 98mm bottom plate. The purpose of this was to force the fibres in the matrix to assume a predominantly horizontal orientation.

The three remaining prisms were then cast. The fibre mix was used to make up the bottom 30mm of the prism depth and the plain concrete which had been set aside in the bucket was used to top up the prisms

to the required 60mm depth. The concrete in the bucket was remixed with a trowel to eliminate any segregation which had occurred, prior to being added to the prism moulds. Nine fibre concrete cubes were cast thereafter. The surfaces of the prisms and cubes were finished with a trowel during vibration.

The reason for making nine prisms per set were as follows :

- the three plain prisms would provide a control, i.e. plain unreinforced concrete strength;
- the three partially reinforced prisms and the three fully reinforced prisms would show whether partial reinforcing would impart the same strength to a concrete matrix as full reinforcing.

Immediately after finishing, the specimens were placed under a polyethylene sheet at room temperature for 24 hours. They were then demoulded, labelled with a water resistant ink and transferred to a water storage tank to cure until tested. The water in the tank was maintained at a temperature of 22°C.

FLEXURAL TESTING PROCEDURE - The prisms and cubes were removed from the tank 7 days after casting and painted with white distemper paint. This aided the visual inspection of the prisms for cracking during flexural loading. (The use of PVA or Micatex paint is advised against because of the elastic nature of the dried paint.) The paint was allowed to dry sufficiently, care being taken not to place the prisms in areas of draft. The prisms were then centred on the support bearings which had been set 400mm apart. The head of the testing machine was lowered slowly until the load bearings were

in contact with the prism surface at the third points between the supports. Plate 5.3 shows the test set-up of a prism loaded to failure.

Plate 5.3 : Prism undergoing third-point loading

Once contact was reached, the load was applied at a constant rate of 1 kN/min. The prism was constantly inspected until the first crack became visible. In most cases the applied load indicator would flicker slightly, sometimes even drop by 0.1 - 0.2 kN when cracking occurred. Loading would continue at the same rate until the ultimate load was reached.

CALCULATIONS - Where the fracture initiated within the middle third of the span length, the flexural strength was calculated as follows :

$$\sigma_{cb.c}\ ,\ \sigma_{cb.u} = \frac{P\,\ell}{b\,d^2}$$

where $\sigma_{cb.c}\ ,\ \sigma_{cb.u}$ = cracking, ultimate flexural strength (MPa)

P = applied load as indicated by machine in N , for the relevant strength

ℓ = span length (400mm)

b = average width of specimen (100mm)

d = average depth of specimen (60mm) .

If the fracture occurred outside the middle third of the span by not more than 5% of the span length the MOR was calculated as

$$\sigma_{cb.c}\ ,\ \sigma_{cb.u} = \frac{3\,P\,a}{b\,d^2}$$

where a = average distance between line of fracture and the nearest support (mm) .

For fractures occurring beyond this point, the result was disregarded.

5.4.2 Shear Strength Testing

APPARATUS - The same Denison Universal Testing machine as was used for flexure was used in the shear testing, although different support and loading devices were required.

The load-bearing rig in which the shear sample was fastened is shown in Plate 5.4.

The base of the rig was produced by welding two 100 x 50mm channel sections 160mm apart. A thick steel plate was welded onto the rear

Plate 5.4 : Shear testing rig

section of the channels. Four 16mm diameter bolts passed through the 4 corners of the welded plate, the bolt ends being welded to the plate itself for rigidity. The shear specimen was placed as shown in Plate 5.4, and a thick plate was then bolted down onto the specimen. For increased rigidity a 50 x 50 x 8mm angle section was placed on top of the uppermost plate, closest to the applied load before the bolts were tightened. The load was applied vertically by a steel section which fastened onto the head of the testing machine. Plate 5.5 shows the shear testing set-up.

The working drawings of the shear specimen support rig are given in Appendices C.

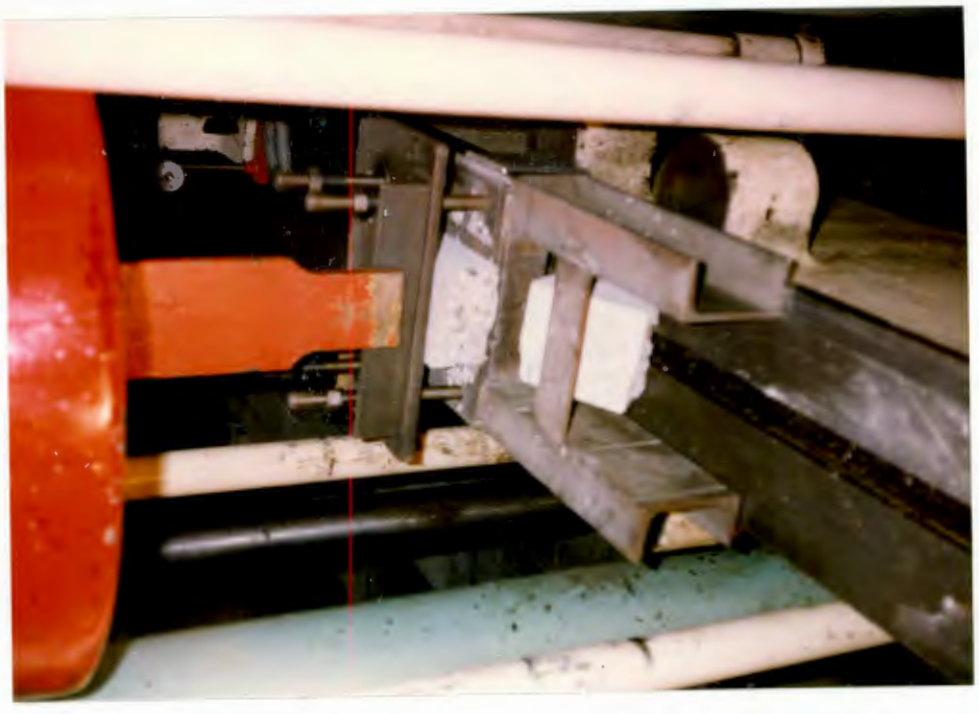

Plate 5.5 : Specimen failed under shear loading

SPECIMEN PREPARATION AND CURING - Fortunately the specimens used in the shear test were the same concrete prisms which had just undergone flexural strength testing. After the prisms had reached their ultimate load capacity, they were quickly loaded and strained until the prism broke into two halves, i.e. of the 9 prisms tested in flexure, eighteen samples became available for the shear strength tests. The shear test was performed immediately after flexural testing had been completed.

TESTING PROCEDURE - The prism specimen was so placed on the support rig that the section of the prism outside the middle-third of the span for flexural loading was protruding from the support plates. This ensured that the end-third of the span, which had not been subjected to the same failure stresses as the middle-third span, was used in the shear test.

A 100mm long, 16mm diameter half-round rod was placed 10mm from the support face of the rig, across the width of the specimen. A steel ballbearing was then placed on the centre of the rod, in the middle of the prism. The loading plate was then slowly lowered until it was in contact with the ballbearing. Loading proceeded at a rate of 4 kN/minute until shear failure occured.

CALCULATIONS - If the shear failure occurred at either the support face, the loading point or along the 10mm space between the two, the shear strength was determined as :

$$\sigma_s = \frac{V}{w.d}$$

where σ_s = shear strength (MPa)

V = maximum applied shear load (N)

w = width of test specimen (100mm)

d = test specimen depth (60mm) .

For those tests where the prism cracked behind the support face, the result was disregarded.

5.4.3 Cube Compression Tests

APPARATUS - The 100 x 100 x 100mm cubes were tested in compression with an "Amsler" Compression Testing Machine of 3000 kN load capacity. The loading range of 600 kN was used for testing. Plate 5.6 shows a front view of the machine.

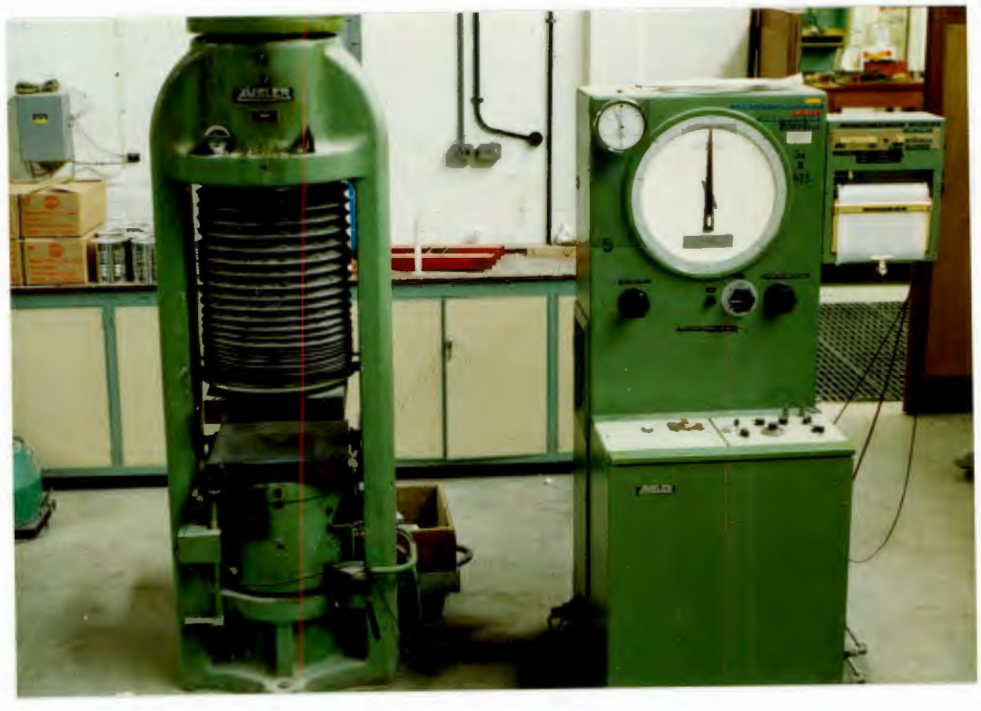

Plate 5.6 : Amsler compression testing machine

TESTING PROCEDURE - Three days after being cast with the flexural prisms, plain concrete cubes 1-3 and fibre concrete cubes 1-3 were removed from the curing tank. They were then loaded in compression at a rate of 150 kN/minute (i.e. 15MPa/min) until failure occurred. The same procedure was followed with plain and fibre concrete cubes 4-6 and 7-9 after 7 days and 14 days respectively.

As with conventional concrete, SFRC exhibits a gain of strength with time. The aim of the cube tests was to observe the effect of the fibres on the compressive strength of concrete with increasing curing periods, and how this effect varied with increasing concentrations of fibre.

CALCULATIONS - The compressive strength of the 100 x 100 x 100mm cube was simply calculated as follows :

$$f_{cu}\ ,\ f_{cf} = \frac{P}{\ell . w}$$

where f_{cu} , f_{cf} = compressive strength of plain-cube, fibre-concrete cube (MPa)

P = maximum applied load as indicated by machine (N)

ℓ = length of cube (100mm)

w = width of cube (100mm) .

5.4.4 Evaluation of Test Results

The Law of Mixtures theory (Chapter 3, section 3.3) was applied to the flexural strength results in order to determine the average and maximum bond strengths. Thereafter an ultimate flexural strength analysis based on conventional reinforced concrete beam theory (with the steel fibres taking the place of the normal reinforcing) was carried out to determine the volume of steel fibres required to impart the same strength to a concrete slab as a 50 x 50mm spaced, 3.15mm diameter wire mesh. The calculations gave a value of 1.24% fibre by volume, so a rounded value of 1.25% was chosen.

The flexure and shear strength tests were then repeated on prisms reinforced with 1.25% and 1.50% binding wire fibres by volume. The central deflection of the prisms under loading was recorded with dial gauges (20mm deflection capacity). The load vs deflection plots obtained enabled the toughness of the fibre-concrete to be determined.

The next phase of the test program involved impact tests on fibre and mesh reinforced arches and slabs. It was therefore deemed

essential to subject the different fibre-concretes to some form of impact test, before a fibre type selection was made based purely on the flexural and shear strength results. The American Concrete Institute (ACI) Impact Test was decided on.

5.4.5 ACI Impact Test

APPARATUS - Examination of Plate 5.7 will facilitate the description of the testing apparatus.

Plate 5.7 : Equipment used for the ACI Impact Test

The equipment for the test consists of :

- a standard, manually operated 10 pound hammer with an 457mm (18 inch) drop (shown on left)
- a 62mm diameter steel ball (shown top right) and
- a flat rectangular baseplate on which four positioning lugs are welded, with a positioning bracket bolted onto two of the opposing lugs, as shown in the bottom right of Plate 5.8. Appendix D contains the working drawings of the test equipment, showing the positioning bracket bolted in place.

SPECIMEN PREPARATION - 63.5mm (2½ inch) thick by 152mm (6 inch) diameter concrete samples were required for the test. Their preparation is outlined below.

Cement, sand, stone and water were weighed off in sufficient quantities to cast four 152mm diameter by 305mm cylinders and six 100 x 100 x 100mm cubes. Once the required workability of the fresh mix had been reached, three cubes were cast in two layers and compacted on a vibrating table. Two cylinders were then cast in two layers, each layer being compacted by 25 strokes with a tamping rod (the same rod as used in a slump test). The cylinders were then vibrated briefly on the vibrating table, the surfaces being finished off during vibration.

Next the preweighed 1.25% fibres by volume were slowly added to the remaining mix in the pan, the process taking about 4-5 minutes. Three cubes were cast, in three layers with each layer being compacted with the tamping rod prior to vibrating. Two cylinders

were then cast, each in 10 layers with each layer being compacted with the abovementioned rod. The surface of the cubes and cylinders were finished with a trowel during vibration. The casting of the cylinders in 10 layers was chosen to see whether some sort of parallel could be drawn between the ACI Impact Test and the impact tests conducted on the slabs later on in the programme. Since the bottom 30mm half of the slabs were to be fibre reinforced, by casting the 305mm deep cylinders in 10 layers the fibres in both specimens would be forced into a predominantly horizontal, 2-directional orientation.

The cubes and cylinders were cured in the same manner as the flexural specimens. Seven days after casting, the cylinders were cut with a diamond saw into 63.5mm deep cylinders. Because of the high slump of the mix (90mm), segregation sometimes occurred in the uppermost region of the plain concrete cylinders. Even the top few millimetres of the fibre-reinforced concrete cyclinders consisted mainly of mortar due to the compaction with the rod. The top and bottom 20mm of each cylinder was therefore cut off and discarded, three 63.5mm cylinders being cut from the remaining length.

TESTING PROCEDURE - The thickness at the centre and at each edge of the specimens was measured prior to placing it on the base-plate within the four positioning lugs. The positioning bracket was then bolted into place and the steel ball placed on top of the specimen within the bracket. The drop hammer was placed with its base resting on the steel ball, and thereafter raised and dropped repeatedly on the ball. A small cone drilled on the base of the

hammer in contact with the steel ball effectively prevented the hammer from bouncing off the ball during the test. The number of blows required to cause the first visible crack on the top of the specimen and thereafter, to open the cracks sufficiently so that the fractured specimen pieces touched 3 of the 4 positioning lugs was recorded. The latter case is regarded as ultimate failure.

Plate 5.8 : ACI Impact Test in progress

Plate 5.8 shows the Impact Test in progress, and Plate 5.9 shows how the ultimate failure differs between the plain control specimens and those fibre-reinforced. Note the actual crushing of the matrix beneath the ball for the fibre-reinforced specimens.

Plate 5.9 : 1.25% Wirand fibre-reinforced specimens on left and plain concrete control specimens on right tested to ultimate failure

CALCULATIONS - Unlike the flexure and shear tests, the ACI Impact Test does not involve any calculations. The function of the test is to give comparative values between the different materials tested, both for the number of blows to cause cracking and to cause "ultimate failure".

Again, the binding wires excelled over the other fibre types. The flexure, shear and impact tests therefore conclusively proved the superiority of the binding wire fibres as a means of strengthening a concrete matrix.

Table 5.1 : Properties of steel fibres

Description	(1) Shreddic	(3) Wirand	(2) ME403(25)	(2) ME403(35)	(2) Binding-wire
x-sectional shape					
Dimensions (diam. x length)	0.25 x 10	0.30 x 25	* 0.4 x 25	* 0.5 x 35	0.71 x 71
Aspect ratio (ℓ/D)	40	83-1/3	62-1/2	70	100
Tensile strength (MPa)	2150	2186	340	340	489

1. Produced in South Africa 2. Imported 3. Local production discontinued

* = Equivalent diameter D = Diameter

CHAPTER 6

EXPERIMENTAL PROGRAM

(APPLICATION PHASE)

6.1 GENERAL

The series of tests conducted on the five different groups of fibre-reinforced concrete under the Efficiency and Proving Phase of the test program proved beyond doubt the marked improvement in the material properties of concrete reinforced with 0.71mm diameter x 71mm long binding-wire fibres. All the results obtained were evaluated on a comparative basis with plain unreinforced concrete where possible. The aim of the Application Phase therefore was to investigate the effectiveness of fibre-reinforced concrete in thin plate and shell construction relative to conventional mesh-reinforced concrete.

Two different specimen shapes were tested, slabs and arches. Partially fibre-reinforced slabs were subjected to static and impact loading, identical tests being performed on mesh-reinforced slabs. The tests were then repeated on fibre-reinforced and mesh-reinforced arches respectively. The purpose behind testing the two different shapes lay in their envisaged applications; the slabs could represent walls and the arches a form of light, industrial roofing material.

6.2 SLAB TESTS

A slab size of 2.1m x 2.1m x 0.06m was decided on as a typical wall dimension of a room in a small dwelling. The slabs were cast horizontally on a large wooden shutter, with 60 x 60mm angle rolled steel sections forming the side shutters. The wooden base was pre-treated with shutter oil for about 5 days to ensure that it was thoroughly watertight. The steel side shutters were oiled before being bolted onto the wooden base. The small gaps between the side shutters, where they met perpendicularly at the corners, were filled in with plasticine.

6.2.1 Slab Preparation

In all, twelve slabs were cast. Table 6.1 outlines the reinforcing and testing sequence.

Table 6.1 : Details of slab test panels

Slab No.	Type of Reinforcement		Type of Test
1 - 3	Mesh		Static
4 - 6		Fibre	Static
7 - 9	Mesh		Impact
10 - 12		Fibre	Impact

MESH-REINFORCED SLAB - Once the wooden base and steel side shutters had been oiled and all gaps filled with plasticine, a

2 x 2m sheet of galvanised mesh was placed within the 2.1 x 2.1m area enclosed by the steel side shutters. Twelve millimetre high concrete spacers were placed beneath the mesh at various intervals so as to position the latter at three quarters of the slab depth beneath the slab surface. The slab was then cast in three batches, the mix quantities by weight per batch being :

Water = 19.83 ℓ kg
Cement = 38.14 kg
} $\frac{w}{c}$ Ratio = 0.52

Sand 96.45 kg

Stone 96.45 kg .

The constituents were mixed as usual in a tilting drum mixer. Once the required slump had been attained, the fresh concrete was discharged into two pre-moistened wheelbarrows. Six 100 x 100 x 100mm cubes were cast in 2 layers, each layer being rodded 25 times. The cubes were then compacted briefly on a vibrating table while their surfaces were finished with a trowel. The mix in the wheelbarrows was quickly reworked with a spade, and dumped into the mould. A shovel was used to spread and compact the fresh concrete.

The same procedure was followed for batches 2 and 3, i.e. in all 18 cubes were cast at six per batch. Once the mould had been completely filled with concrete, the latter was quickly but evenly compacted with an internal poker vibrator. A heavy steel roller was then used to remove any concrete in excess of the 60mm depth. The roller, resting on the 60mm high angle-iron side shutters, was passed back and forth, striking off any excess material. The surface of the slab was finally finished with a trowel.

FIBRE-REINFORCED SLAB - The fibre-reinforced slabs were cast in 4 batches, the first two batches consisting of fibre-reinforced concrete and the last two of unreinforced, plain concrete. Mix quantities by weight per batch were :

Water = 15.08 ℓ kg
Cement = 29.01 kg
} $\frac{W}{C}$ Ratio = 0.52

Sand 73.34 kg

Stone 73.34 kg .

The first batch was mixed in the same manner as for the mesh-reinforced slab. Once the six cubes had been cast, the drum mixer was restarted and 6.788 kg of 0.71mm diameter x 71mm long Binding Wire fibre (equivalent to 1.25% V_f) was manually added by shaking handfuls into the mixer. This process took between 6-9 minutes; a quicker rate caused the fibres to pile up on each other with resulting fibre balls in the mix. However where the addition of fibres took more than 9 minutes, overmixing and drying out of the mix usually caused the same problem. The SFRC was then discharged into pre-wetted wheelbarrows and dumped into the mould. A shovel was required to manually spread the fibre-concrete. Once the fibre mix from batch no. 2 had been evenly spread, the same tamper (used to compact the flexural strength specimens in Chapter 5) was used to compact the fibre mix evenly. Conventional internal vibration with the poker vibrator proved difficult because of the stiffness of the mix and the thin slab depth. The poker would leave deep furrows which were difficult to fill in. The slab was therefore vibrated by lying the shovel face flat on the mix surface, pressing the poker hard onto the shovel surface and slowly pulling the shovel around the whole slab. This worked very well, with no segregation being observed.

The depth of the SFRC was regulated at approximately 30mm by a simple device as shown in Plate 6.1. The device is held along the top bar as shown, and the bottom sharpened end is then pushed firmly into the mix, perpendicular to the mix surface. The device is rotated clockwise and anti-clockwise about the central rod axis until the point makes contact with the mould base. The marker plate welded 30mm above the tip indicates the depth of the mix in that area, whether more concrete is required or whether an excess exists requiring removal.

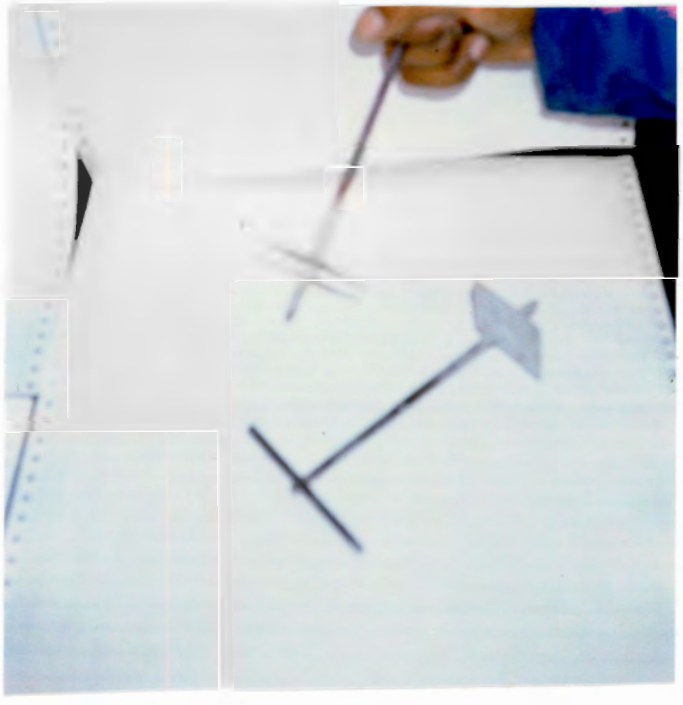

Plate 6.1 : Fibre-mix depth measuring device

Once the depth of the slab had been checked, the rod holes were closed by lightly vibrating the surrounding area with the poker tip. While the SFRC was compacted, etc., the drum mixer was thoroughly cleared of all remaining fibres. Batch 3 was then mixed, the 6

cubes cast and the remaining mix spread evenly over the compacted 30mm deep fibre mix. Batch 4 followed the same procedure, and was used to bring the slab to the required depth. The top plain concrete layer was compacted and then vibrated by immersing the poker horizontally. The poker was slowly moved about the slab to compact all the concrete evenly, but with sufficient speed to prevent it from sinking through the highly workable top layer into the SFRC layer underneath. The steel roller was then used to strike off any excess concrete, and the surface thereafter finished with a trowel.

6.2.2 Slab Curing

After the surface had been finished, the slab was cured under sheets of black, impermeable polyethylene. The cubes were placed under a polyethylene sheet at room temperature for 24 hours. They were thereafter demoulded, labelled and numbers 1-3 per batch placed in a water curing tank and numbers 4-6 per batch placed under the polyethylene sheets of the slab and allowed to cure with the latter.

A rough calculation using elastic analysis showed that the slab could support its own weight after 2 days. As an extra safety precaution, the steel side shutters were stripped off and the slab carefully and slowly lifted up and moved only after 3 days. The slab was lowered onto an empty space on the laboratory concrete floor (which had been thoroughly pre-wetted to prevent moisture absorption) and together with the cubes immediately covered up again and allowed to continue curing. The mould was subsequently cleaned, oiled, and prepared for the next cast.

6.2.3 Static Testing

All testing was done 7 days after casting. The cubes 1-3 from the curing tank and the cubes 4-6 curing with the slab were first tested in compression with the Amsler Machine, at a loading rate of 150 kN/minute (15 MPa/minute). From the results, the strength variation between batches and between the water cured and slab cured cubes could be observed. The slab was then carefully lifted and moved to the test bed. The slab support system consisted of three 127 x 76mm taper flange I-beams, placed perpendicular to each other (resting on large concrete blocks). A 30mm wide by 5mm thick rubber strip was placed on the top flange of each beam to protect the slab from damage. The slab was carefully lowered onto this set-up, so that the slab ends were flush with the flange ends as shown by the sketch in Figure 6.1. The slab was thus simply supported on three sides, with one free edge.

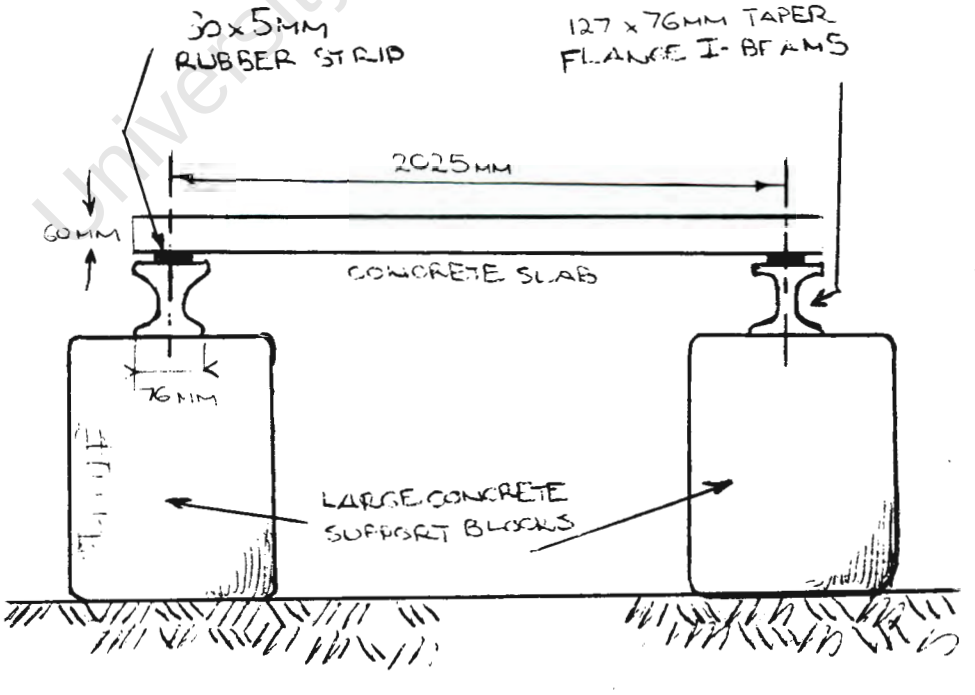

Figure 6.1 : Front view of the simply supported slab as viewed from the free edge

The slabs were loaded in the centre with a 200 kN Amsler jack. The loading rate was controlled via a Wolpert Dynamometer (Plate 6.2). A scale of 200 kN with increments of 0.2 kN per division was used. The load was spread via a load spreader over four points at 380mm centres in the direction of simple support to free edge and 330mm centres in the direction of simple support to simple support. A 80 x 80mm by 5mm thick rubber pad was placed on the slab at each point to prevent the load spreader from locally crushing the concrete.

Two 50mm deflection dial gauges were placed 100mm on either side of the slab centre, along the centre line running from the simply supported to the free edge. The deflection gauges were fixed onto a steel bar, which in turn was supported by stands at the free edge and at the opposite simply supported edge respectively. A third 50mm deflection dial gauge was used to measure the deflection at the free edge.

The 200 kN jack was screwed down until the swivel head of the jack made complete contact with the load spreader. The Amsler-Wolpert test rig was then switched on, and the hydraulically operated jack slowly lowered until the dynamometer showed the slightest loading. This signified that the rubber pads underneath the load spreader and the rubber strips beneath the slab had been adequately compressed to remove any "give" . The dial guage readings were now recorded as at zero load. Plate 6.3 shows the test set-up of a slab about to be statically loaded.

Plate 6.2 : Amsler jack and Wolpert dynamometer

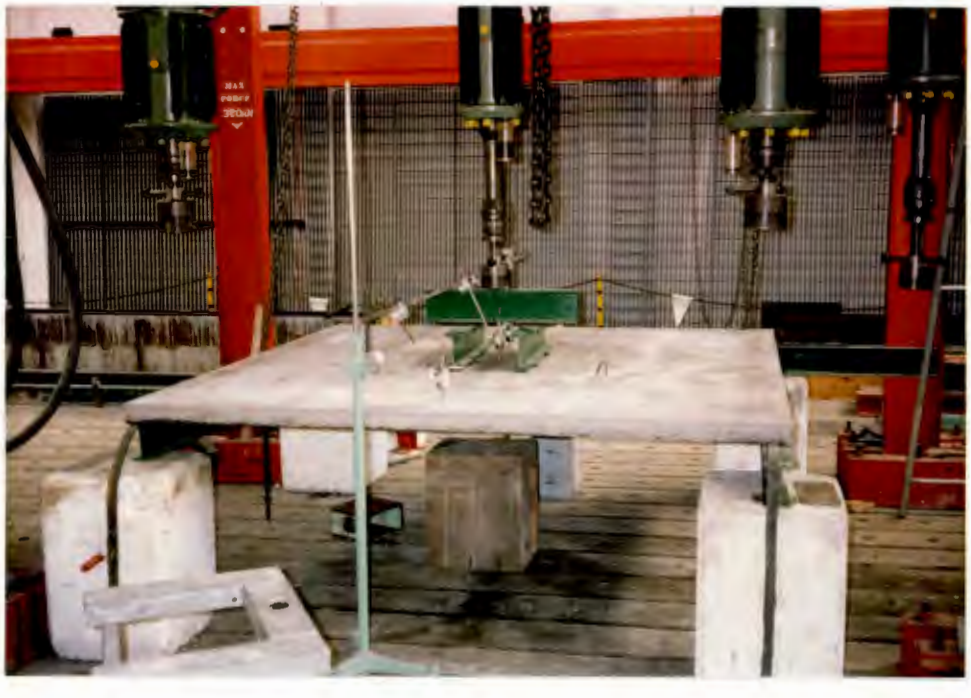

Plate 6.3 : Slab ready for static loading

Initially the slab was loaded in increments of 1 kN, the dial gauges being read between increases. Up to the load at which cracking of the slab occurred, the load could by hydraulically "locked", i.e. held steady while the dial gauges were read. The onset of cracking was detected by the inability to maintain a constant loading with the jack, because of the gradual downward deflection of the cracked section. Thereafter loading was continued in increments of 2 kN. As each increment was completed the dial gauges were read quickly. The total deflection at ultimate load was difficult to record accurately because of the rapid deflection associated with that load. Once the ultimate load capacity of the slab had been exceeded, the load was removed, the jack and load spreader moved aside and the slab removed.

6.2.4 Impact Testing

The same support system as used for the statically loaded slab tests was utilised. Unlike the static loading rate of the previous tests, slabs 7-12 were loaded dynamically, in the form of impacts. This was achieved by dropping weights from various heights.

The weight consisted of a nylon bag filled with dry sand, on top of which three 400 kN weights were fixed, to give a total mass of 160.7 kg. The contact area of the weighted nylon bag was 330 x 380 mm. (It is pointed out that the four load application points in the statically loaded slabs also enclosed an area of 330 x 380mm; these points were actually chosen to parallel the loading area of the impact tests.) A mild steel wire was used to fix the sandbag system

to a crane hook. The overhead crane was then manipulated to centre the bag over the marked loading area. The bag was then raised to reach a 100mm gap between the underside of the bag and the slab surface. The initial slab position, and subsequent deflections was monitored using the simple apparatus shown in Plate 6.4. The maximum (elastic) deflection on impact was measured by a telescoping radio antenna, while the permanent (plastic) deformation was measured with a movable pointer. Both gauges were fixed to a stand, which was placed underneath the centre of the slab.

Plate 6.4 : Impact deflection measuring apparatus; the movable pointer is on the right, the radio antenna at top left

Plate 6.5 : Wooden strip (200mm) used to obtain the required drop height

The antenna was extended until it touched the underside of the slab, the length of the movable part being recorded as at zero loading. The movable pointer was screwed up until the pointer tip made contact with the underside of the slab, and the height of the rod recorded. The weighted bag was subsequently dropped onto the slab by cutting the mild steel wire. The bag was then lifted up to a height of 200mm, the remaining length of the antenna recorded, the movable pointer screwed up to touch the slab bottom and the scaled length recorded. The bag was then released again by cutting the wire. This procedure was repeated for height increments of 100mm until a total drop height of 600mm had been reached. Thereafter the drop height increased by 200mm intervals. Wooden rods cut to 100mm - 1400mm lengths were used to gauge the drop heights (see Plate

6.5). The test was ended when the mesh reinforced slabs had deformed considerably or when the fibre-slabs looked about to disintegrate.

6.3 ARCH TESTS

6.3.1 Arch Dimensions

The arch base was chosen to have the same 2.1 x 2.1m plan area as the slabs. The arch had a constant radius of curvature, i.e. it had a circular shape. The slope of the arch at the springing was 1:4, and the highest point at the underside of the crown was 125mm above ground level. The thickness of the arch was intended to be 60mm as for the slabs, however, the mould manufactured had only 54mm deep sides. The ends of the mould were so shaped that the concrete arch would have a 75mm flat, horizontal bearing surface. The arch mould was reinforced with several channel sections welded along the spine of the mould, to prevent any buckling and downward sagging of the mould under the weight of the concrete during curing (see Plate 6.6).

Figure 6.2 shows a sketch of a typical concrete arch with all relevant dimensions included.

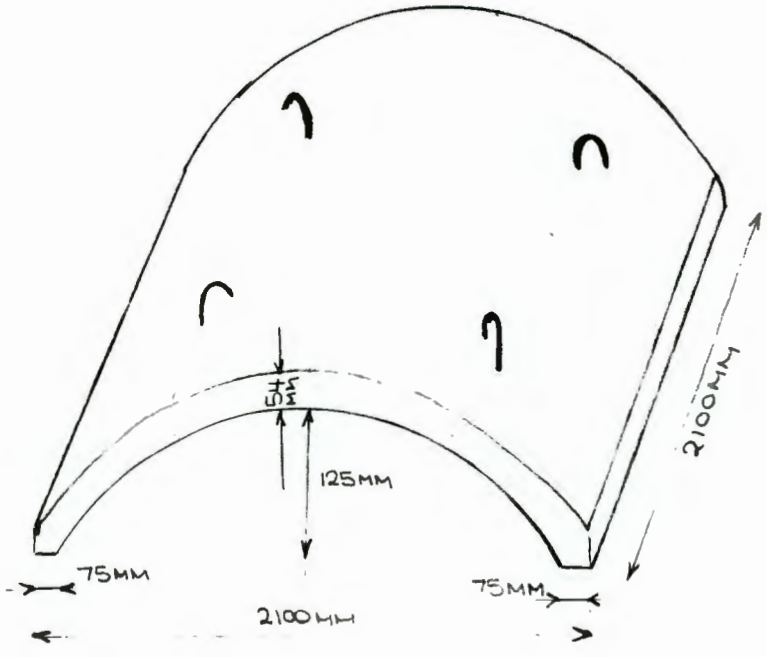

Figure 6.2 : Diagrammatic view of arch, with lifting hooks in place

Plate 6.6 : Arch mould made from 5mm steel plate. Note channel side supports and end sections of later supports. The large I-beam placed under the crown of the arch can be seen in the middle front.

6.3.2 Arch Preparation

Nine arches were cast, the first of which was used for "trouble-shooting" to detect problems/deficiencies in the testing procedure (Table 6.2).

Table 6.2 : Details of arch test panels

Arch No.	Type of Reinforcement		Type of Test
1,2	Mesh		Static
3,4		Fibre	Static
5,6	Mesh		Impact
7,8		Fibre	Impact

MESH-REINFORCED ARCH - The steel mould was first thoroughly covered with a thin layer of shutter oil. A 2 x 2m square mesh sheet was thereafter shaped to fit the curvature of the mould. Concrete spacers of 10.5mm depth were attached to the mesh at various intervals to position the mesh approximately three quarter way down the slab depth. Four lifting hooks were passed through the mesh as indicated by Figure 6.2. The arch was then cast in 3 batches, the mix quantities per batch weighing :

Cement	17.54 kg
Water	33.73 ℓ (kg)
Sand	85.29 kg
Stone	85.29 kg .

Six cubes were prepared from each batch. The same mixing and casting procedure as for the mesh-reinforced slabs was followed.

Care had to be taken when compacting the mix with the poker vibrator, because of the downward movement of the concrete on the slopes. This downward movement of the mix was aggravated even further when the poker made contact with the steel mould. The excess concrete overflowing the base of the mould was removed with trowels. A heavy steel bar was thereafter rolled from the base of the arch to the crown, all material in excess of the 54mm depth being removed or used to fill in regions of lesser depth. This process was repeated on the other side of the arch. Trowels were used to fill in the smaller holes and to finish the arch surface.

FIBRE-REINFORCED ARCH - The binding wire fibre-reinforced arches were cast in 4 batches, the first two containing the fibres and the remaining two consisting of plain concrete. The batch quantities by weight are given below :

Cement	13.878 kg
Water	26.69 ℓ (kg)
Sand	67.49 kg
Stone	67.49 kg .

The concrete constituents were mixed as usual, and 6 cubes cast before 6.582 kg of Binding Wire fibre was added. The fibre mix was spread and compacted in the same manner as was used for the fibre-reinforced slabs. The sharpened rods used to measure the mix depth (see Plate 6.1) were ground down and resharpened to leave an effective depth of 27mm (half the 54mm arch depth) between the point and the plate above. Batches 3 and 4 consisting of plain, un-reinforced concrete were then dumped, spread out, compacted with the tamper and vibrated quickly but evenly. The surface was afterwards

levelled and finished in the same manner as the mesh-reinforced arches.

6.3.3 Arch Curing

Following surface finishing, the arches were covered with black polyethylene sheets and left to cure. Once all the cubes were cast, they were covered with a black polyethylene sheet at room temperature, left for 24 hours, and then demoulded. The cubes were labelled and cubes 1-3 per batch placed in the water tank to cure, cubes 4-6 with the arch.

After 3½ days the arch was removed from the mould and together with cubes 4-6 from batches 1-4 moved to a clear space to continue curing until tested.

6.3.4 Static Testing

Seven days after casting, the cubes were tested in compression using the Amsler cube tester, at a constant loading rate of 150 kN per minute. The variation between batches and curing conditions was noted. The arch was then carefully lifted and moved to the test bed. Unlike the simply supported slabs, the arches were to be pinned at the ends. The concrete blocks were thus removed and the arch lowered onto the test bed. The self-weight of the arch combined with the downward force during static loading would ensure no vertical movement of the arch at its supports. Horizontal movement was restrained by screwing horizontal bolts against the ends of the arch. The restraining setup is best described with reference to Figure 6.3.

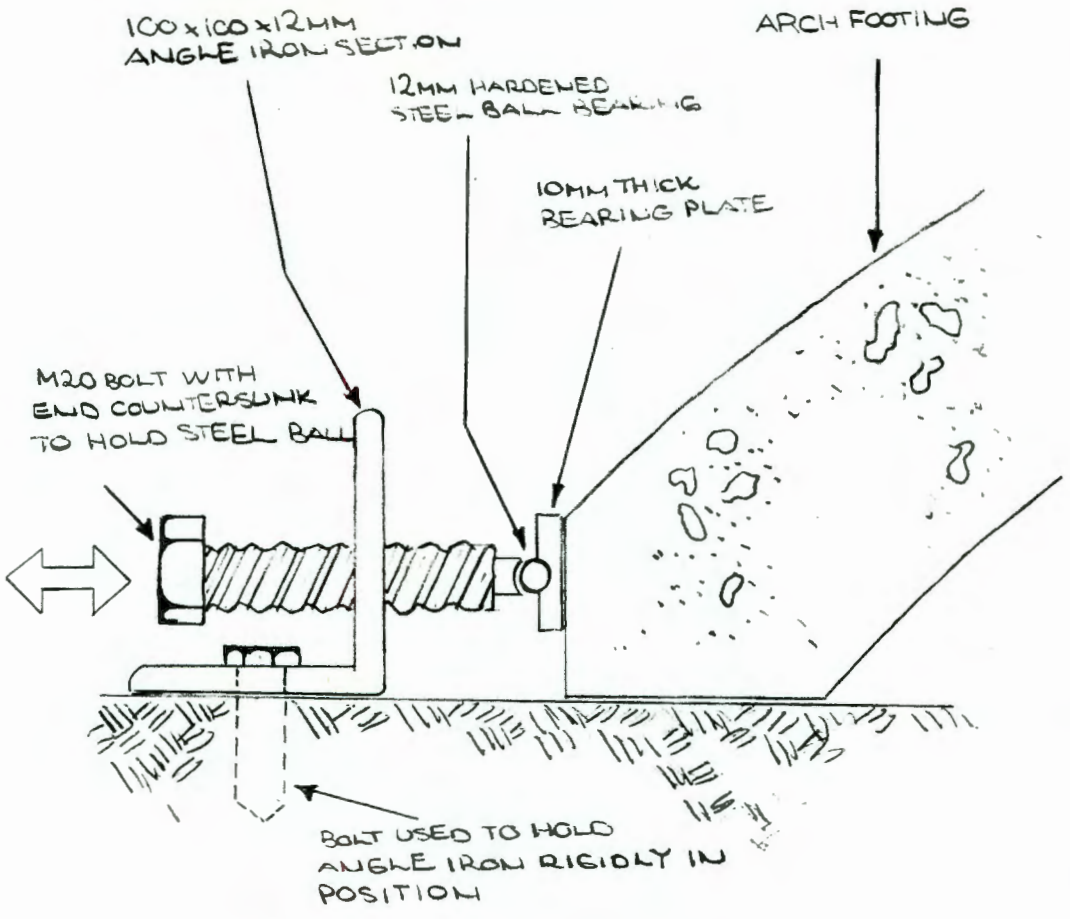

Figure 6.3 : Diagrammatic close-up of arch support

A steel ball was placed at the tip of the steel bolt (which had been grooved to keep the ball in place) and a 38mm diameter x 17mm thick bearing plate was pressed against the steel ball on the other side. The bolt was then screwed forward until the bearing plate made contact with the side of the arch, the surfaces flush to one another. Five of these support bolts were situated across the width of the arch base. The bolts were initially tightened manually and afterwards all given half a turn with a spanner. The arch was thus effectively prevented from moving laterally or vertically resulting in a pinned-end support condition.

The centre of the arch ridge was marked and a long, 5mm thick by 40mm wide rubber strip placed on either side of the centre line. A two metre long 127 x 76mm (taper flange) I-section was laid on these strips, its longitudinal axis coincidental with the crown centre line. An extension was fitted to the 200 kN jack to lower it down to the I-section. Next, the loading head of the jack was screwed down until the swivel head lay resting flat on the upper flange.

Three 50mm dial gauges were placed along the arch crown, one at either end and the third 100mm of the arch centre. The two end gauges were spaced 50mm perpendicular to the centre line to avoid interference from the rubber strips. The dial gauges were attached to a steel rod, which in turn was supported by stands at the arch ends (see Plate 6.7).

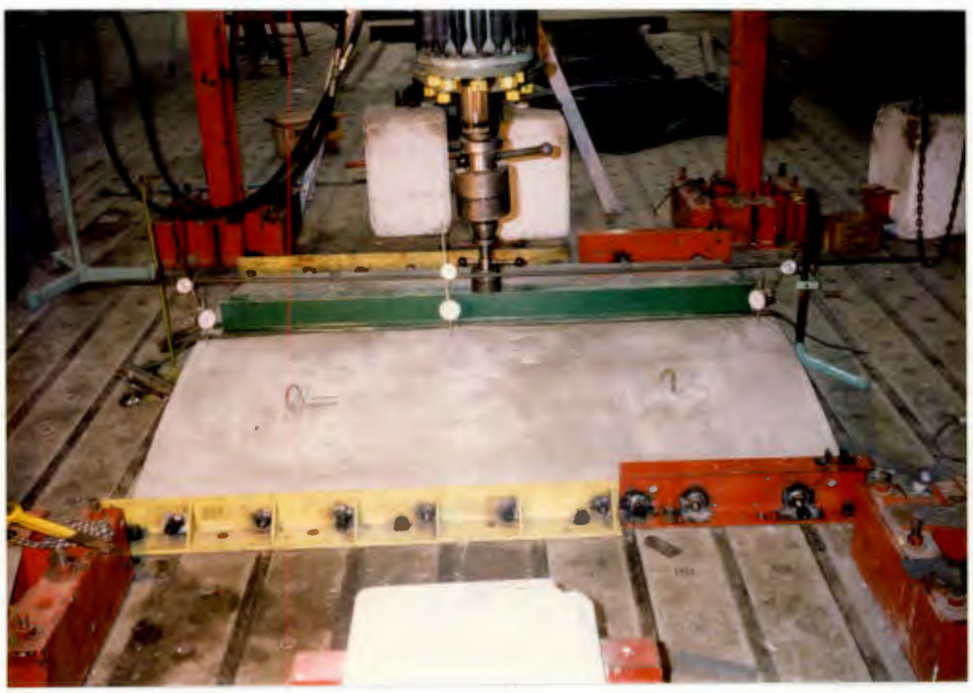

Plate 6.7 : A side view of an arch undergoing static testing. Note positioning of dial gauges.

Plate 6.8 shows an arch undergoing a static test as viewed from the front. The 38mm diameter by 17mm thick arch support bearing plates are clearly visible as shiny cylinders at equal spacings along the arch base. The steel ball between the bearing plates and the horizontally adjustable bolts can just be seen on closer examination.

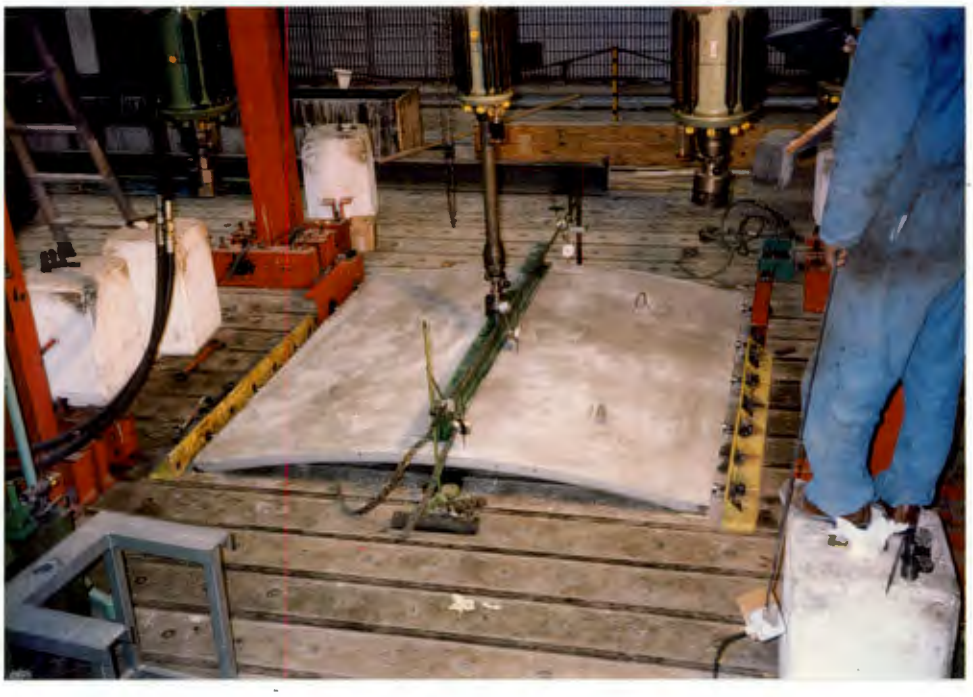

Plate 6.8 : Front view of test set-up

The dial gauge readings were taken at zero load. Initially the load was increased by increments of 1 kN, the dial gauges being read off prior to each increase. The commencement of cracking was detected by the operators' inability to "lock off" the applied load. The loading was thereafter increased by 2 kN increments. Initially the post-crack loading was easily controllable to allow for deflection readings. However, as the ultimate capacity of the arch was

approached, the deflection of the arch increased at such a quick rate that only the middle dial gauge could be read accurately. Once the ultimate load had been reached and the bearing capacity of the arch dropped, the test was stopped.

6.3.5 Impact Testing

The same end restraint system was used for the arches subjected to impact loading. The same 160.7kg sandbag/weights combination was used to load the arch. The 2 metre long 127mm x 76mm (taper flange) I-section used for the static loading was replaced by a 1.98m long, 178 x 102mm (taper flange) I-section for greater strength and rigidity. A 488mm diameter by 10mm thick plate was welded onto the top flange at the beam centre to form a stable base onto which the weight could be dropped. The I-beam was securely held in position by two G-clamps at either end, to prevent the former from falling over on impact. The G-clamps were very firmly tightened onto rectangular hollow sections, which themselves were rigidly clamped to the Amsler jack support rig (see Plates 6.9 and 6.10).

A 50mm deflection dial gauge attached to a small stand was placed on both ends of the arch crown. These dial gauges were used to record the permanent (plastic) deformation of the arch under impact loading. The total (i.e. elastic and plastic) deformation of the arch was measured via a simple little device as shown in the sketch below.

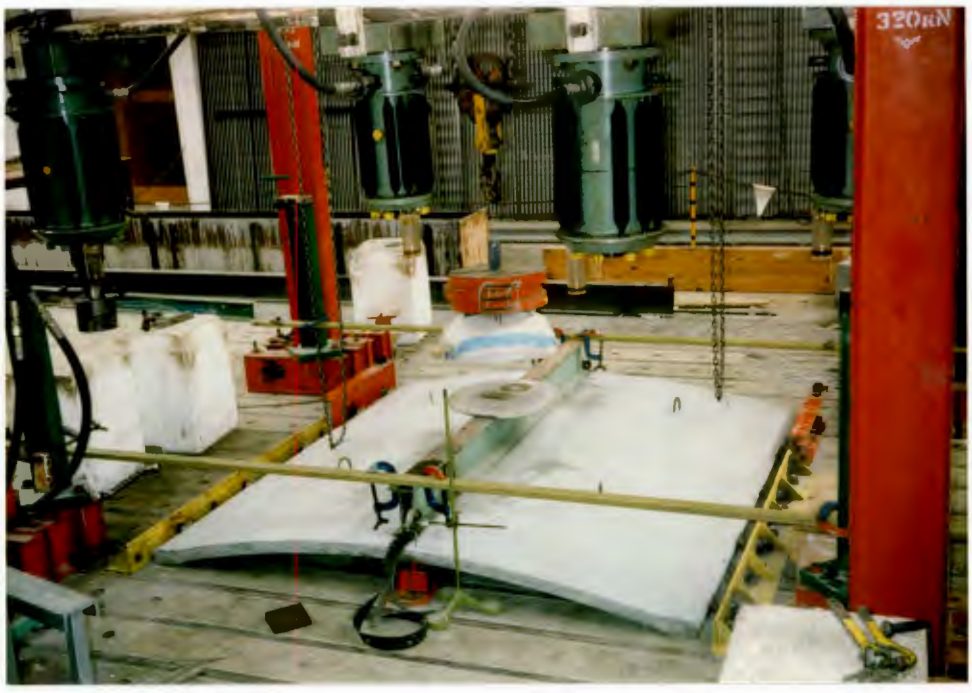

Plate 6.9 : Front view of the concrete arch with the I-beam and attached plate in position. Note the sway restraint system of G-clamps (blue) and hollow channel sections (green).

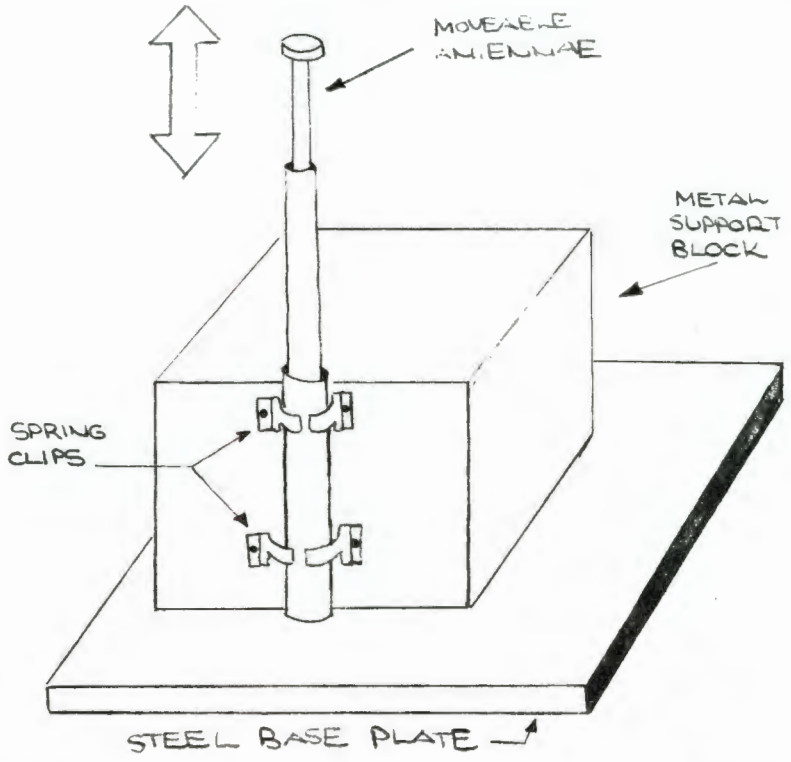

Figure 6.4 : Total impact deformation measuring apparatus

These devices were placed just underneath each open end of the arch, the telescoping antenna section raised until it touched the underside of the crown, and the length of the movable portion recorded as at zero loading. The dial gauge values were also read off, the values recorded designating deflection at zero load. The sandbag system was then raised 100mm above the round plate and thereafter dropped by cutting the wire. The bag was next lifted to a height of 200mm above the plate, the dial gauge readings recorded and the remaining length of the telescoping antenna measured with a ruler. The bag was then released and the whole process repeated for successive 100mm drop height increments. Cracking usually occurred after the 300 or 400mm drop height. Height increments were continued by 100mm up to a height of 600mm , and by 200mm thereafter, i.e. 800, 1000mm, etc., to observe the post-crack behaviour of the arch.

Plate 6.10 below shows a mesh-reinforced arch about to be subjected to the 160.7 kg impact load from a height of 300mm.

NOTE ON IMPACT TESTING - during the first impact test, after the 400mm drop had occurred, the concrete sections in immediate contact with the bearing cylinders showed signs of crushing, with small pieces breaking off the top surface of the slab above the contact point. It was realised that this was caused by the insufficient bearing area of the cylinders. An 80 x 50mm x 8mm thick plate was subsequently welded onto each cylinder to increase the area of contact. Thereafter, disruption of the concrete at the contact face usually became visible only after the 500mm or 600mm drop,

increasing in severity with increasing drop heights. The deflections recorded for drop values in excess of and including 800mm should thus be treated with caution, making allowances for possible inaccuracies.

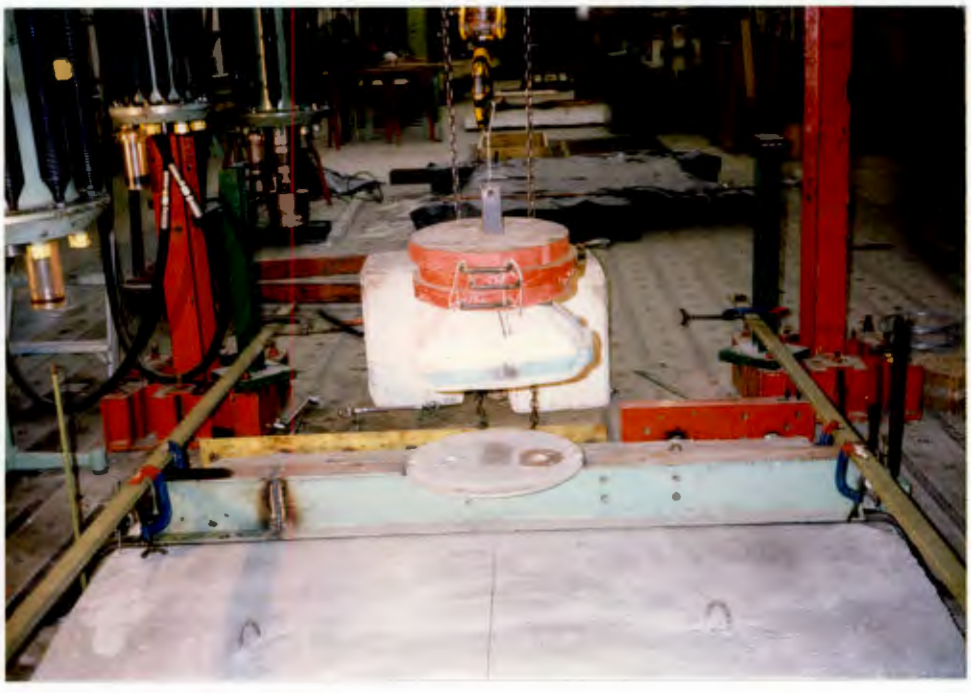

Plate 6.10 : Arch Impact Test in progress

CHAPTER 7

EFFICIENCY AND PROVING PHASE

(TEST RESULTS AND DISCUSSION)

7.1 RESULTS OF TRIAL TESTING

Previous static and impact loading tests on chicken mesh reinforced concrete slabs undertaken at the University of Cape Town illustrated the energy absorbing capacity of the composite[91]. However, the single chicken-mesh layer provided only a third of the minimum steel required for the intended slab application. It was thus decided that trial flexural and shear tests should be carried out to investigate the influence of two or more chicken mesh layers on the concrete strength.

The results showed marginal increases in flexure and shear strengths of prisms reinforced with two layers of chicken mesh. The initial conclusion reached was that the two layers of chicken mesh were insufficient to affect the material properties of the concrete matrix, and that the tests should be repeated on samples reinforced with four layers of chicken mesh. The results of the flexural testing and shear strength determination are given below in Table 7.1(a) and 7.1(b) respectively.

Table 7.1(a) shows that the flexural strength of the prisms reinforced with 4 layers of chicken mesh was lower than the control flexural strength. Additionally, those prisms with the mesh near

the bottom of the prism depth exhibited the lowest flexural strengths. Examination of the fracture surface showed small air pockets trapped between the bound layers of chicken mesh, despite the careful casting and vibration of the prisms to prevent just such an occurrence. Inspection of the bottom of the prism depth showed that the matrix between the mesh and prism base consisted largely of mortar. It is believed that these two factors may have caused the decreased flexural strengths. The results of the shear tests (Table 7.1(b)), also showed a decrease in strength as the number of chicken mesh layers increased. From the trial test it was concluded that the chicken mesh was not a suitable reinforcing material, actually weakening the concrete if used excessively. The efficiency and proving phase was subsequently initiated to determine which of the five different fibre types available was most suited as a reinforcing material. The cube compression, flexure and shear test results are presented and discussed below.

* SPECIAL NOTE : Throughout the following discussions, the term RELATIVE STRENGTH INCREASE is used. This means that the strength of a, say, partially SFR prism is compared RELATIVE to the control strength, and is expressed as a percentage. Example; the relative first-crack flexural strength increase;

$$= \frac{\sigma_{cb.c} - \sigma_{mb}}{\sigma_{mb}} \times 100 \quad .$$

Where the term STRENGTH INCREASE is used (i.e. without RELATIVE), then the comparison is between the actual data, i.e. comparing the ultimate flexural strength of prisms reinforced with 1.50% V_f directly to those reinforced with 2.25% V_f .

7.2 FLEXURAL STRENGTH OF SERIES A-E

The results of the flexural tests conducted on beams 1-6 and 7-9 per series are given in Tables 7.2 and 7.3 respectively. The low control flexural strength of Series E most probably resulted from using cement of a different batch than was used for all the other specimens.

7.2.1 First Crack Flexural Strength

Graphs showing the variation of flexural strength against the product of fibre volume and aspect ratio ($V_f \cdot \ell/D$) are commonly used to determine the effect of increasing the fibre concentration. The aspect ratio remains constant and therefore variations in flexural strength are attributed directly to variations in V_f . However, since five different types of fibres (all of differing aspect ratios) were being investigated, this form of graph would be seriously distorted. The flexural strength was therefore plotted against the fibre volume only and the influence of the differing aspect ratios and fibre shapes on the individual plots studied.

Figure 7.1 shows the flexural cracking strengths of the partially reinforced prisms from Series A-E. The Binding Wire reinforced prisms (Series E) are observed to show the greatest strength increase with increasing fibre volume. The first-crack flexural strength of the fully reinforced prism, Series A-E are shown in Figure 7.2. The plots are observed to be similar to those of Figure 7.1 except that of Series D which shows higher strength increases for the fully SFR prisms. Again the Series E prisms show the greatest strength increase with increasing V_f .

Of particular interest in Figures 7.1 and 7.2 is the decrease in flexural strength of the prisms reinforced with 2.25% V_f Shreddic fibres. Plate 7.1 shows the dense fibre concentration of prisms reinforced with 1.50% Shreddic fibres, and it is thought that at 2.25% V_f the Shreddic fibres actually interfered with the matrix structure thereby weakening the composite.

Although Figures 7.1 and 7.2 show the flexural strength increases/decreases, they do not differentiate between the different control flexural strengths. In order to see how each fibre type strengthens/weakens the plain concrete, the relative flexural strength increase was plotted against V_f . Figure 7.3 shows the relative first-crack flexural strength increase of the partially reinforced prisms against V_f . The Series E prisms are observed to show the greatest increase in strength, reaching 93% for the prisms reinforced with 2.25% V_f .

Figure 7.4 shows the relative first-crack flexural increase of the fully reinforced prisms plotted against V_f for Series A-E. The prisms of Series E again show the greatest relative flexural strength increase. The next best relative strength increase is that of Series D (ME430(35mm) fibres). The similarity between Figures 7.3 and 7.4 is apparent.

7.2.2 Ultimate Flexural Strength

The ultimate flexural strengths of the partially reinforced prisms of Series A to E are shown in Figure 7.5. The prisms of Series E are seen to exhibit the greatest flexural strengths from

approximately 1% V_f to 2.25% V_f . It is interesting to note the parallel plots of Series C and D, Series D exhibiting higher flexural strengths as expected.

Figure 7.6 shows the ultimate flexural strength of the fully reinforced individual fibre types at various fibre volumes. Again, the similarity in plots between the partially reinforced (Figure 7.5) and the fully reinforced prisms (Figure 7.6) is apparent. In order to eliminate the difference in control strengths for comparing the effect of the fibres, the relative ultimate flexural strength increase was plotted against the fibre volume.

In both figures, the Series E prisms show the greatest relative strength increase by far. These increases are noted to be linear with increasing V_f . The prisms reinforced with Shreddic fibres (Series A) exhibited the usual peak in strength at 1.50% V_f followed by a decrease in relative strength.

The following observations were made from Figures 7.1 through 7.8 :

(i) the presence of steel fibres on the concrete matrix unmistakenly delays the onset of cracking in prisms subjected to flexural load;

(ii) high aspect ratios do not always guarantee greater flexural strengthening; viz. the higher flexural strengths of Series D (ℓ/D = 70) compared to Series B (ℓ/D = 83). This observation supports the review of Chapter 4 in that the fibre shape and consequent bond strength and shear stress collectively influence a fibre's effectiveness in reinforcing a concrete matrix;

(iii) the plot of Series E in Figures 7.3 - 7.4 and 7.7 - 7.8 is linear between 0.75% V_f and 2.25% V_f . Assuming that a linear relationship exists, a regression analysis of the Series E data enables the minimum volume of Binding Wires required to initiate flexural strengthening to be determined as :

$$V_{f(MIN)} = \text{between } 0.40 - 4.47\% \; V_f \quad ;$$

(iv) the partially SFRC prisms exhibited flexural strengths close to the fully SFRC prisms;

(v) the Binding Wire fibres (of Series E) had the greatest strengthening effect on a concrete matrix. It should be noted though that the 2.25% Binding Wire mix was very difficult to mix and cast. The mix was nearly unworkable, and nonhomogeneous with clumps of fibres and segregated stone clearly visible.

7.2.3 Comparison of Partially and Fully Reinforced Prism Flexural Strengths

One of the main objectives of the Efficiency and Proving Phase of the experimental programme was to determine whether prisms partially reinforced with steel fibres would develop the same strength as fully reinforced samples. The close similarity between the plots of Figures 7.3, 7.4, 7.7 and 7.8 demonstrates clearly the equality of the partially and fully reinforced prisms. Figure 7.9 is a bar-graph representation of the abovementioned figures. For each of the three sets of flexural prisms per series, the difference in first-crack and ultimate strength between the partially and fully reinforced prisms is recorded as a percentage. The blue shading represents cases where the fully reinforced prisms exhibited greater flexural strengths and the red shading vice versa.

Figure 7.9 shows that the majority of the partially SFRC prisms exhibited flexural strengths (with first-crack and ultimate) within 10% of the fully SFRC prism flexural strengths. Considering the variability in strength of plain concrete, this variation is very small. From Figure 7.9 the following conclusions were drawn :

(i) concrete prisms reinforced with steel fibres over only a partial section of the depth exhibited the same flexural strengths as those samples with fibre reinforcing throughout the full depth,

(ii) the partially and fully fibre reinforced prism strengths were equal when reinforced with fibres of high aspect ratio (Wirand, ME430(35mm) and Binding Wire) at 1.50% V_f .

It should be remembered that the same fibre-mix was used to cast the bottom half of the partially reinforced prisms as was used to cast the full depth of the fully reinforced prisms. In effect, therefore, a partially reinforced prism will contain half the number of fibres as a fully reinforced prism. To compare a partially and fully fibre reinforced prism containing the same volume of fibres, one would need to compare a sample of the former reinforced with, say, 1.50% V_f and a sample of the latter reinforced with 0.75% V_f . Figure 7.10(a) shows the difference in relative flexural cracking strength while Figure 7.10(b) shows the difference in the relative ultimate flexural strength of such a case. The 1.50% V_f partially reinforced prisms are observed to exhibit flexural strengths far higher than the 0.75% V_f fully reinforced prisms.

The lower flexural strength of the partially ME430(35mm) fibre reinforced prisms was due to the high control strength, which resulted in a smaller relative strength increase than that calculated for the 0.75% V_f fully reinforced prisms. Plates 7.2 and 7.3 show (from left to right) three fully reinforced prisms and three partially reinforced prisms containing 0.75%, 1.50% and 2.25% by volume of ME430(35mm) fibre respectively. The left prism in Plate 7.2 has the same volume of fibres as the middle prism of Plate 7.3. The higher concentration of fibres in the bottom half of the partially reinforced prism is clearly visible, and but for the high control strength the latter would have exhibited a higher flexural load capacity.

Plates 7.4 and 7.5 show the difference in fibre concentration between fully reinforced and partially reinforced prisms containing (from right to left) 0.75% , 1.50% and 2.25% volume of Binding Wire fibres. The dense fibre concentration at 1.50% V_f for the middle partially reinforced prism (Plate 7.5) is clearly visible compared to the scattered fibres of the 0.75% V_f fully reinforced prism (Plate 7.4). The ultimate flexural strength was consequently 59.8% higher for the partially reinforced prism (see Figure 7.10(b)).

7.3 SHEAR STRENGTH OF SERIES A-E

The shear strengths of beams 1-9 per set for Series A-E are given in Table 7.4 (see end of written text).

To eliminate variations of control shear strengths the relative shear strength increase was plotted against the fibre volume (Figures 7.11 and 7.12). The relative shear increase was calculated as :

$$\% \text{ increase} = \frac{(V_{PART} - V_{CONTROL})}{V_{CONTROL}} \times 100$$

and

$$= \frac{(V_{FULLY} - V_{CONTROL})}{V_{CONTROL}} \times 100 \quad .$$

The highest increase in relative shear strength of the partially reinforced prisms (Figure 7.11) was found to occur for the ME430(35mm) partially reinforced prisms. Between 1.50% V_f and 2.25% V_f however, the shear strength increased only marginally. This may have been caused by fibre-balls forming in the mixing of the concrete, which effectively reduces the volume of fibres available for distribution. Whenever detected during mixing, the fibre-balls were broken up to ensure even distribution of fibres. Plate 7.6 shows an ME430(35mm) fibre ball on left and a ME430(25mm) fibre-ball at right which were observed in mixes containing 2.25% V_f . Fibre-balls were also observed in the mix reinforced with 2.25% Wirand fibres (Series B). Plate 7.7 shows a fibre-ball detected on the fracture face of a partially reinforced prism. This probably accounts for the drop in relative shear strength between 1.50% - 2.25% V_f .

Figure 7.12 shows the relative shear strength of the fully reinforced prisms plotted against V_f . Once again the plot of Series E shows the greatest increase in relative strength. Generally, the plots of Series B-E are linear, the plots of Series

of A showing the usual drop in relative shear strength between 1.50 - 2.25% V_f .

As a check to whether the partially and fully reinforced prisms were being properly cast and tested, the difference in shear strengths between the 1.50% V_f partially reinforced and 0.75% V_f fully reinforced prisms of Series A-E were compared (Figure 7.13). The variations in Series B, D and E were minor, as expected. Series A showed a 10% higher strength for the fully reinforced prism and for Series C the partially reinforced prisms were found to be 12.7% stronger in shear. Both these differences are reasonably low.

From the test results and Figures 7.11 - 7.13 the following conclusions were drawn :

(i) the relative shear strength of the fully SFRC prisms increased linearly as the V_f increased. However, there is a limit to the quantity of steel fibre which can be added to a concrete matrix, beyond which the homogeneity of the composite and its mechanical properties are adversely affected;

(ii) the partially reinforced prisms did not show a relationship described in (i), whereas the fully reinforced prisms distinctly showed such a relationship. It is therefore recommended that more testing be carried out on partially reinforced prisms to observe whether some type of trend can be detected.

(ii) at an early stage of curing the fibres have a major influence on the young, "green" concrete, binding the matrix together. With increased curing time, the concrete hardens with a corresponding increase in load absorbing capacity. The influence of the fibres therefore decreases and it is believed that after the concrete gains its maturity strength, the contribution of the fibres will level off at a constant value.

7.4.2 Variation in Strength with Increasing Fibre Volume

To compare the influence of the different fibres on the matrix compressive strength, Figures 7.15, 7.16 and 7.17 were plotted which show the relative compressive strength increase after 3,7 and 14 days. From Figures 7.15 through 7.17 the following observations were made :

(i) the relative compressive strength increased linearly with increasing V_f when the cubes were tested after 3 days. However, after 7 and 14 days curing, this linearity was only apparent up to the 1.50% V_f mark,

(ii) the cubes reinforced with 2.25% Binding Wire fibres exhibited relative strengths substantially lower than the cubes reinforced with 1.50% V_f . It is thought that the segregation of the fibres and stone occurring with the 2.25% V_f mix, combined with the inability to compact this unworkable mix caused these lower strengths. Plate 7.8 shows from left to right cubes reinforced with 2.25% V_f Shreddic, Wirand, Binding Wire and an unreinforced control cube. The superior binding ability of the Shreddic and Wirand fibres over the Binding Wire is clearly visible,

7.4 EFFECT OF FIBRE TYPES A-E ON COMPRESSION STRENGTH

The plain control and fibre cubes were cast from the same mixes as the flexural specimens. Table 7.5 shows the control cube strengths (i.e. unreinforced) and fibre cube strengths after 3.7 and 14 days for each set of Series A-E. The relative increase in cube strength is calculated as :

$$\% \text{ increase} = \frac{f_{cf} - f_{cu}}{f_{cu}}$$

where f_{cf} = compressive strength of SFRC cube

f_{cu} = control cube strength.

The mean compressive strength (f_{cu}), standard deviation (σ_n) and coefficient of variation ($c = \sigma/f_{cu}$) for the control cubes after 3,7 and 14 days was determined as :

$$f_{cu(3)} = 24.7 \text{ MPa}, \ \sigma_n = 1.95, \ c = 7.9\%$$
$$f_{cu(7)} = 33.8 \text{ MPa}, \ \sigma_n = 1.91, \ c = 5.6\%$$
$$f_{cu(17)} = 40.4 \text{ MPa}, \ \sigma_n = 1.10, \ c = 2.7\% \ .$$

7.4.1 Variation of Strength With Increased Curing

The relative compressive strength increase for each test series was plotted against time of curing (3-14 days) to observe the effect of the fibres on the concrete matrix and how this effect varied for differing fibre concentrations with time (Figures 7.14(a) to 7.14(e)). From Figures 7.14(a) - 7.14(e) the following observations were made :

(i) generally, as the fibre concentration increased the relative strength increased though not always proportionately. (This is expanded on in Section 7.4.2 below.)

(iii) as the concrete matures and consequently hardens, the fibres with non-uniform cross-sections appear to exert less influence on the composite behaviour. Comparing Figures 7.16 and 7.17 with Figure 7.15 shows a definite "separation" of those fibres with a tubular shape (Series A, B and E) to those with irregular cross-sectional areas (Series C and D).

It is thought that the "separation" mentioned above is attributable to two factors :

- the orientation of the fibres, and
- the non-uniform cross-sectional shape along the length of the fibre types C and D.

When the cubes are cast in 2-3 layers and compacted, the fibres are forced to assume a predominantly 2-dimensional (horizontal) orientation. Prior to loading, the cubes are rotated 90°, and the fibres therefore assume a predominantly 2-dimensional (vertical) orientation. As the cube is loaded in compression, the interfacial shear stress between the fibre and the surrounding matrix would enable the fibre to absorb some of the applied load while the concrete matrix absorbed the remainder. Because of the uniform cross-sectional area of fibre types A, B and E, the interfacial shear stress and resulting fibre compressive stress should be roughly linear. The irregular shape along the length of fibre types C and D however will probably result in stress concentrations. The author believes that this non-uniform stress absorbtion of fibre types C and D is the cause of the lower compressive strengths of such composites.

7.5 IMPACT STRENGTH OF SERIES A-E

The results of the impact testing are given in Table 7.6. The most impressive performance was obtained from the Binding Wire reinforced samples. The first-crack impact strength was nearly double that of the Melt Extract fibre reinforced samples, while the ultimate impact strength averaaged at a massive 312 blows. One of the tests was actually stopped after 400 blows because by then the superior action of the Binding Wire reinforced samples had been amply demonstrated.

One notes the very large coefficients of variation for the number of blows required to cause cracking of the specimen. This was due to the difficulty in spotting the first hairline crack combined with the very slow propagation of these cracks in the fibre-reinforced test specimens. It was also later discovered that those test specimens cut from the top and bottom of each cylinder gave substantially lower cracking and ultimate strengths. These results were subsequently discarded. Despite the high coefficients of variation in the number of blows to cause cracking, it should be noted that the coefficients are very much lower for the number of blows required to cause ultimate failure.

The ACI Impact Test clearly demonstrates the significant improvement in impact resistance of SFRC over plain concrete. The Binding Wire fibres were seen to have the greatest strengthening influence.

7.6 THEORETICAL EVALUATION OF TEST RESULTS

7.6.1 Determination of a Flexural Strength Equation

The Law of Mixtures equation (3.7) is given as :

$$\sigma_{cb.c} \text{ , } \sigma_{cb.u} = A.\sigma m_b \, V_m + \beta \, \tau_{AV} \, V_f \, \frac{\ell}{D} \qquad (3.7)$$

for which constants A and B are determined statistically from experimental results. Equation (3.7) implies that the modulus of rupture for the SFRC composite increases in proportion to the volume percentage of the fibres (V_f) and the fibre aspect ratio (ℓ/D) . This agrees with the findings of a conducted by Johnston[77]. Assuming this relationship, the flexural test data was analysed using five different methods to determine constants A and B (see Appendix F.1). Since the first term on the right hand side of equation (3.7) represents the contribution of the matrix at maximum load, constant A is constrained to a maximum value of 1. Two of the analysis methods yielded values of constant A in excess of unity, and were thus discarded. The remaining three methods of analyses are discussed below.

Swamy and Mangat Approach This analysis utilises the Law of Mixtures equation (3.7) which has been modified to include length and volume efficiency fectors (see reference 31 for formulae derivation). The final form of the equation is :

$$\sigma_{cb} = A\,\sigma_{mb} + 2\,\tau\,\ell/D\;0.41V_f$$

or

$$\sigma_{cb} = A\,\sigma_{mb}\,V_m + 0.82\,\tau\,V_f\,\ell/D \qquad (7.1)$$

which can be rewritten as :

$$\frac{\sigma_{cb}}{V_f\,\ell/D} = \frac{A\,\sigma_m(1 - V_f)}{V_f\,\ell/D} + 0.82\,\tau \quad . \qquad (7.2)$$

(This last term in equation (7.2) is equal to B of equation (3.7).)

When the first crack in the flexural prism occurs, the interfacial bond stress τ in equation (7.2) corresponds to the average bond

stress τ_{AV} at which bond slip commences. Further loading causes progressive debonding and subsequent crack propagation. Eventually the ultimate failure load will be reached, at which stage the interfacial shear stress will reach the ultimate bond strength τ_u between the fibres and the matrix, and failure by fibre pullout occurs. Equation (7.2) at these two stages is written as :

at first crack
$$\frac{\sigma_{cb.c}}{V_f\,\ell/D} = \frac{\sigma_m(1 - V_f)}{V_f\ell/D} + 0.82\,\tau_{AV} \qquad (7.3a)$$

at failure
$$\frac{\sigma_{cb.u}}{V_f\,\ell/D} = \frac{\sigma_m(1 - V_f)}{V_f\ell/D} + 0.82\,\tau_u \quad . \qquad (7.3b)$$

Equations (7.3a) and (7.3b) are of a linear form. By plotting the flexural test data of the left hand side of equation (7.3a), (7.3b) against the first term on the right hand side of the equation, one should obtain a straight line of slope A and an intercept of 0.82 τ, equal to B.

Figures 7.18 and 7.19 show the plots for the partially reinforced prisms at cracking and at the ultimate failure loads. Figures 7.20 and 7.21 show the data of the fully reinforced prisms at first-crack and ultimate failure stages. The results show a consistent pattern which is most pronounced for the first-crack load cases (Figures 7.18 and 7.20). The best fit line for each plot was obtained by a linear regression analysis. Constants A and B obtained from the analysis are shown in Table 7.7 (see end of written text). From the last term of equations (7.3a) and (7.3b) the average and ultimate bond stress was calculated :

$$0.82\,\tau_{AV,u} = B$$

i.e.
$$\tau_{AV,u} = B/0.82 \quad .$$

The partially reinforced prisms exhibited an average bond strength of 1.8 MPa and an ultimate bond strength of 2.5 MPa. For the fully reinforced prisms the average bond stress was 1.7 MPa and for ultimate load, a value of 2.45 MPa was calculated. The close correlation of the bond stresses (τ_{AV} difference of 7.5% and τ_u difference of 3.1%) confirms the validity of the test approach. Figures 7.18 - 7.21 also show that the influence of differing fibre aspect ratio (for the range tested) on the bond stress developed is negligible.

Composite strength vs $V_f \cdot \ell/D$ approach Figures 7.22 through 7.25 show the plots of first crack and ultimate composite flexural strength against $V_f \cdot \ell/D$ for the partially and fully reinforced prismatic specimens respectively. The best-fit line was determined using linear regression analysis. The cracking flexural strengths of the partially reinforced prisms (Figure 7.22) and fully reinforced prisms (Figure 7.24) showed very good correlation with the regression line. It should be noted though that those points deviating most from the regression lines in Figures 7.22 through to 7.25 are the same data associated with nonlinear flexural strength increases (see Figures 7.7 and 7.8), e.g. those prisms reinforced with 1.50% V_f Shreddic, 0.75% ME430(35mm), 2.25% ME430(35mm) and 2.25% V_f Binding Wire. If these data points are "excluded" from the plots, then the linear relationship between the composite strength and the product of $V_f \ell/D$ is clearly visible.

The bond strengths determined from constant B were :

partially reinforced τ_{AV} = 1.60 MPa, τ_u = 2.3 MPa

fully reinforced τ_{AV} = 1.50 MPa, τ_u = 2.6 MPa .

These values are slightly lower than those obtained for the preceding analysis.

Composite strength vs $W_f \cdot \ell/D$ approach Figures 7.26 through 7.29 show the plots of composite strength against the product of fibre weight (W_f) and their ratio (ℓ/D). The plots are very similar to those of Figures 7.22 through 7.25. The product $W_f \cdot \ell/D$ is preferred to $V_f \cdot \ell/D$ because;

i) steel is normally priced by weight, and

ii) the product $W_f \cdot \ell/D$ combines cost (W_f) with performance ℓ/D.

The slope A and intercept B determined from the regression analysis are given in Table 7.7. From constant B, the average and ultimate bond strengths were calculated as :

partially reinforced, first crack $\tau_{AV} = 1.8$ MPa , $\tau_u = 2.1$ MPa

fully reinforced, ultimate $\tau_{AV} = 1.4$ MPa , $\tau_u = 2.4$ MPa .

The average bond strengths differ by 24.5%, and the ultimate bond strengths by 12.1%. These variations are noted to be three times greater than that obtained from the Shah and Mangat method of analysis.

Final choice of constants All three methods of analysis yielded constants A and B (and resulting bond strength values) fairly close to one another. A statistical analysis of the predicted strengths given by the various equations with the experimental results was thus carried out (see Appendix F.1).

The findings of the analysis show that the equations of the second method (composite strength vs $V_f \cdot \ell/D$) generally predicted strengths lower than those obtained experimentally. Although the strength equations for the partially reinforced prisms determined by the last method showed the closest correlation to test results, the strength equations as determined by the Shah and Mangat approach yielded the best overall comparison.

The final form of the first-crack and ultimate flexural equation for the partially reinforced composite was thus taken as :

$$\sigma_{cb.c} = 0.877\ \sigma_m(1 - V_f) + 1.474\ V_f\ \ell/D \qquad (7.4)$$

$$\sigma_{cb.u} = 0.873\ \sigma_m(1 - V_f) + 2.072\ V_f\ \ell/D \qquad (7.5)$$

From equation (7.4) the average bond stress at first-crack is given by τ_{AV} = 1.80 MPa, and at ultimate failure the ultimate bond stress given by equation (7.5) is τ_u = 2.5 MPa.

The first-crack and ultimate flexural equations for the fully reinforced composite was taken as :

$$\sigma_{cb.c} = 0.963\ \sigma_m(1 - V_f) + 1.371\ V_f\ \ell/D \qquad (7.6)$$

$$\sigma_{cb.u} = 0.932\ \sigma_m(1 - V_f) + 2.010\ V_f\ \ell/D \qquad (7.7)$$

for which the average bond stress τ_{AV} = 1.67 MPa and the ultimate bond stress τ_u = 2.45 MPa.

7.6.2 Relationship between Fibre-spacing and Flexural Strength

The first-crack flexural strengths obtained were plotted against the spacing equations (3.8) through (3.13) to observe whether some relationship/pattern could be detected. Equations (3.9) and (3.10) were modified for the Series D and E results to take into account the greater length and volume efficiency factors for these predominantly 2-directionally aligned fibres. The modified spacing equations were :

$$\text{For first-crack modulus of rupture } S_c = 21.28 \sqrt{\frac{d}{V_f \ell}} \qquad (7.8)$$

$$\text{For ultimate modulus of rupture } S_c = 19.01 \sqrt{\frac{d}{V_f \ell}} \, . \qquad (7.9)$$

Figures 7.30 and 7.31 show the plots of the ultimate modular ratio against Romualdi's spacing equation (3.8). The data shows wide scatter with no detectable relationship. The same data plotted against Krenchell's spacing equations (3.11) to (3.13) show an equal amount of scatter (Figures 7.32 and 7.33). The fibre spacing of the latter was noted to be lower than that obtained by Romualdi's equation.

Finally, the flexural cracking modulus of the partially reinforced prisms was plotted against spacing equations (3.9) and (7.8) for the data of Series A-C and D-E respectively, as shown in Figure 7.34(a). The plot showed a clear pattern of increasing modular ratio associated with decreasing fibre-spacing. A theoretical curve relating the first-crack spacing equation (7.8) to the first-crack flexural strength prediction equation (7.4) shows very good correlation with the test data. The ultimate flexural modulus data

plotted against the ultimate spacing showed the same pattern although the points were more spread out (see Figure 7.34(b)). The ultimate strength prediction equation (7.5) plotted against the ultimate spacing equation (7.9) yielded a curve which also showed good correlation with the test results.

The first-crack and ultimate modular ratios for the fully reinforced prisms, plotted against the cracking and ultimate spacing (Figures 7.35(a) and 7.35(b)) showed the same pattern as detected for the partially reinforced prisms. The theoretical curves drawn, based on flexure equations (7.6) - (7.7) and spacing equations (7.8) and (7.9), are seen to follow this pattern very well, confirming the unique relationship which exists between fibre-spacing and flexural strength.

7.6.3 Relationship between Flexural and Shear Strength

If the plots of the relative increase in flexural strength (Figures 7.7 and 7.8) are compared with these showing the relative increase in shear strength (Figure 7.12(a) and (b)) for increasing fibre concentration, certain simularities are observed. The first-crack and ultimate flexural strengths of Series A-E was therefore plotted against the shear strength (Figures 7.36 and 7.37), all the units being in MPa.

The plot obtained for the partially reinforced test data (Figure 7.36) showed that an increase in flexural strength was generally accompanied by an increase in the shear strength. The best-fit line obtained by linear regression was of the form :

$$\sigma_{c.b\ u} = 1.508\ \sigma_s + 1.954 \quad . \qquad (7.10)$$

The data for the fully reinforced prisms showed a distinct relationship between the flexural and shear strength (Figure 7.37). The best-fit line yielded a flexural strength of 0.33 MPa for a zero shear strength. Theoretically the flexural strength should also be equal to zero, and its is thought that this discrepancy is probably due to the sometimes large variation in flexural and shear strength encountered for the same set of specimens.

The theoretical equation obtained by linear regression, for the fully reinforced prisms (all units in MPa);

$$\sigma_{c.b\ u} = 1.922\ V_u + 0.33 \quad . \qquad (7.11)$$

The magnitude of the slope and constant in equation (7.10) is seen to be quite different to that obtained for equation (7.11). A possible explanation for this is

(i) the partially reinforced prisms exhibited flexural strengths slightly lower than the fully reinforced prisms. This may account for the shallower slope of equation (7.10);

(ii) the shear strength of the partially reinforced prisms was <u>less than</u> that of the fully reinforced ones, as expected. The flexural strengths however were usually similar, as mentioned in (i) above. If the partially and fully reinforced specimen data are plotted together (Figure 7.38), because of the lower shear strengths of the partially reinforced specimens however, this data will lie to the left of the fully reinforced data. The best-fit line therefore yielded an intercept of magnitude 0.74 MPa higher than that obtained for the fully reinforced samples. The best-fit line was :

$$\sigma_{cb.u} = 1.725\ V_u + 1.07 \quad .$$

Figures 7.37 through 7.38 clearly show the relationship between the shear strength and flexural strength of a SFRC specimen. Additional testing is required to observe whether this relationship exists at very low and very high shear strengths.

7.6.4 Cost Analysis

The current cost of fibre types A-E per kilogram, inclusive of railage (for fibres not produced in Cape Town), discount where offered and Government Sales Tax (G.S.T.) of 12% are :

Shreddic	-	R 4.95
Wirand	-	R 4.95
ME430(25mm)	-	R 9.01
ME430(35mm)	-	R 9.01
Binding Wire (Cape Gate)	-	R 4.98
(C.W.I.)	-	R 4.34
(Allans Meshco)	-	R 3.02 .

(The Binding Wire fibres were produced by cutting up 50 kg spools into fibres of the required length. The three prices given above are therefore inclusive of material cost and cutting cost.) From the prices quoted, the ME430(25Mm) and ME430(35Mm) fibres are the most expensive, because they are imported from Australia. The Binding Wire fibres produced at Allans Meshco are the cheapest.

7.6.5 Determination of Fibre Volume Required

All the tests performed under the "efficiency and proving phase" of the test programme involved the comparison of SFRC composites with plain, unreinforced concrete specimens. In the next step of the

testing programme, the performance of Binding Wire reinforced concrete slabs and arches subjected to static and impact load were to be compared with the performance of mesh-reinforced arches and slabs. It was therefore necessary to calculate the volume of fibres required to impart the partially reinforced slabs and arches with the same strength as mesh reinforcing.

An ultimate strength analysis using conventional reinforced concrete beam theory was used to determine the volume of fibre required. The assumed stress distributions at failure and the ultimate strength calculations are given in Appendix G. The calculations showed that 1.24% by volume of Binding Wire fibres was required. A rounded value of 1.25% V_f was decided on.

7.6.6 Calculation of Toughness Index for Binding Wire Reinforced Specimens

Once the volume of Binding Wire required had been determined, two additional sets of flexural tests were conducted on prisms reinforced with 1.25% V_f and 1.50% V_f , before the application phase of the program began.

The deflection of the prisms under loading was measured at the beam centre and on either side, at the points of load application, using 20mm travel dial gauges. Generally ultimate failure occurred at or near the central deflection gauge, but when the failure occurred near one of the points of load application, the dial gauge readings on that side were used. The load deflection plots for the 1.25% V_f partially and fully reinforced prisms are shown in Figures 7.39(a) and 7.39(b). The plots for the prisms reinforced with 1.50% V_f are shown in Figures 7.40(a) and 7.40(b).

Load vs deflection plots of the type in Figures 7.39(b) and 7.40(b) are typical where the bond length ℓ_f is near to ℓ_{CRIT} and the fibre strength near 500 MPa[88]. The curves can be divided into three regions. The first corresponds to the linear elastic deformation of the prism until first-crack occurs. The deflection now becomes nonlinear while the load increases up until the fibres begin to debond. The second region of the curve represents the debonding of the fibres and is limited by the load when the fibre is debonded along its full length. The third part of the curve corresponds to the load transferred to the matrix by the shear stresses and friction. The sudden drops in the observed load in region three occur as some of the fibres fail or become completely debonded.

The plots of Figures 7.39(a) and 7.40(a) can also be divided into these three regions although region two is observed to be much smaller, i.e. debonding of the fibres occurs over a smaller deflection range. This was expected because the partially reinforced prisms only have fibres over the bottom half depth. As the cracks propagate under increased loading, a stage will be reached where the cracks propagate through the unreinforced matrix and therefore the load capacity will drop off quicker than for the fully reinforced prisms. The sudden drop between the second and third region occurs when the fibres become fully debonded along their length and the residual load capacity thereafter is attributable to the shear stresses and friction between the matrix and fibre.

The Toughness Index is calculated as the area under the load vs deflection curve up to the deflection point 1.9mm divided by the area under the load vs deflection curve up to the first-crack load.

$$\text{Toughness Index} = \frac{A_{\text{TOTAL 1.9mm}}}{A_{\text{FIRST-CRACK}}} \quad .$$

The values of the index calculated from Figures 7.39 and 7.40 are given in Table 7.8 (see end of written text). For the 1.50% V_f reinforced prisms the index was greater for the fully reinforced prisms. This was expected due to the much higher energy absorbing capacity of the fully reinforced beams. The indices of the partially and fully 1.25% V_f reinforced prisms however, were close despite the much higher energy absorption of the fully reinforced specimens. In this instance the index can be misleading because since the area up to first-crack is the divisor in the calculation, a mix having a high first-crack strength can have a low index. This is the case for the 1.25% V_f fully reinforced prisms.

Despite the shortcomings of the index in situations as above, the load vs deflection plots of Figures 7.39 through 7.40 show the increased energy absorbing capacity of the fibre-reinforced prisms over the control prisms. The index varied between 6 and 10.6 for the composites compared with 1.0 for the control specimens.

Table 7.1(a) : Results of trial flexural tests

Type of Reinforcing	Control modulus of rupture (MPa)	Ultimate flexural strength - mesh in middle (MPa)	Coefficient of variation (%)	Ultimate flexural strength - mesh on bottom half (MPa)	Coefficient of variation (%)	Cube strength (MPa)
Chicken mesh 2 layers 25mm apertures	4.06	4.33	5.5	4.07	1.3	35.5
Chicken mesh 4 layer 25mm apertures	5.33	4.63	7.9	4.04	6.4	35.3

Table 7.1(b) : Results of trial shear tests

Type of Reinforcing	Control, un-reinforced (MPa)	Mesh in middle (MPa)	Coefficient of variation (%)	Mesh in bottom half (MPa)	Coefficient of variation (%)	Control cube strength (MPa)
Chicken mesh 2 layers 25mm apertures	2.32	2.75	5.5	2.39	16.3	35.5
Chicken mesh 4 layer 25mm apertures	2.88	2.80	6.6	2.37	4.6	35.3

Table 7.2 : Properties of flexural prisms partially reinforced

Type and size of fibre (diam. x length, mm)	% Fibre by volume	Control modulus of rupture (MPa)*	Flexural cracking strength (MPa)†	Ultimate flexural strength (MPa)	Coefficient of variation (%)	Cube strength (MPa)
	0.75 B	5.44	5.11	5.11	9.2	36.3
Shreddic 0.25 x 10	1.50 B	4.33	5.60	6.28	1.0	33.4
(40)	2.25 B	4.37	4.70	5.06	5.4	33.9
	0.75 B	4.40	4.44	5.17	1.1	34.1
Wirand 0.30 x 25	1.50 B	4.26	5.25	5.36	2.0	34.7
(83.33)	2.25 B	4.63	5.95	6.17	1.0	34.0
	0.75	4.26	4.37	4.50	1.33	35.3
Melt Extract (ME430)	1.50	4.18	5.11	5.48	2.6	33.0
0.4 x 25	2.25	4.26	5.07	5.40	1.9	32.7
(62.5)						
	0.75	4.37	4.63	5.61	3.0	36.4
Melt Extract (ME430)	1.50	4.63	5.56	5.78	1.6	36.7
0.5 x 35	2.25	4.41	6.33	6.70	2.1	34.3
(70)						
	0.75	3.71	4.11	4.30	6.1	29.7
Binding Wire 0.71 x 71	1.50	3.71	7.11	7.50	1.3	31.6
(100)	2.25	3.74	7.22	9.39	4.2	31.3
	1.25	4.28	6.00	9.23	6.3	33.1
#	1.50	4.22	6.30	8.00	4.2	33.5

† = Determined by visual inspection and/or by flick of load indicator

B = Brass-coated

* = Plain, unreinforced concrete prisms

= Repeat test

Table 7.3 : Properties of flexural prisms fully reinforced

Type and size of fibre (diam. x length, mm)	% Fibre by volume	Control modulus of rupture (MPa)*	Flexural cracking strength (MPa)†	Ultimate flexural strength (MPa)	Coefficient of variation (%)	Cube strength (MPa)
	0.75 B	5.44	5.50	5.50	2.0	36.3
Shreddic 0.25 x 10	1.50 B	4.33	5.98	6.68	3.4	33.4
(40)	2.25 B	4.37	5.15	5.48	2.6	33.9
	0.75 B	4.40	4.33	4.48	3.2	34.1
Wirand 0.30 x 25	1.50 B	4.26	5.40	5.68	1.3	34.7
(83.33)	2.25 B	4.63	5.60	5.89	6.6	34.0
	0.75	4.26	4.63	4.78	1.9	35.3
Melt Extract (ME430)	1.50	4.18	4.78	4.96	6.4	33.0
0.4 x 25	2.25	4.26	5.74	6.04	3.7	32.7
(62.5)						
	0.75	4.37	5.50	6.78	5.7	36.4
Melt Extract (ME430)	1.50	4.63	5.61	5.67	5.8	36.7
0.5 x 35	2.25	4.41	7.07	7.67	2.1	34.3
(70)						
	0.75	3.71	4.52	4.89	9.9	29.7
Binding Wire 0.71 x 71	1.50	3.71	7.55	9.41	8.6	31.6
(100)	2.25	3.74	7.63	10.15	20.0	31.3
	1.25	4.28	6.67	9.13	9.5	33.1
#	1.50	4.22	6.07	8.26	10.5	33.5

† = Determined by visual inspection and/or by flick of load indicator

B = Brass-coated

* = Plain, unreinforced concrete prisms

= Repeat test

Table 7.4 : Shear strengths of SFRC samples

Type and size of fibre (diam. x length, mm)	% Fibre by volume	Control unreinforced (MPa)	Partially reinforced (MPa)	Coefficient of variation (%)	Fully reinforced (MPa)	Coefficient of variation (%)	Cube strength (MPa)
Shreddic 0.25 x 10	0.75	2.52	2.24	17.5	3.38	7.8	36.3
	1.50	2.06	2.56	6.0	3.61	10.1	33.4
	2.25	1.92	2.16	3.6	2.68	2.4	33.9
Wirand 0.30 x 25	0.75	1.93	2.03	11.1	2.42	4.9	34.1
	1.50	1.92	2.48	14.0	2.62	11.9	34.7
	2.25	1.84	2.27	21.6	2.72	11.4	34.0
Melt Extract (ME430)	0.75	1.78	2.18	4.4	2.28	6.6	35.3
	1.50	1.67	2.48	5.2	2.74	9.5	33.0
	2.25	1.67	2.67	9.2	2.96	9.2	32.7
Melt Extract (ME430)	0.75	1.79	2.55	7.8	2.75	3.8	36.4
	1.50	1.83	2.87	5.6	2.71	5.2	36.7
	2.25	1.81	2.89	12.2	3.24	7.0	34.5
Binding Wire 0.71 x 71	0.75	1.82	2.21	8.2	2.37	11.8	31.6
	1.50	1.85	2.36	8.1	3.84	9.2	33.5
	2.25	1.93	2.23	28.4	4.96	17.8	31.3

Table 7.5 : Results of cube compression test

Type and size of fibre (diam. x length, mm)	% Fibre by volume	Relative increase (%) after 3 days			Relative increase (%) after 7 days			Relative increase (%) after 14 days		
		Control (MPa)	Fibre (MPa)	Increase (%)	Control (MPa)	Fibre (MPa)	Increase (%)	Control (MPa)	Fibre (MPa)	Increase (%)
Shreddic 0.25 x 10	0.75	24.5	28.6	17	36.3	39.6	9	40.8	45.5	12
	1.50	23.8	29.5	24	33.4	43.3	30	39.3	48.5	23
	2.25	24.9	32.1	29	33.9	43.3	28	40.4	50.3	24
Wirand 0.30 x 25	0.75	26.5	30.2	14	34.0	39.3	16	41.3	44.7	8
	1.50	25.2	31.5	25	34.7	45.1	30	40.4	49.7	23
	2.25	26.2	36.5	38	34.0	47.5	40	41.4	51.8	25
Melt Extract (ME430) 0.4 x 25	0.75	25.8	28.4	10	35.3	40.8	16	42.0	47.1	12
	1.50	23.5	28.7	22	33.0	39.3	19	41.3	46.3	12
	2.25	21.4	28.6	34	32.7	38.3	17	39.4	45.9	16
Melt Extract (ME430) 0.5 X 35	0.75	26.2	29.7	13	36.4	39.3	10	42.3	45.9	8.5
	1.50	27.6	32.2	17	36.7	41.0	12	40.3	47.1	11
	2.25	27.8	33.6	21	34.3	39.0	14	39.7	45.6	14
Binding Wire 0.71 x 71	0.75	23.6	26.7	13	29.7	32.5	10	33.1	36.1	8
	1.50	22.3	30.5	37	31.6	42.9	30	38.6	45.7	18
	2.25	21.5	26.2	22	31.3	36.8	18	38.9	43.1	11

Table 7.6 : ACI impact test results

Description	Type of fibre and dimensions (diam. x length, mm)			
	Wirand 0.3 x 25	ME430(25mm) 0.4 x 25	ME430(35mm) 0.5 x 35	Binding Wire 0.71 x 71
Control impact strength				
- blows to first-crack, (c.o.v %)	6 (23.8)	24 (17,3)	20 (7.1)	10 (7.0)
- blows to failure, (c.o.v %)	10 (7.4)	31 (12.4)	31 (20.7)	14 (6.5)
Composite impact strength				
- blows to first-crack, (c.o.v %)	28 (39.4)	46 (22.0)	46 (11.7)	88 (42.0)
- blows to failure, (c.o.c %)	111 (7.1)	132 (16.2)	121 (19.5)	312 (22.8)
Control cube strength	33.4	33.0	35.2	32.9

† c.o.v = coefficient of variation

Table 7.7 : Correlation of flexural strength prediction equations with experimental results

Method of analysis		Equation constants		Flexural strength (experiment) / Flexural strength (calculated)	
		constant A	constant B	Mean	coefficient of variation (%)
Swamy and Mangat	CR	0.877	1.474	0.998	8.4
	ULT	0.873	2.072	0.993	14.0
	CR	0.963	1.371	1.000	10.7
	ULT	0.932	2.010	1.000	15.5
$V_f \frac{\ell}{D}$ vs	CR	0.882	1.465	0.996	8.4
	ULT	0.919	1.760	1.012	14.2
	CR	0.906	1.177	1.085	10.8
	ULT	0.924	1.973	1.011	15.9
$W_f \frac{\ell}{D}$ vs	CR	0.912	1.320	1.000	8.6
	ULT	0.908	1.908	0.995	14.0
	CR	1.000	1.200	0.994	10.8
	ULT	0.912	2.128	0.990	15.1

Table 7.8 : Toughness Indices of SFRC specimens

Beam type		Area up to first-crack Nmm^2	Area up to 1.9mm deflection Nmm^2	Toughness Index	
1.50% V_f					
PARTIALLY REINFORCED	1	550	4299	7.81	
	2	825	5044	6.24	6.79
	3	803	5070	6.32	
FULLY REINFORCED	1	413	5298	12.83	
	2	525	5296	10.09	10.68
	3	932	5777	9.13	
1.25% V_f					
PARTIALLY REINFORCED	1	-	-	-	
	2	806	4702	5.84	5.98
	3	840	5138	6.17	
FULLY REINFORCED	1	825	5278	6.40	
	2	1056	5798	7.37	5.93
	3	1020	6188	5.91	

KEY TO FIGURES 7.1 THROUGH 7.40

COLOUR	FIBRE TYPE	SERIES NO.
	SHREDDIC	A
	WIRAND	B
	ME430(25mm)	C
	ME430(35mm)	D
	BINDING WIRE	E

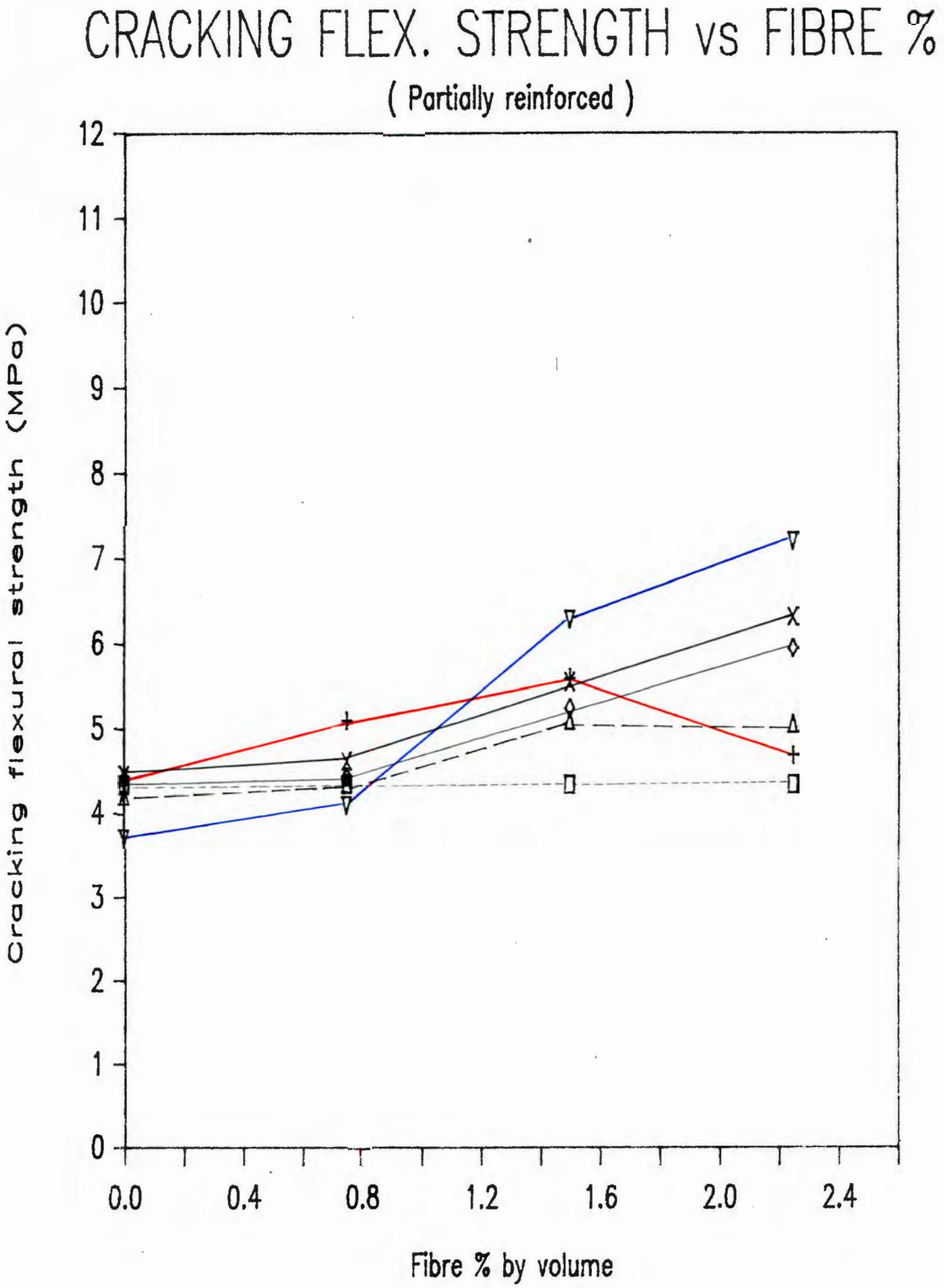
CRACKING FLEX. STRENGTH vs FIBRE %
(Partially reinforced)
Cracking flexural strength (MPa)
12
11
10
9
8
7
6
5
4
3
2
1
0
0.0
0.4
0.8
1.2
1.6
2.0
2.4
Fibre % by volume

Figure 7.1

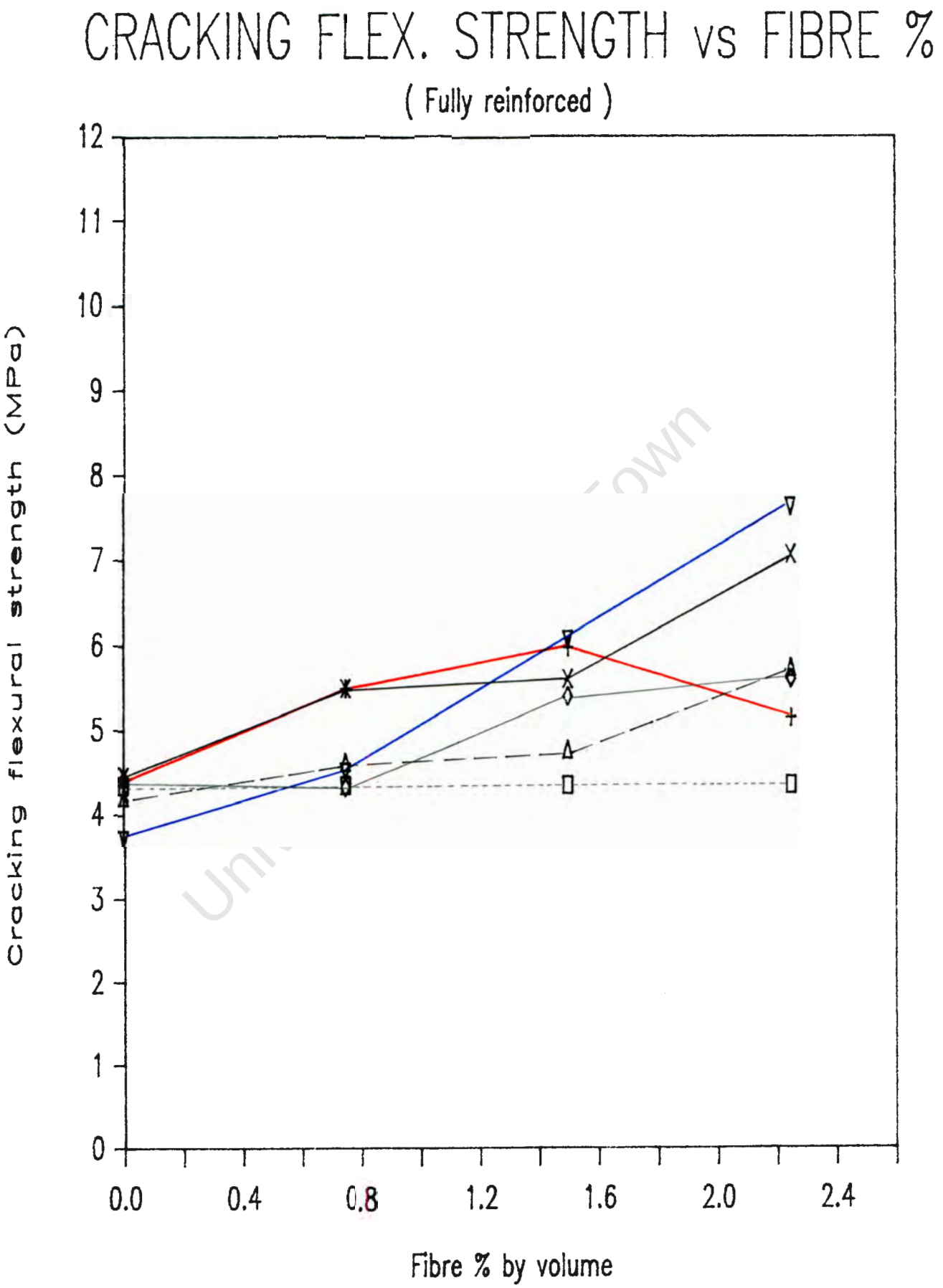
CRACKING FLEX. STRENGTH vs FIBRE %
(Fully reinforced)
Cracking flexural strength (MPa)
12
11
10
9
8
7
6
5
4
3
2
1
0
0.0
0.4
0.8
1.2
1.6
2.0
2.4
Fibre % by volume

Figure 7.2

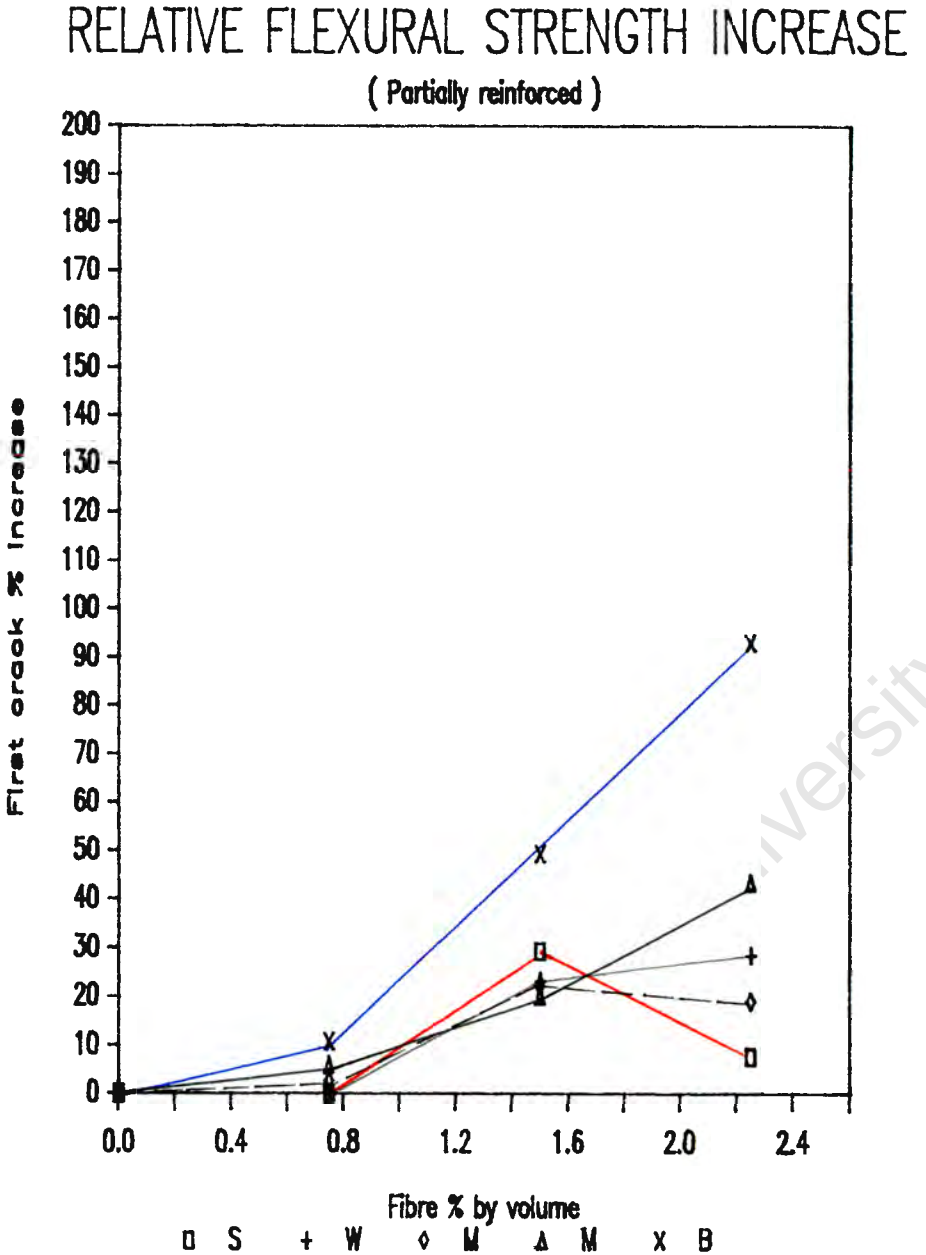

Figure 7.3

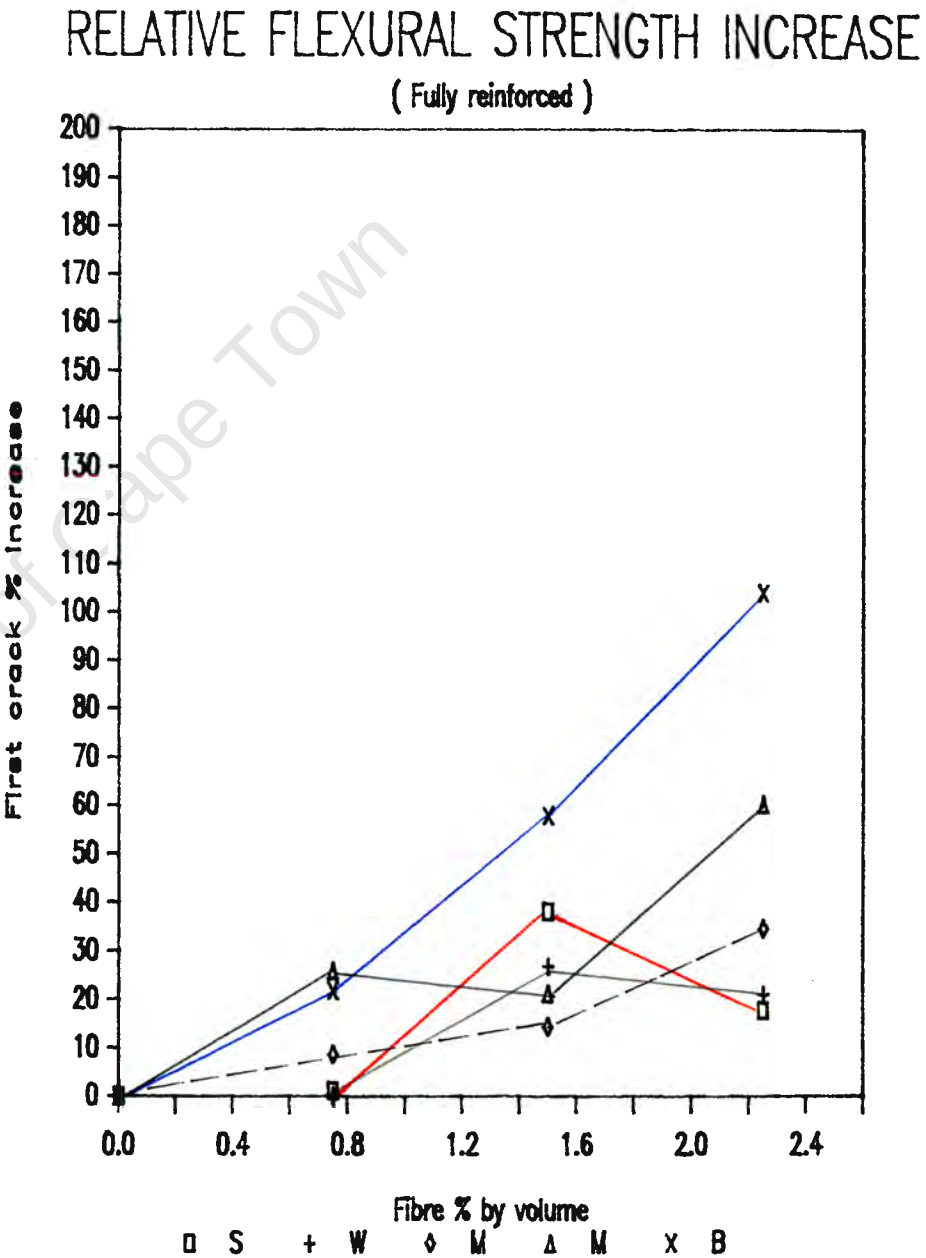

Figure 7.4

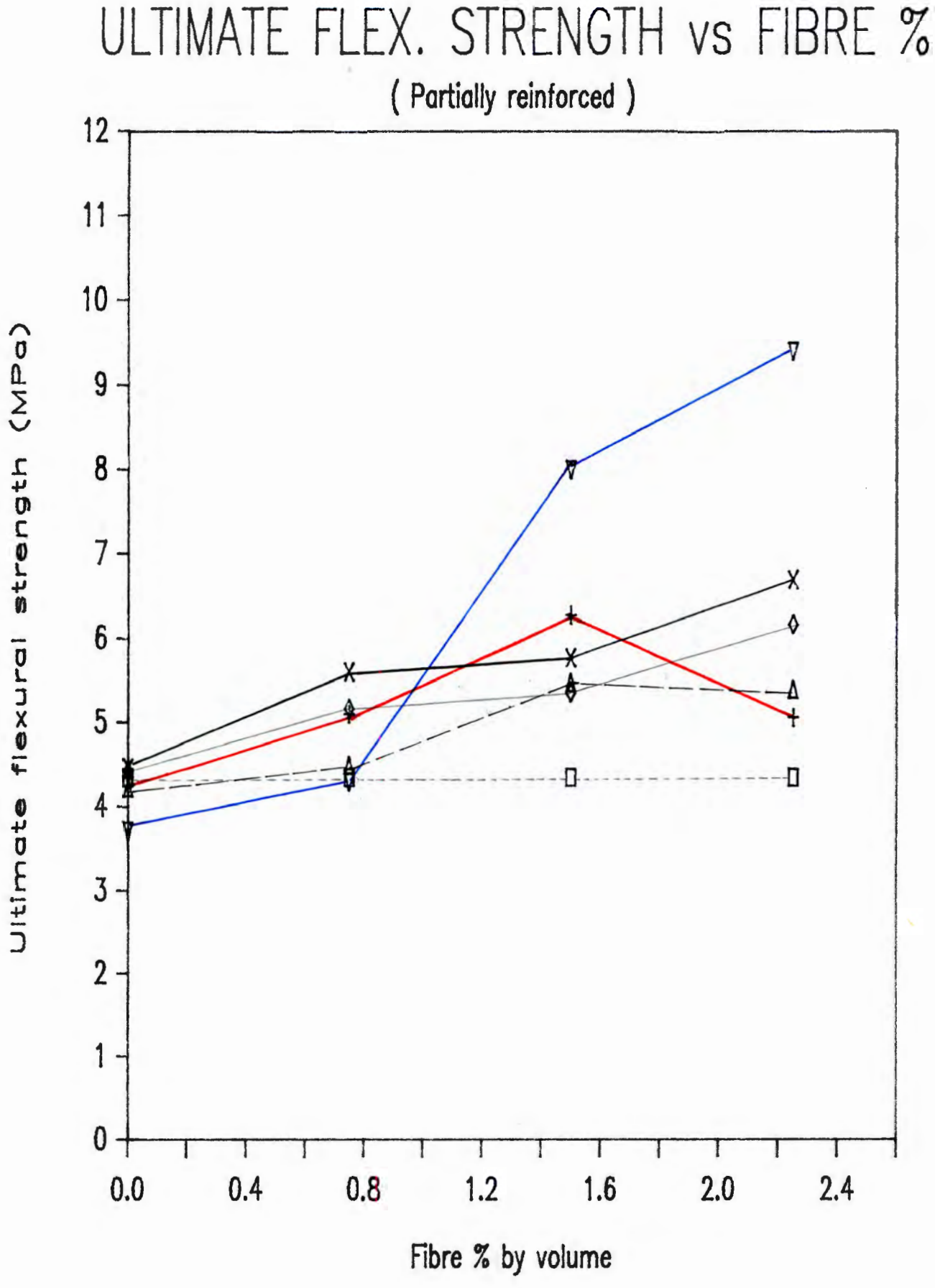
ULTIMATE FLEX. STRENGTH vs FIBRE %
(Partially reinforced)
Ultimate flexural strength (MPa)
12
11
10
9
8
7
6
5
4
3
2
1
0
0.0
0.4
0.8
1.2
1.6
2.0
2.4
Fibre % by volume

Figure 7.5

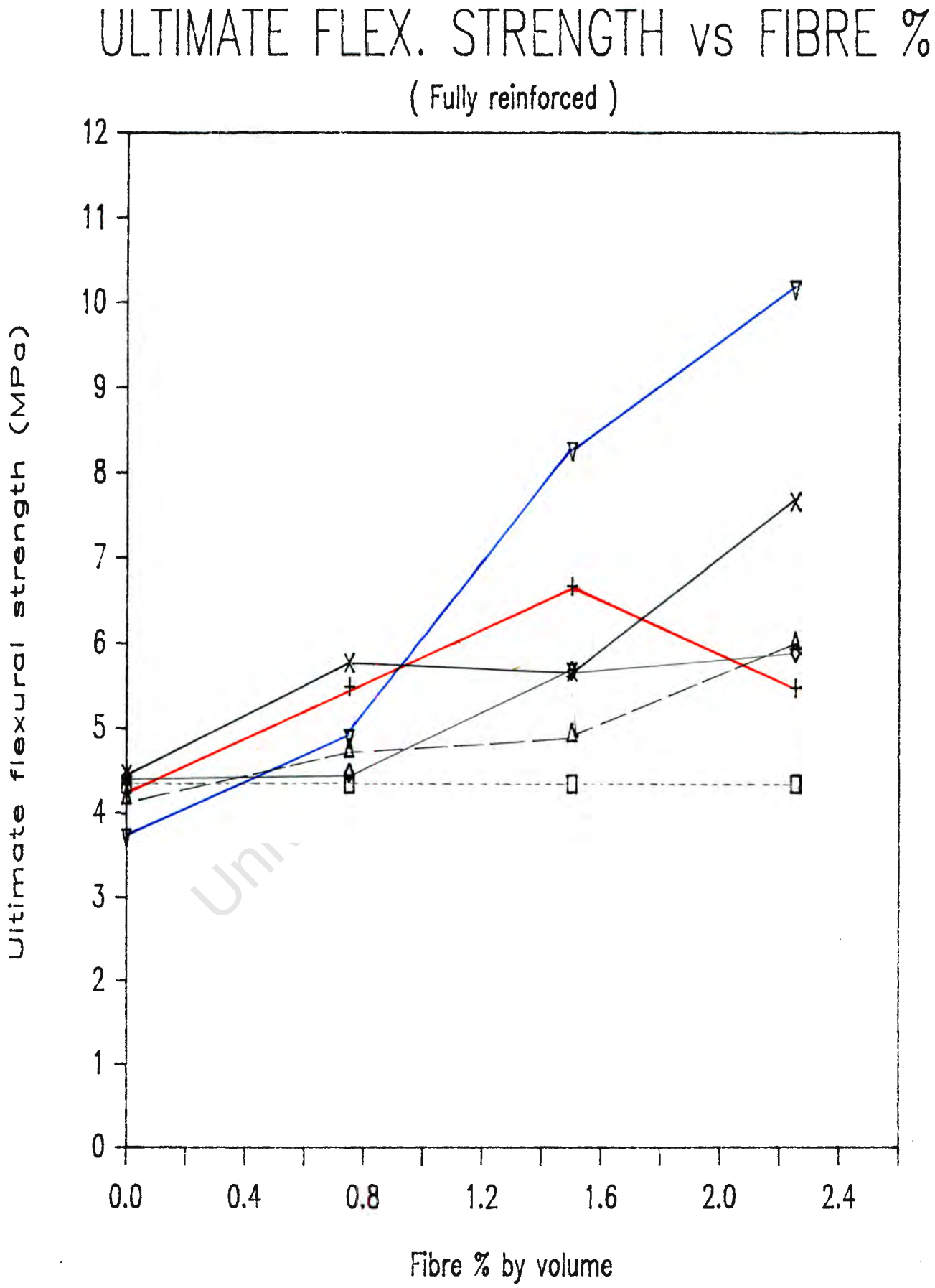
ULTIMATE FLEX. STRENGTH vs FIBRE %
(Fully reinforced)
Ultimate flexural strength (MPa)
12
11
10
9
8
7
6
5
4
3
2
1
0
0.0
0.4
0.8
1.2
1.6
2.0
2.4
Fibre % by volume

Figure 7.6

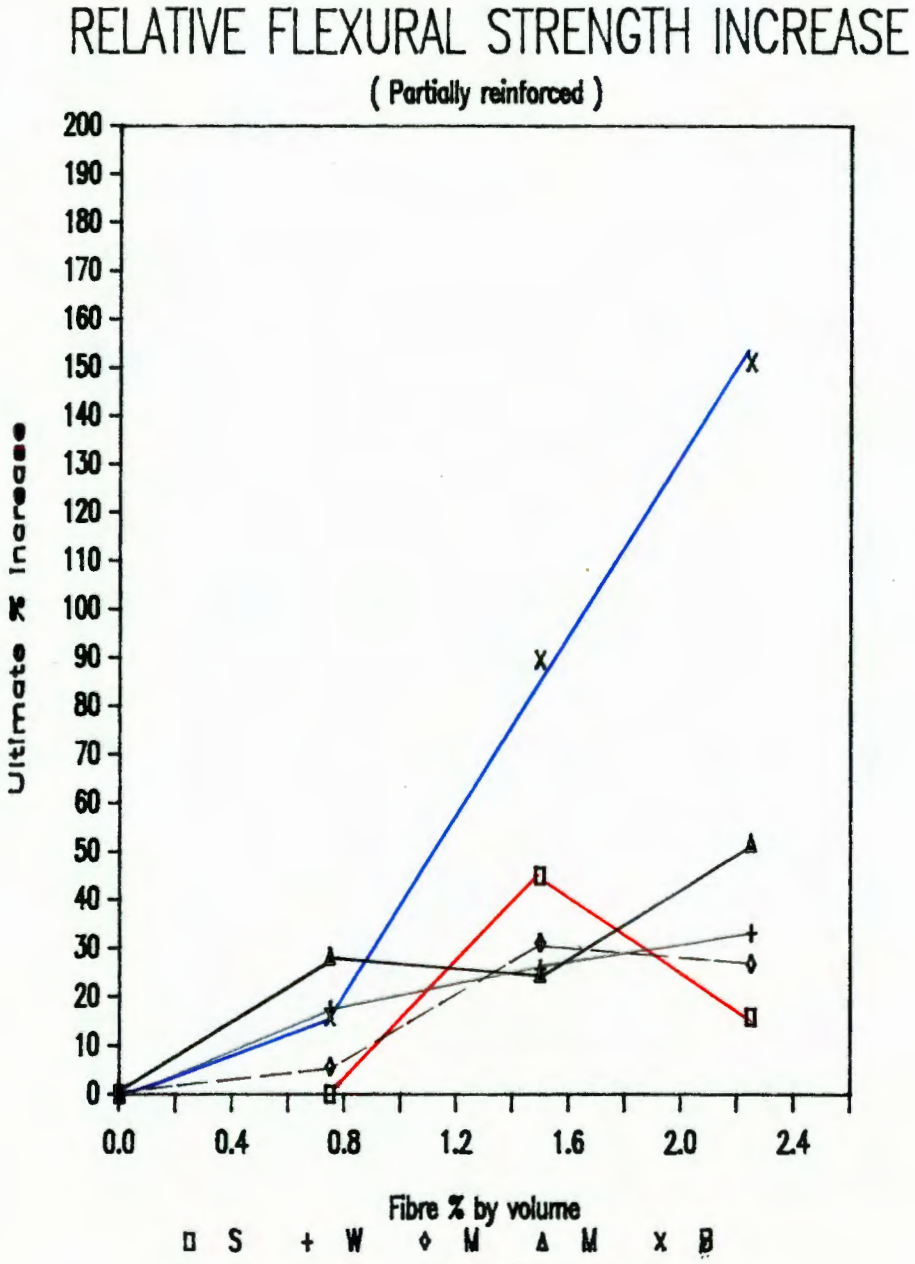

Figure 7.7

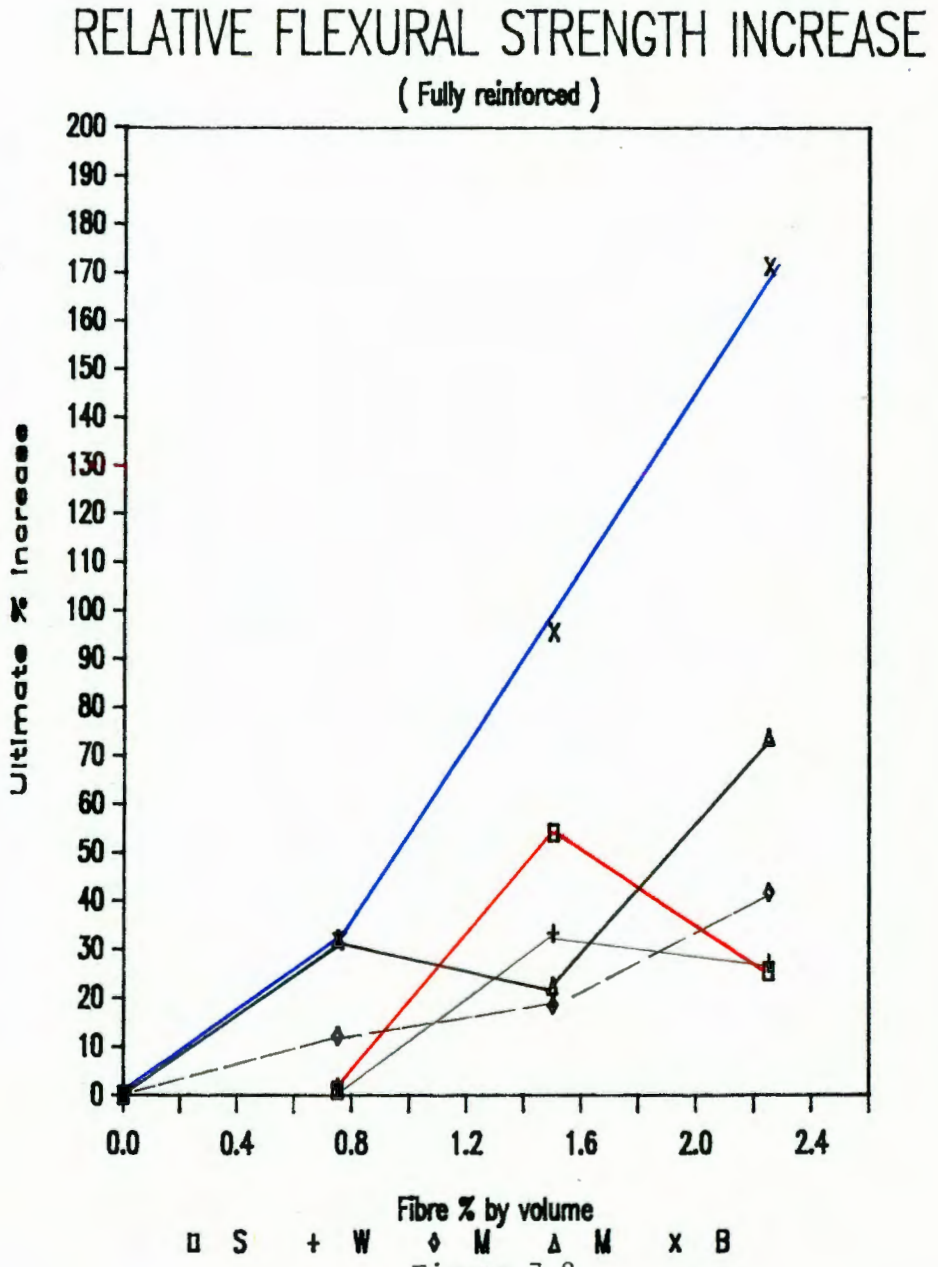

Figure 7.8

Figure 7.9 : Comparison of partially reinforced flexural strengths to fully reinforced flexural strengths

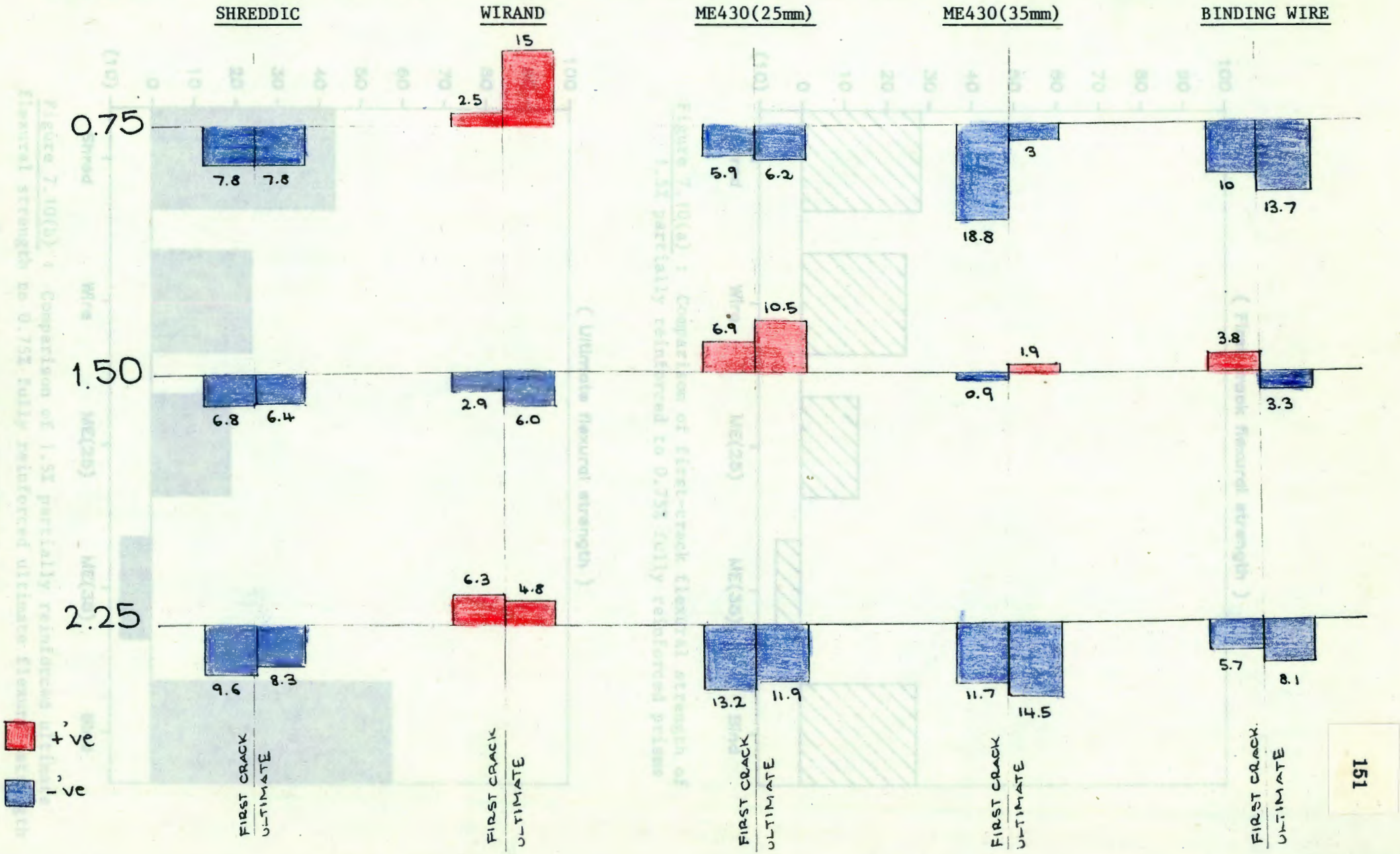

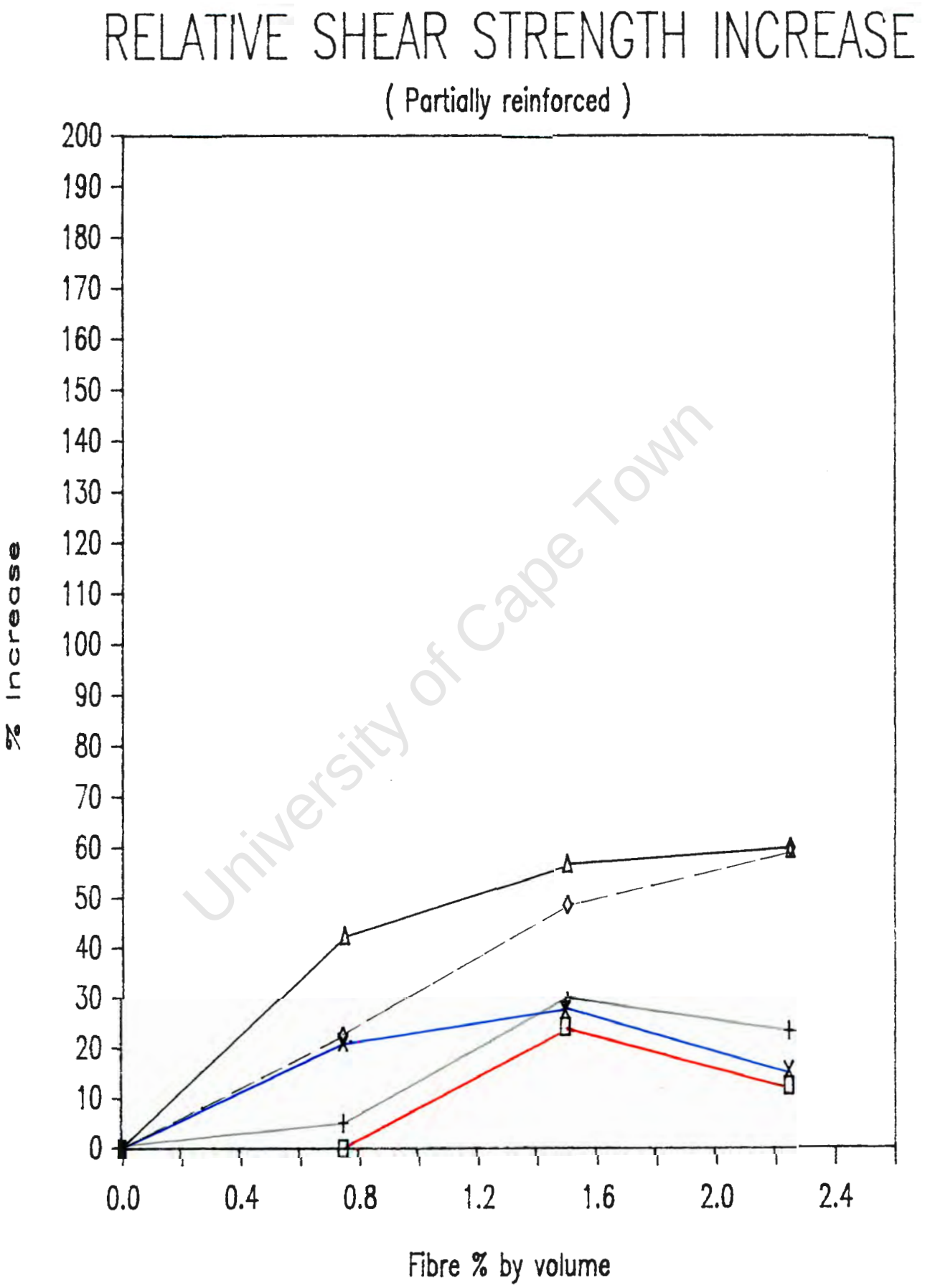

Figure 7.11

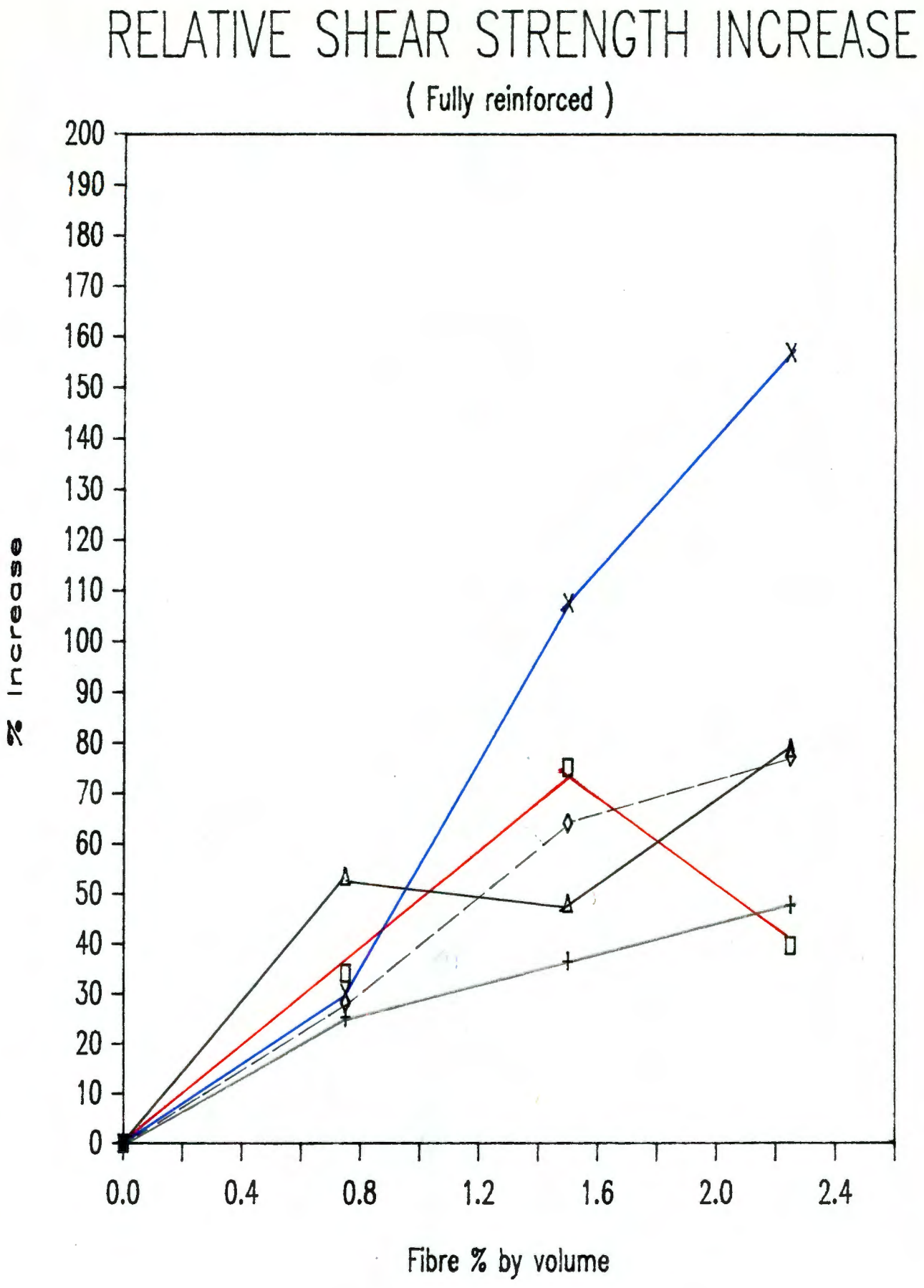
RELATIVE SHEAR STRENGTH INCREASE
(Fully reinforced)
% Increase
200
190
180
170
160
150
140
130
120
110
100
90
80
70
60
50
40
30
20
10
0
0.0
0.4
0.8
1.2
1.6
2.0
2.4
Fibre % by volume

Figure 7.12

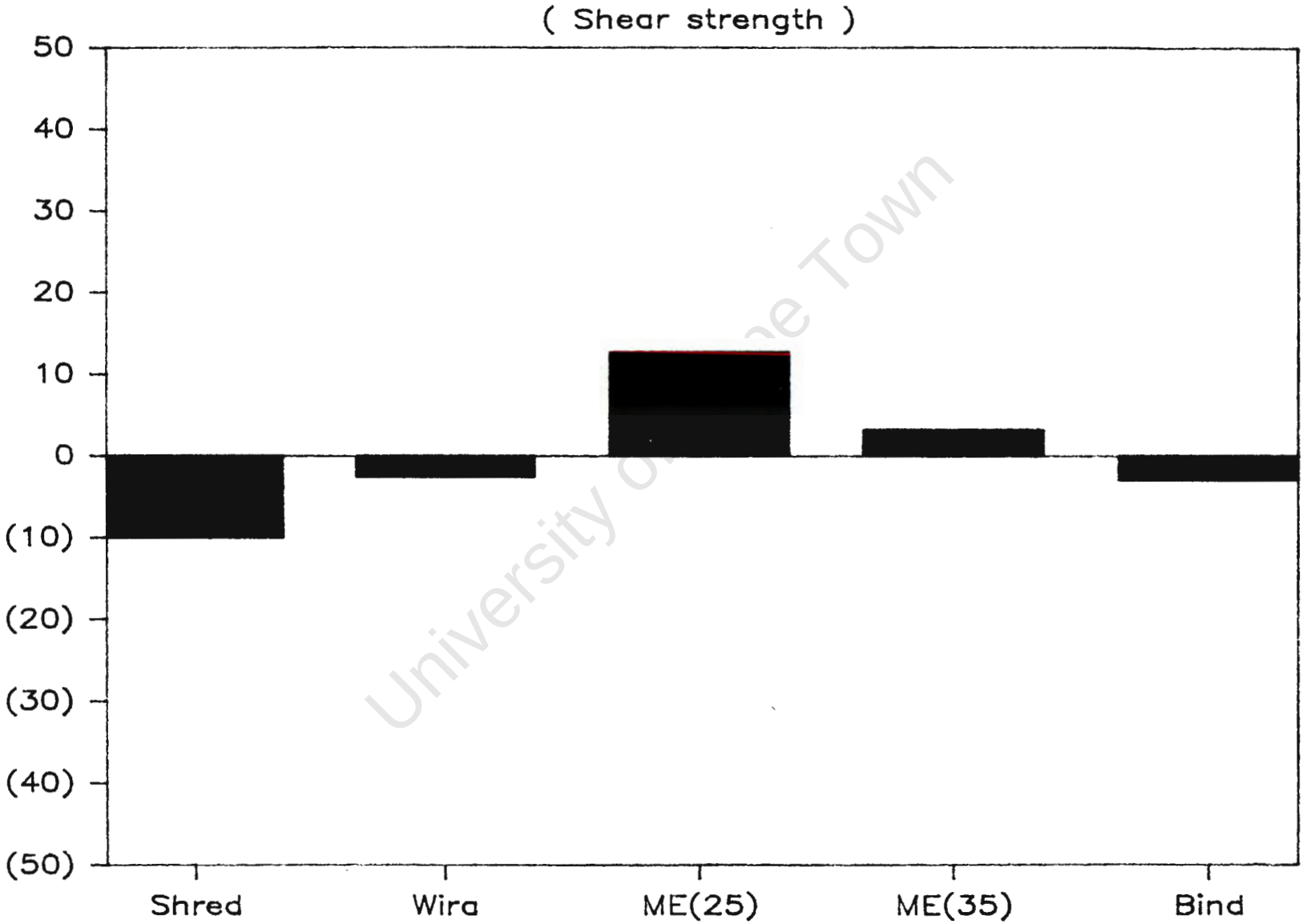

Figure 7.13 : Comparison of 1.5% partially reinforced shear strength to 0.75% fully reinforced shear strength

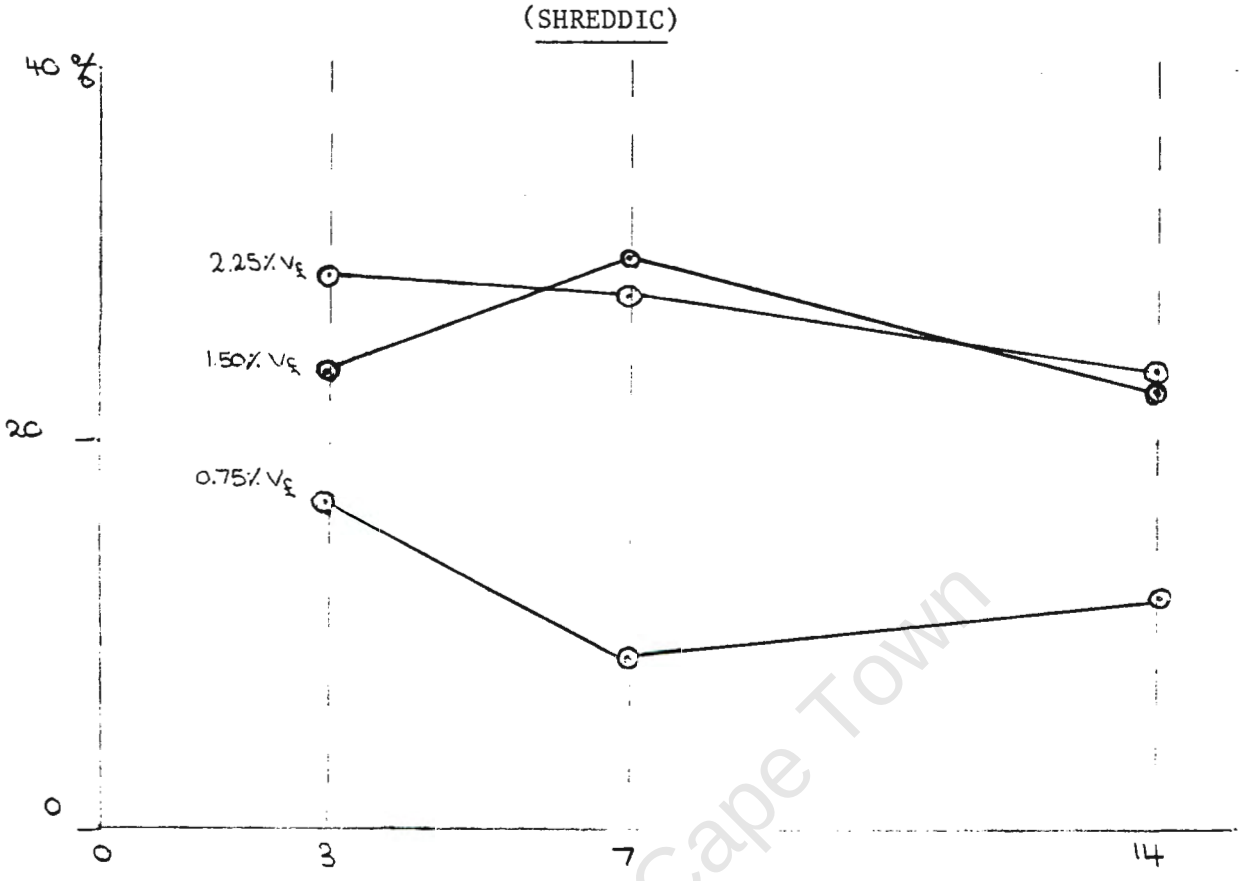

Figure 7.14(a) : Variation of relative compressive strength increase with increasing curing period

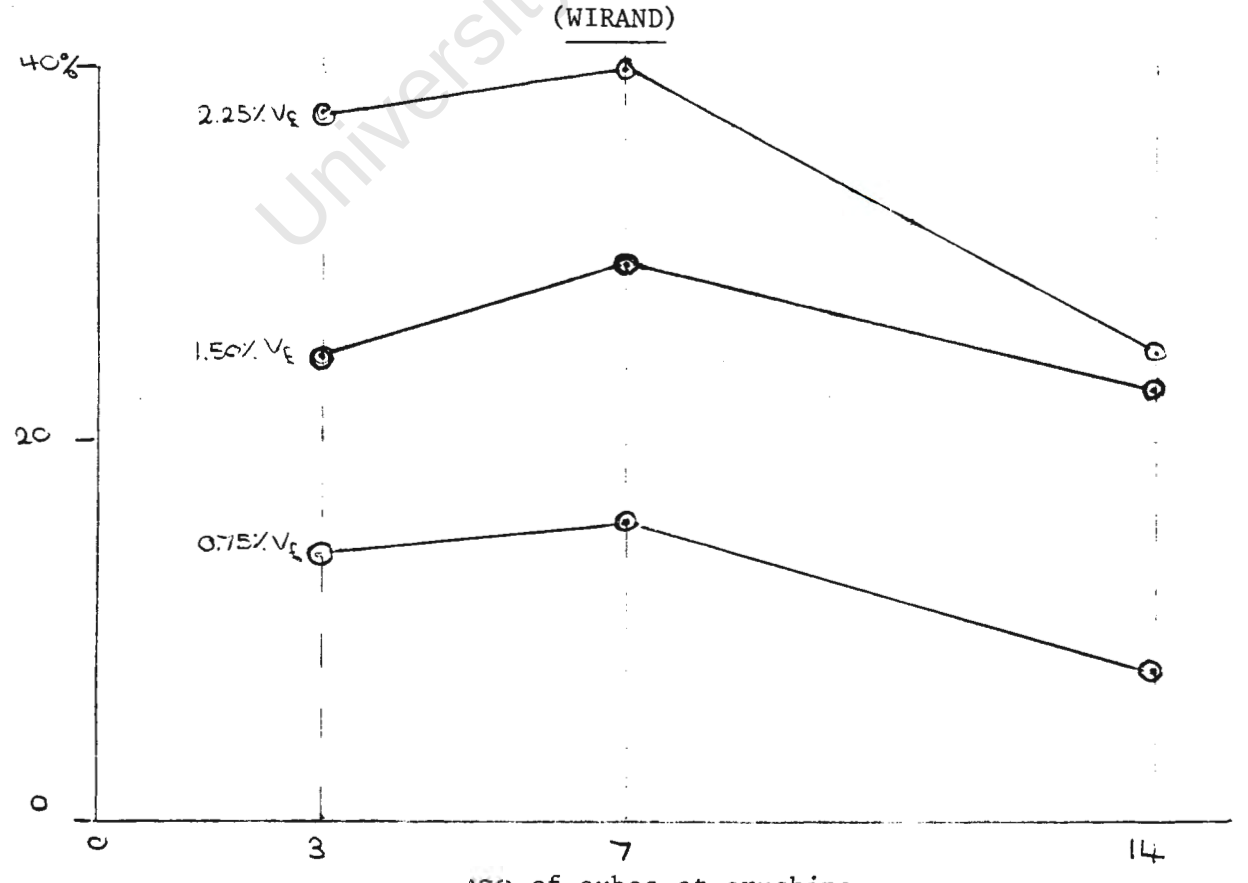

Figure 7.14(b) :

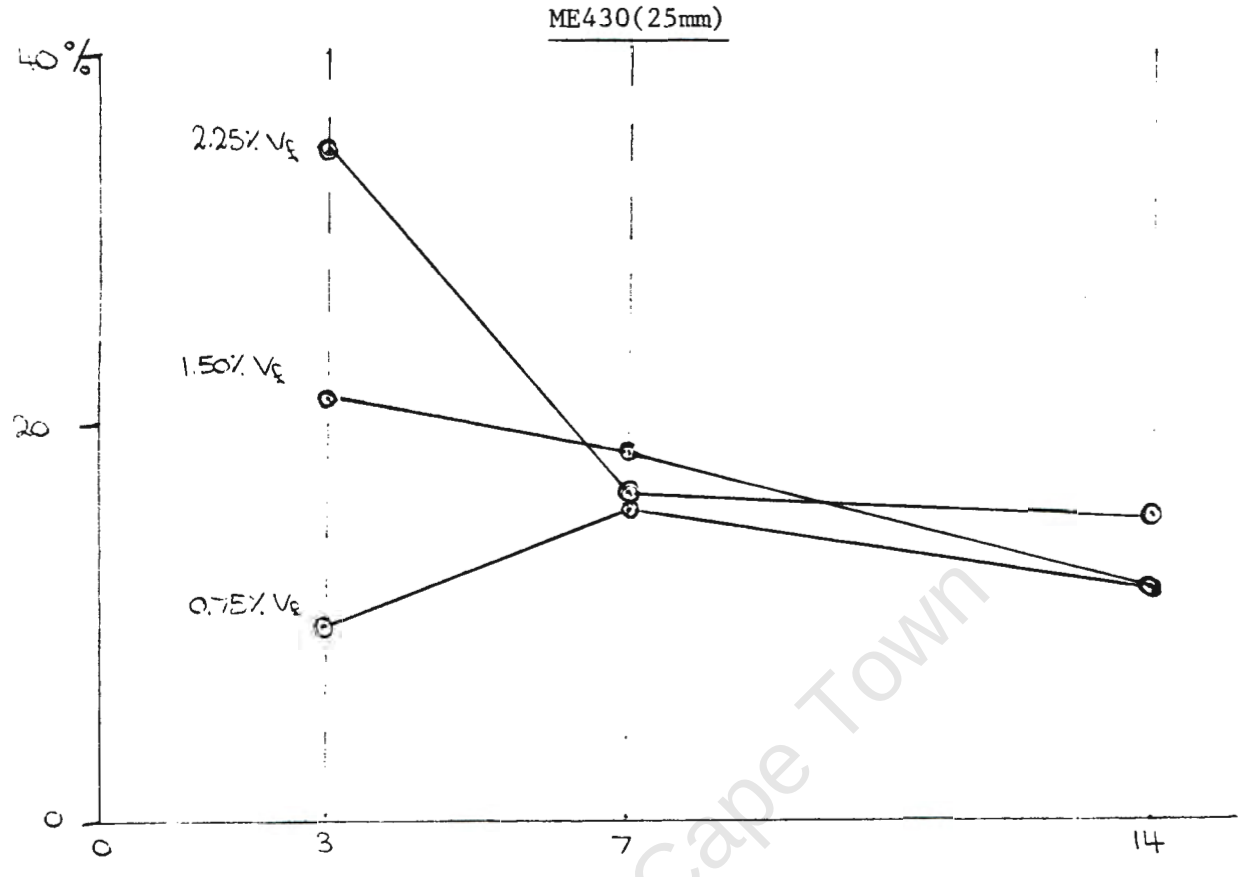

Figure 7.14(c) : Variation of relative compressive strength increase with increasing curing period

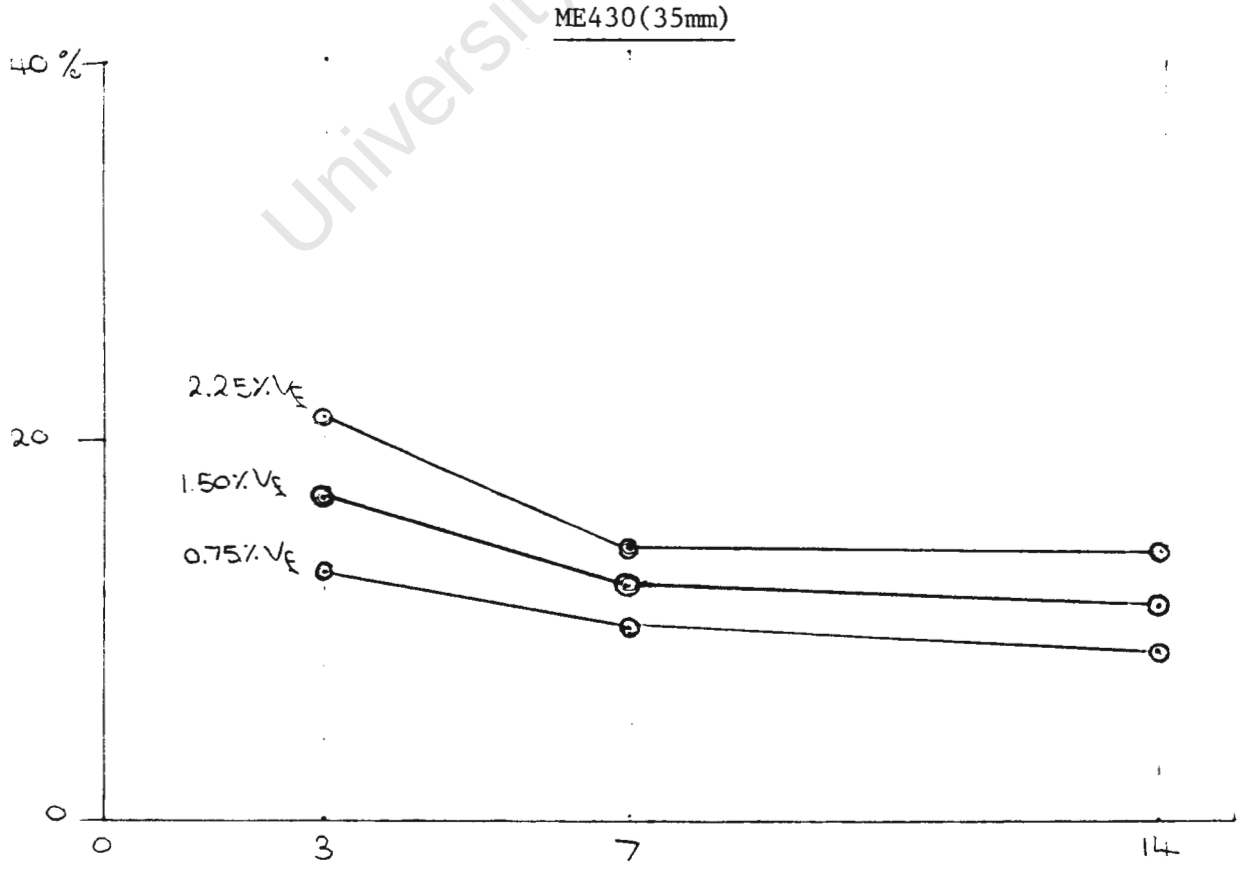

Figure 7.14(d) : age of cubes at crushing

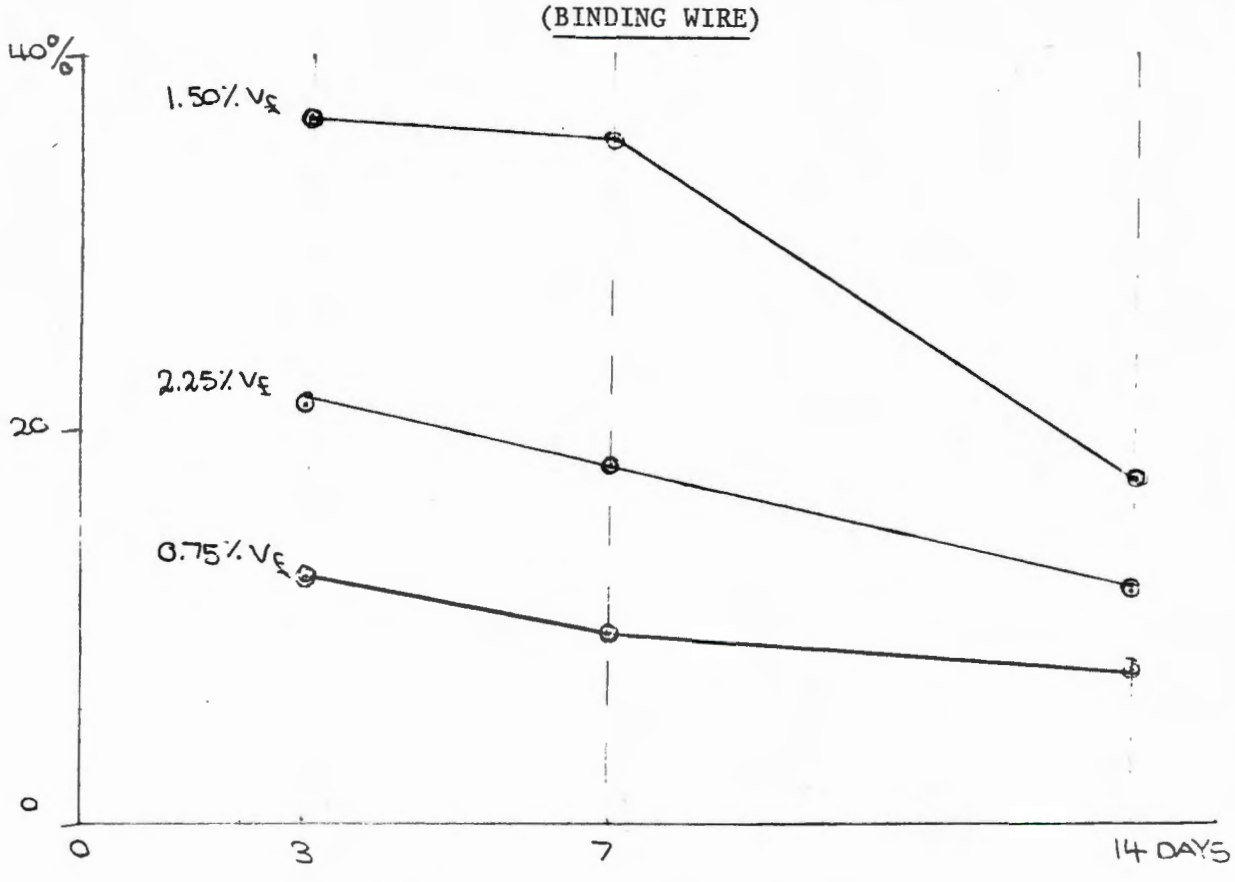

Figure 7.14(e) : Variation of relative compressive strength increase with increasing curing period

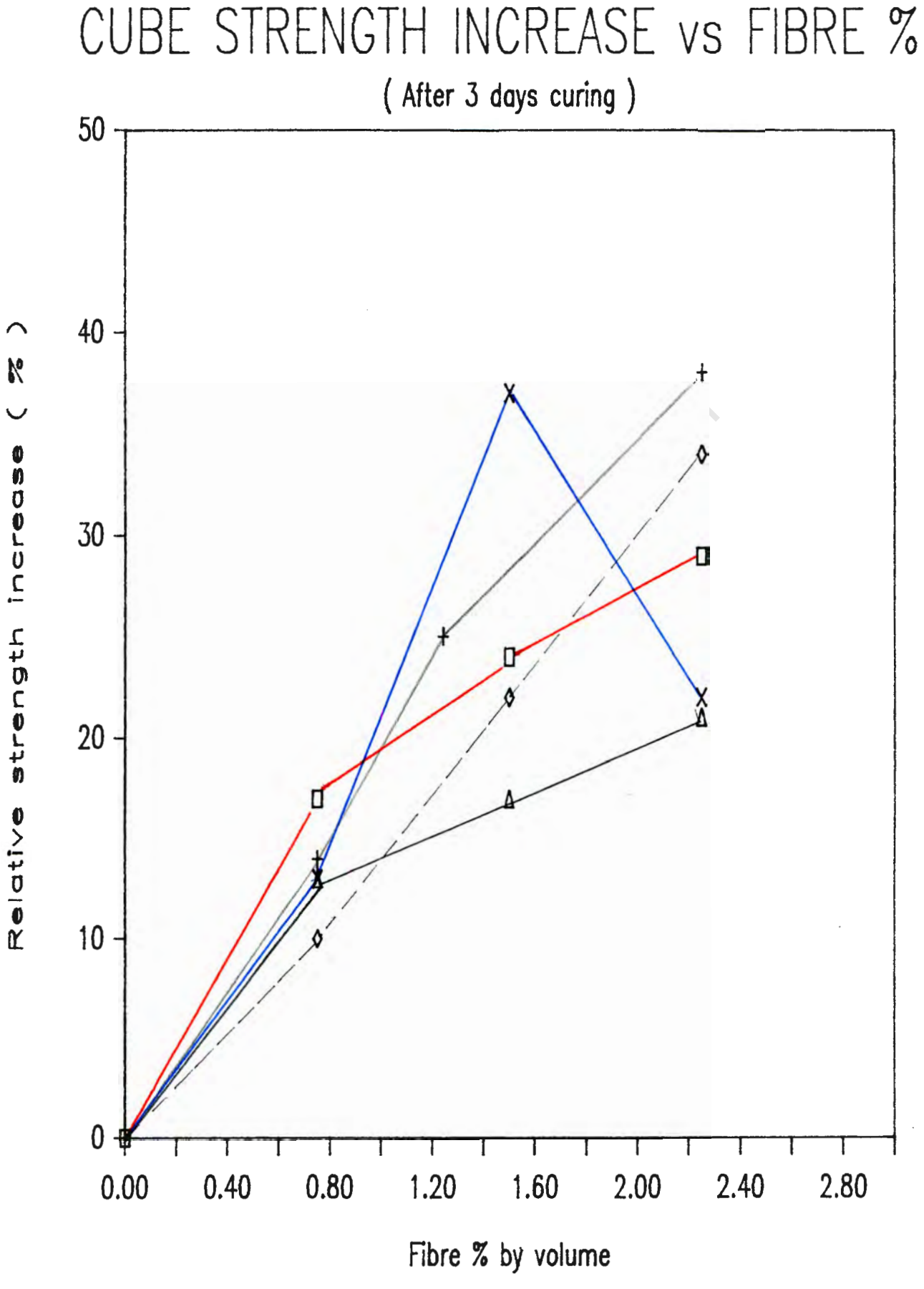
CUBE STRENGTH INCREASE vs FIBRE %
(After 3 days curing)
Relative strength increase (%)
50
40
30
20
10
0
0.00
0.40
0.80
1.20
1.60
2.00
2.40
2.80
Fibre % by volume

Figure 7.15

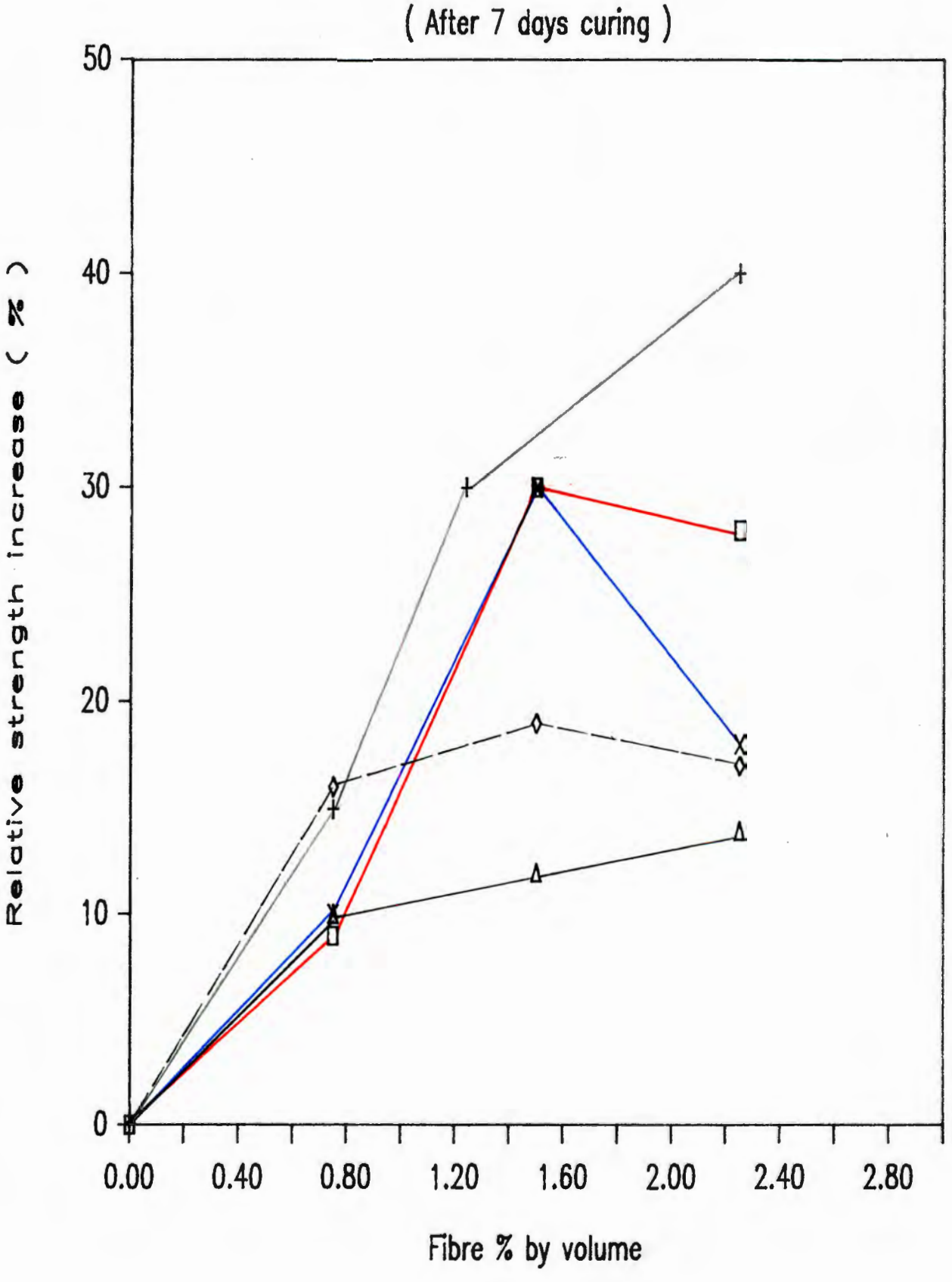
(After 7 days curing)
Relative strength increase (%)
50
40
30
20
10
0
0.00
0.40
0.80
1.20
1.60
2.00
2.40
2.80
Fibre % by volume

Figure 7.16

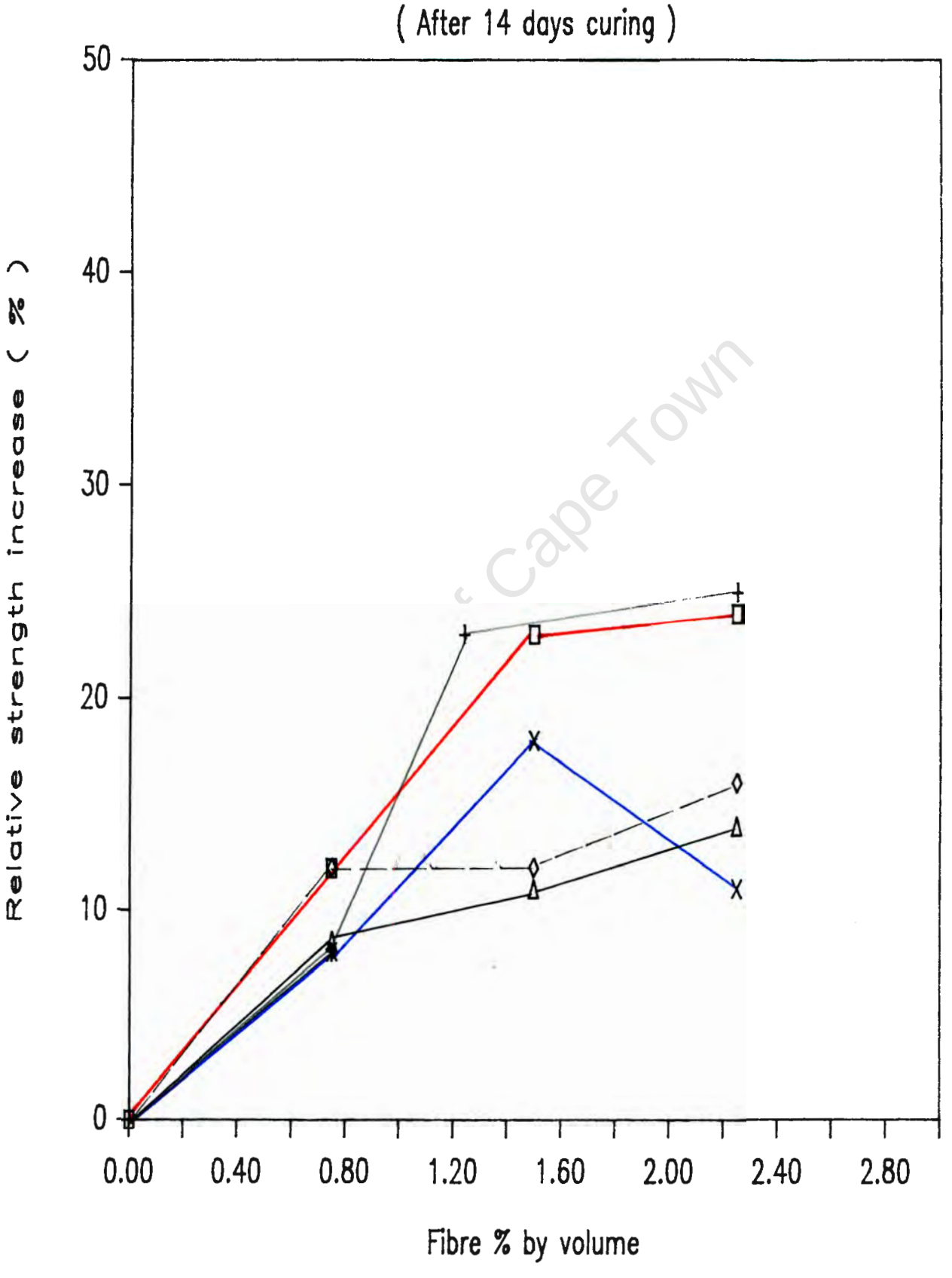

Figure 7.17

Figure 7.18 : SHAH AND MANGAT ANALYSIS METHOD

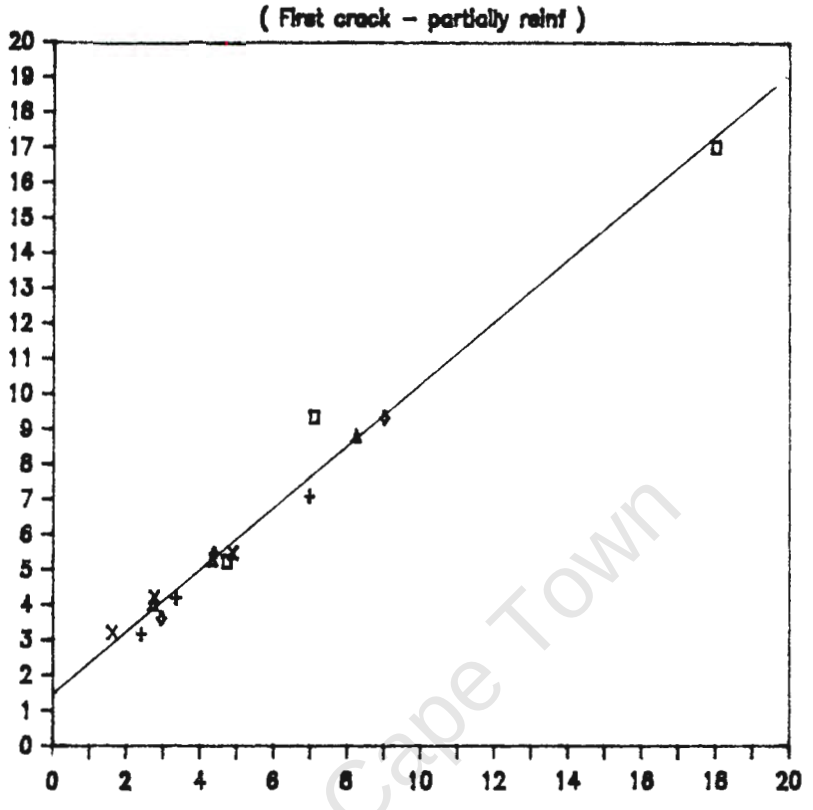

Figure 7.19 SHAH AND MANGAT ANALYSIS METHOD

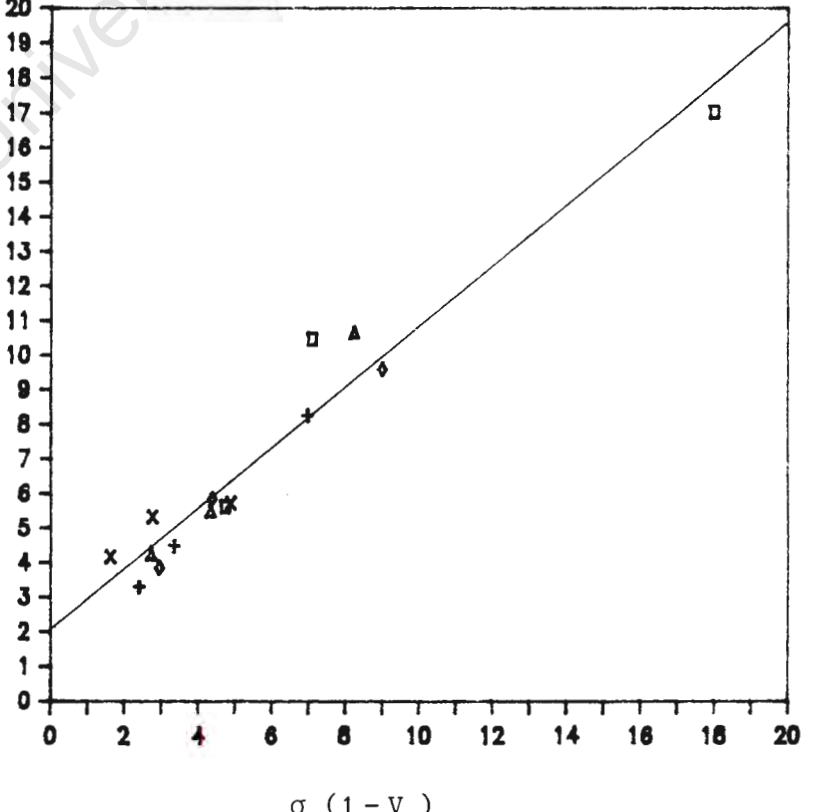

Figure 7.20 : SHAH AND MANGAT ANALYSIS METHOD

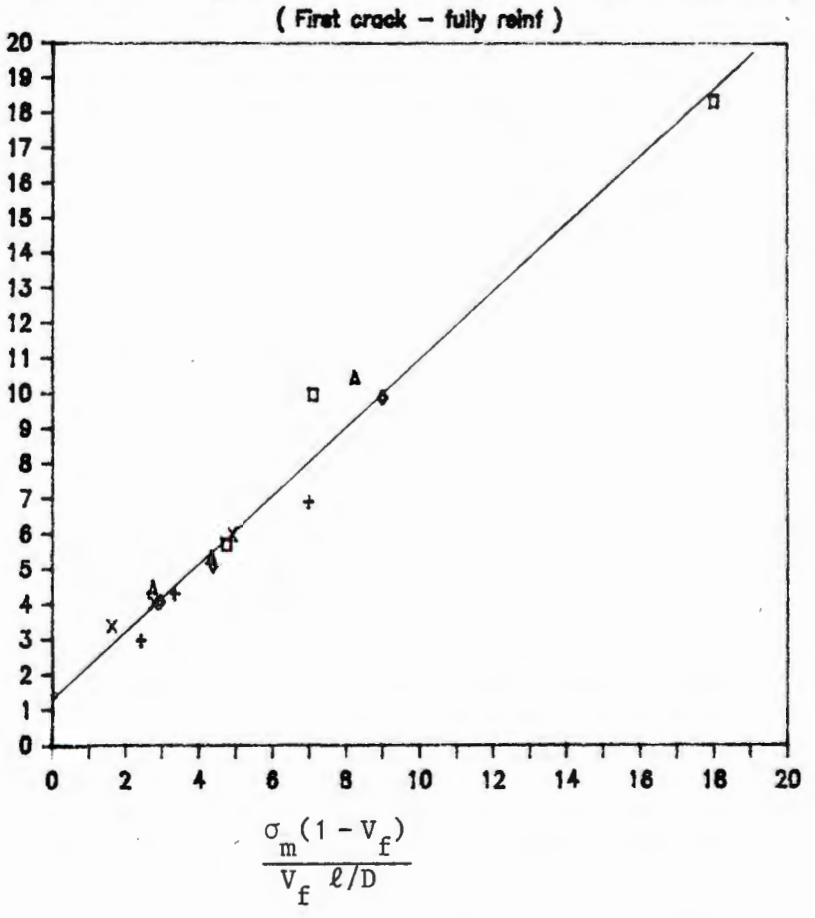

Figure 7.21 : SHAH AND MANGAT ANALYSIS METHOD

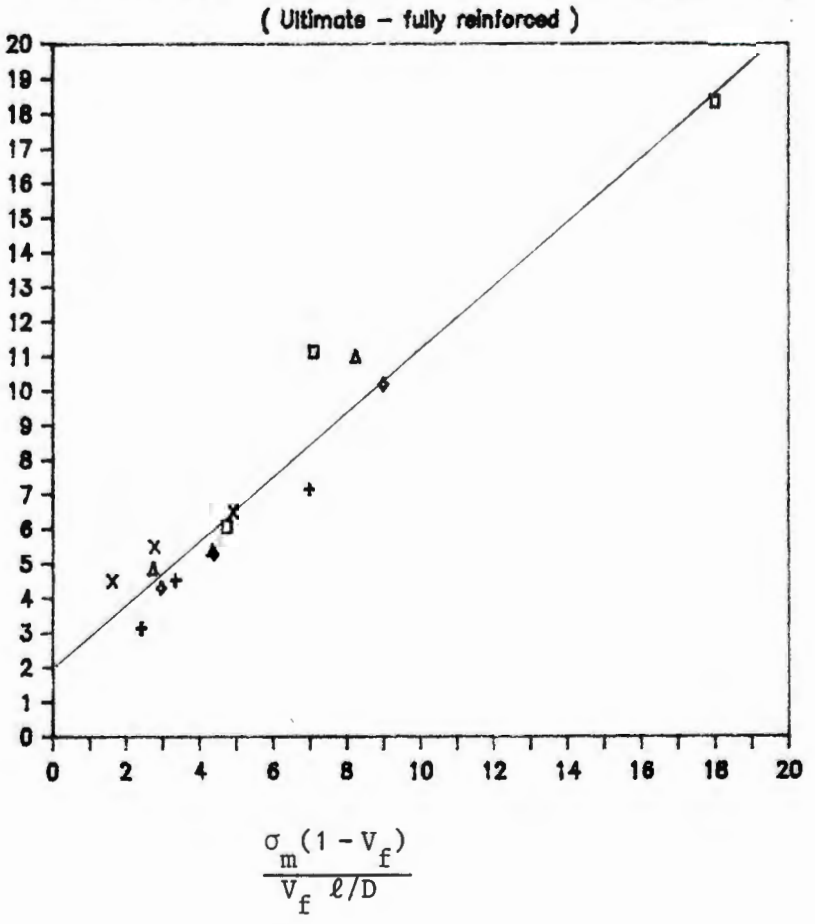

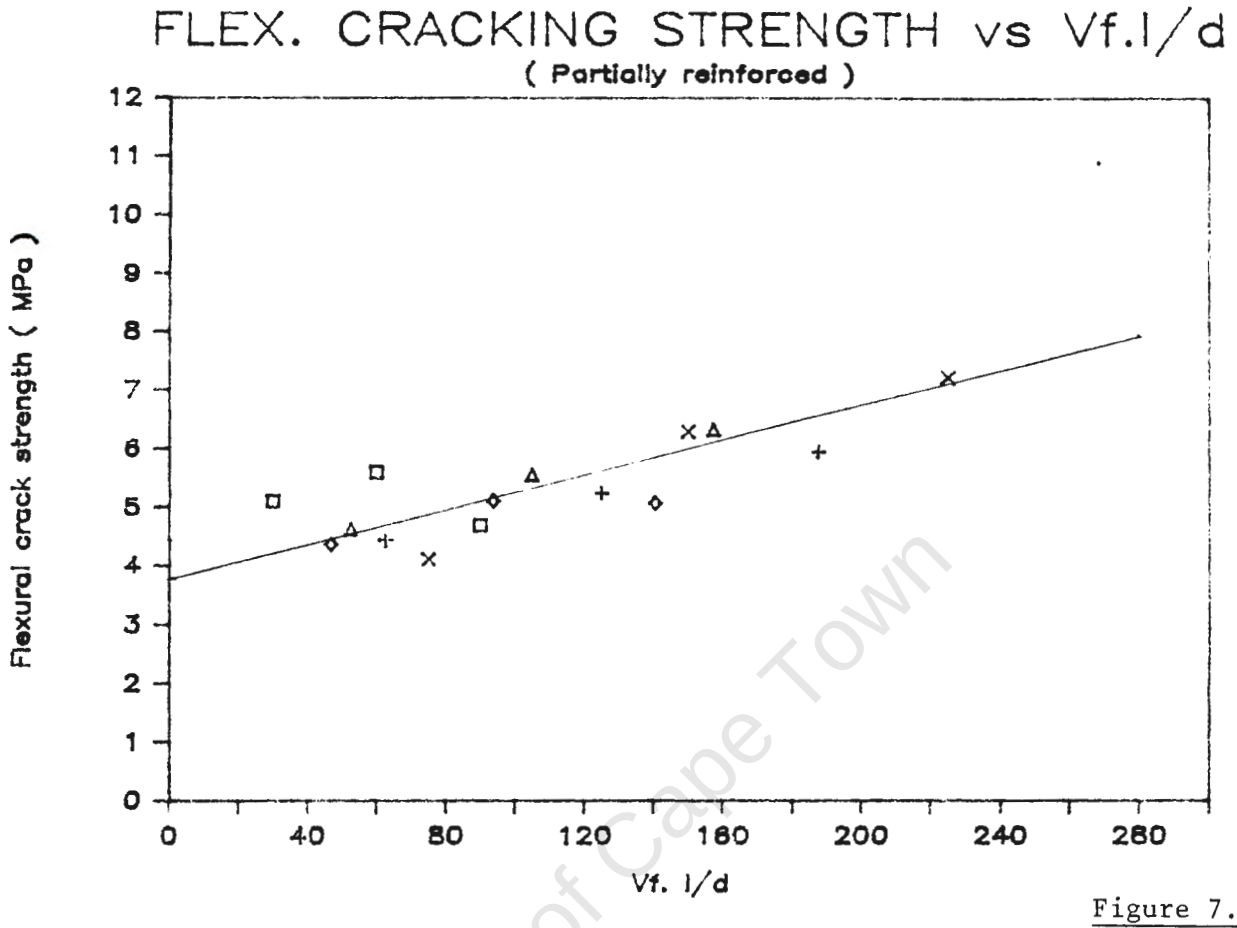

Figure 7.22

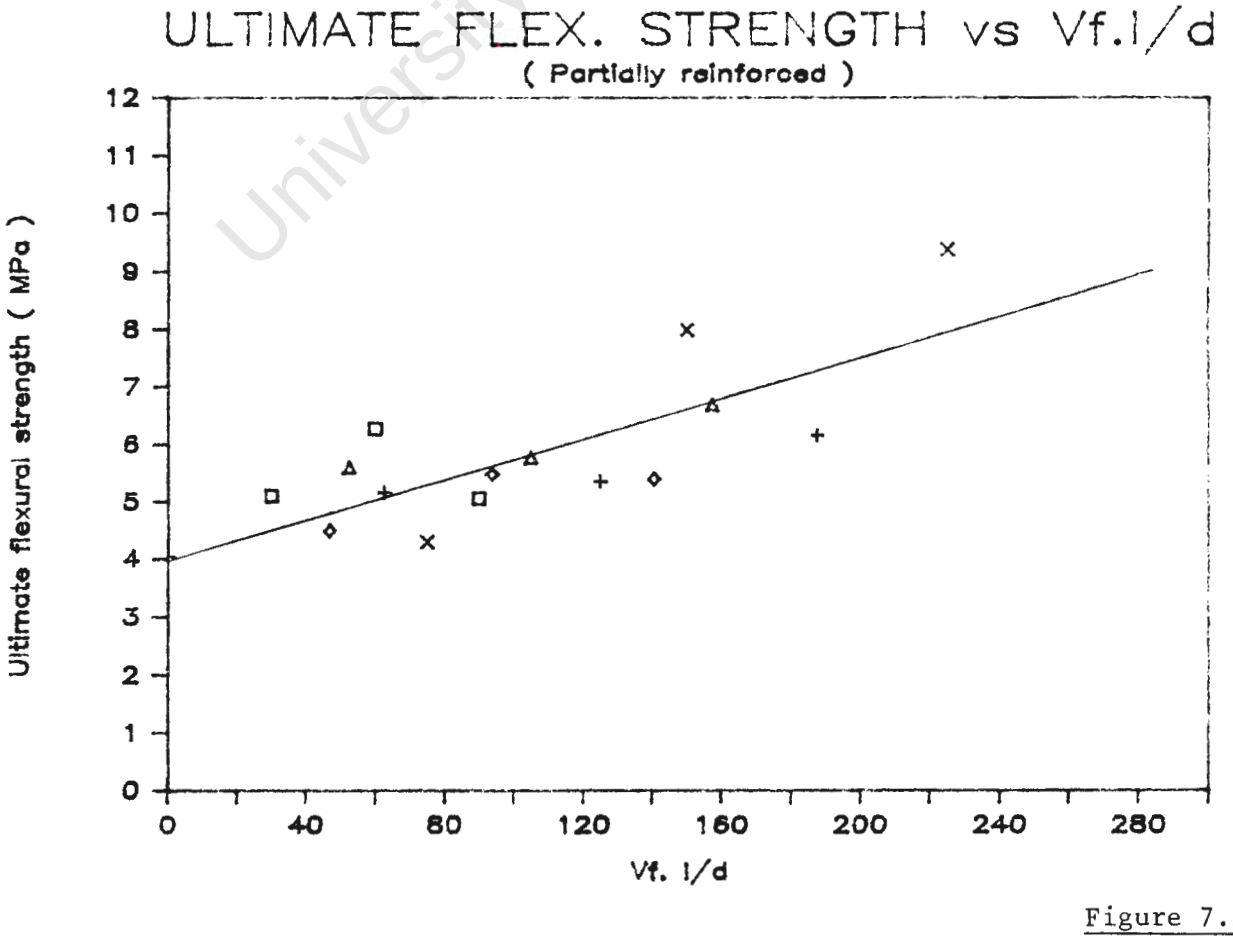

Figure 7.23

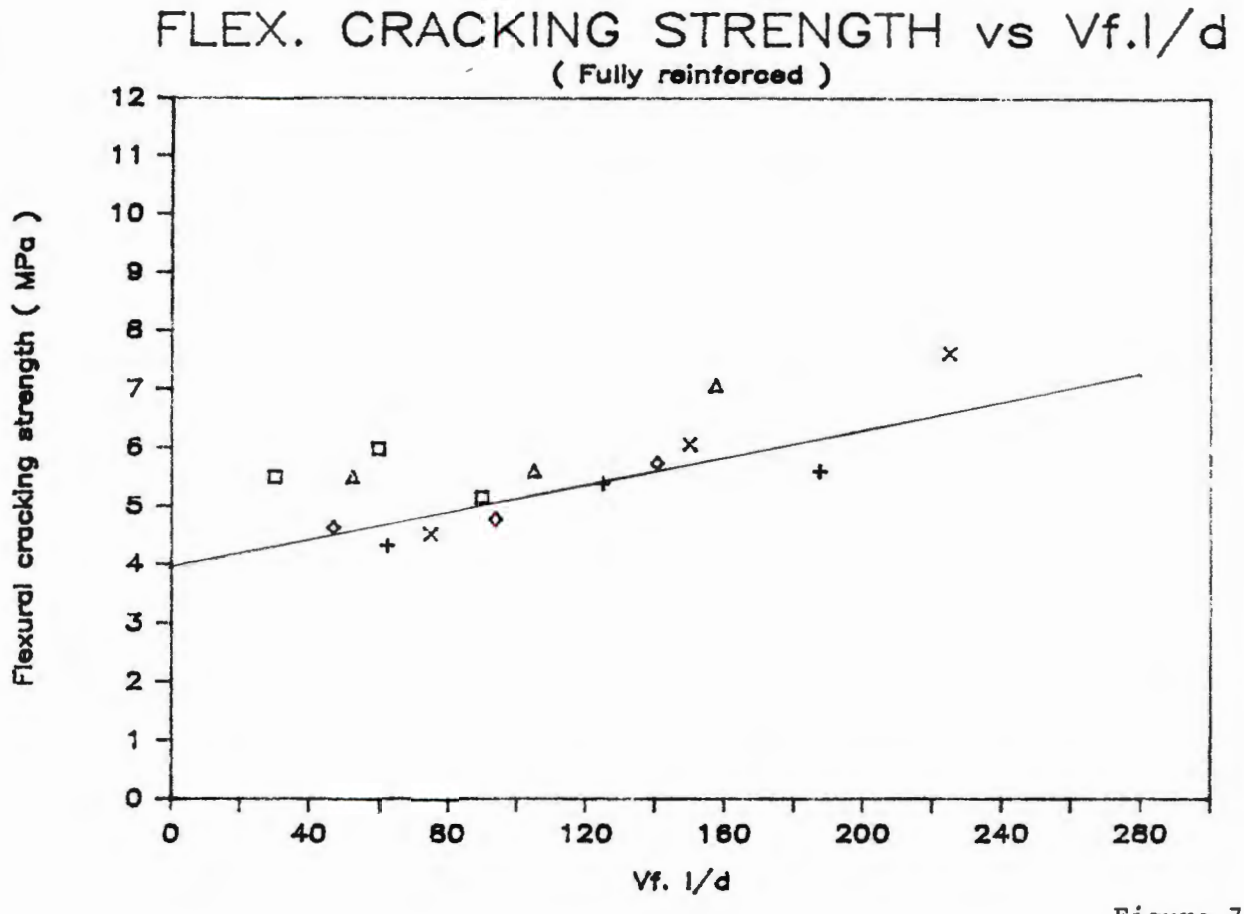

Figure 7.24

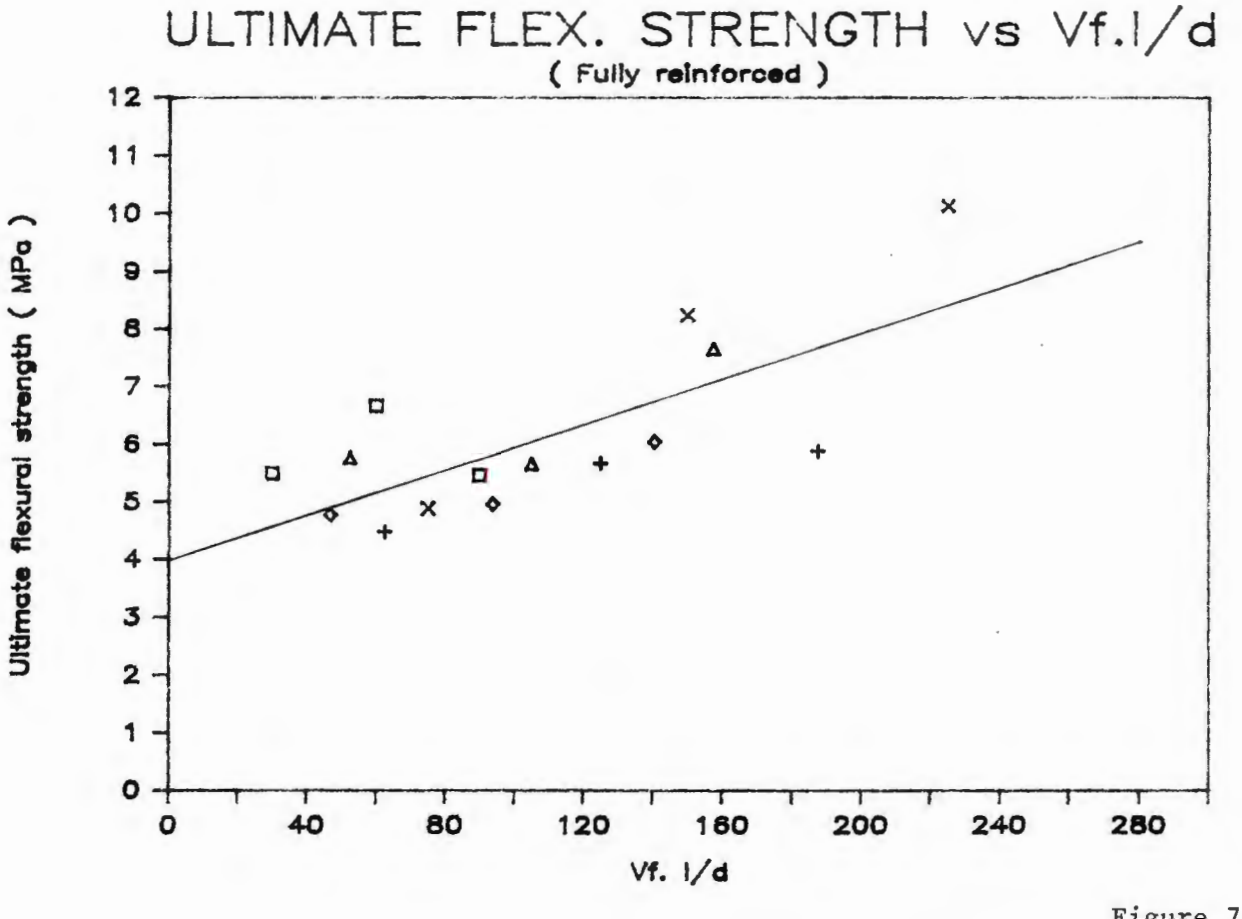

Figure 7.25

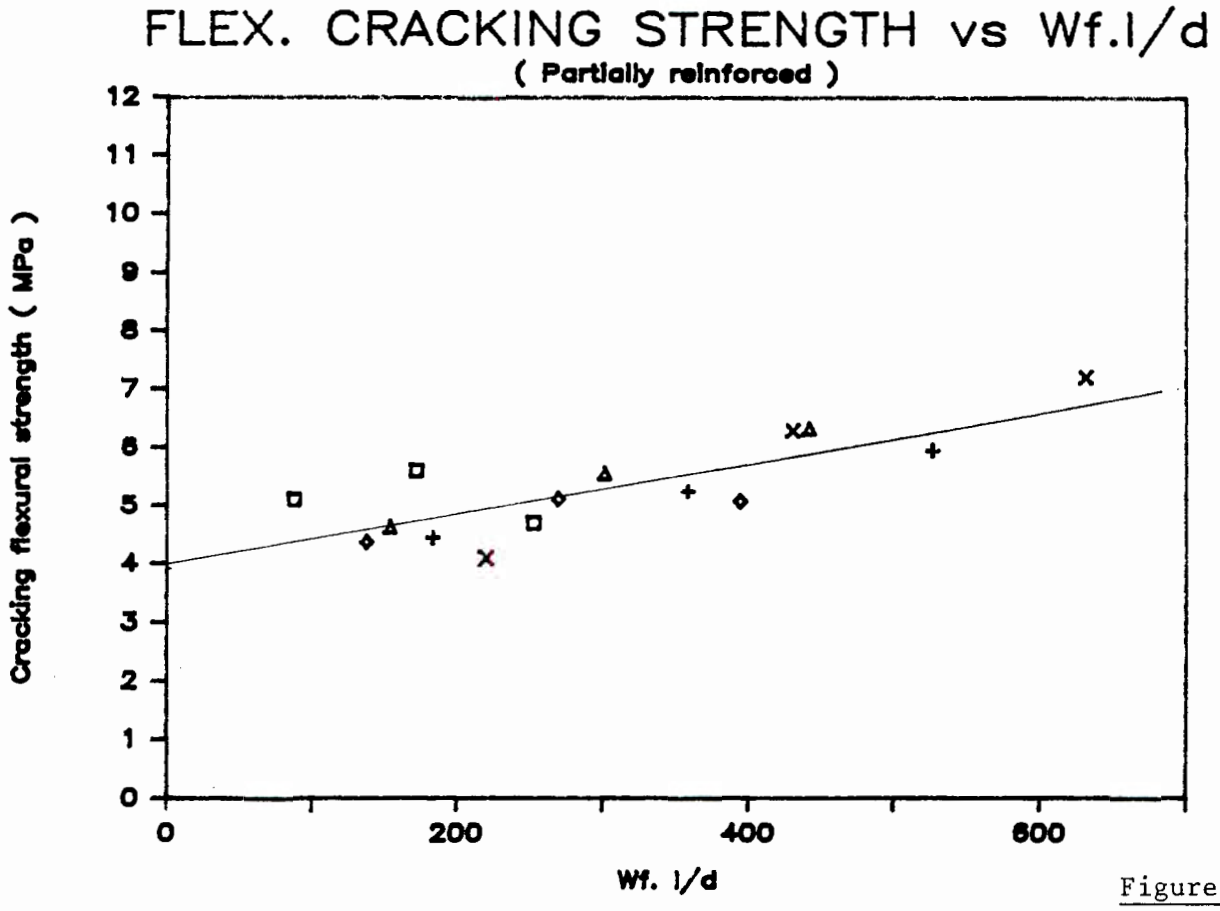

Figure 7.26

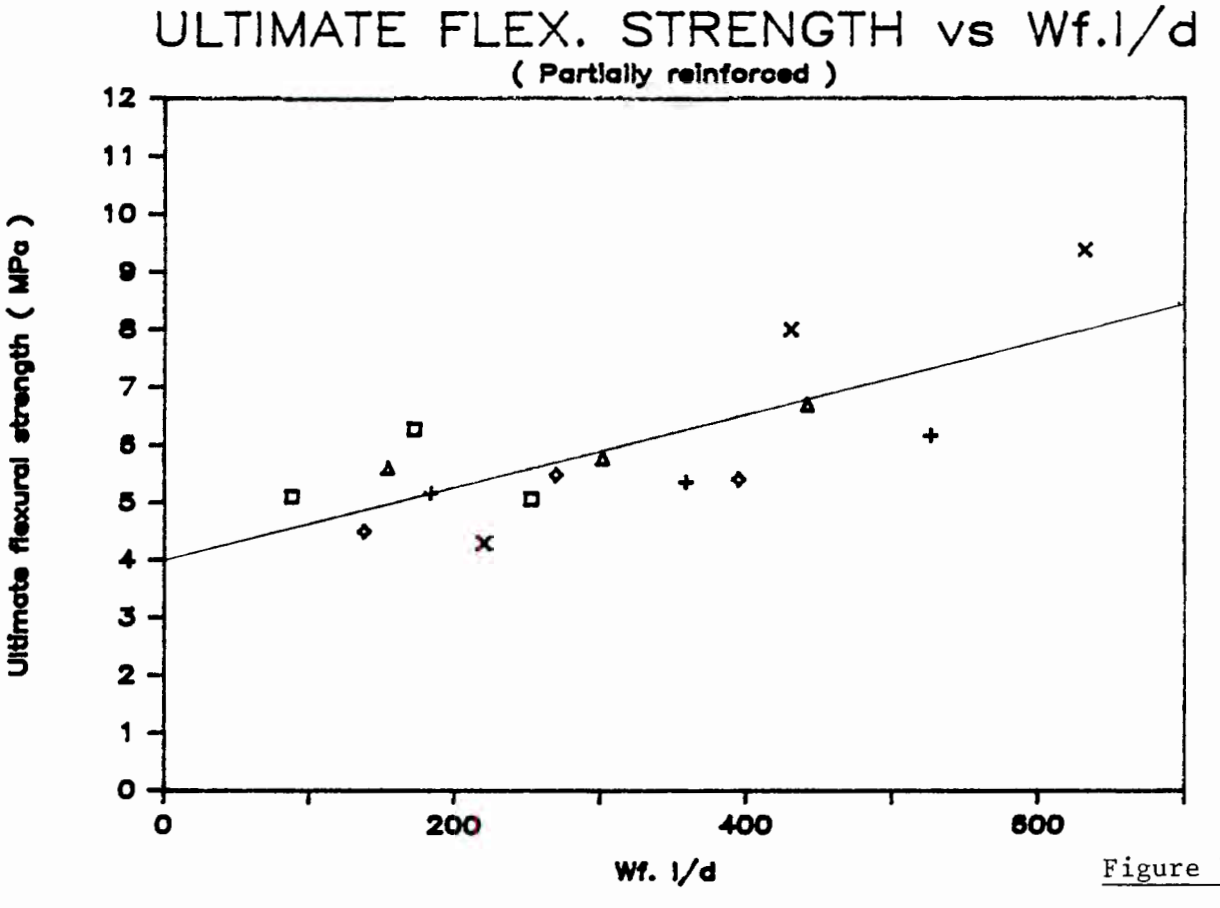

Figure 7.27

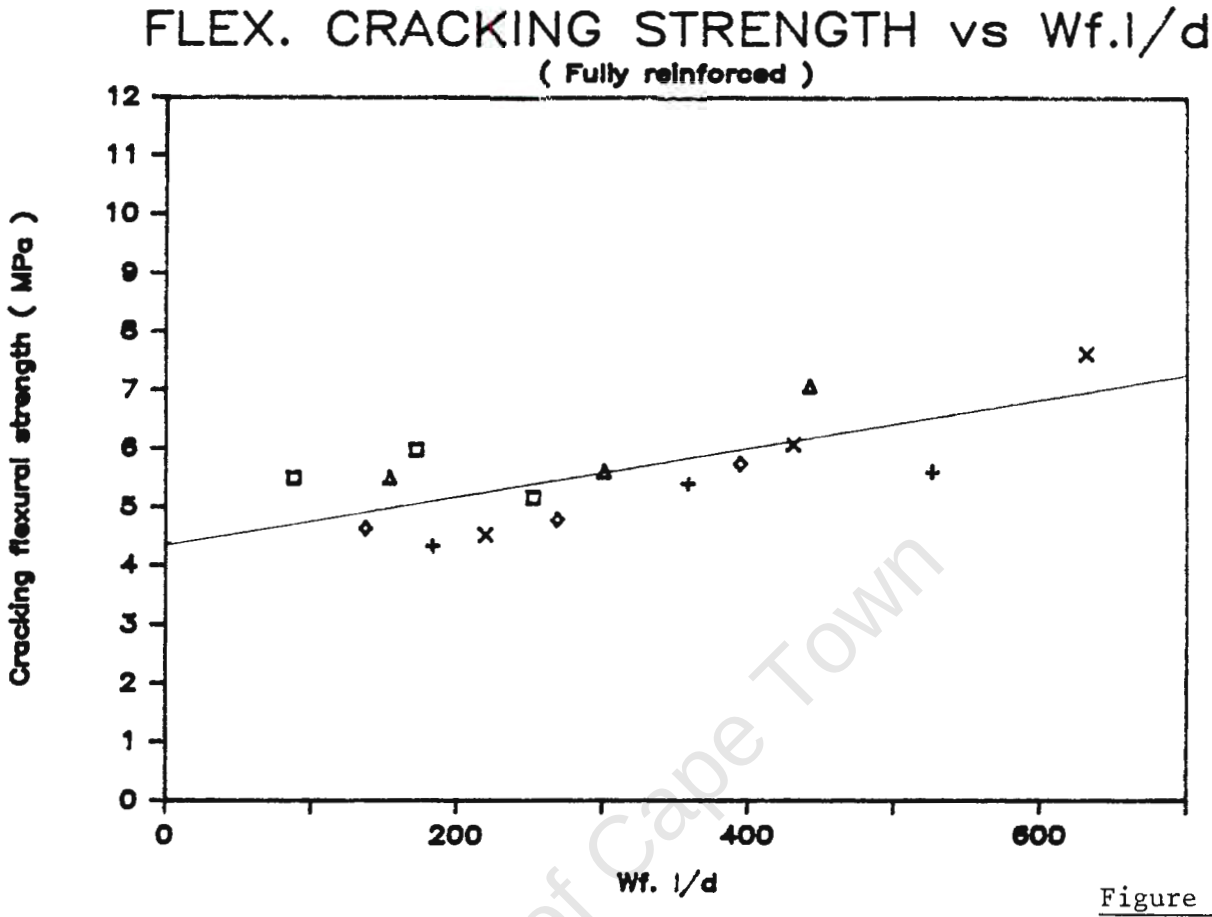

Figure 7.28

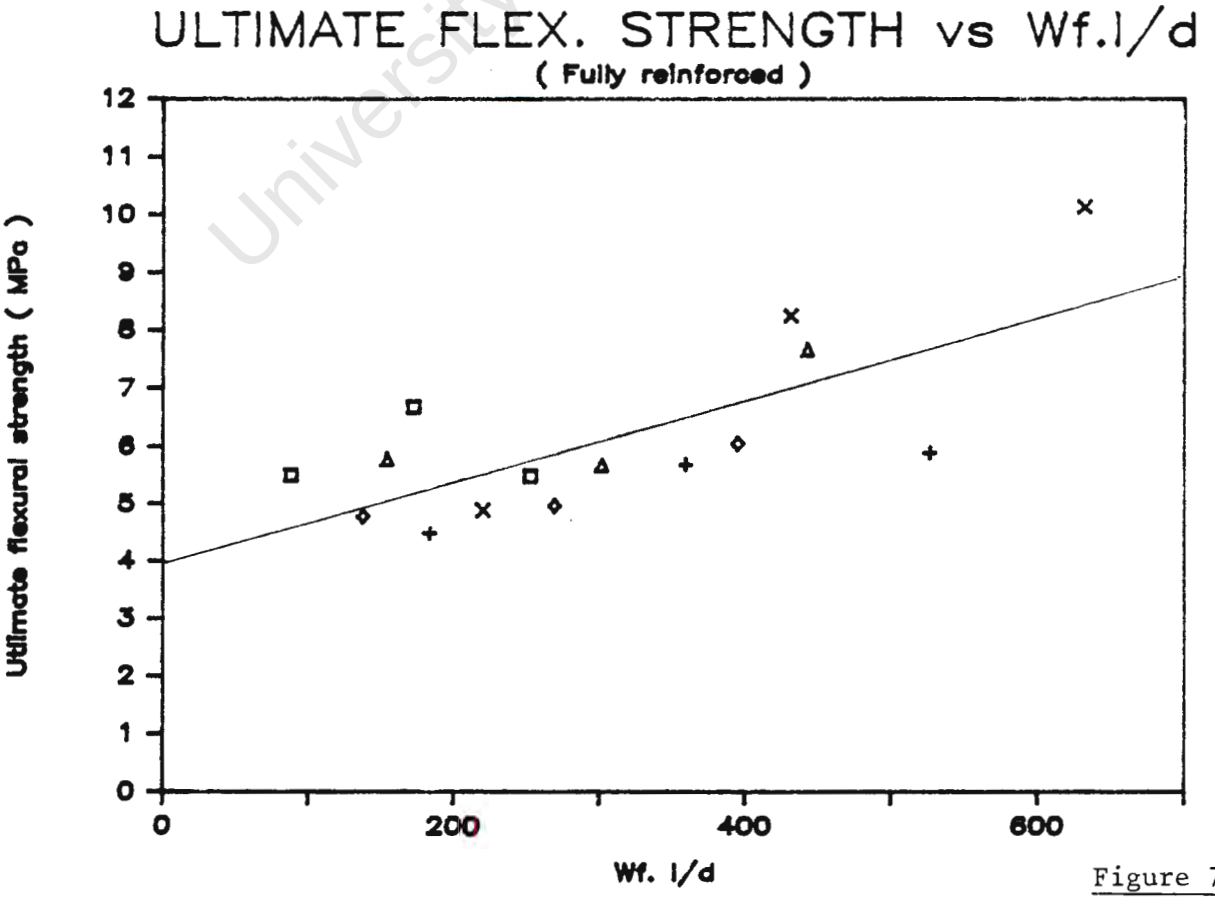

Figure 7.29

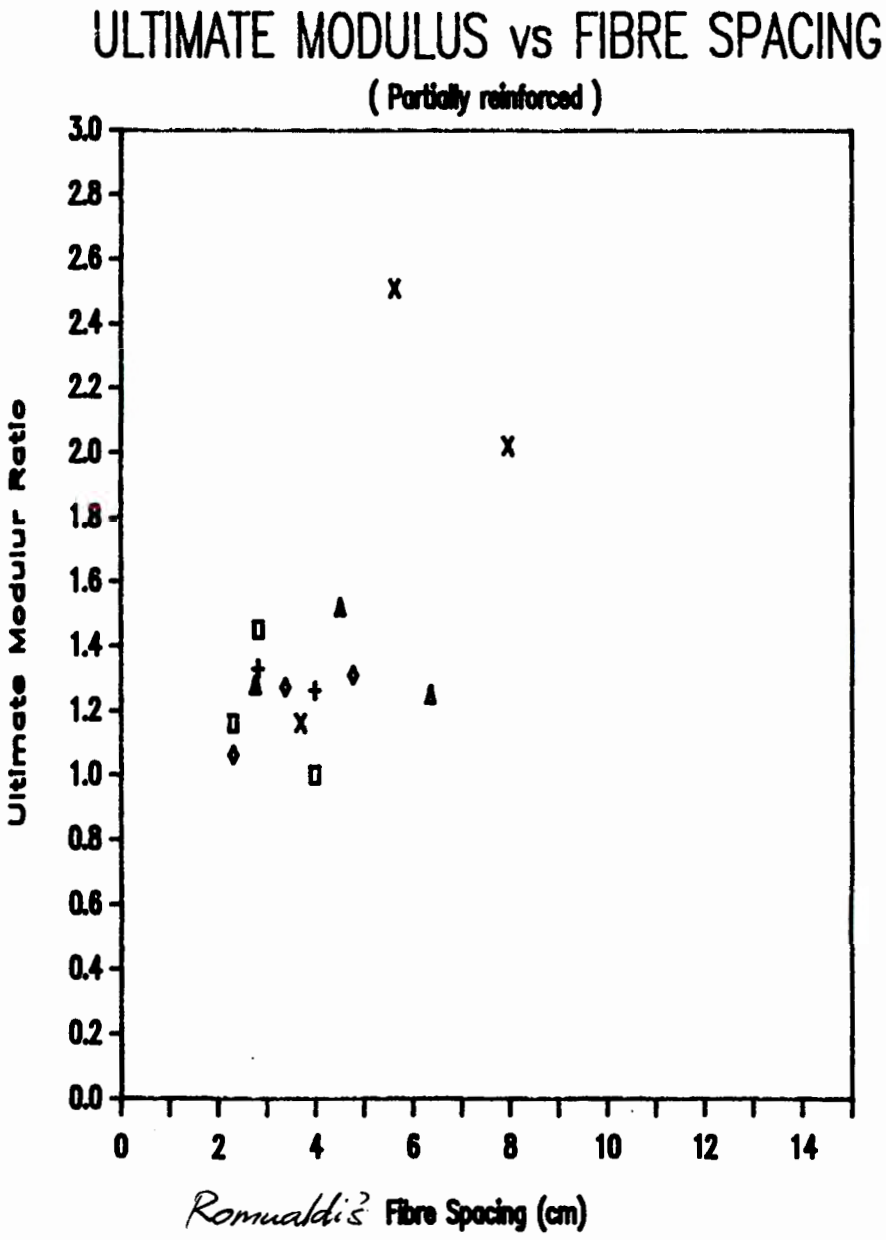

Figure 7.30

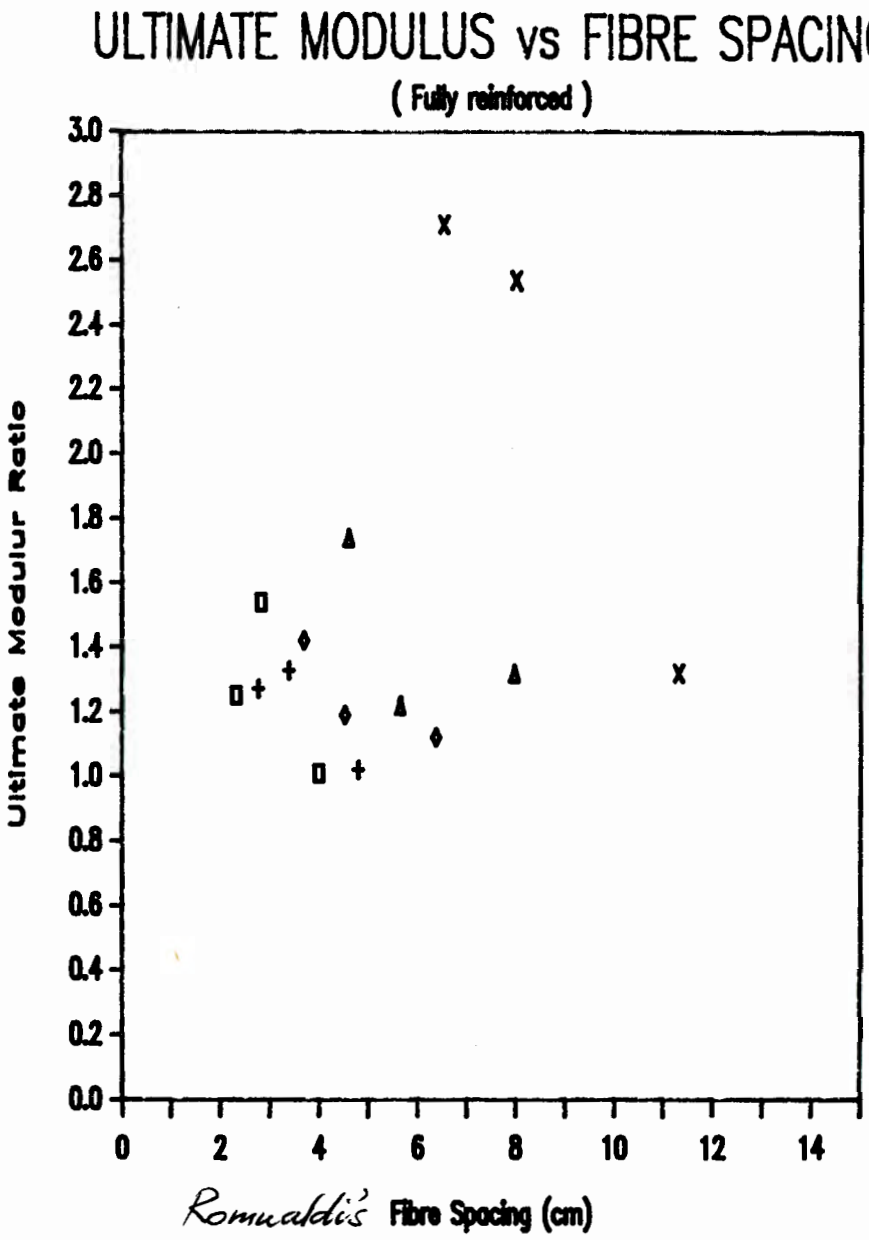

Figure 7.31

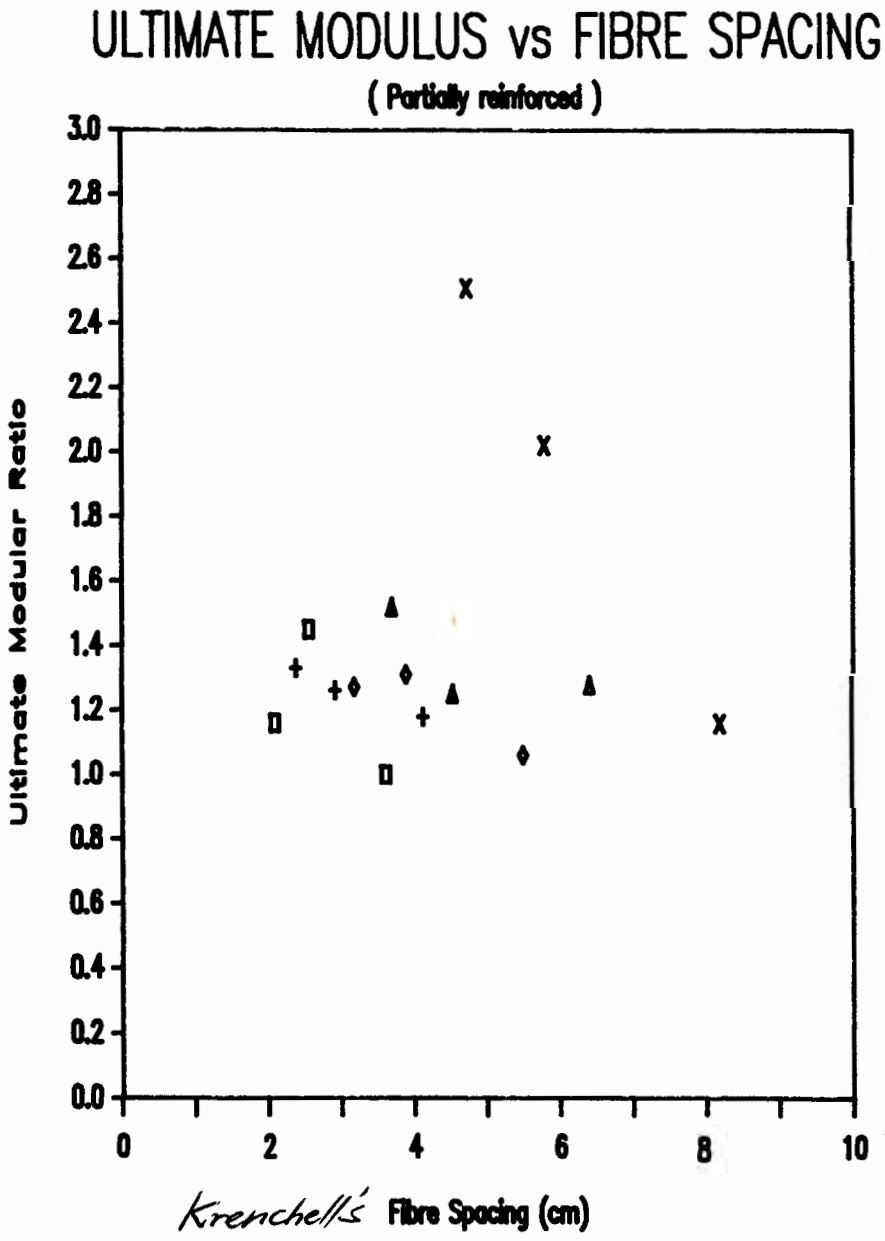

Figure 7.32

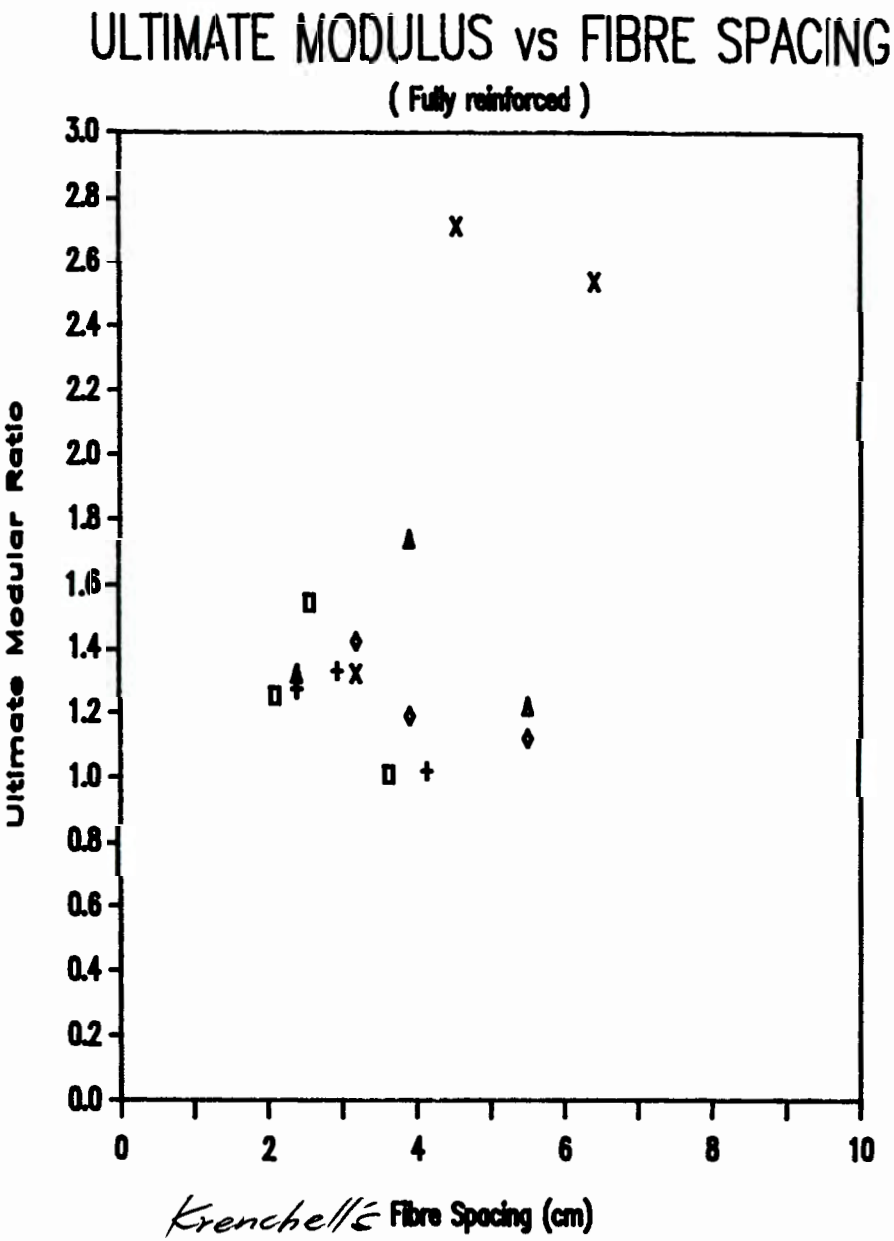

Figure 7.33

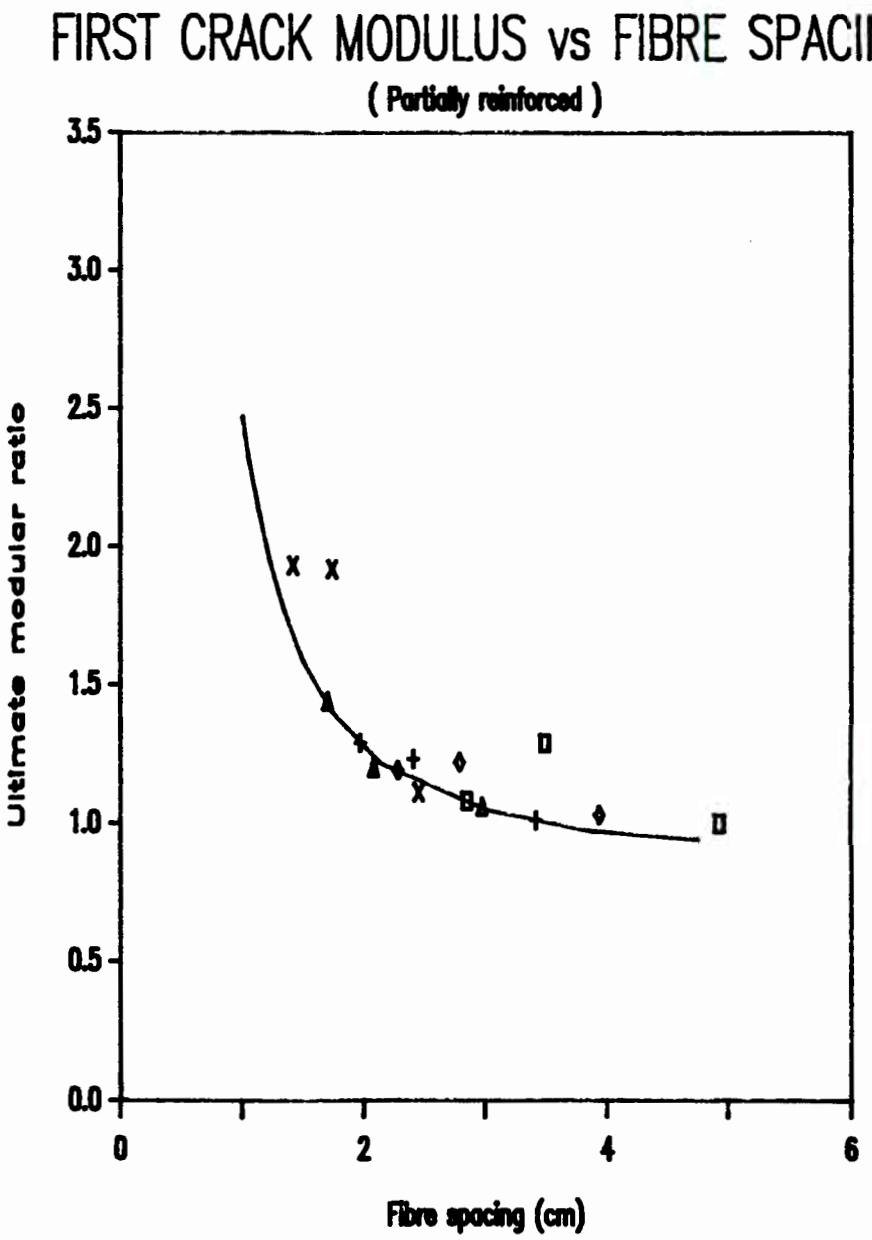

Figure 7.34(a)

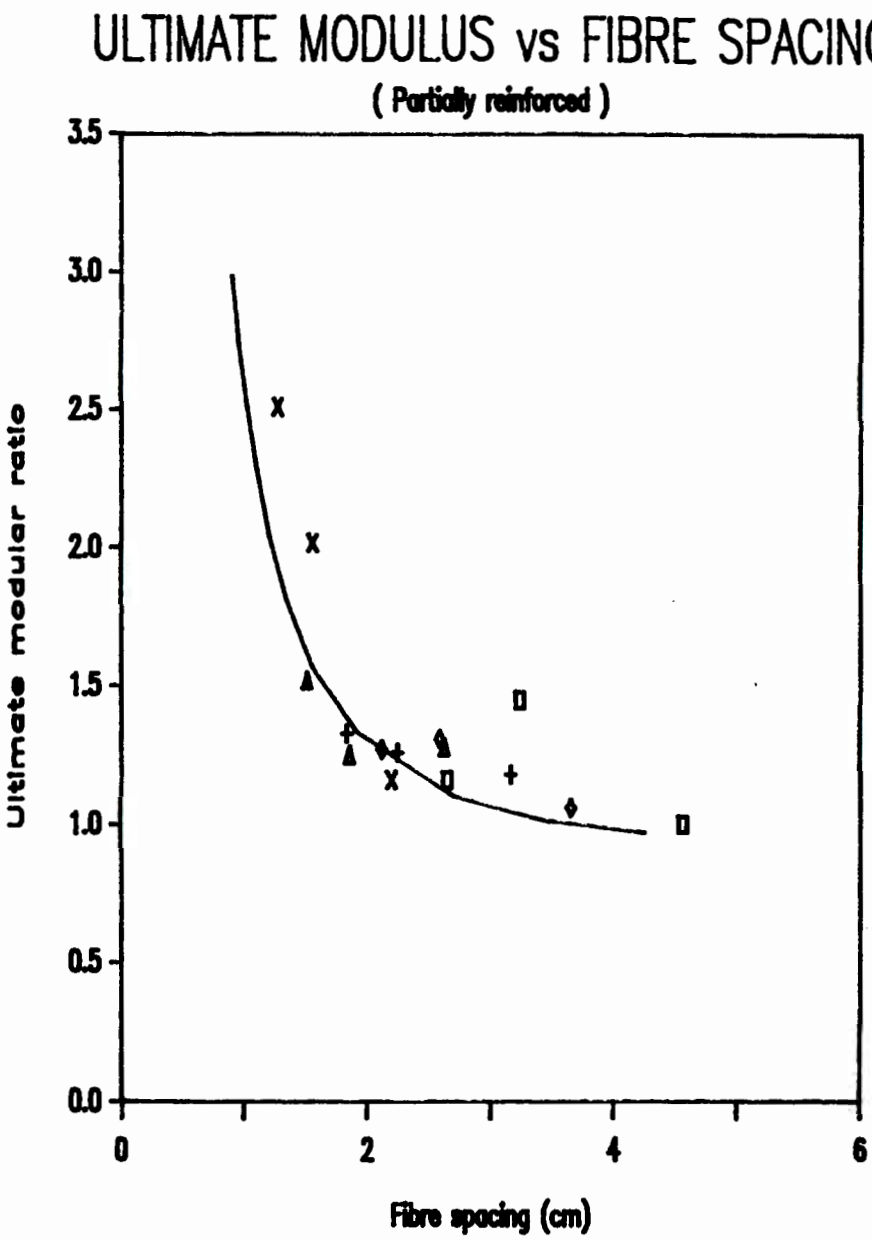

Figure 7.34(b)

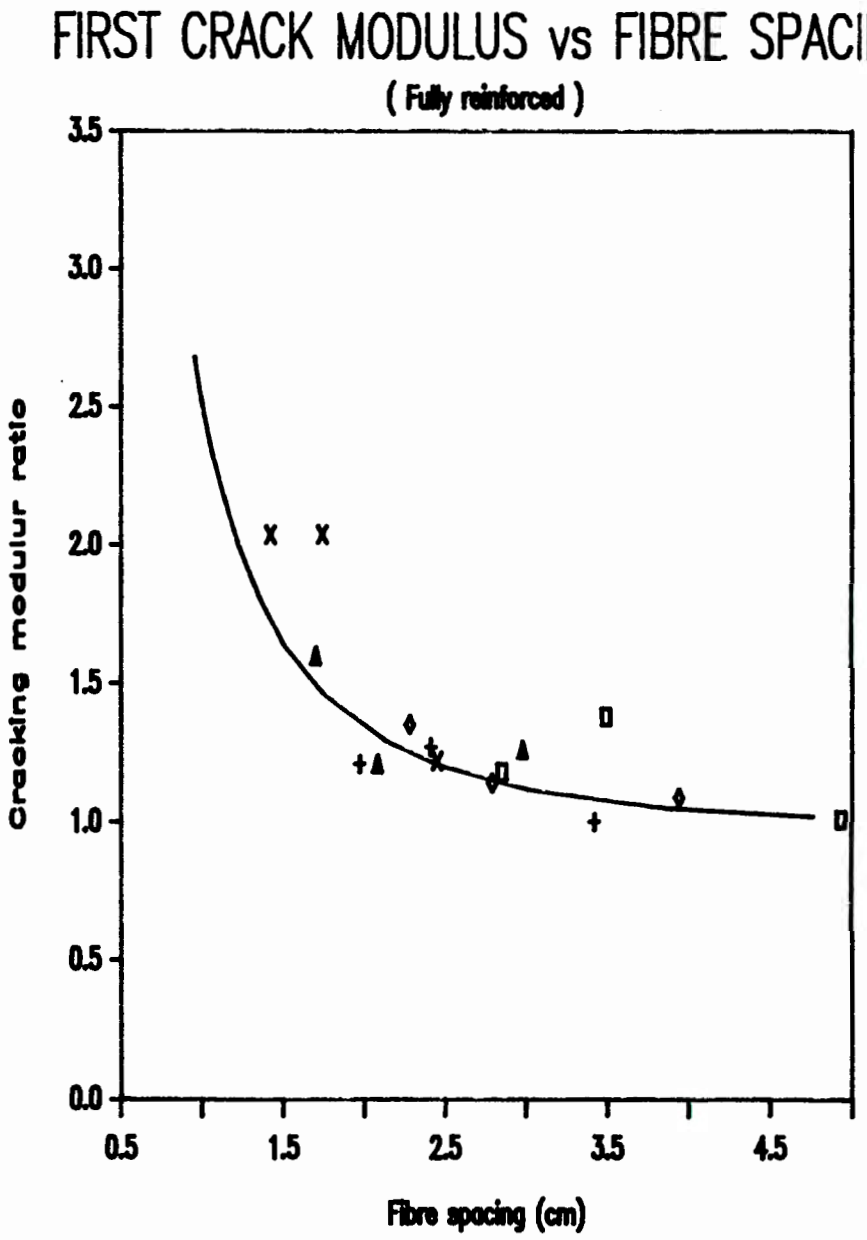

Figure 7.35(a)

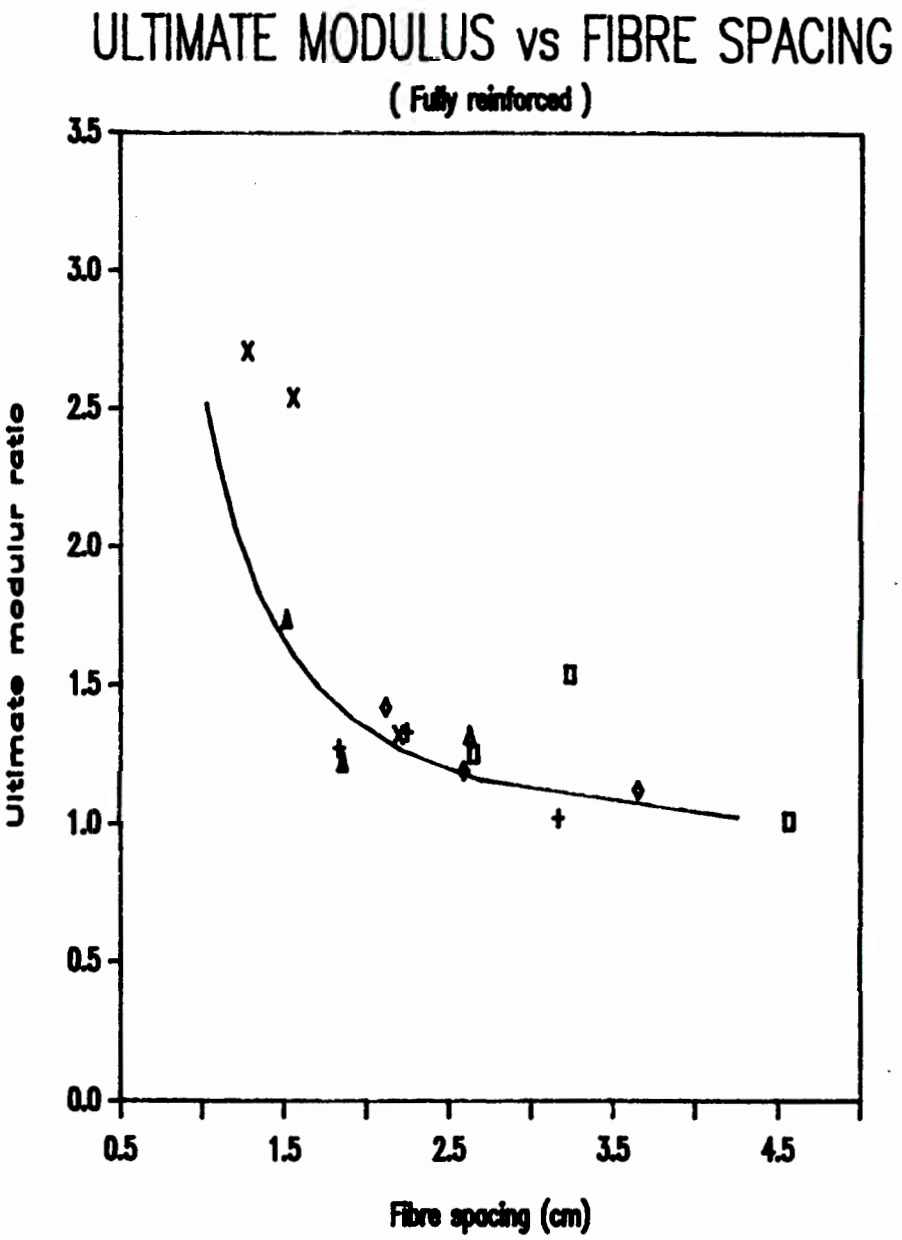

Figure 7.35(b)

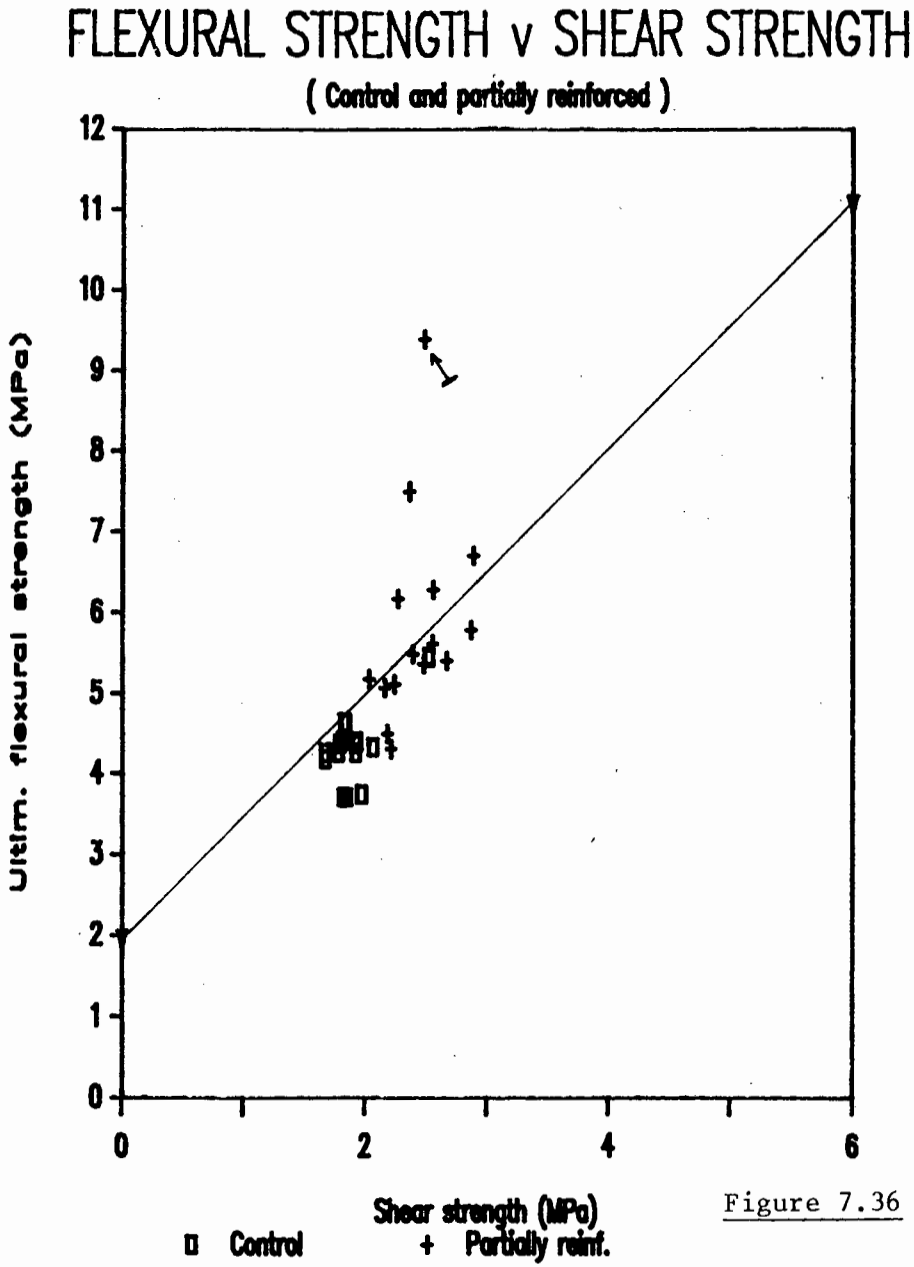

Figure 7.36

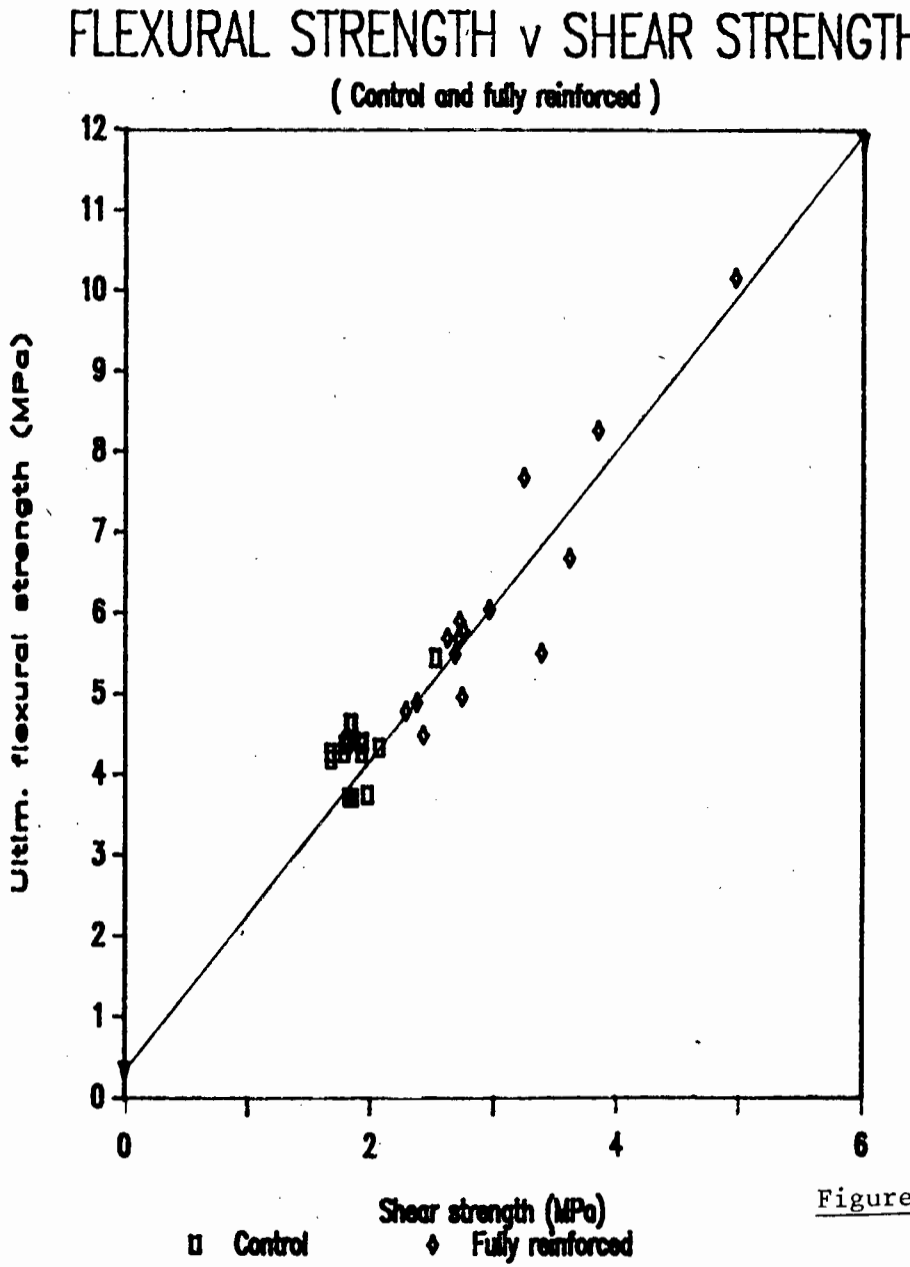

Figure 7.37

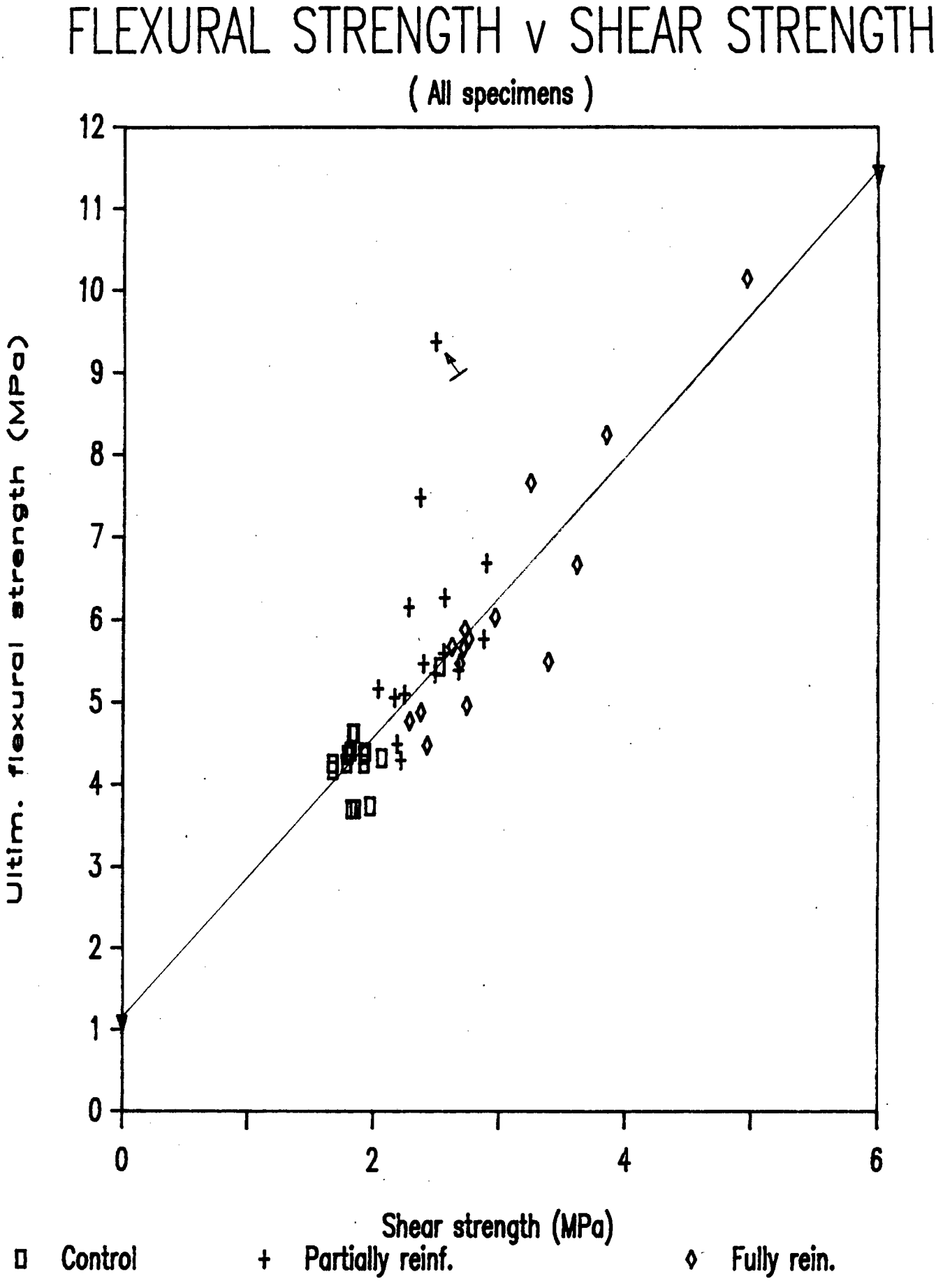
FLEXURAL STRENGTH v SHEAR STRENGTH
(All specimens)
Ultim. flexural strength (MPa)
12
11
10
9
8
7
6
5
4
3
2
1
0
0
2
4
6
Shear strength (MPa)
Control
Partially reinf.
Fully rein.

Figure 7.38

Figure 7.39(a): 1.25% Vf LOAD DEFLECTION CURVES

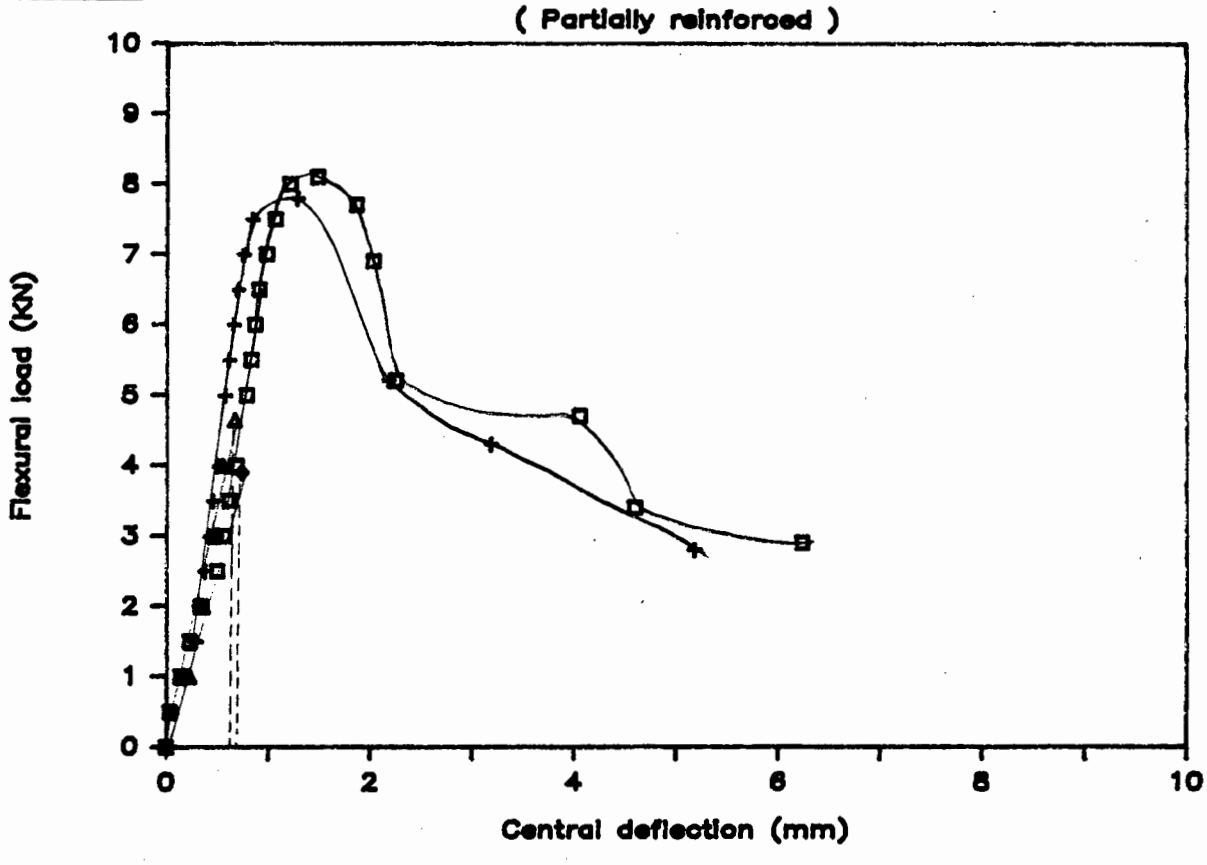

Figure 7.39(b): 1.25% Vf LOAD DEFLECTION CURVES

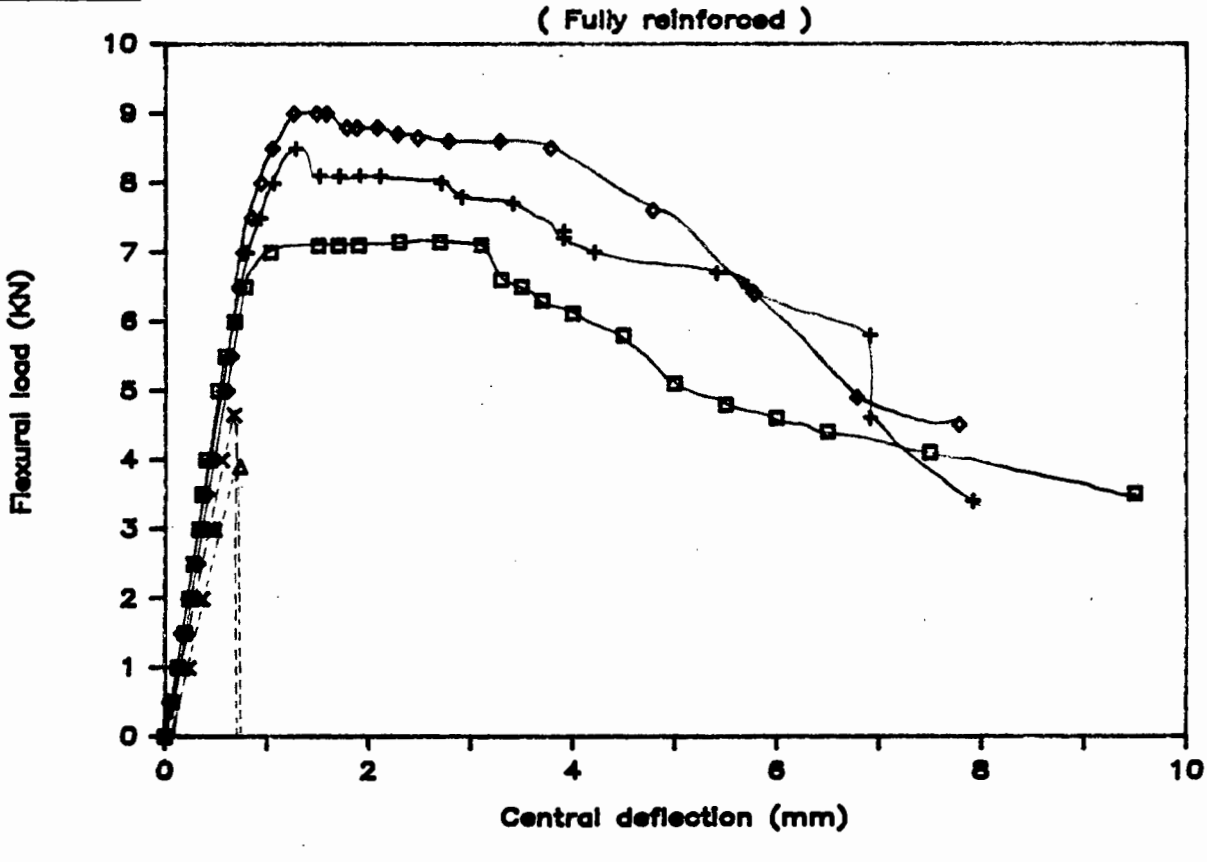

Figure 7.40(a) :1.50% Vf LOAD DEFLECTION CURVES

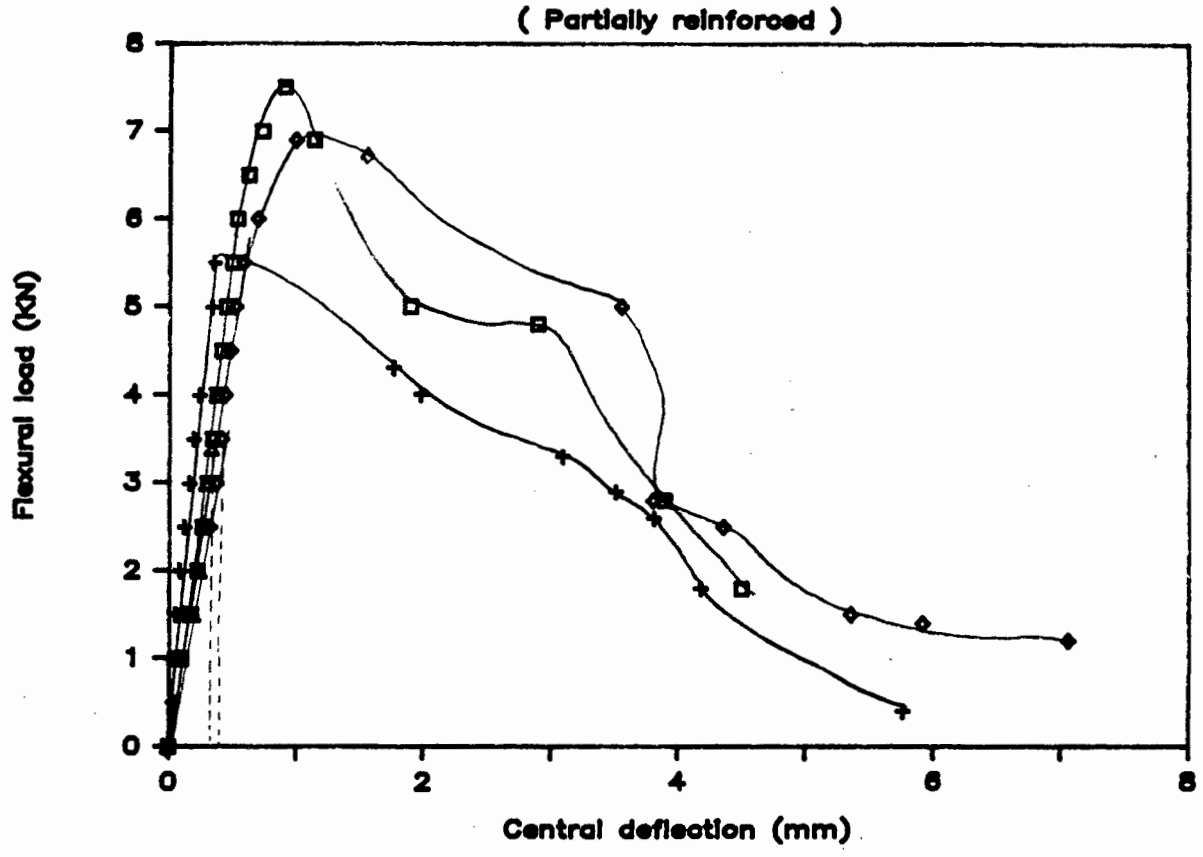

Figure 7.40(b) :1.50% Vf LOAD DEFLECTION CURVES

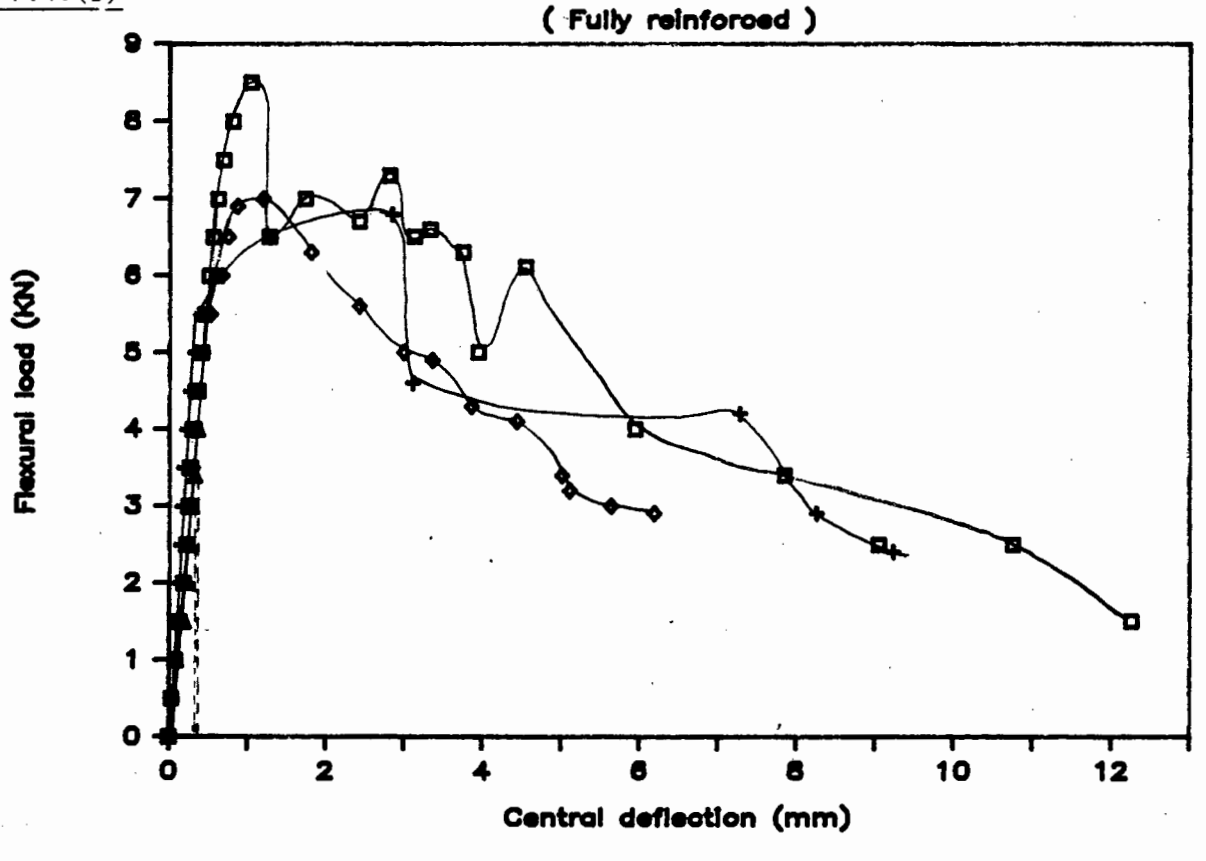

Plate 7.1 : Prisms partially reinforced (left) and fully reinforced (right) with 1.50% Shreddic fibres

Plate 7.2 : Fully reinforced prisms containing from left to right) 0.75%, 1.50% and 2.25% by volume of ME430(35mm) respectively

Plate 7.3 : Partially reinforced prisms containing (from left to right) 0.75%, 1.50% and 2.25% by volume of ME430(35mm) fibres respectively

Plate 7.4 : Prisms fully reinforced with (from left to right) 2.25% - 0.75% by volume of Binding Wire

Plate 7.5 : Prisms partially reinforced with (from left to right) 2.25% - 0.75% by volume of Binding Wire

Plate 7.6 : Examples of fibre balls (ME430(35mm) on left and ME430(25mm) on right) which were detected when mixing concrete with fibre concentrations of 2.25%

Plate 7.7 : Fibre ball detected in prism partially reinforced with 2.25% by volume of Wirand fibre

Plate 7.8 : Cubes reinforced with (from left to right) 2.25% Shreddic, Wirand, Binding Wire and an unreinforced control cube

CHAPTER 8

TEST RESULTS AND DISCUSSION

(APPLICATION PHASE)

8.1 GENERAL

From the Efficiency and Proving Phase it was determined that the Binding Wire fibres were the most suitable of the five types to use for reinforcing. The results of the static and impact tests carried out on mesh and fibre-reinforced slabs are given below. Thereafter the results of the same tests conducted on mesh and fibre-reinforced arches are presented.

8.2 SLAB TESTING RESULTS

Table 8.1 shows the sequence of testing :

Table 8.1 : Details of slab test panels

Slab no.	Type of reinforcement		Test
1-3	Mesh		Static
4-7		Fibre	Static
8-10	Mesh		Impact
11-13		Fibre	Impact

It will be noted that four fibre-reinforced slabs were tested under static load compared to three mesh-reinforced. Because the third fibre-reinforced slab exhibited strengths below the preceeding two slabs, a fourth sample was cast and tested to observe whether this strength variation was normal. The data of all the tests is given in Appendix I).

8.2.1 Static Tests

MESH-REINFORCED SLABS - The load vs central deflection curves obtained for the mesh reinforced slabs are shown in Figure 8.1. Figure 8.2 shows the plot for the deflection at the free edge. The curves are identical. On both plots the deflection is initially linear with increasing load, until cracking occurs, which is signified by the deviation in the initial linear plot. Visual observation of the slabs under load usually confirmed the onset of cracking; slab 1 was observed to crack after 10 kN load, slab 2 deflections were observed to increase nonlinearly after 7 kN load and for slab 3 the loading had to be adjusted manually after the 7 kN load. Unfortunately the deflection at ultimate load is not shown in Figures 8.1 and 8.2, because the 50mm deflection travel of the dial gauges had been exhausted. The plots do, however, clearly show the linear elastic deflection of the slab with increasing load, followed by crack initiation and thereafter gradual yielding of the reinforcing mesh as the load increases to ultimate. At ultimate load, a series of audible snaps occurred, signifying failure of the mesh reinforcing. The ultimate load capacities of slabs 1-3 were 26.6, 28.4 and 26.6 kN respectively.

Plate 8.1 shows the yield pattern of mesh-reinforced slab 1 as viewed from the top. The curved yield lines appeared on the surface of the slab after the ultimate load capacity had been reached. They are thought to be due to a form of punching shear. The yield patterns observed for slabs 1-3 were sketched to facilitate yield line analysis, in Figures 8.3(a) through 8.3(c).

PARTIALLY FIBRE-REINFORCED SLABS - Figures 8.4 and 8.5 show the plots of the load vs central deflection and load vs free edge deflection respectively for the four partially fibre-reinforced slabs tested. During testing the deflection at the centre of slab 1 was observed to increase suddenly at the 3 kN load mark. This is evidenced in Figure 8.4 by the deviation of the plot from linearity. For slab 2 the load had to be manually kept steady for dial gauge reading after the 7 kN load point. A jump in the load-deflection plot indicates that cracking of the slab did occur at this load. For slab 3, the load could not be "locked off" after 11 kN loading, indicating that cracking had occurred, although no deviation in the load vs deflection was observed.

The third fibre-reinforced slab tested, exhibited an ultimate strength somewhat lower than the first two fibre slabs (17.8 kN compared to 19.8 and 19.6 kN). A fourth slab was cast and tested, which yielded an ultimate load capacity of 18.8 kN and exhibited deflections more in accordance with slabs 1 and 2 (see Figure 8.5). The general yield pattern observed at ultimate failure of the partially reinforced slabs is sketched in Figure 8.6. Unlike the mesh-reinforced slabs, only one crack was observed to run from the

free edge to the load application points. The rest of the yield pattern closely approximated that of the mesh-reinforced slabs.

It should be noted that the deflection axis of Figures 8.4 and 8.5 only reaches 6mm, compared to 50mm in Figures 8.1 and 8.2. If the deflections of the partially fibre-reinforced slabs are directly compared to that of the mesh-reinforced slabs under loading (Figures 8.7(a), (b) and 8.8(a), (b)), the former are seen to exhibit only a fraction of the latter's deflection. For an 18 kN applied load, the average central deflection of the fibre-reinforced slabs was 4.6mm compared to 15.7mm for the mesh-reinforced slabs. At ultimate failure though, the deflections of the fibre slabs increased so rapidly that no accurate readings could be recorded to compare with the mesh-reinforced slab deflections.

It is believed that the large deflections recorded for the mesh-reinforced slabs was due to the yield pattern - the slab developed a few major cracks which widened considerably as the load was increased. The fibre-reinforced slabs, however, developed only one visible central crack (see sketch Figure 8.5) and it is believed that a number of closely spaced, hairline cracks (which were not visible to the naked eye) developed which would account for the decreased crack width and deformation at all stages of loading. In Plate 8.2 a pile of tested slabs is shown of which the bottom three are mesh-reinforced and the top three partially fibre-reinforced. The mesh-reinforced slab "pieces" were observed to rotate about their yield lines when picked up, whereas the top three fibre slabs exhibited significant post-cracking stiffnesses even after failure.

DISCUSSION OF RESULTS

The failure mechanism of the mesh-reinforced slabs showed that the steel was controlling, i.e. yielded first. A yield line analysis using the Work Method was carried out to determine the yield moment capacity (see Appendix I.3). A value of 3.01 kNm per metre length of slab was obtained, which compares favourably with the 3.40 kNm per metre moment capacity as predicted by the ultimate sectional analysis.

The average maximum load sustained by the four partially fibre-reinforced slabs was 19.01 kN. This load capacity was substantially lower than the 27.2 kN average obtained for the mesh-reinforced slabs. The yield line analysis carried out for the fibre slabs subsequently yielded a rather low 2.34 kNm per metre length ultimate moment capacity (see Appendix I.3).

From the results it is obvious that the partially SFRC slabs had an insufficient fibre content, i.e. the V_f used was too low. After a critical examination of the calculation steps in Appendix G, the author believes that the problem lies with equations (G.4) and (G.5) as proposed by Hannant (reference 89). Equation (G.4) determines the number of fibres (N) bridging a crack of unit length. Equation (G.5) then assumes that <u>all</u> these fibres are stressed uniformly. Thus no orientation factor has been applied to the value of N , and this results in a far too high value for F_{ft} in equation (G.5). If an orientation factor of 0.64 is applied to N , the value of V_f determined is equal to 2.39%. This quantity is seen to be nearly double of that actually used, and would certainly have increased the ultimate load capacity of the partially SFRC slabs.

8.2.2 Impact Tests

MESH-REINFORCED - The results of the Impact Tests performed on the mesh-reinforced and partially fibre-reinforced slabs are given in Appendix I.4 and I.5. The mesh-reinforced slab 1 cracked after the 400mm drop height, the crack width measuring 0.3mm. After the 500mm high drop, the central crack had widened to 0.9mm. Very fine cracks were observed at the free-edge of slab 2 after the 300mm high drop. After the 500mm high drop one of the cracks was visible on the top of the slab. The third mesh-reinforced slab was observed to have cracked after the weight had been dropped from 400mm. After the 600mm drop height, this crack was visible on the top of the slab.

The three slabs exhibited similar crack patterns as shown in Figures 8.9(a), (b) and (c). These patterns were much the same as those occurring for the statically loaded mesh-reinforced slabs. For the 1200mm plus drop heights, however, the slabs tended to deform more along a few of the yield lines, as shown by Plate 8.3. The third mesh-reinforced slab was subjected to the impact load from as high as 1.6 metres to observe whether the slab would collapse. The slab in Plate 8.3 shows the large deformation of the slab associated with a 1.6m drop height, but still no collapse. The test was stopped here as sufficient data had been obtained and considering the deflections were probably way beyond the allowable service ability limits of structural and building codes.

The permanent deflection and total (i.e. elastic plus permanent) deflection of the mesh-reinforced slabs measured for the various impact drop heights is plotted in Figure 8.10. The three slabs are

seen to have exhibited the same deflections up to the 800mm drop height, and begin to deviate thereafter. This was expected as the slabs had by then deformed considerably along slightly differing yield lines.

PARTIALLY FIBRE-REINFORCED SLABS - Slabs 1 and 2 first cracked along the centre line from the free edge up to the load impact point after the 400mm drop height. Slab 3 was observed to have very fine hairline cracks along the same route after the weight had been dropped from a 300mm height. With increasing drop heights, a number of cracks were seen to radiate outwards from the point of impact, as shown by Figures 8.11(a), (b) and (c). After the 500m drop height the cracks had opened, widened substantially, and at the 600mm drop height slab 2 completely failed, breaking up into three pieces. Slab 1 and 3 also failed catastrophically after being subjected to the impact weight dropped from 700mm. Plate 8.4 shows the fractured sections of slab 1 after such an impact drop.

The permanent and total (i.e. elastic and permanent) deflections recorded for the increasing drop heights are plotted in Figure 8.12. If one compares the yield line patterns of slabs 1 and 3 (Figures 8.11(a) and (c)), the similarity is apparent which accounts for their similar impact vs deflection plots. The yield pattern of slab 2 was more in accordance with that observed for the statically loaded, partially fibre-reinforced slabs. The large deflections measured after (and including) the 500mm drop height can be attributed to the increasing number of fibres which by then had debonded fully and were being pulled out, while the remainder of the fibres were in the process of debonding and/or yielding.

DISCUSSION OF SLAB IMPACT RESULTS - The impact testing was conducted to see whether the partially SFRC slabs and mesh-reinforced slabs satisfied the requirements of the "Minimum Agreement Norms and Technical Advisory Guide (MANTAG). Table 8.2 shows the MANTAG resistance criteria of walls to impact damage by a sandbag (soft body) impact[92]. The equivalent impact energy values in Table 8.2 can be compared to the tests conducted by converting the 160 kg mass system and drop height;

$$\text{ENERGY EQUIVALENT} = \underset{\text{(kg)}}{\text{SANDBAG-MASS SYSTEM}} \times \underset{\text{(m)}}{\text{DROP HEIGHT}} \times 9.81$$

$$= 1570 \times \text{Drop Height (joules)} .$$

Figures 8.13(a) and (b) show the energy vs permanent displacement curves obtained for the mesh and partially SFRC slabs.

Table 8.2 states that for an external wall subjected to impact load of 265 joules (Nm) from the outside, the resulting cracks may not be wider than 0.5mm and the permanent deformation of the wall must be less than 1/600th of the wall height. The effective slab width was 2.025 metres which would allow for a permanent deflection of 3.4mm. The energy equivalents as read off curves 8.13(a) and (b) for this deflection are;

Mesh-reinforced slab $\approx$ 480 joules

partially SFRC slab $\approx$ 560 joules

indicating that both types of reinforced slabs were more than strong enough, the partially SFRC slab over twice the MANTAG requirement. The drop height for the fibre-reinforced slab at 560 J equivalent energy was 360mm as read off Figure 8.12. Since slabs 1 and 2 only cracked after the 400mm drop, while the crack width in slab 3 was

only 0.25mm at the same height, the partially SFRC slabs adequately met both MANTAG requirements. At 480 J energy, a drop height of 310mm was read off Figure 8.10 (mesh-reinforced slabs). Since the mesh-reinforced slabs 1-3 first cracked after the impact load had been dropped from 400, 300 and 400mm heights, the mesh-reinforced slabs also adequately met the MANTAG requirements.

Table 8.2 shows that the external walls should be capable of withstanding a 412 J impact energy without collapsing. All three partially SFRC slabs withstood the impact drop from a 500mm height, which is equivalent to 785 joules. The mesh-reinforced slabs, however, were capable of absorbing in excess of 2500 joules. The partially SFRC and mesh-reinforced slabs therefore met this MANTAG requirement with ease. It should be noted that the deflections in Figures 8.13(a) and (b) were cumulative for the increasing drop heights. If a new slab had been used for each new drop height (as is expected by the MANTAG Table 8.2) the permanent deflections would have been far less and the associated energy equivalents for a 3.34mm deflection much higher.

8.3 ARCH TEST RESULTS

8.3.1 Static Tests

The load vs crown deflection curves obtained for the mesh-reinforced arch 1 and 2 are shown in Figure 8.14. The deflections were taken as the average of three dial gauges placed across the width of the crown. (See Appendix J.1 for recorded results.) Assuming as usual that the inability to "lock off" the applied load indicated the initiation of cracking, arch 1 cracked somewhere between 13 and 14

kN, and arch number 2 between 11-12 kN. There are, however, no visible deviations or kinks in the load-deflection plots in Figure 8.14 at these loads. The ultimate load capacity of arch 1 was 45.2 kN, while arch number 2 failed at 44.1 kN.

Figure 8.15 shows the load vs crown deflection curves obtained for partially SFRC arches 1 and 2. (Test results given in Appendix J.2.) Initially the plots are identical up until 30 kN applied load. Arch number 1 cracked somewhere between 13 and 14 kN applied load. During the actual testing of arch 1 the dial gauges were observed to "flicker" at 13.8 kN load, which tends to support the above assumption. Arch 2 was thought to have cracked between 10 and 11 kN applied load. However, no deviation from the plot of arch number 2 is visible. The ultimate load capacity of arch 1 was 42.1 kN, and for arch 2 equal to 44.5 kN.

DISCUSSION OF RESULTS - If one compares the cracking and ultimate load capacities of the mesh-reinforced and partially SFRC arches, they are seen to be very similar. Additionally, if Figures 8.14 and 8.15 are compared, the plots of the two different reinforced arches are observed to be nearly identical. The mesh-reinforced and partially SFRC arches therefore exhibited nearly equal static strengths, whereas for the slab shaped test panels the fibre-reinforced specimens were much weaker than those reinforced with mesh. The improved performance of the fibre reinforcing in the arch and test specimens is therefore seen as primarily a result of the test panel shape rather than the fibre contribution.

For the average ultimate load of 44.65 kN, the ultimate moment at the crown was equal to 5.47 kNm per metre length and the axial thrust was 137.48 kN (using elastic analysis). This is somewhat higher (20%) than the ultimate moment of resistance of 4.55 kN/m as determined from an ultimate sectional analysis (see Appendix J.3 for calculations).

8.3.2 Impact Tests

The permanent (plastic) and total deflections recorded for the arch test specimens subjected to impact loading are given in Appendix J.4 and J.5.

The impact drop height vs crown deflection curves recorded for the mesh-reinforced arches are shown in Figure 8.16. The permanent deflections of arches 1 and 2 are seen to be nearly half the magnitude of the total deflections. Visual observation (using a bright halogen lamp) revealed fine hairline cracks on the crown underside of arch 1 after the 400mm high drop and on arch 2 after the 300mm high drop. With successive impact loads these cracks widened slowly. The test was stopped after the impact load had been dropped from 1.2 metres, because by then the central crack had propagated to the top of the crown.

Figure 8.17 shows the impact drop height vs crown deflection curves of the partially SFRC arches. The two plots are very similar with only the permanent deflections deviating from the 0.6 metre high drop onwards. Comparing Figures 8.16 and 8.17 one will note the lower deflections of the partially SFRC arches at all drop heights. The deflections are generally between 2-3mm less indicating that the steel fibres bridging the crack held the fractured sections together

better than the intermittently spaced mesh reinforcing. This only occurs for impact loading though, and is not apparent for static loading.

NOTE ON IMPACT TEST RESULTS - Figures 8.16 and 8.17 both show a surprising variation in the shape of the plot beyond the 0.6 metre drop height. Up to the 0.6 height, the plots are curvilinear yet beyond this drop height the plots appear to be linear. The only explanation for this uncharacteristic change concerns the effectiveness of the arch support set-up. As mentioned in section 6.3.5, disruption of the concrete occurred at the bearing points after the 600mm high impact drop, increasing in severity with succeeding impact loadings. Once the impact load had been dropped from a height of 1 metre the concrete in immediate contact with the bearing plates was seen to be crushed and "crumbly". The plots of Figures 8.16 and 8.17 above the 0.6 metre high impact drop should thus be disregarded because of their doubtful accuracy.

Table 8.2 : MANTAG criteria for resistance of walls to impact damage by sandbag impact (1 joule = 1 Nm)

Type of wall	Height of swing of 30 kg sandbag			
	Internal walls External walls (impact from 'inside')		External walls (impact from 'outside'	
	Without causing appreciable cracking or permanent deformation*	Without causing collapse	Without causing appreciable cracking or permanent deformation*	Without causing collapse
Masonry or heavyweight construction	450 mm (132 J)	900 mm (265 J)	900 mm (265 J)	1 400 mm (412 J)
Lightweight construction	450 mm (132 J) (framing) 300 mm (88 J) (cladding)	900 mm (265 J)	900 mm (265 J)	1 400 mm (412 J)

NOTE: The figures in brackets are the energy equivalents.

* Cracks formed must not be wider than 0,5 mm and their aggregate length must not exceed 300 mm. Permanent deformation or displacement of a wall must not be more than 1/600th of its height.

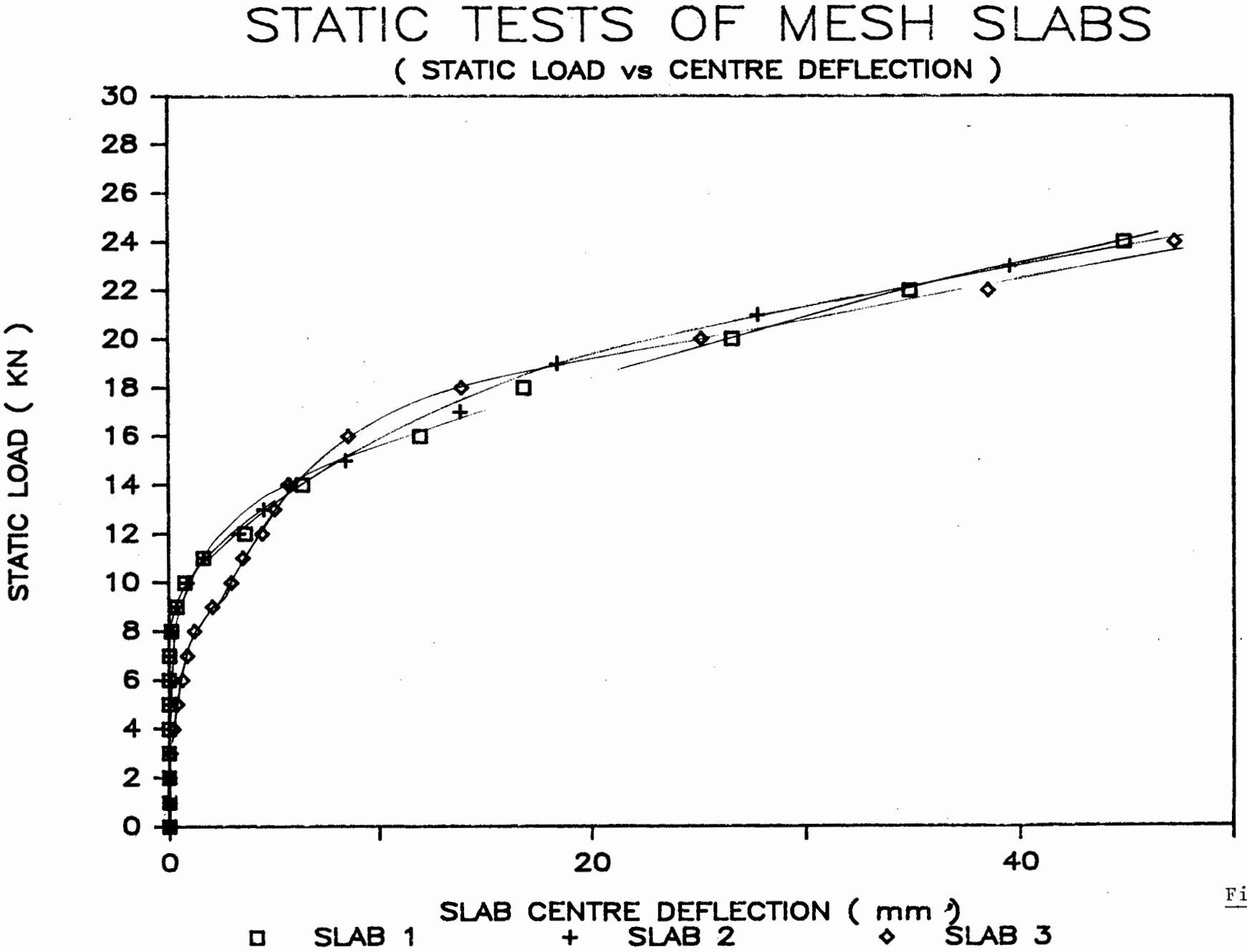
STATIC TESTS OF MESH SLABS
(STATIC LOAD vs CENTRE DEFLECTION)
STATIC LOAD (KN)
30
28
26
24
22
20
18
16
14
12
10
8
6
4
2
0
0
20
40
SLAB CENTRE DEFLECTION (mm)
SLAB 1
SLAB 2
SLAB 3

Figure 8.1

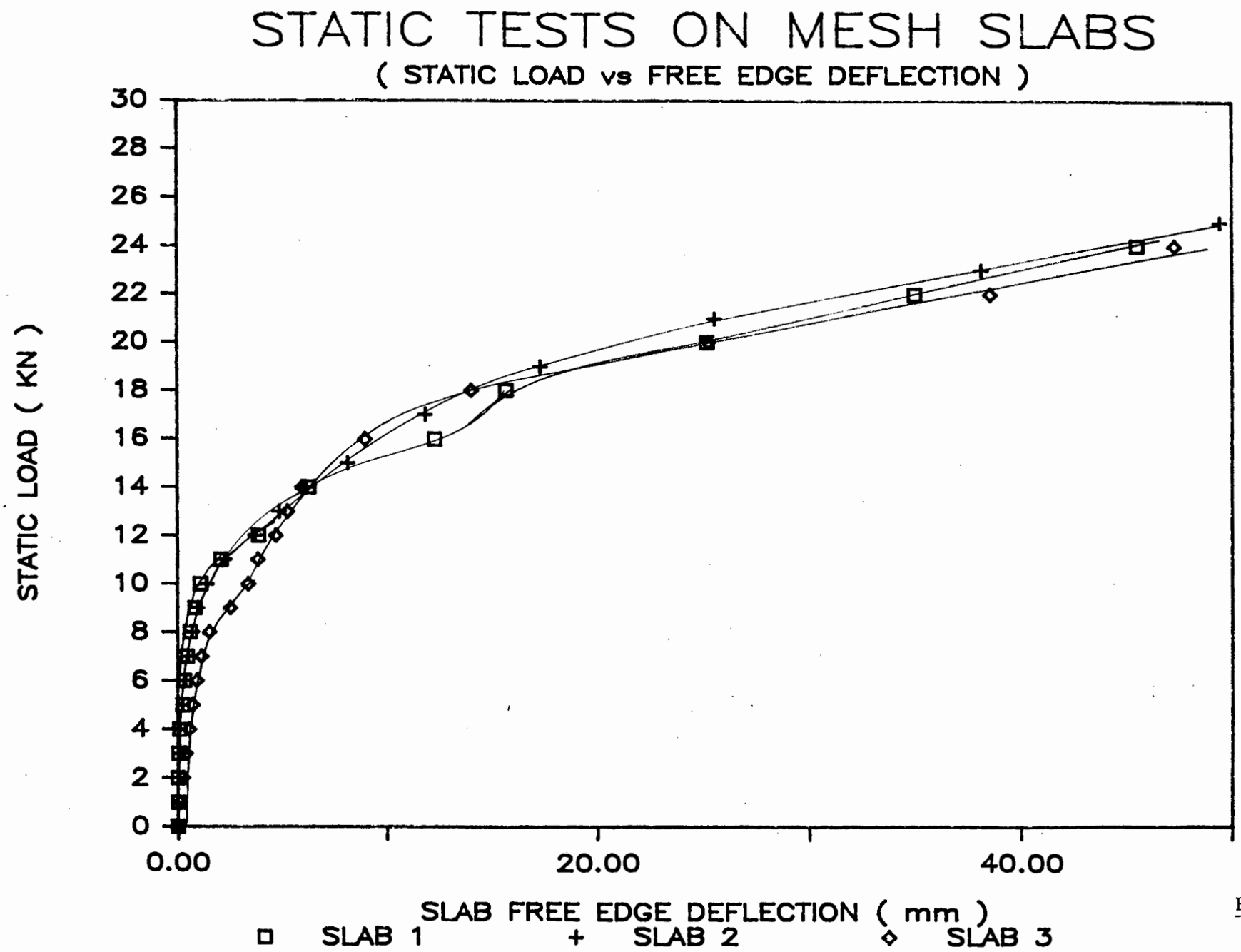
STATIC TESTS ON MESH SLABS
(STATIC LOAD vs FREE EDGE DEFLECTION)
STATIC LOAD (KN)
30
28
26
24
22
20
18
16
14
12
10
8
6
4
2
0
0.00
20.00
40.00
SLAB FREE EDGE DEFLECTION (mm)
SLAB 1
SLAB 2
SLAB 3

Figure 8.2

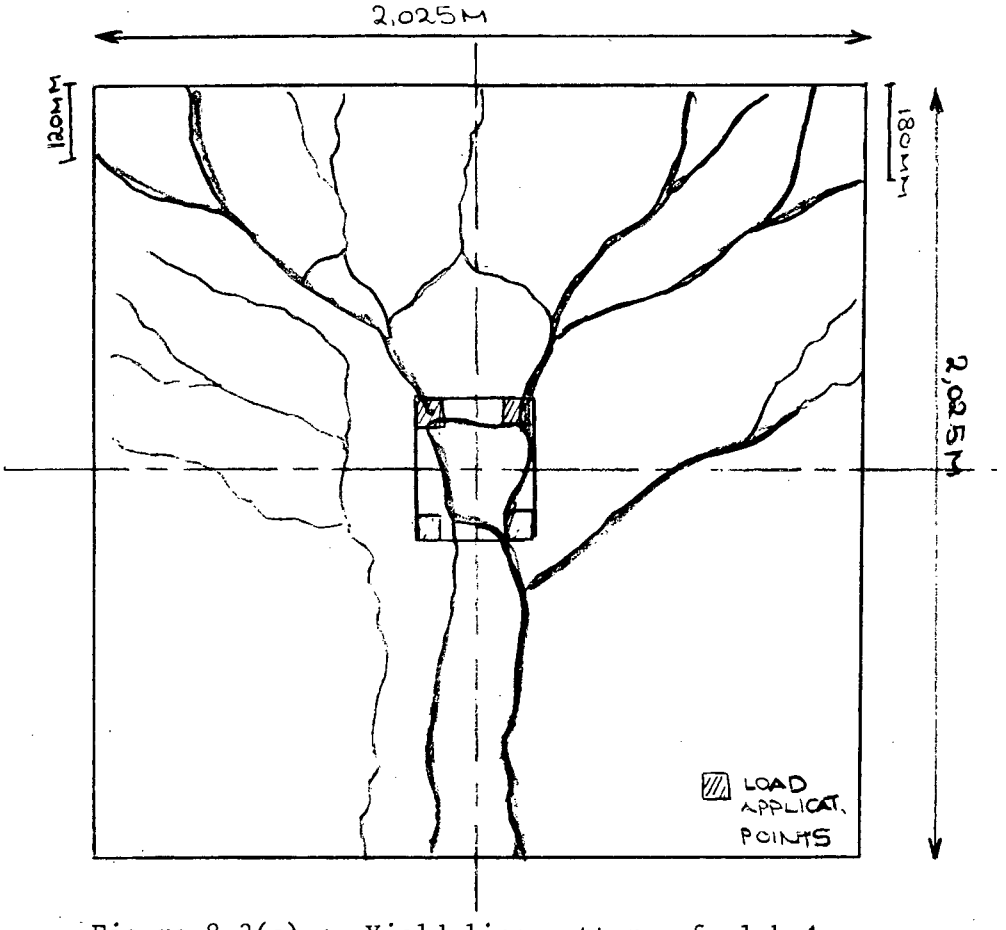

Figure 8.3(a) : Yield line pattern of slab 1

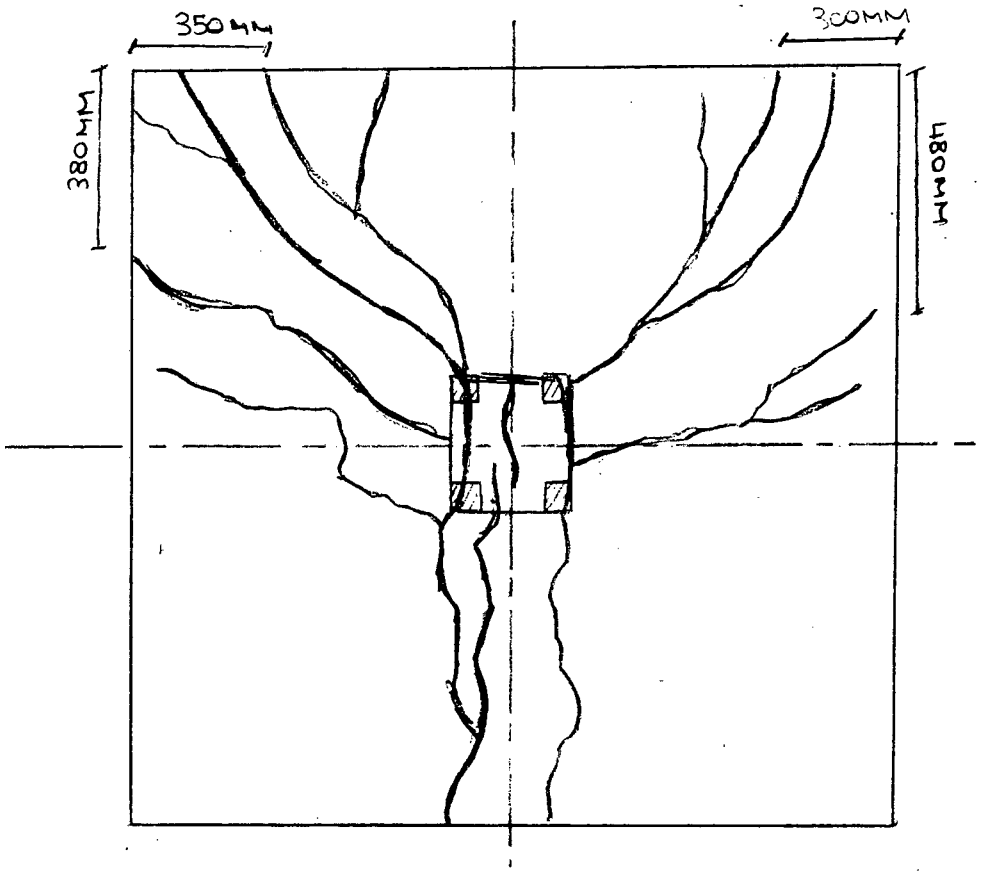

Figure 8.3(b) : Yield line pattern observed for slab 2

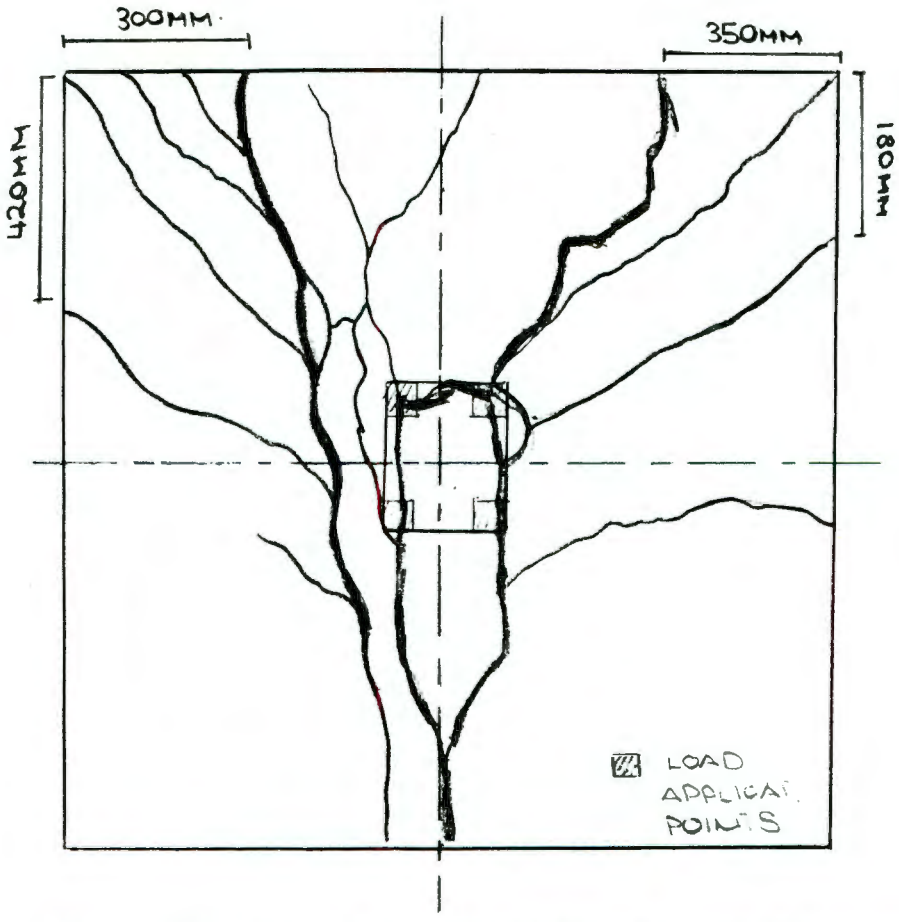

Figure 8.3(c) : Yield line pattern observed for slab 3

Plate 8.1 : Yield lines of slab 1 as viewed from the top of the slab. The large crack on the left side occurred during slab removal.

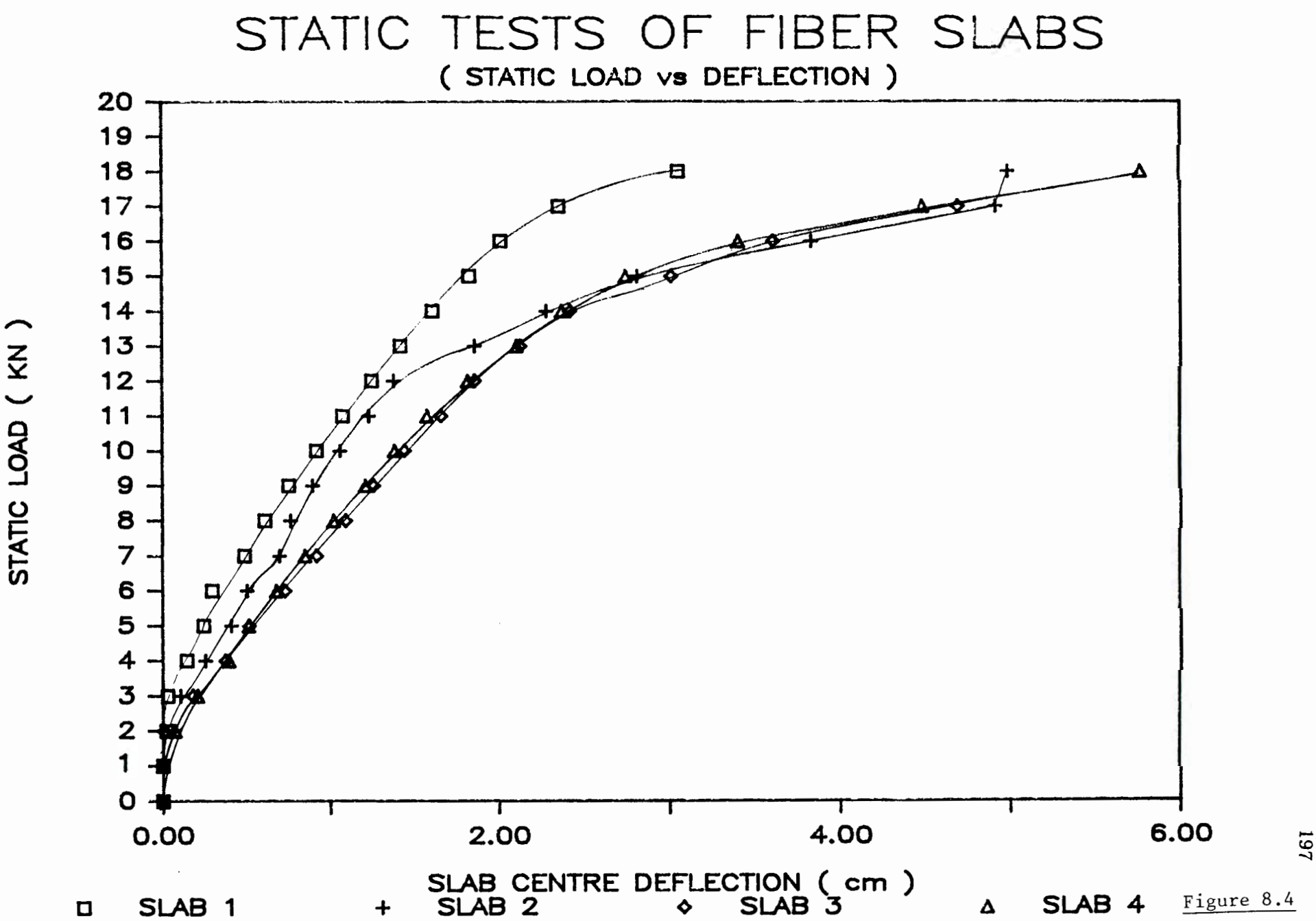
STATIC TESTS OF FIBER SLABS
(STATIC LOAD vs DEFLECTION)
STATIC LOAD (KN)
20
19
18
17
16
15
14
13
12
11
10
9
8
7
6
5
4
3
2
1
0
0.00
2.00
4.00
6.00
SLAB CENTRE DEFLECTION (cm)
SLAB 1
SLAB 2
SLAB 3
SLAB 4

Figure 8.4

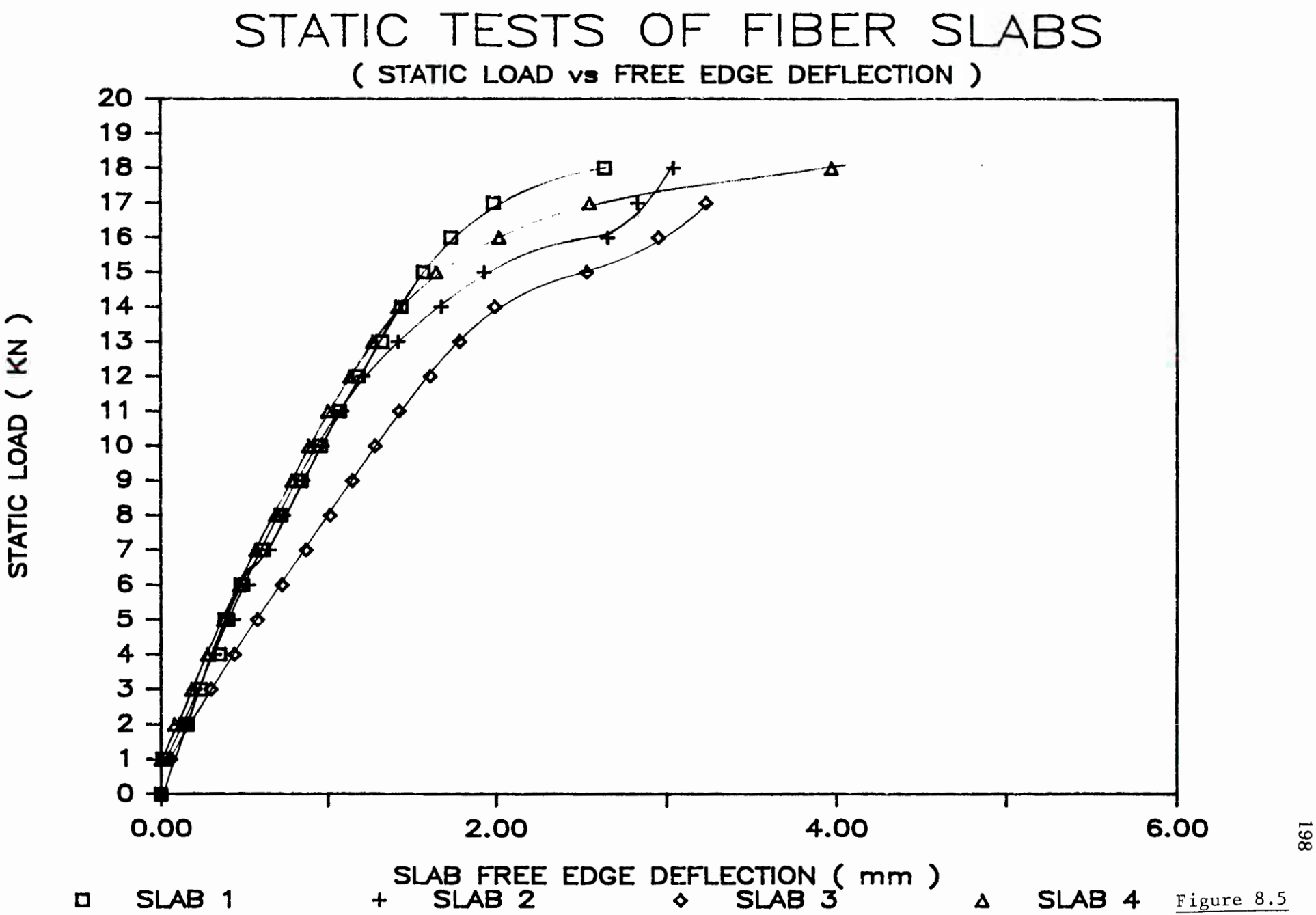
STATIC TESTS OF FIBER SLABS
(STATIC LOAD vs FREE EDGE DEFLECTION)
STATIC LOAD (KN)
20
19
18
17
16
15
14
13
12
11
10
9
8
7
6
5
4
3
2
1
0
0.00
2.00
4.00
6.00
SLAB FREE EDGE DEFLECTION (mm)
SLAB 1
SLAB 2
SLAB 3
SLAB 4

Figure 8.5

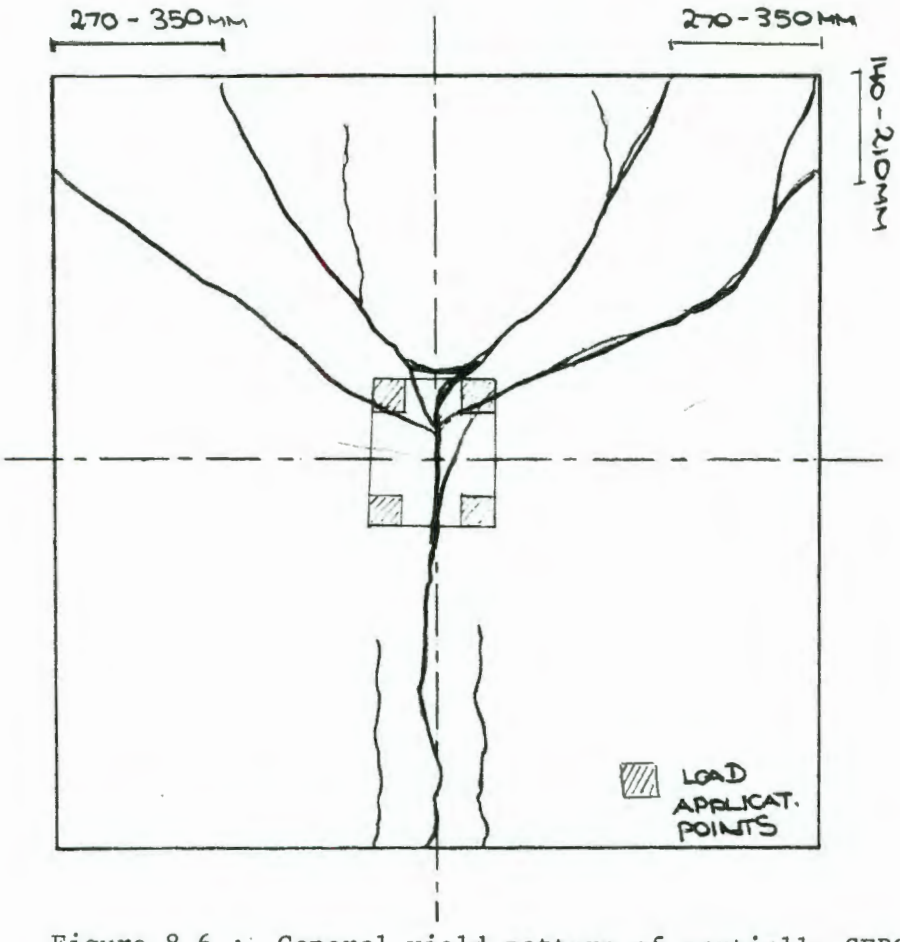

Figure 8.6 : General yield pattern of partially SFRC slabs observed under static loading

Plate 8.2 : A group of tested slabs; the top three were partially fibre-reinforced, the bottom three mesh-reinforced. Note different post-cracking stiffnesses.

Figure 8.7(a) : STATIC TESTS OF MESH SLABS

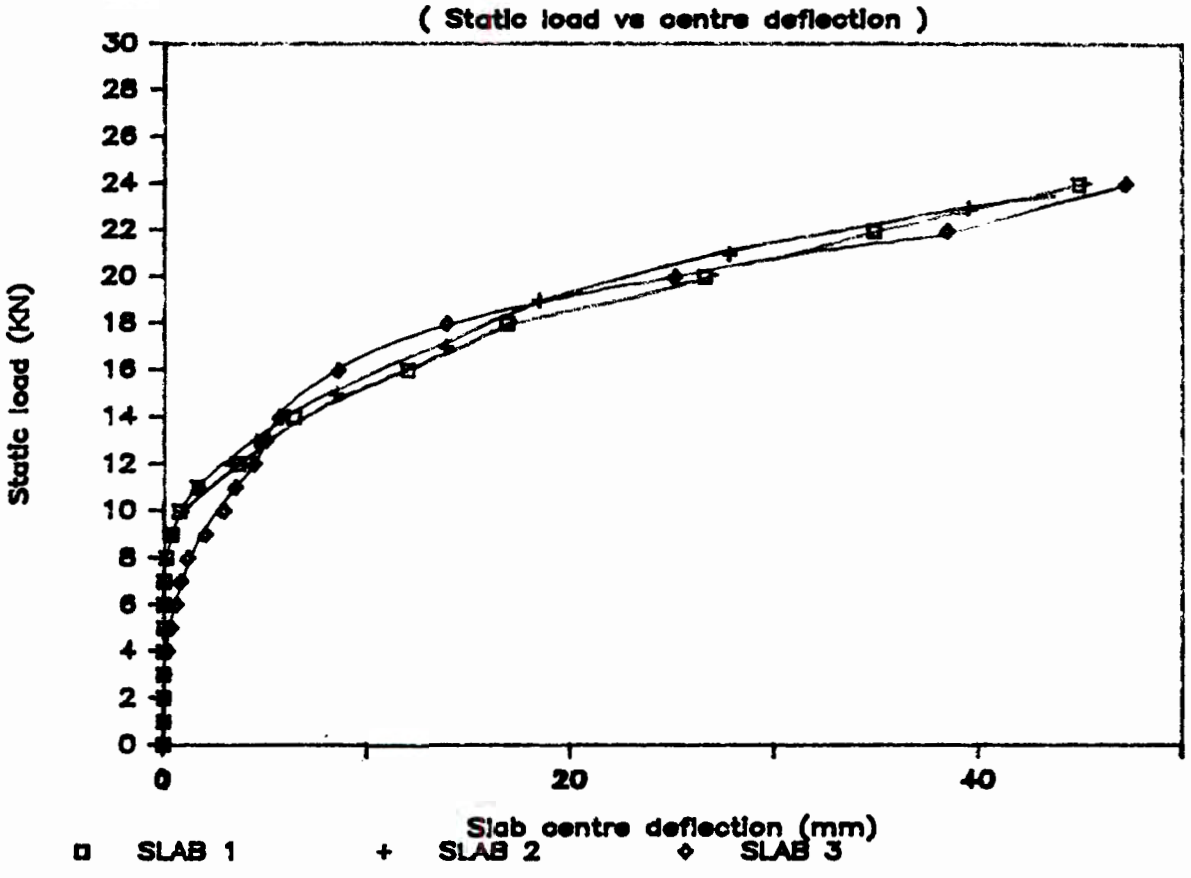

Figure 8.7(b) : STATIC TESTS OF MESH SLABS

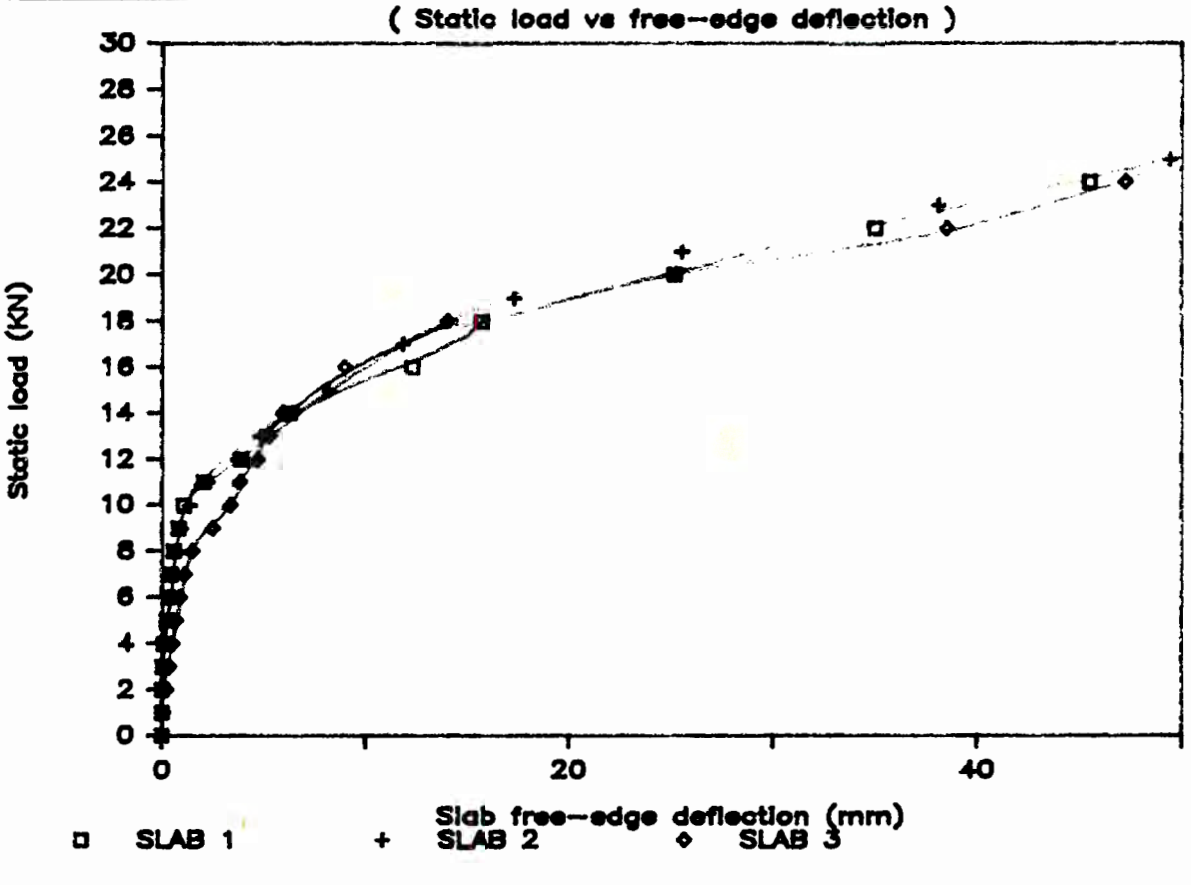

Figure 8.8(a) :STATIC TESTS OF FIBRE SLABS

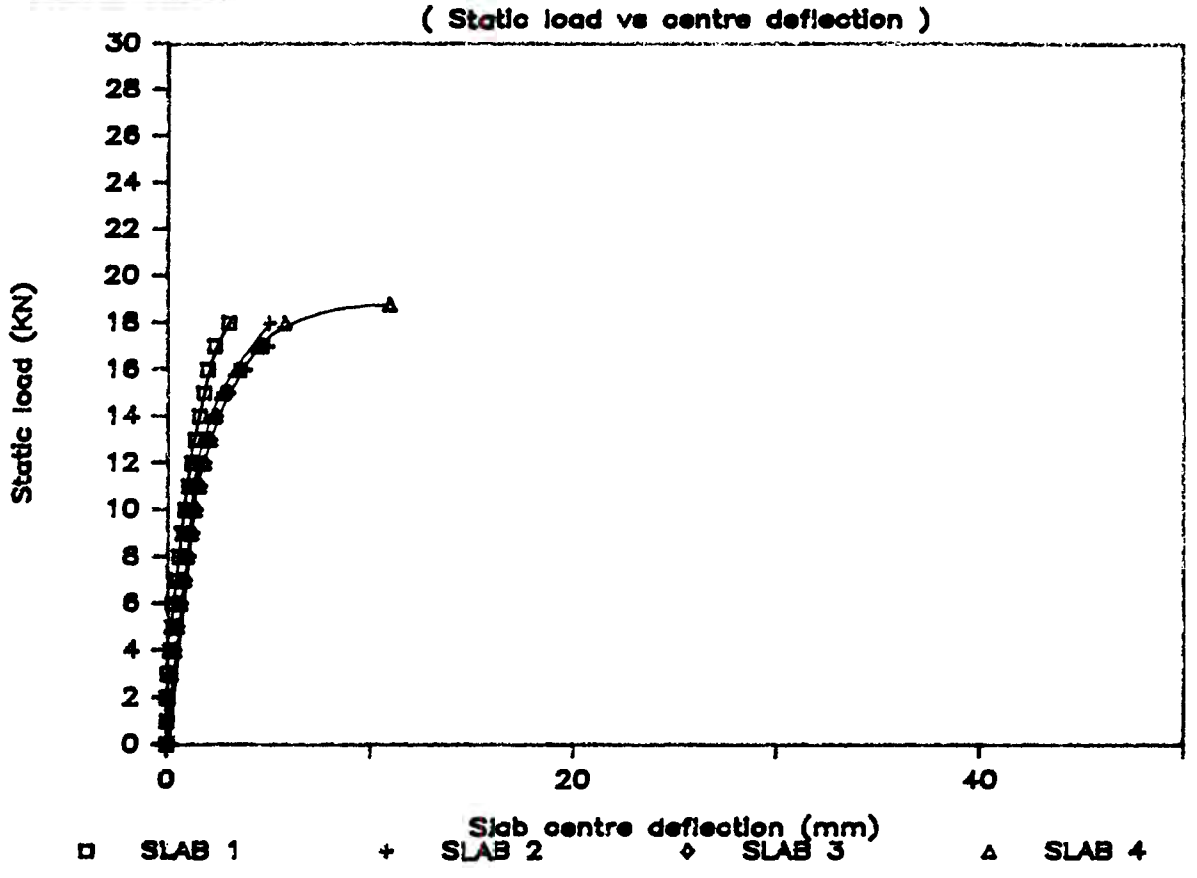

Figure 8.8(b) :STATIC TESTS OF FIBRE SLABS

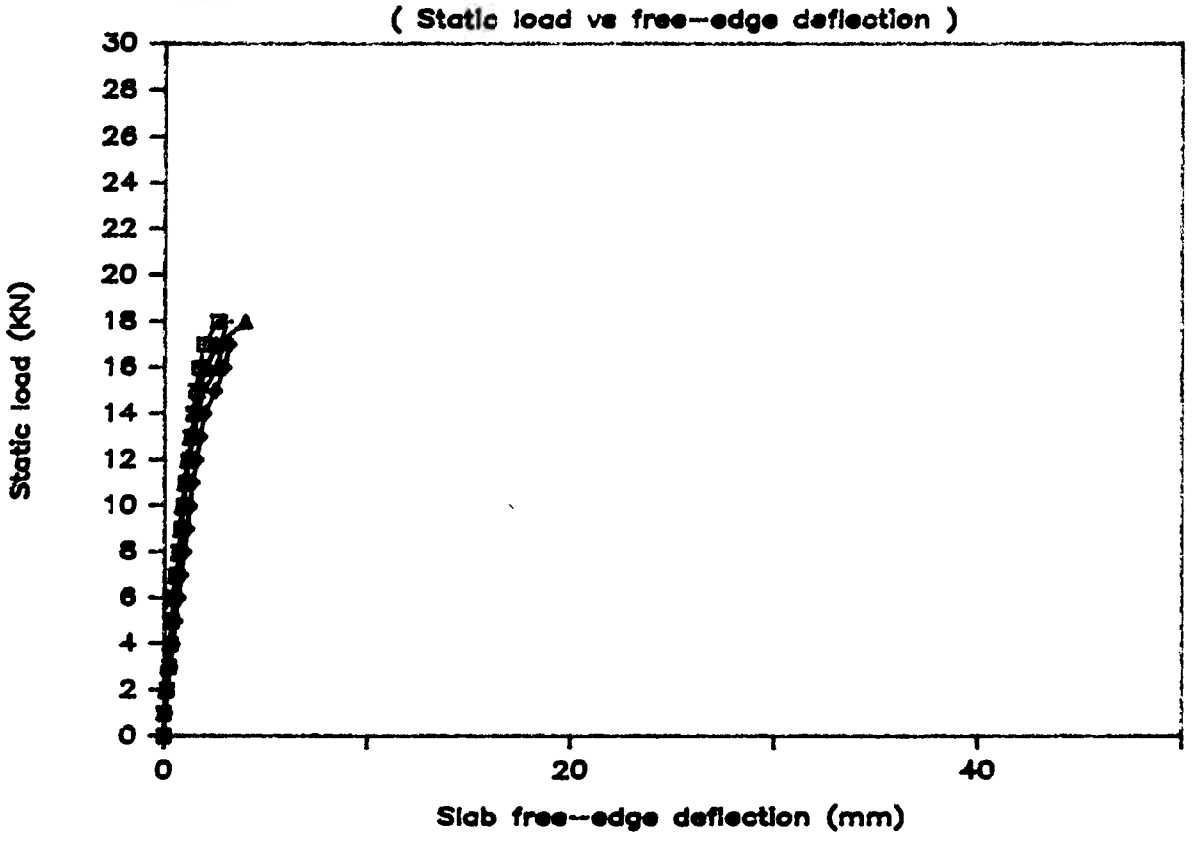

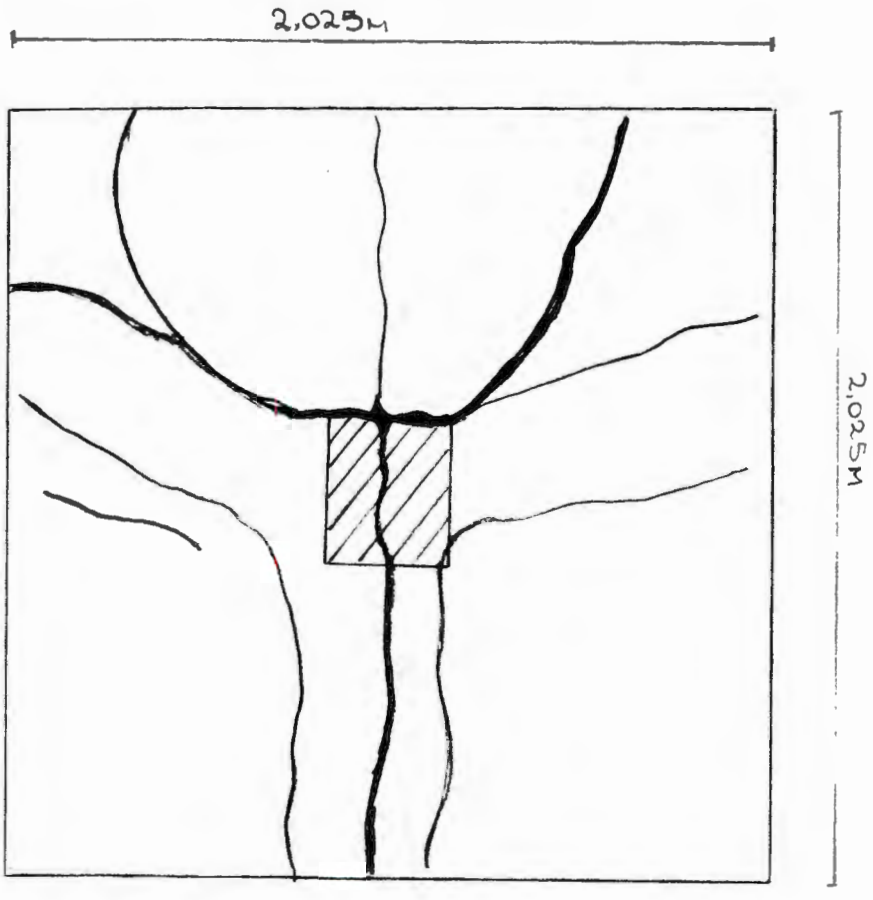

Figure 8.9(a) : Crack pattern of mesh reinforced slab 1, failure occuring along dark lines

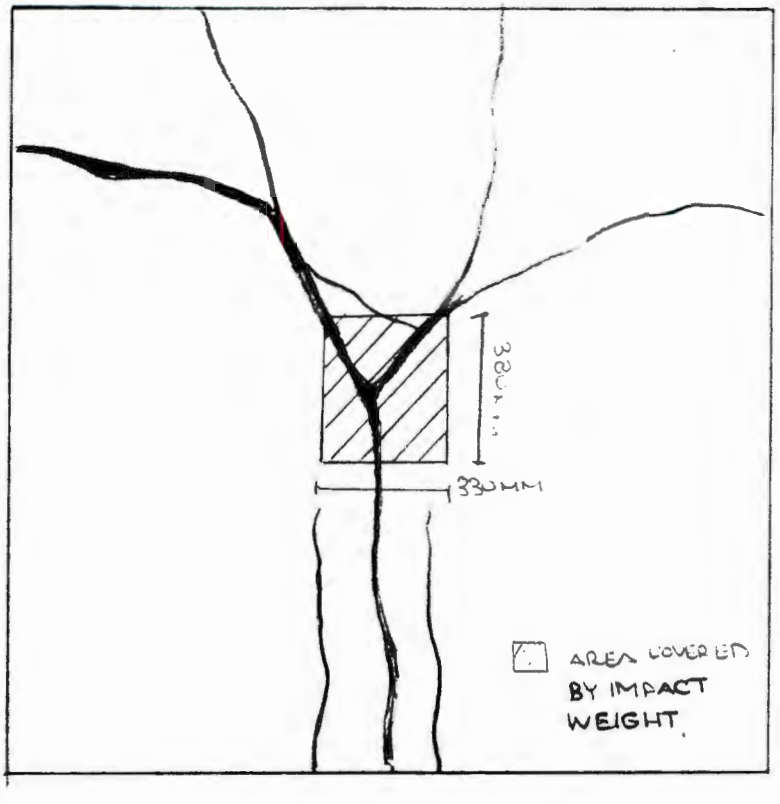

Figure 8.9(b) : Crack pattern of mesh reinforced slab 2 resulting from impact loading

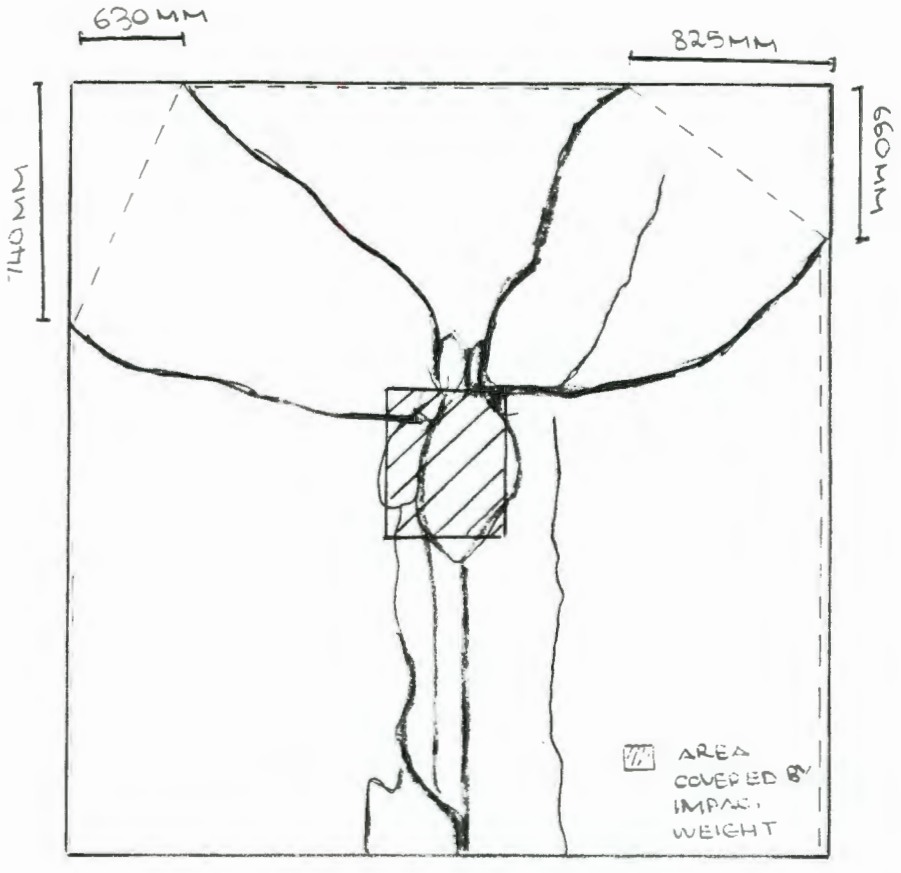

Figure 8.9(c) : Yield pattern of slab 3 subjected to impact loading. The axis of rotation of the fractured panels are shown as dotted lines.

Plate 8.3 : View of mesh reinforced slab 2, just after being subjected to the impact weight from a drop height of 1.6 metres

Figure 8.10

IMPACT TESTS OF MESH SLABS

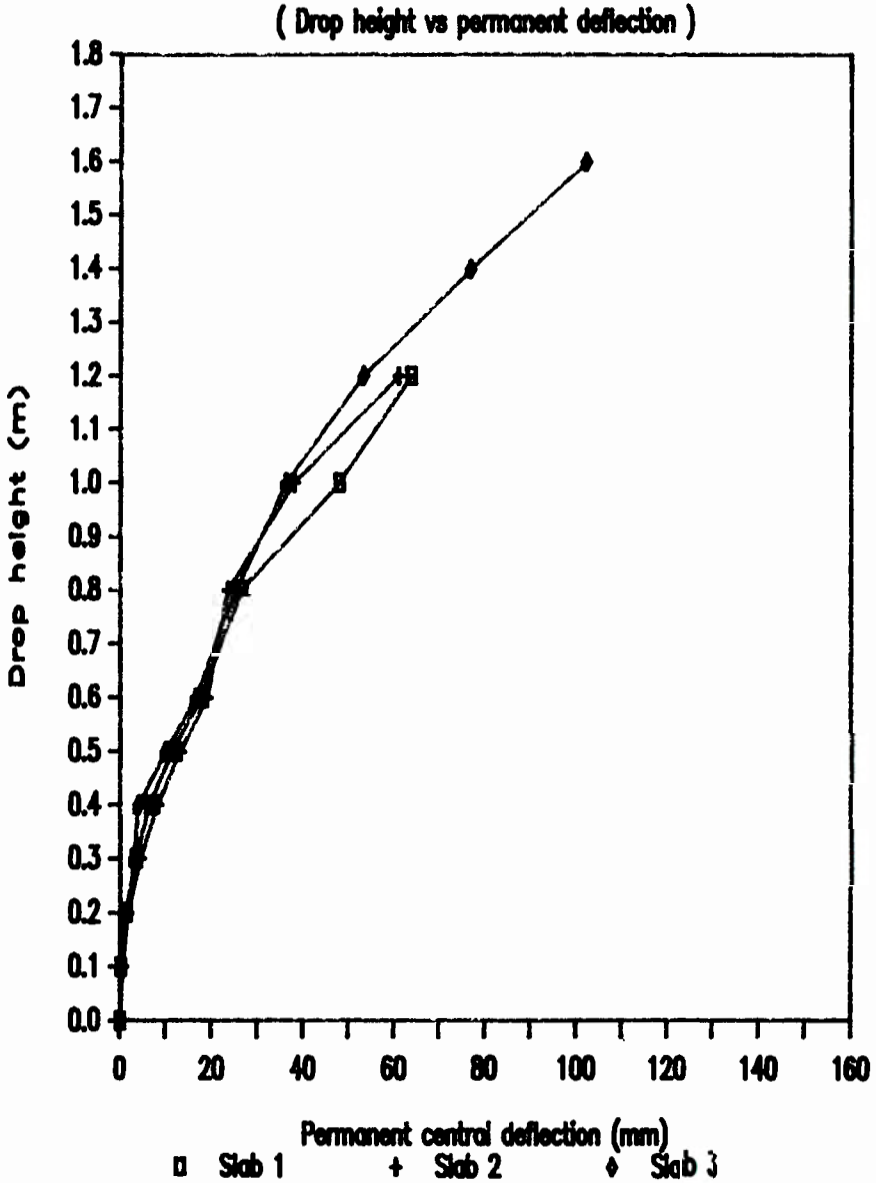

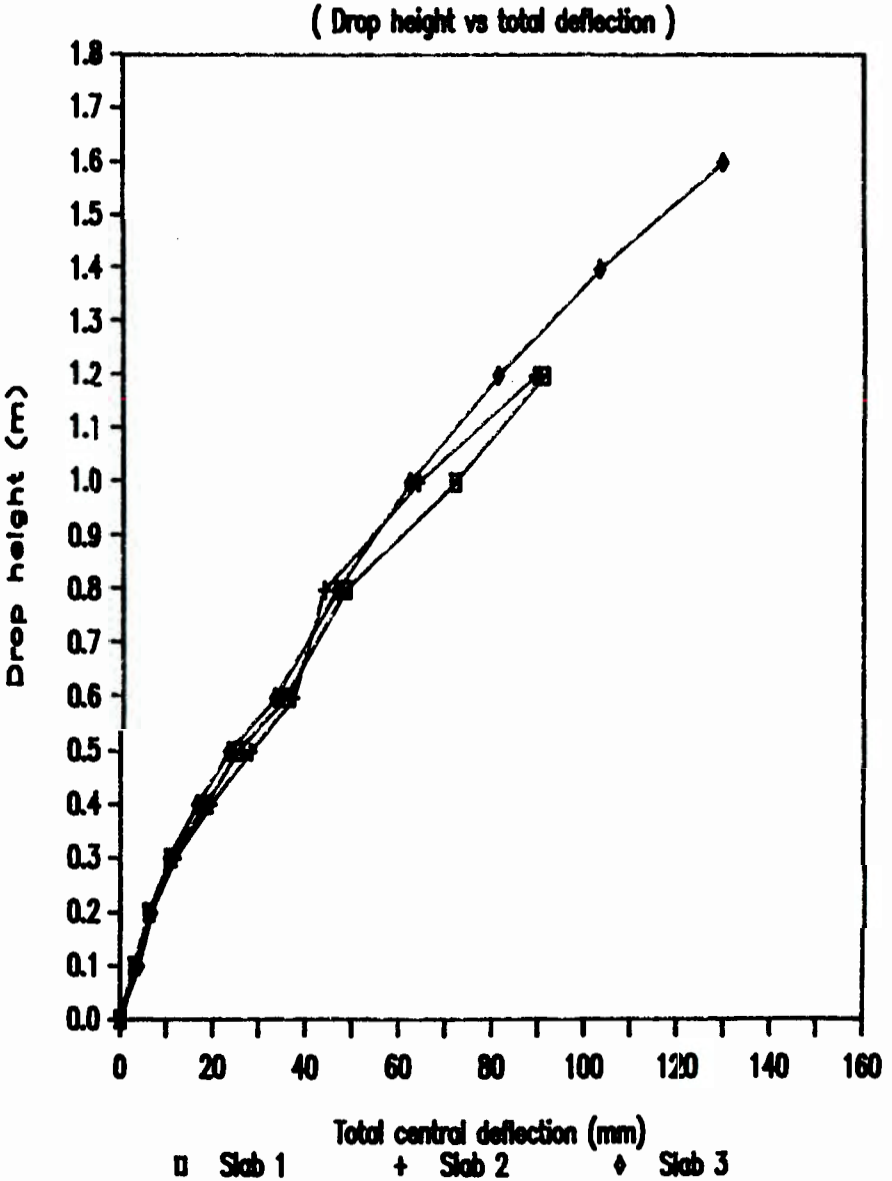

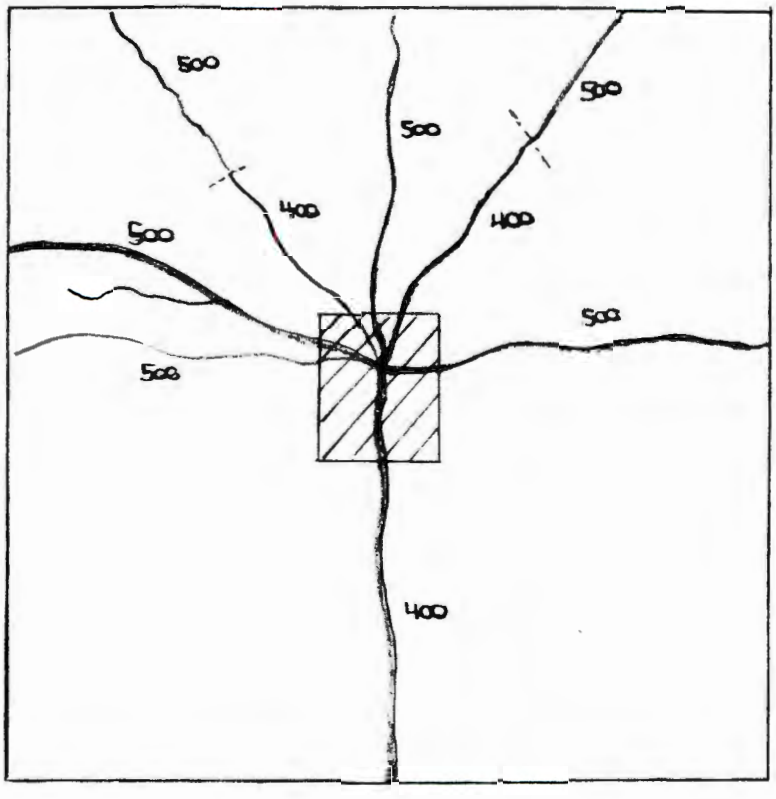

Figure 8.11(a) : Crack pattern and ultimate yield lines (dark) of partially SFRC slab 1. The numbers represent cracks occuring at that drop height.

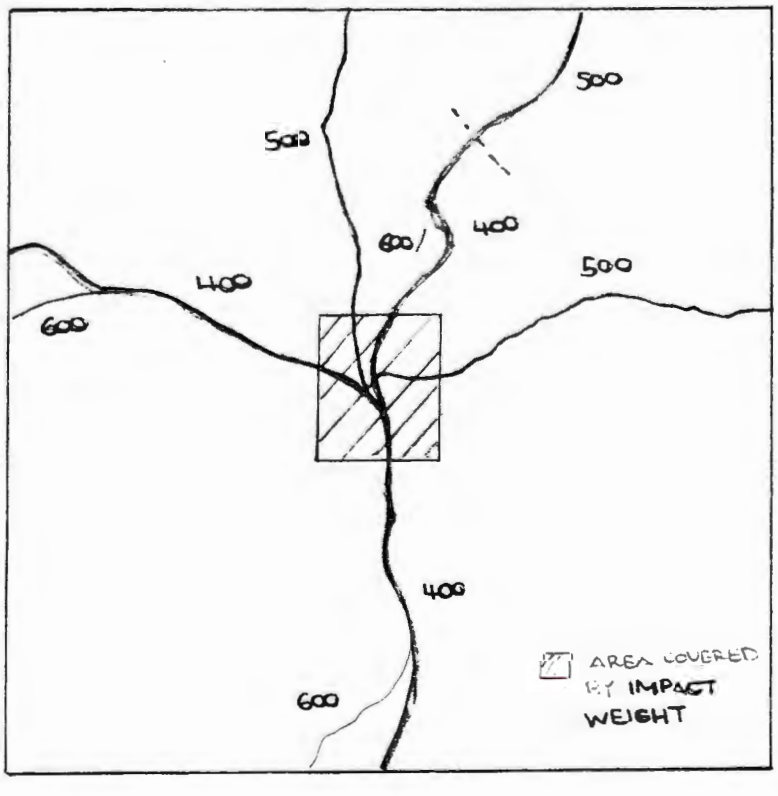

Figure 8.11(c) : Crack pattern and ultimate yield lines (dark) of partially SFRC slab 3

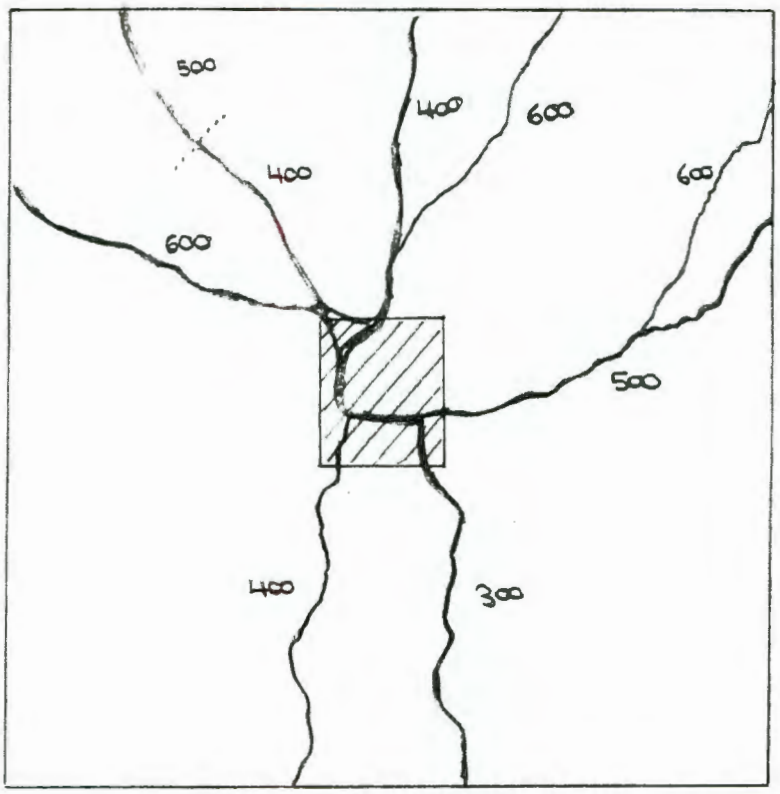

Figure 8.11(b) : Sketch showing crack pattern of partially SFRC slab 2

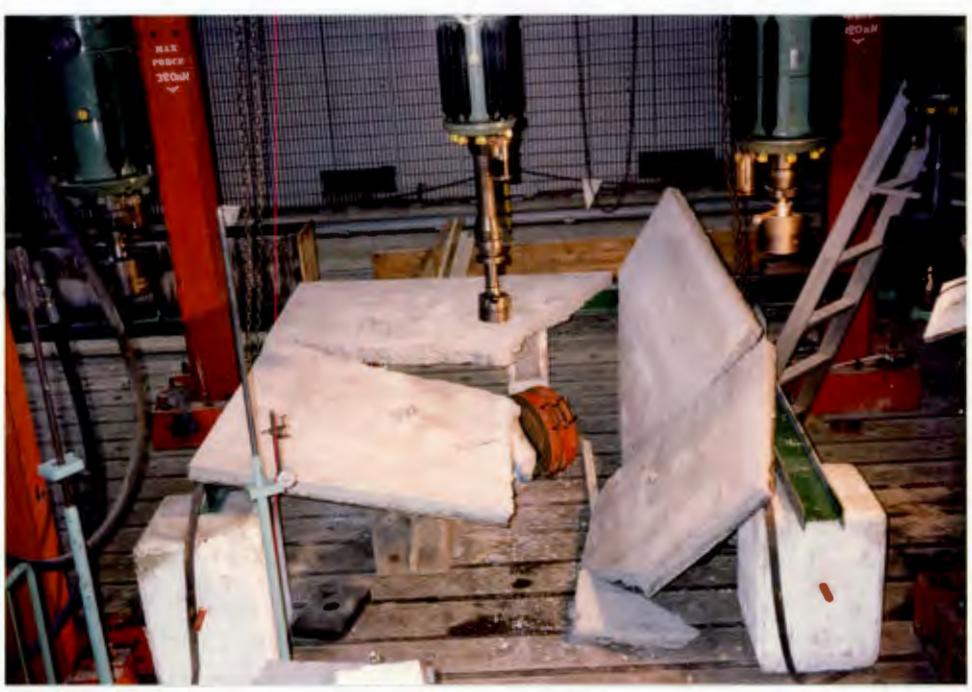

Plate 8.4 : Catastrophic failure of partially SFRC slab 2 after impact loading from a height of 700mm

Figure 8.12

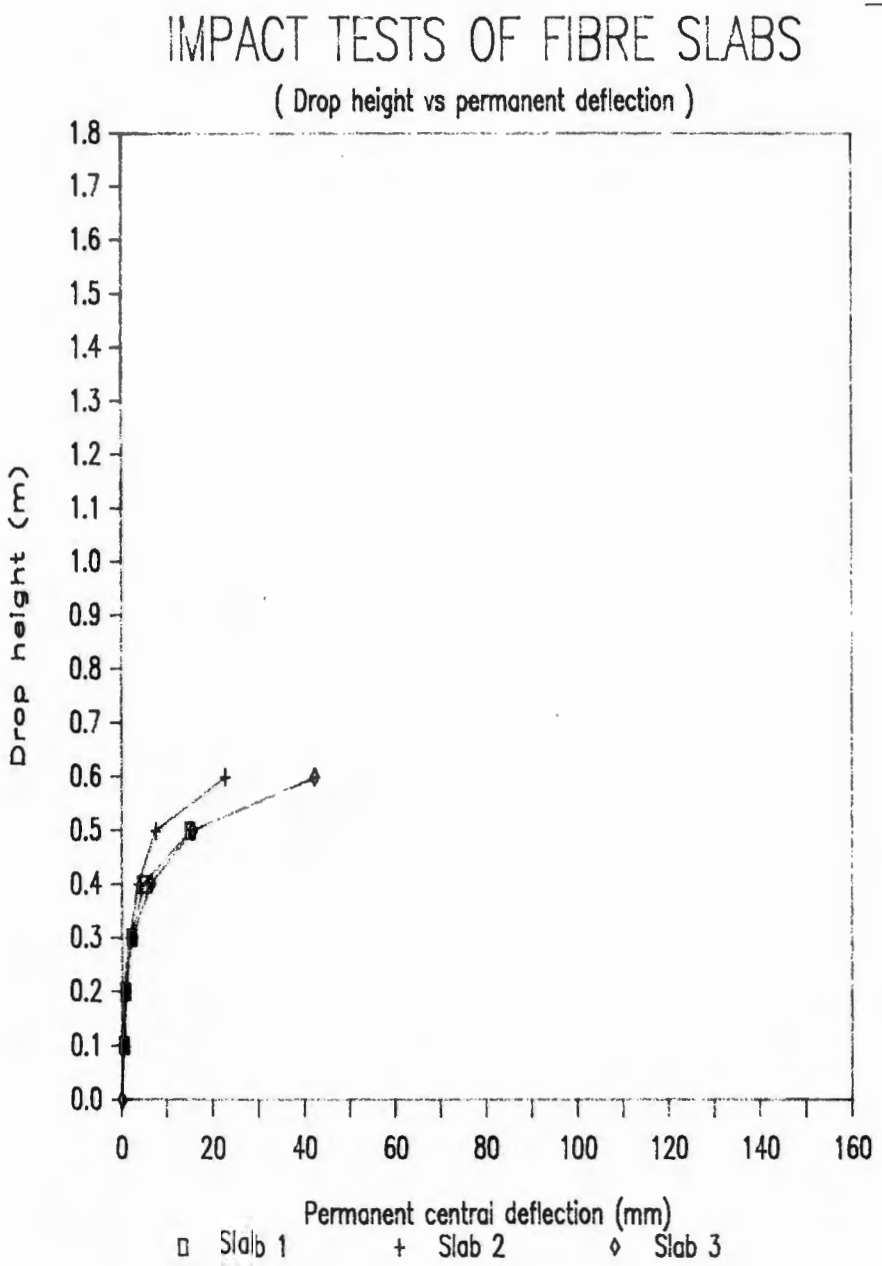
IMPACT TESTS OF FIBRE SLABS
(Drop height vs permanent deflection)
Drop height (m)
1.8
1.7
1.6
1.5
1.4
1.3
1.2
1.1
1.0
0.9
0.8
0.7
0.6
0.5
0.4
0.3
0.2
0.1
0.0
0
20
40
60
80
100
120
140
160
Permanent central deflection (mm)
Slab 1
Slab 2
Slab 3

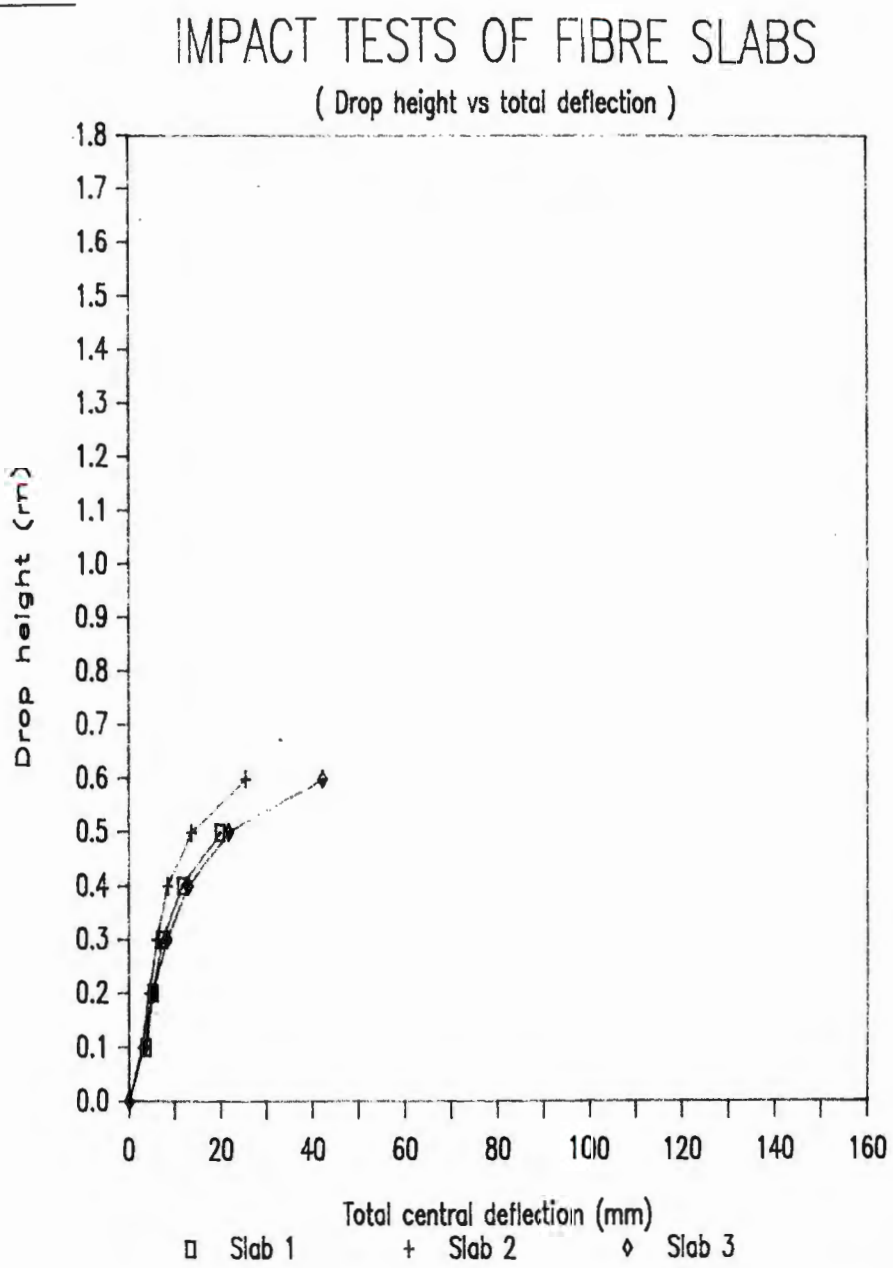
IMPACT TESTS OF FIBRE SLABS
(Drop height vs total deflection)
Drop height (m)
1.8
1.7
1.6
1.5
1.4
1.3
1.2
1.1
1.0
0.9
0.8
0.7
0.6
0.5
0.4
0.3
0.2
0.1
0.0
0
20
40
60
80
100
120
140
160
Total central deflection (mm)
Slab 1
Slab 2
Slab 3

Figure 8.13(a) IMPACT TESTS OF MESH SLABS

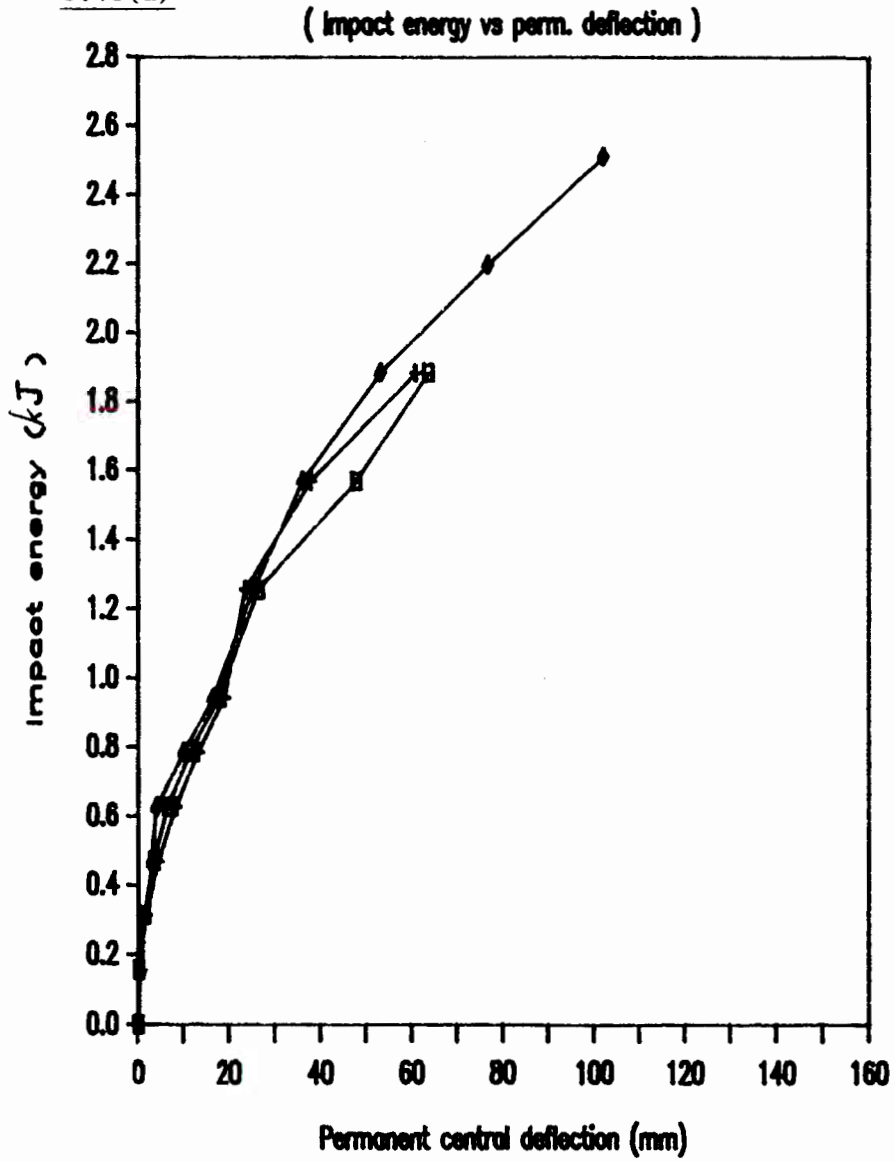

Figure 8.13(b) IMPACT TESTS OF FIBRE SLABS

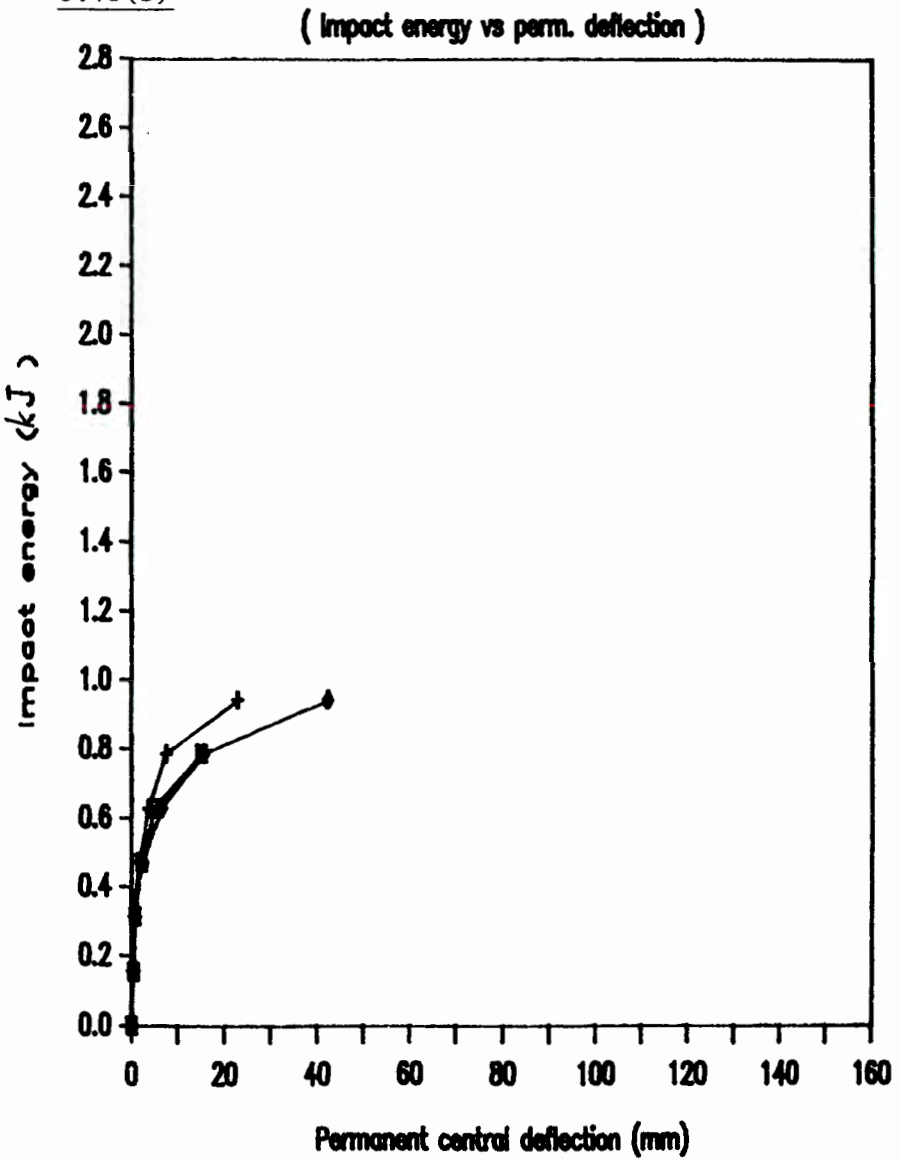

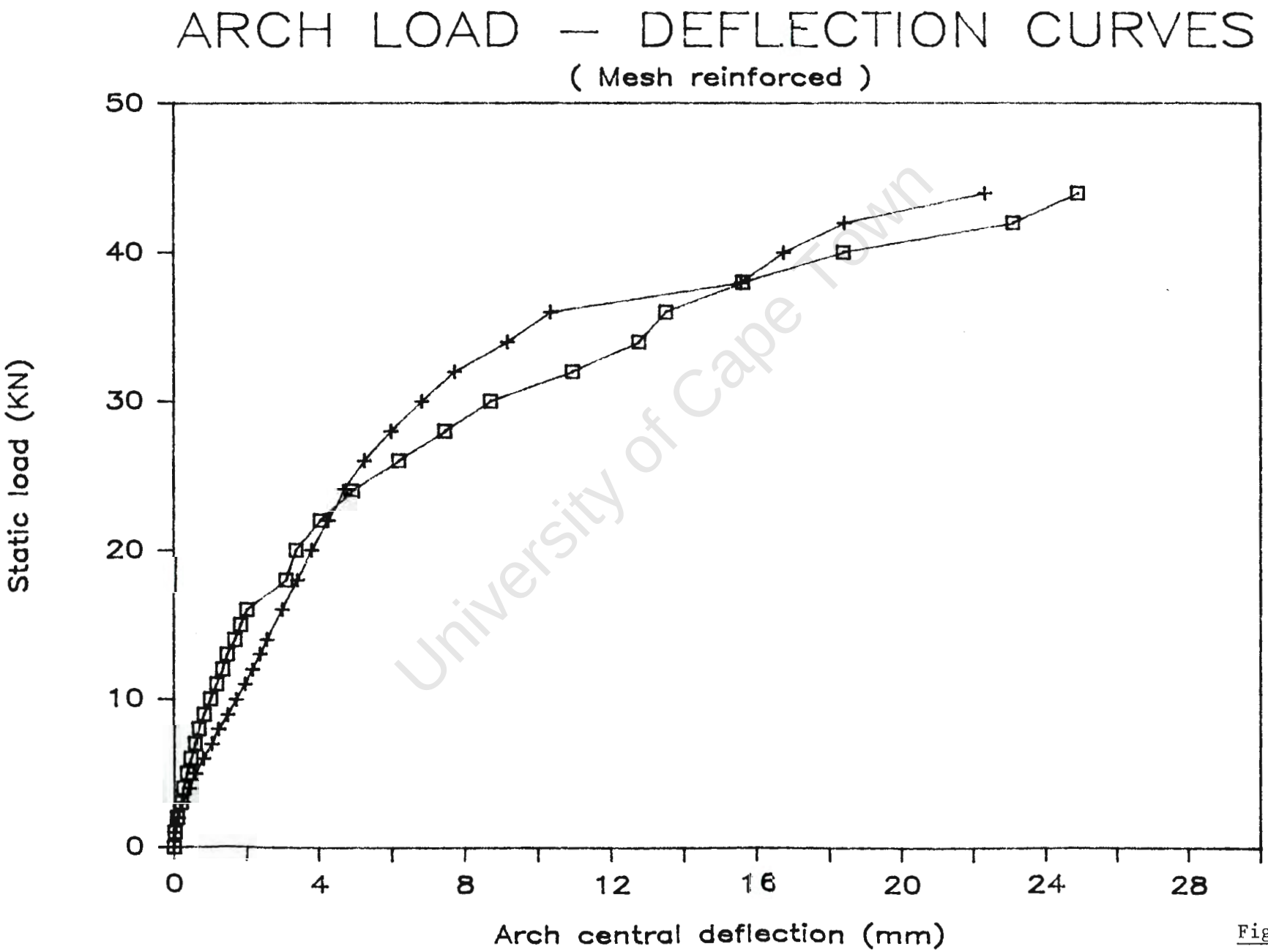

Figure 8.14

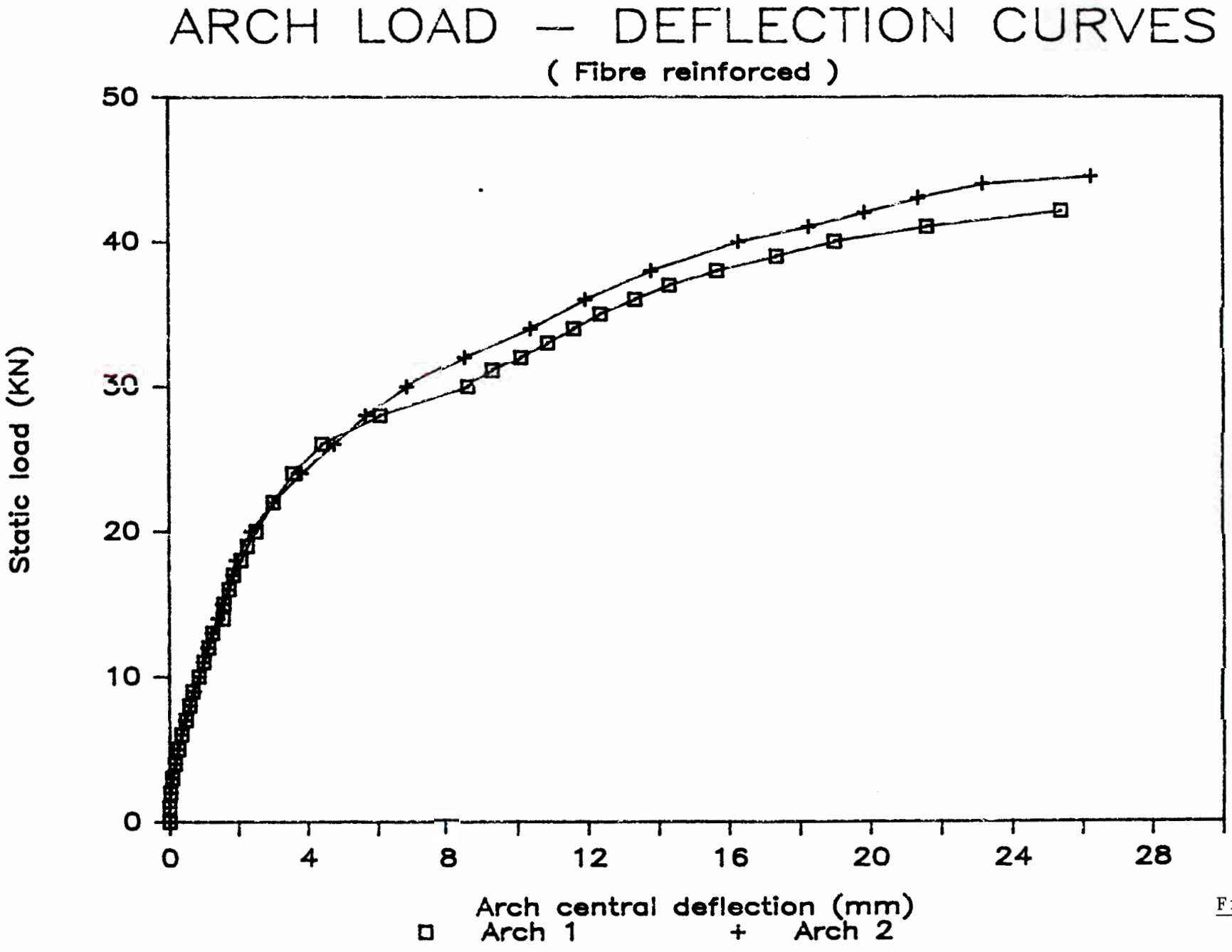
ARCH LOAD — DEFLECTION CURVES
(Fibre reinforced)
Static load (KN)
50
40
30
20
10
0
0
4
8
12
16
20
24
28
Arch central deflection (mm)
Arch 1
Arch 2

Figure 8.15

Figure 8.16

IMPACT TESTS OF MESH ARCHES

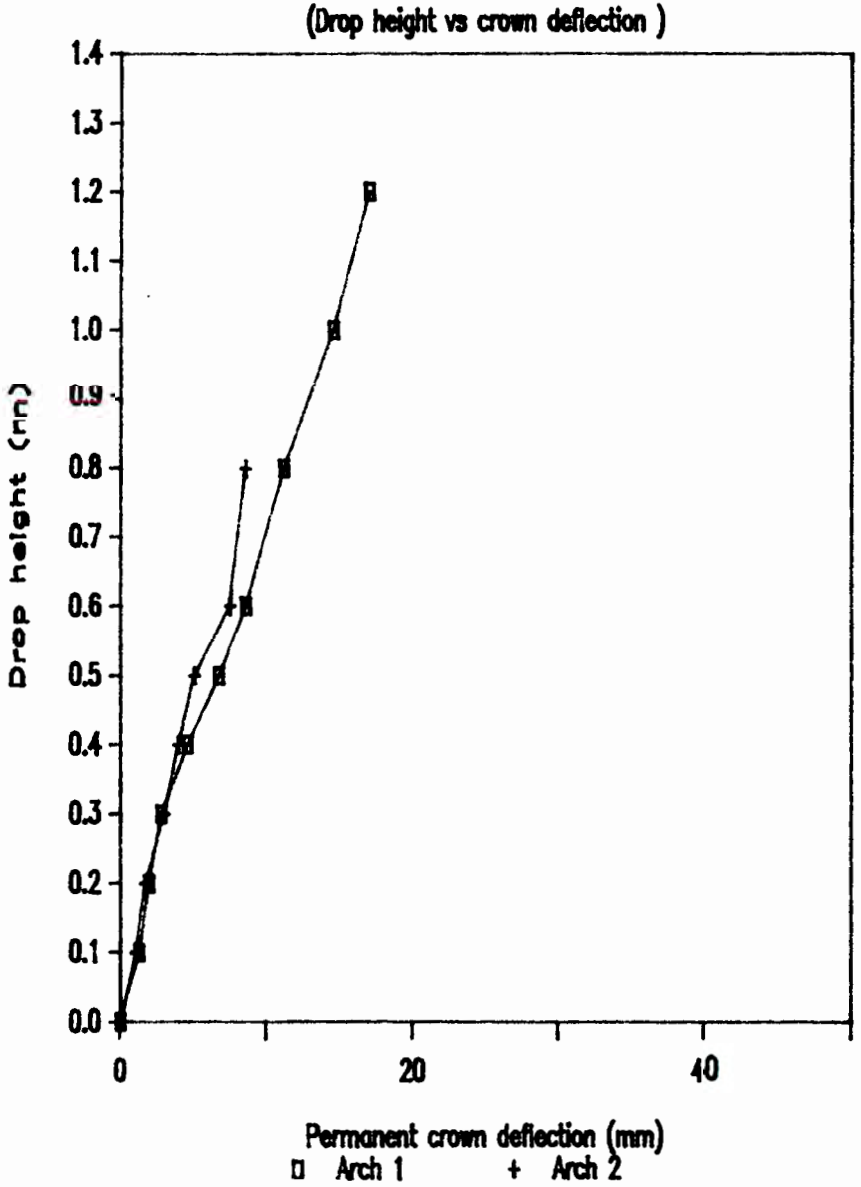

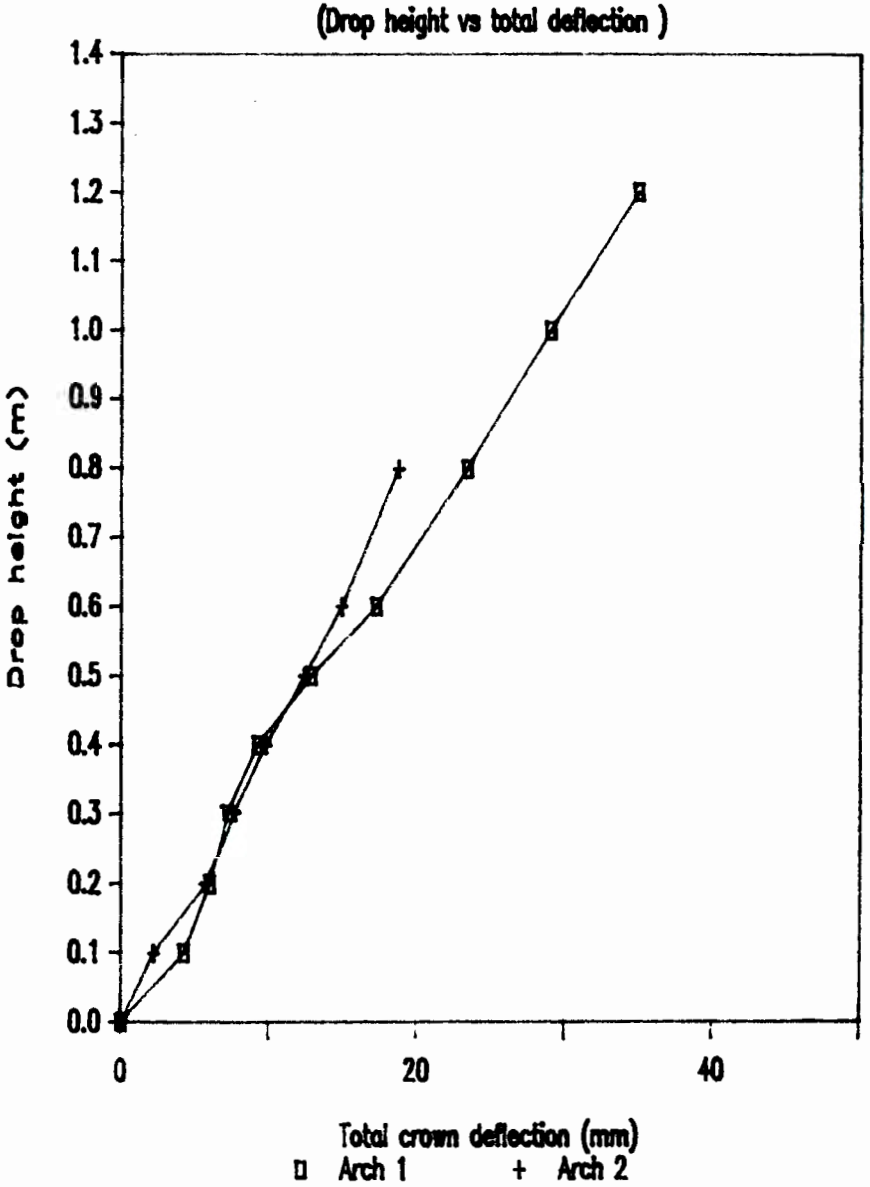

Figure 8.17

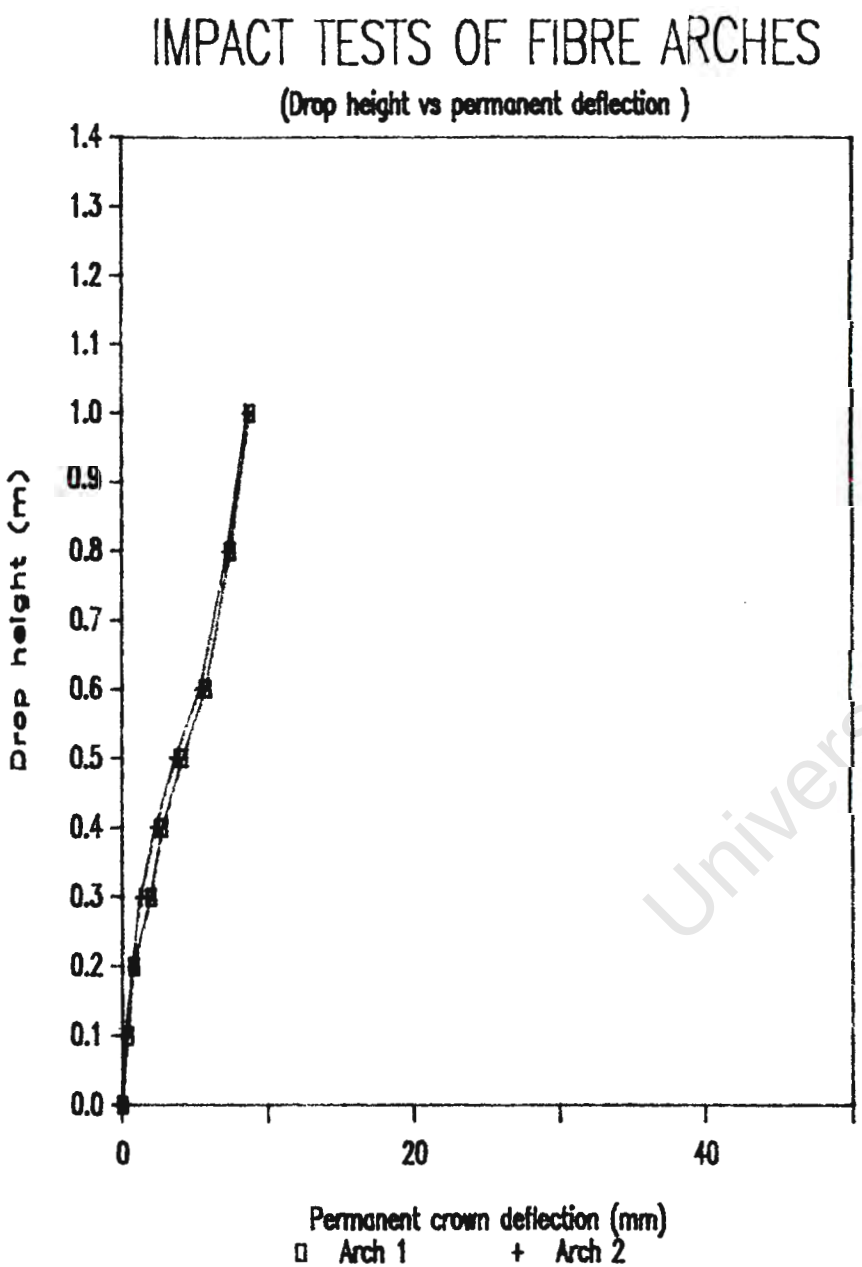

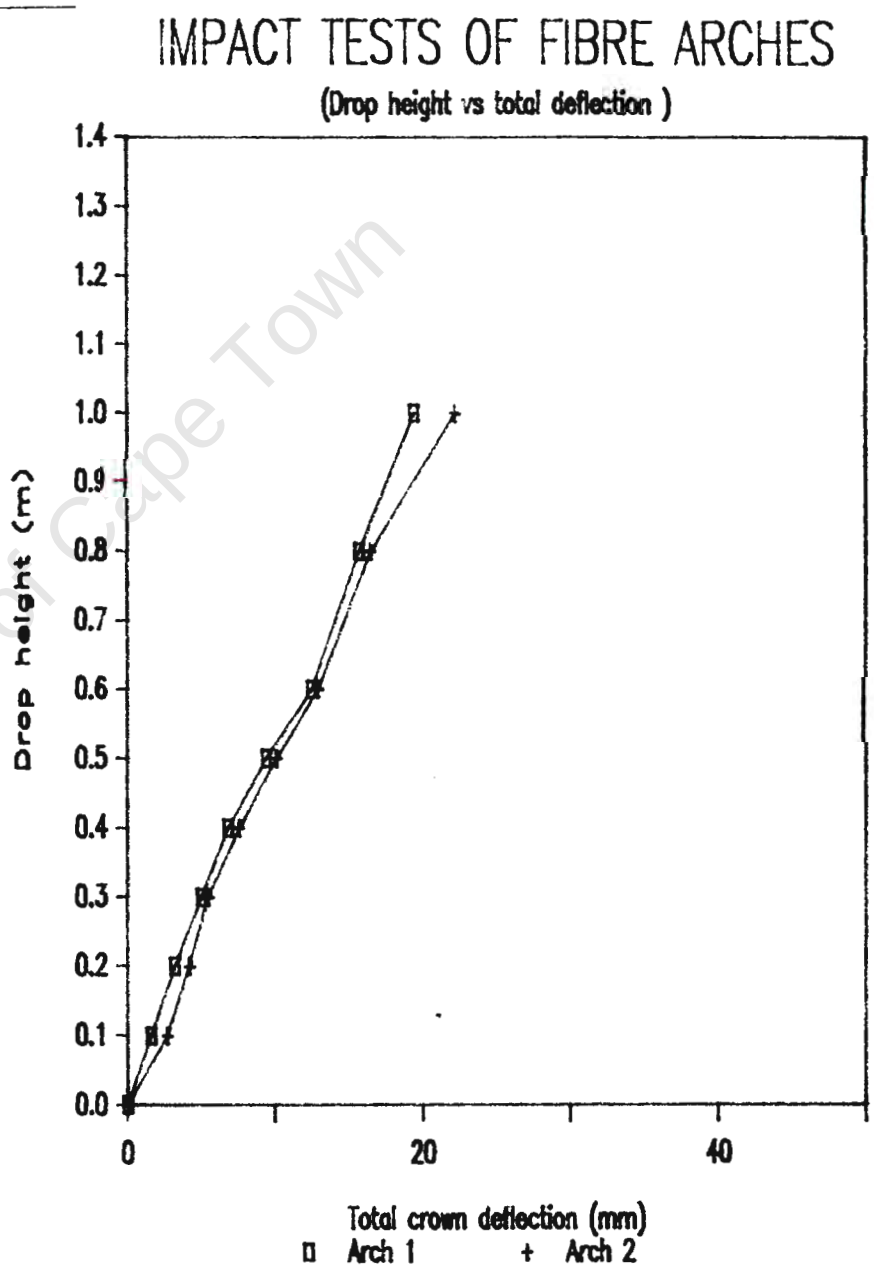

Plate 8.3 : Deformation of mesh-reinforced slab after extensive impact loading

Plate 8.4 : Catastrophic failure of a partially SFRC slab following an impact drop from a 700mm height

CHAPTER 9

CONCLUSIONS

The conclusions drawn from the Efficiency and Proving Phase are presented first, followed by those drawn from the Application Phase.

EFFICIENCY AND PROVING PHASE

1. Various analyses of the flexural strength test data obtained showed that a linear relationship between the flexural strength of SFRC specimens and the product ($V_f \cdot \ell/D$) existed. Theoretical equations, with constants derived from the test data, show good correlation with actual results.
2. An alternative theoretical approach relating the fibre centroid spacing to the SFRC flexural strength also showed very good correlation with test results.
3. The flexural tests conducted on SFRC specimens showed that specimens partially reinforced with steel fibres exhibited flexural strengths very close to those fully reinforced. Since the steel fibres are the most expensive constituent of the matrix, partial reinforcing would enable considerable cost savings.
4. With most fibre types there is a limit to the volume of fibre which can be added to the mix, before the workability and homogenuity of the composite is adversely affected. From the tests, it was observed that fibres with high aspect

ratios could only be used in limited quantities in order to avoid workability problems.

5. While there was an inherently high coefficient of variation between test results of the ACI Impact Test, the increased number of blows required to cause cracking and failure of the SFRC samples was evident. The test clearly showed the significantly improved impact resistance of the SFRC specimens relative to plain concrete.

6. The Efficiency and Proving Phase tests demonstrated the superior influence of the Binding Wire type fibres on the mechanical properties of a concrete matrix. This, combined with the low production cost of the fibres, led to their selection for further testing in the Application Phase.

APPLICATION PHASE

7. Although the 1.25% V_f partially reinforced slabs exhibited lower load capacities than the mesh-reinforced slabs under static loading, the slab deflection of the former was substantially less than that recorded for the latter. This factor is of importance when one considers the low allowable deflections given in most structural and building codes.

8. Under impact loading, the 1.25% V_f partially reinforced slabs showed slightly lower deflections than the mesh-reinforced slabs. Thus, within the limits proposed by MANTAG, the partially SFRC slabs are stiffer. However, for high impact energies the partially SFRC slabs failed catastrophically compared to the mesh-reinforced slabs. It is therefore doubtful whether the partially SFRC slabs would

meet more stringent requirements by, say, the SABS National Building Regulations.

9. Unlike the slab test panels, the partially SFRC and mesh-reinforced arches exhibited the same static load capacity. It was realised that this was due to the test panel shape rather than the effect of the fibres. Under impact loading, the partially SFRC arches exhibited slightly lower deflections than the mesh-reinforced arches, for the same reason.

The application phase of the test program clearly demonstrated the improved performance of partially SFRC compared to mesh-reinforced concrete for the MANTAG criteria. Although the mesh-reinforced slab panels exhibited higher ultimate static and impact load capacities, the deflections associated with these loads are excessive.

CHAPTER 10

RECOMMENDATIONS

Based on the observations made during specimen preparation and subsequent testing it is recommended that :

1. The high aspect ratio of the Binding Wire fibres be reduced so that a less stiffer, more workable mix be obtained. For the high aspect ratio used, fibre balls were observed to occur during mixing with fibre volumes as low as 1.50%. Additionally, the time and effort required to adequately compact the fibre mix nullified any time saved from not having to fix steel mesh in place.
2. When calculating the volume of fibre required to yield the same strength as mesh-reinforcing (Appendix G calculations), an orientation factor of 0.64 be applied to equation (G.4). It is expected that closer correlation of the ultimate static load of the partially SFRC slabs and mesh-reinforced slabs will then occur.
3. A <u>combined</u> partially SFRC and mesh-reinforced section be cast and tested under static and impact loading. The steel fibres will ensure greater rigidity under static loading while the steel mesh will provide for greater impact resistance.

REFERENCES

1. Naaman, A E 'Fibre Reinforcement for Concrete', Concrete International, U.S.A., March 1985, p.21.

2. Naaman, A E, p.21.

3. Hannant, D J Fibre Cements and Fibre Concretes, Chichester, John Wiley and Sons, 1978, p.61.

4. Naaman, A E, p. 24.

5. Hannant, D J, p.101.

6. Naaman, A E, p.25.

7. Hannant, D J, p.115.

8. Ohama, Y 'Properties of Carbon Fibre Reinforced Cement with Silica Fume', Concrete International, U.S.A., March 1985, p.58.

9. Naaman, A E, p.24.

10. Ali, M A 'Carbon-Fibre reinforcement of cement', Cement and Concrete Research, 2(2), 1972, p.201.

11. Ohama, Y, p.58.

12. Hannant, D J, *et al* 'Polypropylene fibres in cement based materials', Composites, 9, No. 2, Science and Technology Press Ltd., April 1978, p.85.

13. Keer, J G and Thorne, A 'Performance of Polypropylene-Reinforced Cement Sheeting Elements', Fibre Reinforcement Concrete, A.C.I. Special Publication SP-81, U.S.A., 1984, p.224.

14. Hannant, D J, p.136.

15. Krenchel, H 'Fibre-reinforced brittle matrix materials', Fibre-Reinforced Concrete, Publication Sp-44, U.S.A., Construction Press Ltd., 1974, p.50.

16. Majumdar, A J 'Discussion on properties of fibre-cement composites', Fibre reinforced Cement and Concrete, RILEM Symposium, Vol. 2, 1975, p.605.

17. Hannant, D J, p.155.

18. Castro, J and Naaman, A E 'Cement mortar reinforced with natural fibres', A.C.I. Journal, January-February 1981, p.69-77.

19. Majumdar, A J 'Properties of fibre-cement composites', Fibre reinforced Cement and Concrete, RILEM Symposium 1, The Construction Press, Lancaster, 1975, p.283.

20. Hannant, D J, p.4.

21. Castro, J, p.72-76.

22. Raunch, W *et al* 'Fibre composite materials', Ceramic Fibres and Fibrous Composite Materials, Vol. 3, Academic Press, New York, 1968, p.60-65.

23. Hannant, D J, p.10.

24. Swamy, R M and Mangat, P S 'A theory for the flexural strength of steel fibre-reinforced concrete', Cement and Concrete Research, Vol. 4, Pergamon Press Inc., U.S.A., 1974, p.316.

25. Gray, R J and Johnston, C D 'The measurement of fibre-matrix interfacial bond strength in steel fibre-reinforced cemtitious composites', Testing and Test Methods of Fibre Cement Composites, RILEM Symposium 1978, The Construction Press, England, p.317.

26. Gray, p.318.

27. Maage, M 'Fibre bond and friction in cement and concrete', Testing and Test Methods of Fibre Cement Composites, RILEM Symposium 1978, The Construction Press, England, p.317.

28. Pinchin, D J 'Interfacial contact pressure and frictional stress transfer in steel fibre cement', Testing and Test Methods of Fibre Cement Composites, RILEM Symposium 1978, The Construction Press, England, p.337.

29. Stroeven, P, *et al* 'Pull-out tests of steel fibres', RILEM Symposium 1978, The Construction Press, England, p.345.

30. Neville, A M 'Testing of hardened concrete', Properties of Concrete, Third Edition, Pitman Publishing Limited, Great Britain, 1981, p.548.

31. Swamy, R N, *et al* 'The mechanics of fibre reinforcement of cement matrices', Fibre Reinforced Concrete, A.C.I. Publication SP-44, Detroit, U.S.A., 1974, p.24.

32. Swift, D G 'The physical significance of the flexure test for fibre cement composites', Testing and Test Methods of Fibre Cement Composites, RILEM Symposium 1978, The Construction Press, England, p.467-468.

33. Swamy, R N and Al-Ta'an, S A 'Deformation and ultimate strength in flexure of reinforced concrete beams made with steel fibre concrete', A.C.I. Journal, September-October 1981, U.S.A., p.401.

34. Laws, V and Walton, P L 'The tensile-bending relationship for fibre-reinforced brittle matrices', Testing and Test Methods of Fibre Cement Composites, RILEM Symposium 1978, The Construction Press, England, p.496.

35. Hannant, D J, p.31.

36. "Spacing Concept", State-of-the-Art Report on Fibre Reinforced Concrete, Report No. ACI 544.IR-82, Concrete International, May 1982, p.12.

37. Ibid, p.12.

38. Swamy, R N, p.12-13.

39. "State-of-the-Art Report", Fibre Reinforced Concrete, International Symposium, ACI Publication SP-81, Detroit, U.S.A., P.415.

40. Krenchel, H 'Fibre spacing and specific fibre surface', Fibre Reinforced Cement, RILEM Symposium 1975, The Construction Press Ltd, Great Britain, p.74-75.

41. Ibid, p.78.

42. Swamy, R N and Mangat, P S 'Crack initiation, ductility, fibre reinforced concrete', Cement and Concrete Research, Vol. 5, 1975, p.43-48.

43. Hannant, D J, p.42.

44. Mallick, P K and Broutman, L S Journal of Materials Science, 9, 1974, p.1420.

45. Raunch, W, *et al*, p.65.

46. Kelly, A and Davies, G J 'Metallurgical Review, 10, 1, (1965), p.43.

47. Argon, A S and Shack, W J 'Theories of fibre cement and concrete', Fibre Reinforced Cement and Concrete, RILEM Symposium 1975, The Construction Press, England, p.48-49.

48. Rajagopalan, K and Parameswaran, V S "A discussion of the paper - 'A theory for the flexural strength determination of a steel fibre reinforced concrete'", A.C.I. Journal, Vol. 5, 1970, p.179-180.

49. Cox, H L and Brit, J Journal of Applied Physics, 3, ((1952), p.72.

50. Allen, H G 'Glass-fibre reinforced cement, strength and stiffness', Ciria Report 55, September 1975, p. .

51. Hannant, D J, p.12.

52. Brandt, A M 'On the optimization of the fibre orientation in cement based composite materials', Fibre Reinforced Concrete, A.C.I. Publication SP-81, Detroit, U.S.A., p.277.

53. Brandt, A M, p.270-273.

54. Naaman, A E and Shah, S P 'Bond studies on oriented and aligned steel fibres', Fibre Reinforced Cement and Concrete, RILEM Symposium 1975, The Construction Press Ltd., Lancaster, England, p.174.

55. Brandt, p.279.

56. Laws, V 'The efficiency of fibrous reinforcement of brittle matrices', Journal Physics D : Applied Physics, 4, (1971), p.1739-1744.

57. Schnütgen, B 'Some results of investigations on steel fibre reinforced concrete', Fibre Reinforced Cement and Concrete, RILEM Symposium 1975, The Construction Press Ltd., Lancaster, England, p.105-112.

58. Hannant, D J, p.23.

59. Romualdi, J P and Mandel, J A 'Tensile strength of concrete affected by uniformly distributed and closely spaced short lengths of wire reinforcement', ACI Journal, June 1964, p.657-671.

60. Rajagopalan, K, p.180.

61. Naaman, A E 'Fibre reinforced concrete under dynamic loading', Fibre Reinforced Concrete, A.C.I. Publication SP-81, Detroit, U.S.A., 1984, p.657-671.

62. Johnstone, C D 'Steel fibre reinforced mortar and concrete: A review of mechanical properties', Fibre Reinforced Concrete, A.C.I. Publication SP-44, Detroit, U.S.A., 1974. p.128-135.

63. Fanella, D and Naaman, A E 'Stress strain properties of fibre-reinforced mortar in compression', ACI Journal, July-August 1985, p.477.

64. Hannant, D J, p.64.

65. State-of-the-Art Report on Design with Fibre Reinforced Concrete and Mortar, Item 3, Revision 2, January 1984, p.51.

66. Singh, B, *et al* 'Test methods used to measure the mechanical properties of fibre cement composites at the Building Research Establishment', Testing and Test Methods of Fibre Cement Composites, RILEM Symposium 1978, The Construction Press Ltd., Lancaster, England, p.378-379.

67. Johnstone, C D, p.130.

68. Schnütgen, B, p.114-116.

69. Hannant, D J, p.49.

70. "State-of-the-Art Report", Fibre Reinforced Concrete, p.19.

71. Swamy, R N and Mangat, P S 'A theory for the flexural strength of steel fibre reinforced concrete', Cement and Concrete Research, Vol. 4, Pergamon Press Inc., U.S.A., 1974, p.319.

72. Pakotiprapha, B, Pama R P and Lee, S L 'Mechanical properties of cement mortar with randomly oriented short steel wires', Magazine of Concrete Research, Vol. 26, No. 86, March 1974, p.8.

73. Shah, S P and Rangan, B V 'Fibre reinforced concrete properties', ACI Journal, Vol. 68, No. 2, February 1971, p.127-129.

74. Hughes, B P and Fattuhi, N I 'Load-deflection curves for fibre-reinforced concrete beams in flexure', Magazine of Concrete Research, Vol. 29, No. 101, December 1977, p.199-202.

75. Hannant, D J, p.66.

76. Measurement of Properties of Fibre Reinforced Concrete, ACI Journal, July 1978, p.103.

77. Johnstone, C D, p.131-132.

78. Henager, C H 'A toughness index of fibre concrete', Testing and Test Methods of Fibre Cement Composites, RILEM Symposium 1978, The Construction Press, England, p.80-86.

79. Hughes, B P, p.201.

80. Verhagen, A H 'Impact testing of fibre reinforced concrete: Reflection on possible test methods', Testing and Test Methods of Fibre Cement Composites, RILEM Symposium 1978, The Construction Press, England, p.101.

81. Measurement of Properties of Fibre Reinforced Concrete, ACI Journal, July 1978, p.4-5.

82. Majumdar, A J, p.299.

83. Anderson, W E 'Proposed testing of steel-fibre concrete to minimize unexpected service failures', Testing and Test Methods of Fibre Cement Composites, RILEM Symposium 1978, The Construction Press, England, p.230.

84. State-of-the-Art Report on Fibre Reinforced Concrete, p.20-21.

85. Neville, A M, p.393.

86. State-of-the-Art Report on Fibre Reinforced Concrete, p.20-21.

87. Hannant, D J and Edgington, J 'Durability of steel fibre concrete', Fibre Reinforced Concrete, RILEM Symposium (2), p.159-169.

88. Burakiewicz, A 'Testing of fibre-bond strength in cement matrix', Testing and Test Methods of Fibre Cement Composites, RILEM Symposium 1978, The Construction Press, England, p.360.

89. Hannant, D J, p.23.

90. 'Structural strength and stability (dwellings)', Minimum Agreement Norms and Technical Advisory Guide (MANTAG), Agreement Board of South Africa, July 1985, p.4-5.

91. Uaendere, G N 'Strength of fibre-reinforced concrete slabs', Undergraduate BSc Eng (Civil) Thesis No. 28, University of Cape Town, 1986, p.20-25.

APPENDIX A

EXAMINATIONS WRITTEN BY THE AUTHOR TO COMPLETE THE REQUIREMENTS OF THE DEGREE

Examination		Credit Rating
CIV 502F	Prestressed Concrete (June 1986)	5
CIV 507B	Theory of Elasticity (June 1986)	2
CIV 528F	Road Pavements (June 1986)	3
CIV 508S	Plates and Shells (November 1986)	2
CIV 525S	Contract Law (November 1986)	3
END 510	Engineering Management (November 1986)	5
Thesis:	"An experimental investigation into the effectiveness of steel fibre reinforced concrete relative to conventional mesh reinforced concrete in thin shell construction"	20
	TOTAL	40
	Credit requirements for degree	40

UNIVERSITY OF CAPE TOWN

DEPARTMENT OF CIVIL ENGINEERING

UNIVERSITY EXAMINATION CIV502F (1986)

OPEN BOOK EXAMINATION - 3 HOURS

1. Discuss briefly all the desirable properties of
   (a) the steel used for prestressing, and
   (b) the concrete used for prestressed concrete. (9)

2. Sketch and discuss the concrete stress distributions behind different arrangements and sizes of tendon anchorages. (7)

3. Discuss the advantages of full prestressing vs. partial prestressing vs. reinforcing only, of concrete beams. (9)

4. Give the advantages of pretensioning vs. post-tensioning of concrete members. (10)

5. (a) For the prestressed concrete beam section shown overleaf, find the stresses in the extreme fibres, in the reinforcement and in the tendons at the SLS using an uncracked section analysis. (17)

   (b) What is the degree of prestress κ ? (4)

   (c) Estimate the maximum crack widths on the beam soffit at the SLS by any Code; without doing a cracked section analysis. (9)

6. For the same prestressed concrete beam shown overleaf, find

   (a) the sagging flexural capacity M_u in kNm , by analysing the section, and (20)

   (b) the shear capacity V_u in kN ; (15)

   - both by SABS0100 for the ULS. (MARKS)

   The strands are conventional, horizontal and grouted.

Page 2./ .....

BEAM SECTION : $A = 0{,}480 m^2$, $I = 0{,}0661 m^4$,

$Z_1 = 0{,}09117 m^3$, $Z_2 = 0{,}13916 m^3$,

$a_1 = 725$, $a_2 = 475$

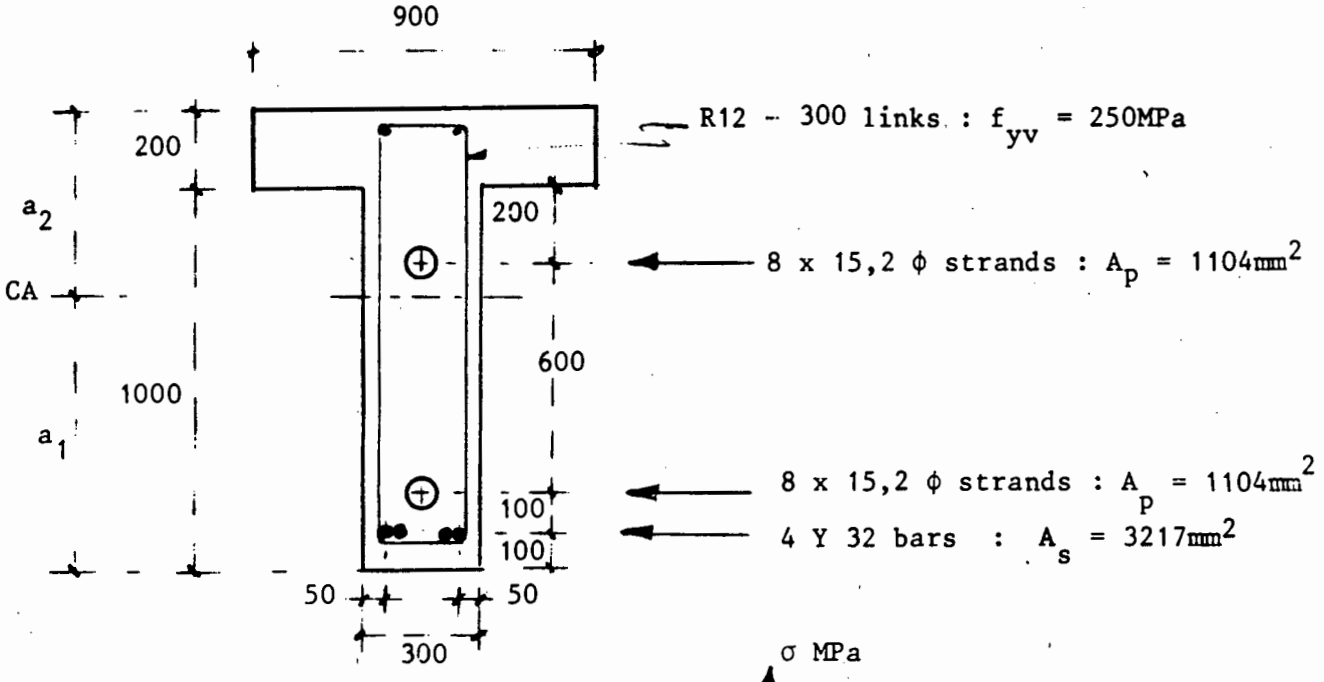

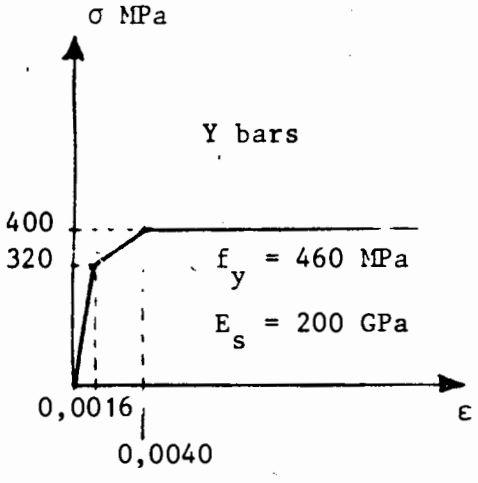

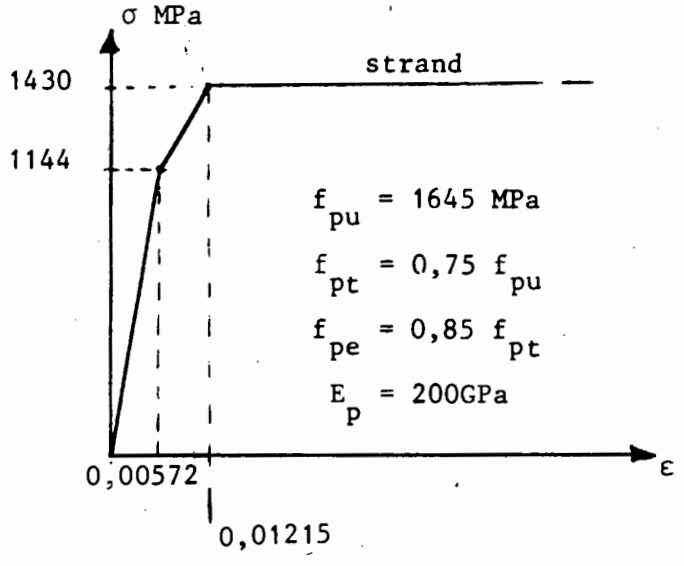

ULS DESIGN STRESS-STRAIN GRAPHS

- Concrete grade f_{cu} = 50 MPa : E_c = 34 GPa

  flexural tensile strength = 2,6 MPa by BS8110

S.L.S. values $\begin{cases} M_d = 900 \text{ kNm} \\ M_{imax} = 1100 \text{ kNm} \\ M_{imin} = 0 \end{cases}$

U.L.S. values $\left\{ \begin{matrix} M = 3000 \text{ kNm} \\ V = 500 \text{ kN} \end{matrix} \right\}$ occurring simultaneously at the same section

UNIVERSITY OF CAPE TOWN

DEPARTMENT OF CIVIL ENGINEERING

UNIVERSITY EXAMINATION : JUNE 1986

CIV 507B : THEORY OF ELASTICITY

Time : TWO HOURS

ANSWER ALL QUESTIONS

(5 PAGES)

QUESTION 1.

(a) The constitutive equations of an isotropic elastic material are

$$[\varepsilon] = \frac{1+\nu}{E}[\sigma] - \frac{\nu}{E}(\sigma_{11}+\sigma_{22}+\sigma_{33})[I] \quad .$$

Show that the mean stress $\sigma_m = \frac{1}{3}(\sigma_{11} + \sigma_{22} + \sigma_{33})$ and volume strain $\varepsilon_v = \varepsilon_{11} + \varepsilon_{22} + \varepsilon_{33}$ are related by

$$\sigma_m = \frac{E}{(1-2\nu)}\varepsilon_v \quad . \qquad (i)$$

By considering (i) for the case when $[\sigma] = p[I]$ where p is a positive constant, explain why a value of Poissons ratio $\nu > \frac{1}{2}$ is physically unacceptable.

(10)

(b) The stress matrix at a point in an elastic material is given by

$$|\sigma| = E\begin{bmatrix} 7 & -\sqrt{3} & 0 \\ -\sqrt{3} & 5 & 0 \\ 0 & 0 & 3 \end{bmatrix}$$

where E is Youngs modulus. Find the principal stresses, the corresponding principal strains (in terms of ν) and the principal directions. If ε_3 is the principal strain corresponding to the smallest principal stress, is it possible for ε_3 to be negative?

(20)

[30]

QUESTION 2

(a) In the problem of torsion of prismatic bars the warping function $\psi(x_1,x_2)$ and Prandtl's stress function $\phi(x_1,x_2)$ are related to each other and to the shear stress σ_{13} and σ_{23} by

$$\sigma_{13} = G\alpha\left(\frac{\partial\psi}{\partial x_1} - x_2\right) = \frac{\partial\phi}{\partial x_2}, \quad G = \text{shear modulus}, \quad \alpha = \text{angle of twist per unit length.}$$

$$\sigma_{23} = G\alpha\left(\frac{\partial\psi}{\partial x_2} + x_1\right) = -\frac{\partial\phi}{\partial x_1}.$$

Show that the equilibrium equations require that ψ be harmonic. Show also that ϕ satisfies $\Delta\phi = -2G\alpha$. Given that ψ satisfies

$$\left(\frac{\partial\psi}{\partial x_1} - x_2\right) n_1 + \left(\frac{\partial\psi}{\partial x_2} + x_1\right) n_2 = 0$$

on the boundary, show that ϕ = constant on the boundary, equal to zero, say.

(15)

(b) Describe the analogy between the torsion problem and the problem of a thin membrance carrying a tension T and subjected to a transverse pressure P. Use the membrane analogy to show that the stress function ϕ for a bar of thin rectangular cross-section is given approximately by

$$\phi = G\alpha\left(\frac{t^2}{4} - x_1^2\right)$$

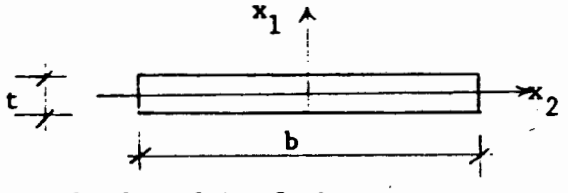

where t is the thickness and b (>>t) is the breadth of the cross-section. If τ is the resultant shear stress at any point on the cross-section, show that the applied couple C and the maximum value τ_{max} of τ are related by

$$C = \frac{1}{3} bt^2.\tau_{max}$$

given that $C = 2\iint\phi\, dA$.

(20)

QUESTION 2

(c) How is the couple C related to Gα for the angle section shown? Give reasons for your answer.

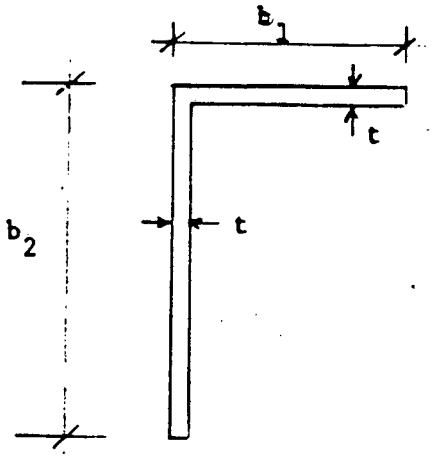

(5)

[40]

QUESTION 3

(a) An isotropic elastic half-space is subjected to a state of one-dimensional strain (i.e. $\varepsilon_{11} = \varepsilon_{11}(x,t) \neq 0$, all other components zero) by the action of a pressure p(t) on its bounding surface. Use the constitutive equation

$$[\sigma] = \lambda\, \varepsilon_v [I] + 2\mu [\varepsilon]$$

and the equations of motion to show that the displacement $u_1 = u$ satisfies the wave equation

$$\frac{\partial^2 u}{\partial x^2} = \frac{1}{c^2} \frac{\partial^2 u}{\partial t^2}$$

in the absence of body forces. Give c in terms of Lamé's constants λ, μ.

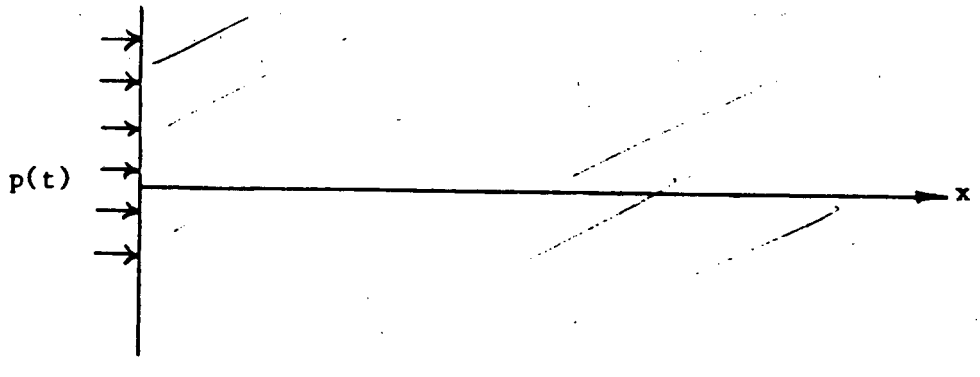

(10)

QUESTION 3

(b) The solution to this problem is

$$u(x,t) = \frac{c}{\lambda+2\mu} \int_0^{t-x/c} p(s)\, ds$$

where $p(s) = 0$ for $s < 0$. Describe the entire displacement history for an arbitrary point x for the case of the pressure history shown below:

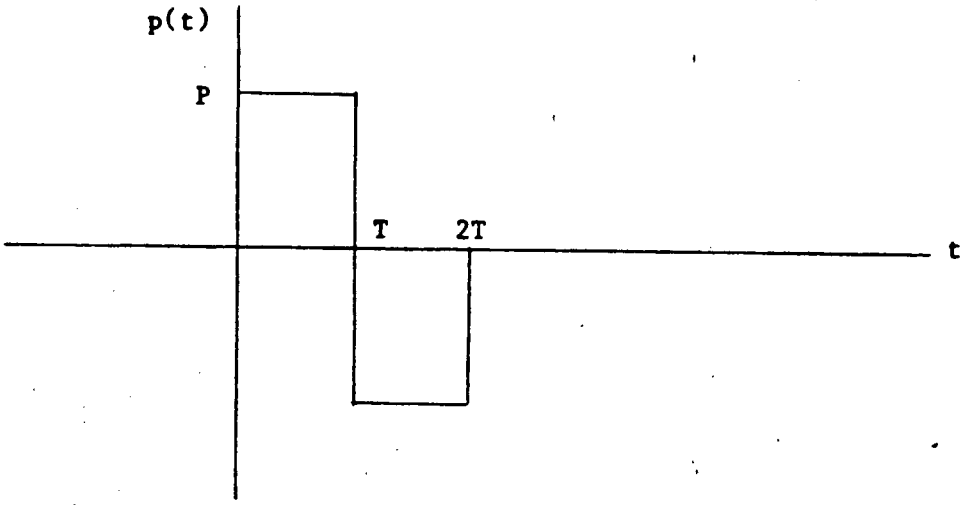

That is, obtain explicit expressions for u(x,t), and explain what happens over the period of time $t > 0$, at a point x.

(20)

[30]

* * * * *

UNIVERSITY OF CAPE TOWN

DEPARTMENT OF CIVIL ENGINEERING

POSTGRADUATE EXAMINATION

CIV 528F 18 JUNE 1986

PAVEMENT DESIGN

TOTAL MARKS 85

NOTE:

* The examination is 4 hours
* Books and references permitted
* Attempt all questions
* Where relevant refer to publications, tables and graphs during calculations.
* Show all working.

1. Refer to Annexure A. (35)

2. An existing Provincial road near Kroonstad is to be rehabilitated. The traffic has increased more than originally allowed for. The authorities wish to retain as much of the existing pavement as possible. Recommend the best solution taking into account that the road cross-section will remain unaltered and that a premix wearing course is to be used.

   The following information is available:

* Current equivalent traffic per lane per day = 180 E80
* The estimated new growth = 6%
* The rehabilitation will be carried out 5 years from now.
* Average CBR along the centreline below the existing pavement is = 10
* The existing layers consist of:

Surfacing - chip and spray		
Basecourse - crusher run	=	100mm
Subbase - natural gravel CBR 30	=	150mm
Selected layers	=	150mm
Total thickness	=	400mm

(10)

3. Using the latest PCA design method for concrete pavements determine whether a concrete pavement complying with the following particulars will be adequate for the subgrade and traffic conditions. The attached calculation sheet should be used.

* Modulus of subgrade reaction k = 50 Mpa
* Untreated subbase = 150 mm
* Concrete pavement = 225 mm
* Modulus of rupture (28 day) = 3,8Mpa
* Rural freeway with premix shoulders
* The following traffic is projected for the slow lane:

Single-axle (KN)	Expected Repetitions
130	650
120	820
115	1 320
105	1 500
95	25 000
85	61 000

Tandem-axled (KN)	Expected Repeitions
240	700
230	1 000
225	1 200
215	4 000
200	5 000
190	9 000
185	15 000
175	35 000

(10)

4. Using the CBR method, design a flexible pavement using the Vickers Vanguard as the design aircraft. Give a recommended balanced pavement layer design from the results obtained.

The following information is available:

Basecourse CBR	= 80
Subbase CBR	= 45
Selected layers CBR	= 20
Subgrade CBR (E9)	= 5
Spacing between adjoining wheels	S = 35 inches
Spacing between tyre edges	d = 20 inches

5. Determine the percentage **voids in the mix** based on both the "Marshall" bulk specific gravity and the maximum theoretical - "Rice´s" Specific Gravity of the sample. Also determine the **voids in the mineral aggregate.**

The following has been determined in a laboratory:

Max. theoretical S.G. of sample	=	2,5415
Bulk S.G. of the sample	=	2,294
Bitumen content	=	6,54%
Bitumen absorption	=	1,07%
Apparent S.G. of bitumen	=	1,01
Bulk S.G. of aggregate blend	=	2,76

(10)

6. Discuss briefly the different means of stabilisation and their agents and also the reasons for stabilisation. State if any types of materials are not recommended for stabilisation and if so give reasons for this.

(10)

UNIVERSITY OF CAPE TOWN

DEPARTMENT OF CIVIL ENGINEERING

FINAL UNIVERSITY EXAMINATION : NOVEMBER 1986

CIV 508S : PLATES AND SHELLS

TIME: 3 HOURS OPEN BOOK

ANSWER ALL QUESTIONS

QUESTION 1

A thin circular plate of thickness h and radius R is subjected to a constant (axisymmetric) traction T per unit length along its edge and normal to it, and in the plane of the plate.

From the potential energy show that the governing differential equation in terms of the stress resultants N_r and N_θ is given by

$$\frac{\partial N_r}{\partial r} + \frac{N_r - N_\theta}{r} = 0$$

where $$N_r = \int_{-h/2}^{h/2} \sigma_r \, dz$$

and given that $$\epsilon_r = \frac{\partial u}{\partial r}$$

$$\epsilon_\theta = \frac{u}{r}$$

and derive the boundary conditions.

QUESTION 2

A thin rectangular plate of thickness h and sides a and b is simply supported on all four edges and loaded with a transverse uniformly distributed load q. Compute the maximum deflection of the plate using a one-term polynomial Ritz approximation.

QUESTION 3

A certain type of stationary variational principle for a thick beam is given by

$$H(x,w,\kappa,\lambda,\mu_1,\mu_2) = \int_0^L \left[\frac{EI}{2}\kappa^2 + \left(\frac{d^2w}{dx^2} - \kappa\right)\lambda + fw\right] dx$$

$$- M_L \frac{dw}{dx}(L) - V_L\, w(L) + \mu_1[w(o)-w_o] + \mu_2\left[\frac{dw}{dx}(o) - \theta_o\right]$$

By using the condition for stationarity of a functional, obtain the governing equations and boundary conditions for this problem.

QUESTION 4

Consider a thick circular plate which rests on an elastic foundation with foundation constant s.

Derive the element stiffness matrices of the displacement finite element method for this special case with axisymmetric loading.

* * * * * * * * *

UNIVERSITY OF CAPE TOWN

DEPARTMENT OF CIVIL ENGINEERING

UNIVERSITY EXAMINATION - NOVEMBER 1986

COURSE CIV 525S - CONTRACT LAW

OPEN BOOK EXAMINATION

Time : 135 Minutes

PLEASE ANSWER ALL QUESTIONS BEARING IN MIND THE NUMBER OF QUESTIONS. IT IS SUGGESTED THAT YOUR ANSWERS BE KEPT AS BRIEF AS POSSIBLE.

TOTAL NUMBER OF MARKS : 100 MARKS

QUESTION 1(a)

You are a director of a construction firm. You are instructed by a development company (DC (Pty) Limited) to build certain houses on Erven owned by individual owners with whom DC (Pty) Limited had entered into contracts for the erection of the houses. As work progressed the individual owners paid DC (Pty) Limited. A dispute breaks out between your company and DC (Pty) Limited causing delays in the building operations which resulted in the individual owners engaging another contractor to complete the houses. You have not yet been paid in full by DC (Pty) Limited for the work done by you for that company. You do not want to give up possession of the building works until you have been paid in full and the individual owners institute proceedings against you for an order claiming possession of the site. Your managing director asks you for your advice in regard to these proceedings.

Advise him as to the prospects of success in the action by the individual owners.

(10 Marks)

Question 1(b) / ....

QUESTION 1(b)

Would your advice be different - and if so - what would you advise if in the circumstances mentioned above it had been agreed between your company, the individual owners and DC (Pty) Limited that although DC (Pty) Limited would be doing the development, your company would in fact be contracting and building directly with and for the individual owners and they were in arrears with payment to you as a result of a dispute which they had with you and with DC (Pty) Limited and they now wished to obtain possession of the building works?

(5 Marks)

QUESTION 2

May a contractor in a lump sum contract claim payment for work done without having completed the work? How can he ensure that he can receive payment for work done before completing the whole work?

(5 Marks)

QUESTION 3

What is the principle of "Quantum Meruit"? Where would this principle apply in regard to construction work and indicate the principles laid down in Middleton v Carr 1949 (2) SA 374 (AD) dealing with that issue?

(10 Marks)

QUESTION 4 / ....

QUESTION 4

What is a delict and distinguish between the rules relating to liability for delict and liability for breach of contract?

(5 Marks)

QUESTION 5 / ....

QUESTION 5

What are : -

(i) fraudulent

(ii) negligent

(iii) innocent

misrepresentations and indicate in each case what claims may be instituted by a Plaintiff suffering as a result of each of the above misrepresentations?

(5 Marks)

QUESTION 6 / ....

QUESTION 6

In what circumstances could a person who expresses an opinion during the course of negotiations with another party be liable to that other party for damages if the opinion was expressed incorrectly? Quote any relevant authority.

(5 Marks)

QUESTION 7 / ....

QUESTION 7

May one contract out of liability for negligence in rendering a service which service one has agreed to do? Write a short note on exemption/disclaimer clauses, quoting any relevant authority.

(10 Marks)

QUESTION 8 / ....

QUESTION 8

What are the duties of the engineer's representative in terms of the General Conditions of Contract 1982 as issued by the South African Institution of Civil Engineers?

(5 Marks)

QUESTION 9 / ....

QUESTION 9

In what circumstances may a contractor have a right under the said General Conditions of Contract to make any claim for additional payment should he encounter adverse physical conditions during execution of the work, and what procedure must he follow?

(5 Marks)

QUESTION 10 / ....

QUESTION 10

When may an extension of time be granted in terms of the said General Conditions of Contract?

(5 Marks)

QUESTION 11 / ....

QUESTION 11

What is the difference between "extra work" and "additional work"? What procedure must be followed by the contractor as a condition precedent to the engineer taking into account any extra or additional work in regard to a request by the contractor for an extension of time for the completion of the works?

(5 Marks)

QUESTION 12 / ....

QUESTION 12

May a penalty in a construction contract be enforced? In what circumstances may the Court intervene to reduce the amount of a penalty imposed in terms of a contract?

(5 Marks)

QUESTION 13 / ....

QUESTION 13

What are the rights of an employer in terms of the General Conditions of Contract 1982 where the estate of a contractor has been sequestrated?

What are the rights of a contractor in terms of the said General Conditions of Contract 1982 in the event of the estate of the employer being sequestrated and what are the consequences of the contractor exercising those rights as laid down in the said General Conditions of Contract?

(10 Marks)

QUESTION 14 / ....

QUESTION 14

Write a short note on the mediation procedure as provided for in the General Conditions of Contract?

(10 Marks)

UNIVERSITY OF CAPE TOWN

DEPARTMENT OF ACCOUNTING

END 510 - INDUSTRIAL ADMINISTRATION PROGRAMME

ACCOUNTING MODULE

Final - November 1986

Marks : 100
Time : 3 Hours

1. This is an open book examination.
2. Answer all five questions.
3. Write on right hand side of the book only.
4. The use of calculators is permitted.
5. This paper consists of 8 numbered pages.

Question	Description	Marks	Time
1	Standard Costing	20	36 min
2	Capital Budgeting	25	45
3	Financial Analysis	20	36
4	Responsibility Accounting	20	36
5	Financial Modelling	15	27
		100	180 min

1

QUESTION 1 (20 marks)

The Remro Company uses standard costs. The purchasing manager, Peter Price, is responsible for material-price variances, and the production manager, Juan Pusher, is responsible for material usage variances and direct-labour price and efficiency variances.

The standard price for metal used as a principal raw material was R2 per kilogram. The standard allowance was six kilograms per finished unit of product.

The standard rate for direct labour was R14 per hour. The standard allowance was half an hour per finished unit of product.

During the past week, 10,000 good finished units were produced. However, strike action caused the production manager to use unskilled labour. Actual labour costs were R78 000 for 6,500 actual hours; 80 000 kilograms of metal were acquired for R1.80 per kilogram, and 71 000 kilograms of metal were consumed during production.

REQUIRED:

1. Compute the material purchase-price variance, material usage variance, direct-labour rate variance, and direct-labour efficiency variance. (10 marks)

2. As a supervisor of both the purchasing manager and the production manager, how would you interpret the feedback provided by the computed variances? (6 marks)

3. What are the budget allowances for the production manager for direct materials and direct labour for the past week? Would they be different if production were 7,000 good finished units? (4 marks)

2

QUESTION 2 (25 marks)

As Financial Director of the Buchin Company, John Northrup has just presented the managing director with his analysis of the proposed addition of a new product, code-named Zim. Northrup summarised his opposition as follows:

Zim should be rejected because it will not earn the minimum required rate of return of 10 percent after taxes. We cannot sell enough units to breakeven, even though our marketing people insist that the product can be sold without increasing our sales force.

Zim is expected to be a highly saleable product for the next ten years. Our market research department has predicted a sales volume of 45,000 units per year at a selling price of R12. But my computations indicate a breakeven volume of 50,000 units per year:

	PER UNIT
Variable costs:	
Direct material	R 5.00
Direct labour	2.00
Variable factory overhead at 25% of direct labour	0.50
Other costs (using companywide absorption rates):	
General factory overhead at 25% of direct labour	0.50
Selling and administrative costs at 1/6 selling price	2.00
Total costs per unit	R10.00

Zim will occupy space that is being vacated by our old product, Yim, which is now obsolete. The new Zim department will incur fixed costs of R100 000 annually. This sum includes R50 000 of annual straight-line depreciation on R500 000 of contemplated new equipment. The equipment is expected to have a ten-year life and zero scrap value. The other R50 000 is composed of various incremental indirect general factory-overhead and selling and administrative expenses.

The breakeven volume is R100 000 divided by R2 contribution per unit, or 50,000 units.

My computation of the breakeven point is conservative in the sense that direct labour could be looked at as being a fixed cost. A special work force will have to be trained. These personnel will not be transferable to other departments and vice versa.

An additional R130 000 will be spent to (a) clean up the area where the new Zim department will go and (b) cover startup and learning costs. This sum can probably be written off immediately for book and tax purposes. Because the R130 000, represents a once-off expenditure, it has been excluded from the breakeven analysis.

Our total working capital investment will immediately increase by about 25 percent of Zim's sales. Because this is fully recoverable as a lump sum whenever we drop Zim from our product line, it too has been excluded from the breakeven analysis.

3

Last year we spent R300 000 on product development and market research for Zim. Although we have written this off immediately for both book and tax purposes, I think it should be amortized over the first five years of Zim sales. Of course, this would make the picture look even gloomier.

The after-tax effects of the above analysis would decrease Zim's attractiveness. The applicable income-tax rate is 48 percent. As you know, our chairman has insisted that we use the same depreciation method for book, tax, and decision purposes because he feels it is somehow dishonest to "keep more than one set of books." The Receiver of Revenue will grant a wear and tear allowance of 10 percent per annum straightline. The company does not qualify for the initial allowance.

REQUIRED:

1. Appraise Northrup's analysis. Be specific by citing all his points with which you disagree. (8 marks)

2. Prepare your analysis of the attractiveness of the proposal based on an annual volume of 45,000 units. Use discounted cash flow. (14 marks)

3. What volume must be sold to make Zim a desirable investment? (3 marks)

4

QUESTION 3 (20 marks)

Du Pont Limited operates in the shoe industry. The company manufactures fashion footwear.

You have been asked to analyse the company's financial position, in particular, to assess the company's management of current assets and use of debt.

The financial statements for 1986 and 1985 are presented below:

Balance Sheet at 31 October 1986 (R000)

	1986	1985
Capital Employed		
Ordinary shareholders' equity	1 815	1 680
Redeemable preference share capital	300	300
Long-term liabilities	825	825
	2 940	2 805
Employment of Capital		
Fixed assets	1 050	960
Net current assets (working capital)	1 890	1 845
	4 005	3 293
Stock	2 325	1 650
Accounts receivable	1 350	1 110
Cash at bank	330	533
	2 115	1 448
Short-term loans	1 575	968
Accounts payable	540	480
	2 940	2 805

The company has 500 000 ordinary shares of R1 each in issue.

5

Income Statement for the year ended 31 October 1986 (R000)

		1986		1985
Sales (All sales are on credit)		9 480		8 250
Less: Cost of sales		7 110		6 105
Gross profit		2 370		2 145
Less: Operating expenses	1 404		1 230	
Depreciation	90	1 494	75	1 305
Net income before interest and tax		876		840
Interest		270		165
Net income before tax		606		675
Less: Taxation		270		240
Net income after tax		336		435
Less: Extraordinary loss		120		-
		216		435
Less: Preference dividends	36		36	
Ordinary dividends	45	81	45	81
Retained income for the year		135		354
Retained income at beginning of year		930		576
Retained income at end of year		1 065		930

Industry average ratios for 1986

Current ratio	2:1
Acid test (Quick ratio)	1:1
Stock turnover (sales/stock)	6 times
Accounts receivable collection period	40 days
Debt ratio	50%
Times interest earned	6 times

REQUIRED:

1. Compute the relevant ratios for 1986 and 1985 required for an analysis of the company's liquidity position and management of current assets. Comment on your findings. (13 marks)

2. Compute the relevant ratios for 1986 and 1985 required for an analysis of the company's use of debt to finance its operations. Comment on your findings. (7 marks)

QUESTION 4 (20 marks)

MBR Limited consists of three divisions which formerly were three independent manufacturing companies. Bader Company and Roach Company merged in 1985 and the merged corporation acquired Mitchell Company in 1986. The name of the Company was subsequently changed to MBR Limited, and each company became a separate division retaining the name of its former company.

The three divisions operate as if they are independent companies. Each division has its own sales force and production facilities. Each division's management is responsible for sales, cost of operations, acquisition and financing of divisional assets, and working capital management. The corporate management of MBR evaluates the performance of the divisions and division managements on the basis of return on investment (that is, net income divided by invested capital).

Mitchell Division has just been awarded a contract for a product which uses a component that is manufactured by the Roach Division as well as by outside suppliers. Mitchell used a cost figure of R3.80 for the component manufactured by Roach in preparing its bid for the new product. This cost figure was supplied by Roach in response to Mitchell's request for the average variable cost of the component and represents the standard variable manufacturing cost and variable selling and distribution expense.

Roach has an active sales force that is continually soliciting new prospects. Roach's regular selling price for the component Mitchell needs for the new product is R6.50. Sales of this component are expected to increase. However, the Roach management has indicated that it could supply Mitchell with the required quantities of the component at the regular selling price less variable selling and distribution expenses. Mitchell's management has responded by offering to pay standard variable manufacturing cost plus 20 percent.

The two divisions have been unable to agree on a transfer price. Corporate management has never established a transfer price policy because interdivisional transactions have never occurred. As a compromise, the financial director has suggested a price equal to the standard full manufacturing cost (i.e., no selling and distribution expenses) plus a 15 percent markup. This price has also been rejected by the two division managers because each considered it grossly unfair.

7

The unit cost structure for the Roach component and the three suggested prices are shown below.

Regular selling price	R6.50
Standard variable manufacturing cost	R3.20
Standard fixed manufacturing cost	1.20
Variable selling and distribution expenses	.60
	R5.00
Regular selling price less variable selling and distribution expenses (R6.50 - .60)	R5.90
Standard variable manufacturing cost plus 20% (R3.20 x 1.20)	R3.84
Standard full manufacturing cost plus 15% (R4.40 x 1.15)	R5.06

REQUIRED:

1. Discuss the effect each of the three proposed prices might have on the Roach Division management's attitude toward intercompany business.

(6 marks)

2. If Mitchell can acquire the component from an outside supplier for R5.90, how would this affect your answer to the above? What is the effect on corporate profits if Mitchell were to acquire the component externally?

(5 marks)

3 Is the negotiation of a price between the Mitchell and Roach Divisions a satisfactory method to solve the transfer price problem? Explain your answer.

(5 marks)

4. Should the corporate management of MBR Limited. become involved in this transfer price controversy? Explain your answer.

(4 marks)

8

QUESTION 5 (15 marks)

PART A

You have approached your Managing Director with a request to purchase a personal computer to assist with financial modeling. The Managing Director is not overly enamoured with the idea as the company has recently upgraded it's mainframe at considerable cost. He feels that if the company is going to allocate resources to computerisation, that these resources be pooled rather than being spread over a number of personal computers. Further, he feels strongly about the pooling of data rather than each personal computer user having his own data base.

REQUIRED:

Write a memo to the Managing Director explaining why his concerns are unjustified and why it is necessary to have a personal computer for financial modeling.

(8 marks)

PART B

It has been suggested that in designing and implementing a financial model, the user should follow a systematic approach starting with the definition of the objective and ending with the verification of the model.

REQUIRED:

Explain why it necessary to follow a systematic approach and discuss the various stages of the design and implementation.

(7 marks)

APPENDIX B.1

BINDING WIRE TENSILE TEST RESULTS

MATERIALS ENGINEERING UCT

DATE 26 06 87

TEST RESULTS:

n	F MAX N/mm2	dL MAX %	S mm2
1	496.26	11.13	.40
2	490.20	10.11	.40
3	487.78	10.89	.40
4	490.20	10.87	.40
5	485.75	10.78	.40
6	486.97	12.04	.40
7	487.78	9.96	.40

**STATISTICAL EVALUATION* n= 7

X	489.28	10.83	.40
S	3.48	.69	.00
V	.71	6.37	.00

where :

F MAX = maximum tensile strength (MPa)

dL MAX = maximum elongation at break (%)

S = cross-sectional area (mm^2)

X = mean ultimate tensile stress

V = coefficient of variation

APPENDIX B.2

RESULTS OF TENSILE TESTS CONDUCTED ON SECTIONS OF THE STEEL MESH

MATERIALS ENGINEERING UCT

DATE 15 06 87

TEST RESULTS:

n	F MAX N/mm2	dL MAX %	S mm2
1	498.33	9.34	7.79
2	497.01	8.98	7.79
3	502.60	9.99	7.79
4	499.97	10.99	7.79
5	503.25	10.02	7.79
6	503.25	8.81	7.79

**STATISTICAL EVALUATION* n= 6

X	500.73	9.69	7.79
S	2.70	.81	.00
V	.54	8.36	.00

where :

F MAX = maximum tensile strength (MPa)

dL MAX = maximum elongation at break (%)

S = cross-sectional area (mm^2)

X = mean ultimate tensile stress

V = coefficient of variation

APPENDIX C

WORKING DRAWINGS OF SHEAR SUPPORT RIG

SCALE 1:25

APPENDIX D

WORKING DRAWINGS OF ACI IMPACT TESTING EQUIPMENT

SCALE 1:25

IMPACT HAMMER SCALE 1:10

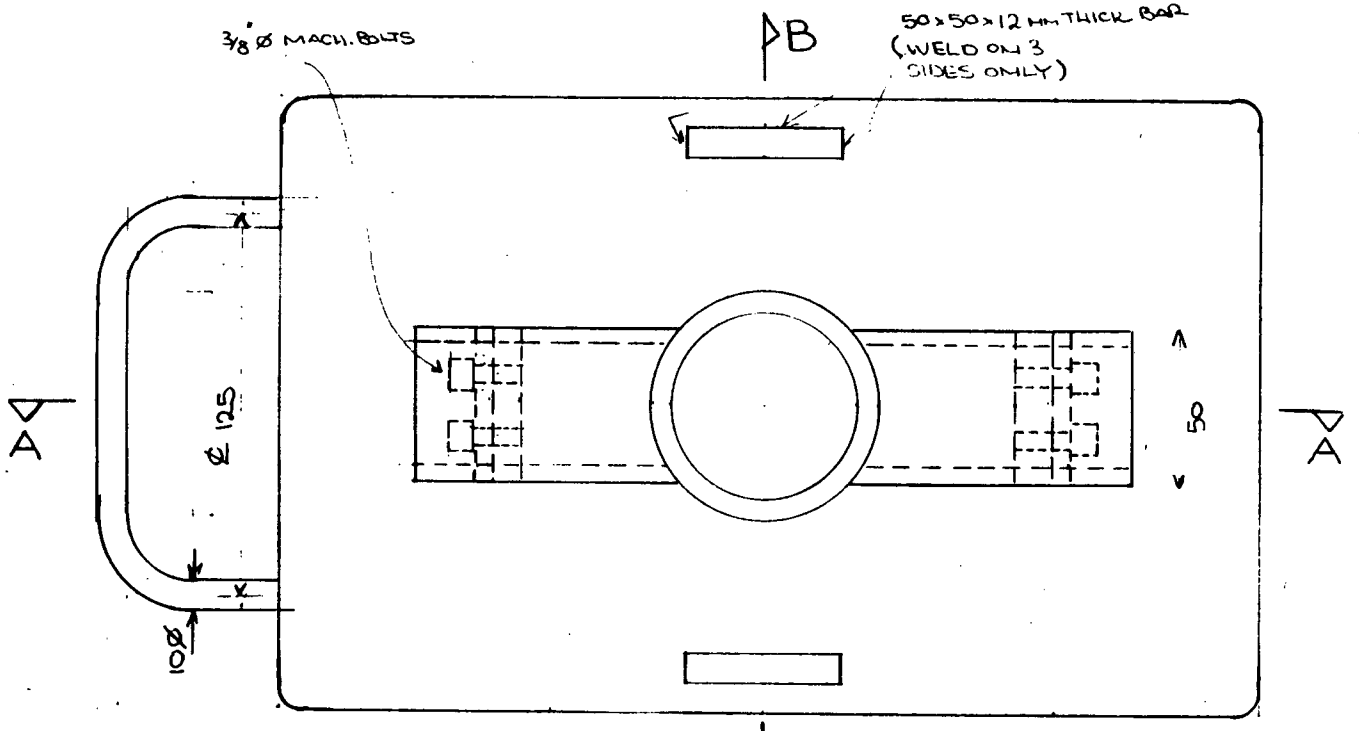

PLAN VIEW OF TEST EQUIPMENT

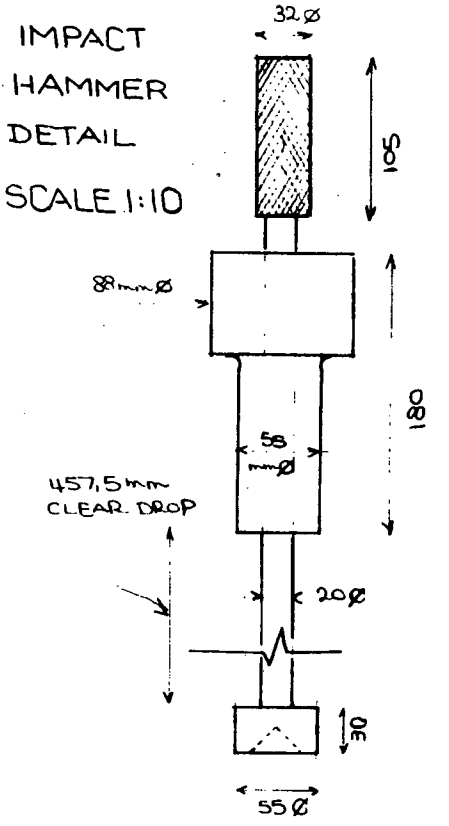

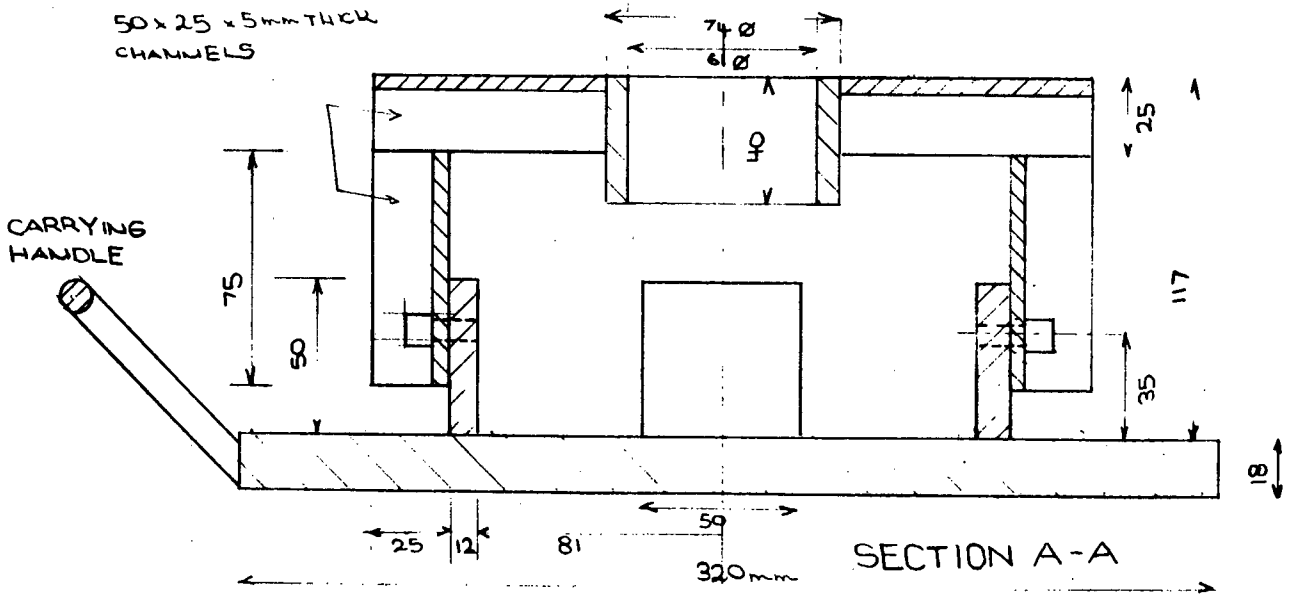

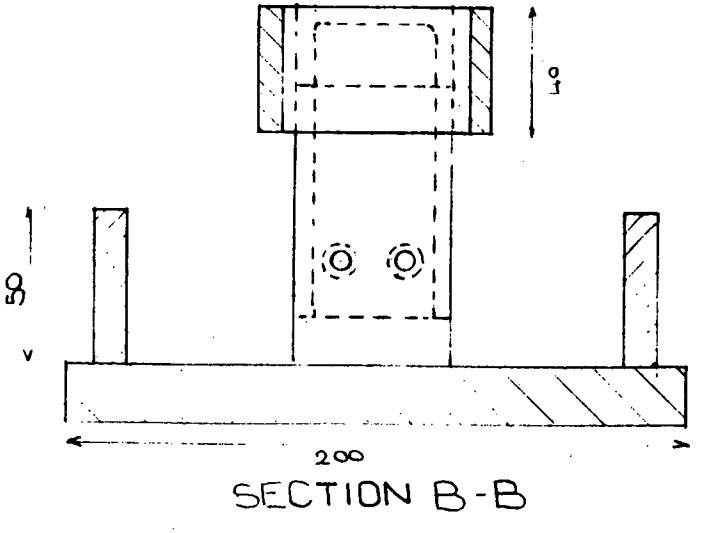

APPENDIX E

LOAD-DEFLECTION PLOTS OF BINDING WIRE REINFORCED PRISMS

E.1 Prisms reinforced with 1.25% V_f

E.2 Prisms reinforced with 1.50% V_f

APPENDIX E.1

PRISMS REINFORCED WITH 1.25% V_f

CONTROL.

1		2	
Load (KN)	Defl. (mm)	Load (KN)	Defl. (mm)
0	0	0	0
1	0.186	1	0.235
2	0.336	2	0.371
3	0.496	3	0.478
3.9	0.746	4	0.562
— o o o —		4.65	0.682
		— o o o —	

PARTIALLY REINFORCED

1		2		3	
Load (KN)	Defl. (mm)	Load (KN)	Defl. (mm)	Load (KN)	Defl. (mm)
0	0			0	0
0.5	0.037			0.5	0.055
1	0.146			1	0.179
1.5	0.234			1.5	0.295
2	0.347			2	0.342
2.5	0.567			2.5	0.383
3	0.575			3	0.425
3.5	0.632			3.5	0.463
4	0.657			4	0.508
5	0.797			5	0.583
5.5	0837			5.5	0.618
6	0.877			6	0.663
6.5	0.917			6.5	0.703
7	0.985			7	0763
7.5	1.074			7.5	0.843
8	1.214			7.68	1.267
8.1	1.486			5.2	2.183
7.7	1.868			4.3	3.183
6.9	2.034			2.8	5.183
5.2	2258			— o o o —	
4.7	4.057				
3.4	4.602				
2.9	6.243				
— o o o —					

FULLY REINFORCED

1		2		3	
Load (KN)	Defl. (mm)	Load (KN)	Defl. (mm)	Load (KN)	Defl. (mm)
0	0	0	0	0	0
0.5	0.068	0.5	0.06	0.5	0.04
1	0.135	1	0.142	1	0.107
1.5	0.200	1.5	0.219	1.5	0.157
2	0.245	2	0.279	2	0.235
2.5	0.285	2.5	0.312	2.5	0.330
3	0.340	3	0.355	3	0.378
3.5	0.372	3.5	0.395	3.5	0.414
4	0.410	4	0.445	4	0.470
5	0.520	5	0.565	5	0.615
5.5	0.595	5.5	0.625	5.5	0.655
6	0.685	6	0.685	6	0.685
6.5	0.790	6.5	0.725	6.5	0.725
7	1.035	7	0.802	7	0.767
7.1	1.505	7.5	0.935	7.5	0.852
7.1	1.705	8	1.065	8	0.947
7.1	1.905	8.5	1.285	8.5	1.057
7.15	2.305	8.1	1.515	9	1.267
7.15	2.705	8.1	1.715	9	1.487
7.10	3.105	8.1	1.915	9	1.587
6.6	3.305	8.1	2.115	8.8	1.787
6.5	3.505	8.0	2.715	8.8	1.887
6.3	3.705	7.8	2.915	88	2.087
6.11	4.005	7.7	3.415	8.7	2.287
5.80	4.505	7.3	3.915	8.65	2.487
5.10	5.005	7.2	3.915	8.6	2.787
4.80	5.505	7.0	4.215	8.6	3.287
4.6	6.005	6.7	5.415	8.5	3.787
4.4	6.505	6.5	5.715	7.6	4.787
4.1	7.505	5.8	6.915	6.4	5.787
3.5	9.505	3.4	7.92	4.9	6.787
				4.5	7.787.

APPENDIX E.2

PRISMS REINFORCED WITH 1.50% V_f

CONTROL

1		2	
LOAD (KN)	DEFL. (mm)	Load (KN)	DEFL. (mm)
0	0	0	0
0.5	0	1.0	0.10
3	0.3	1.5	0.20
4	0.33	2.0	0.25
4.2	0.40	2.5	0.28
—ooo—		3.0	0.3
		3.4	0.34

PARTIALLY REINFORCED

1		2		3	
Load (KN)	DEFL. (mm)	Load (KN)	DEFL. (mm)	Load (KN)	DEFL. (mm)
0	0.	0	0	0	0
1	0.10	1.0	0.02	0.5	0.03
1.5	0.18	1.5	0.06	1	0.08
2	0.23	2.0	0.09	1.5	0.12
2.5	0.27	2.5	0.122	2	0.22
3	0.31	3.0	0.162	2.5	0.33
3.5	0.35	3.5	0.198	3	0.38
4	0.38	4	0.242	3.5	0.42
4.5	0.42	5	0.342	4	0.48
5	0.46	5.5	0.356	4.5	0.49
5.5	0.505	4.3	1.766	5	0.53
6	0.54	4.0	1.986	5.5	0.59
6.5	0.63	3.3	3.096	6	0.70
7	0.74	2.9	3.516	6.9	1.00
7.5	0.91	2.6	3.816	6.5	1.56
6.9	1.15	1.8	4.136	5.0	3.56
5	1.90	0.4	5.766	2.8	3.81
4.8	2.90	—ooo—		2.5	4.36
2.8	3.90			1.5	5.36
1.8	4.50			1.40	5.92
—ooo—				1.20	7.06
				—ooo—	

FULLY REINFORCED

1		2		3	
Load (kN)	Defl. (mm)	Load (kN)	Defl. (mm)	Load (kN)	Defl. (mm)
0	0	0	0	0	0
0.5	0.035	0.5	0.03	0.5	0.035
1	0.08	1	0.06	1	0.085
1.5	0.14	1.5	0.10	1.5	0.132
2	0.19	2	0.13	2	0.182
2.5	0.225	2.5	0.15	2.5	0.237
3	0.260	3	0.17	3	0.272
3.5	0.283	3.5	0.19	3.5	0.307
4	0.328	4	0.23	4	0.343
5	0.423	4.5	0.27	4.5	0.379
5.5	0.458	5	0.33	5	0.439
6	0.513	5.5	0.41	5.5	0.529
6.5	0.566	6	0.62	6	0.679
7	0.629	6.5	1.29	6.5	0.759
7.5	0.70	6.8	2.85	6.9	0.879
8	0.819	4.6	3.12	7	1.199
8.5	1.049	4.2	7.29	6.3	1.819
6.5	1.279	29	8.27	5.6	2.43
7.0	1.739	2.4	9.211	5	3.00
6.7	2.429	— ooo —		4.9	3.37
7.3	2.89			4.3	3.87
6.5	3.139			4.1	4.45
6.6	3.339			3.4	5.02
6.3	3.759	3.4	7.86	3.2	5.12
5.0	3.959	2.5	9.06	3.0	5.65
6.1	4.56	2.5	10.76	2.9	6.20
4.0	5.96	1.50	12.26	— ooo —	
		— ooo —			

APPENDIX F

FLEXURAL STRENGTH EQUATION

F.1 Determination of constants for flexural strength equation (3.7)

F.2 Ratios of the experimental strength to the theoretical strength predicted by the various analysis methods

DETERMINATION OF CONSTANTS FOR FLEXURAL STRENGTH EQUATION (3.7)

Method of analysis: Y AXIS vs. X AXIS	Constants determined for equation 3.7 A (slope)	B (MPa)
CR* – $V_f \cdot l/D$	0.882	1.465
ULT† – $V_f \cdot l/D$	0.919	1.760
CR – $V_f \cdot l/D$	0.906	1.177
ULT – $V_f \cdot l/D$	0.924	1.973
CR – $W_f \cdot l/D$	0.912	1.320
ULT – $W_f \cdot l/D$	0.908	1.908
CR – $W_f \cdot l/D$	1.000	1.200
ULT – $W_f \cdot l/D$	0.912	2.128
CR / □ – $V_f \cdot l/D$	0.728	1.017
ULT / □ – $V_f \cdot l/D$	1.026	1.192
CR / □ – $V_f \cdot l/D$	1.015	0.963
ULT / □ – $V_f \cdot l/D$	1.029	1.363
CR / □ – $W_f \cdot l/D$	0.937	1.17
ULT / □ – $W_f \cdot l/D$	1.015	1.304
CR / □ – $W_f \cdot l/D$	1.030	0.976
ULT / □ – $W_f \cdot l/D$	1.018	1.481
CR / $V_f \cdot l/D$ – □ / $V_f \cdot l/D$	0.877	1.474
ULT / $V_f \cdot l/D$ – □ / $V_f \cdot l/D$	0.873	2.072
CR / $V_f \cdot l/D$ – □ / $V_f \cdot l/D$	0.963	1.371
ULT / $V_f \cdot l/D$ – □ / $V_f \cdot l/D$	0.932	2.010

* CR = First-crack flexural strength

† ULT = Ultimate flexural strength

□ control, unreinforced

▨ partially reinforced

▨ Fully reinforced.

Fibre type and percentage by volume.		FLEXURAL STRENGTH VS $V_f \ell/D$ METHOD				FLEXURAL STRENGTH VS $W_f \ell/D$ METHOD				SWAMY AND MANGAT METHOD OF ANALYSIS			
		A = 0.882 B = 1.465	A = 0.919 B = 1.760	A = 0.906 B = 1.177	A = 0.924 B = 1.973	A = 0.912 B = 1.320	A = 0.908 B = 1.908	A = 1.00 B = 1.20	A = 0.912 B = 2.128	A = 0.877 B = 1.474	A = 0.873 B = 2.072	A = 0.963 B = 1.371	A = 0.932 B = 2.010
SHREDDIC	0.75%	0.983	0.931	1.049	0.986	0.961	0.933	0.940	0.989	0.986	0.957	0.980	0.977
	1.50%	1.207	1.261	1.304	1.305	1.196	1.252	1.158	1.293	1.212	1.264	1.214	1.290
	2.25%	0923	0918	1.045	0.958	0.929	0.904	0916	0943	0.926	0.905	0.962	0.946
WIRAND	0.75%	0.931	1.012	0.923	0.850	0924	1.002	0.846	0.843	0.935	1.012	0856	0.842
	1.50%	0.949	0.884	1.024	0.899	0.959	0865	0.948	0.876	0.951	0.858	0.943	0.885
	2.25%	0.884	0828	0.889	0.747	0.901	0.803	0.826	0726	0.884	0.787	0.809	0.764
ME430(25mm)	0.75%	0.989	0.959	1.057	0.989	0.977	0.951	0.966	0.985	0.993	0.966	0.983	0.979
	1.50%	1.022	1.010	0.990	0.877	1.024	0.991	0912	0.863	1.024	0.989	0.917	0.867
	2.25%	0.885	0857	1.060	0.912	0.897	0.835	0.980	0.890	0.886	0.824	0.967	0.900
ME430(35mm)	0.75%	1.010	1.143	1.209	1.146	0996	1.134	1.107	1.139	1.011	1.152	1.124	1.134
	1.50%	1.000	0.957	1.050	0.902	1.003	0.941	0.964	0887	1.000	0.938	0.961	0.891
	2.25%	1.036	0.996	1.230	1.082	1.053	0968	1.140	1.053	1.037	0.953	1.123	1.068
BINDING WIRE	0.75%	0945	0.915	1.074	1.002	0.945	0.901	0.986	0.987	0.949	0.901	0.989	0.990
	1.50%	1.075	1.238	1.098	1.215	1.092	1.205	1.019	1.183	1.075	1.187	1.000	1.199
	2.25%	1.107	1.283	1.280	1.300	1.149	1.233	1.200	1.250	1.107	1.196	1.143	1.280
MEAN $\bar{x}$		0996	1.012	1.085	1.011	1.000	0.995	0.994	0.990	0.998	0.993	1.000	1.000
COEFFICIENT OF VARIATION (%)		(8.4)	(14.2)	(10.8)	(15.9)	(8.6)	(14.0)	(10.8)	(15.1)	(8.4)	(14.0)	(10.7)	(15.5)

A = Slope of equation (3.07)
B = Intercept of equation (3.07)

Partially reinforced prism
Fully reinforced prism

APPENDIX G

ULTIMATE FLEXURAL STRENGTH ANALYSIS TO DETERMINE V_f REQUIRED

The volume of binding wire required to give a partially reinforced section the same ultimate capacity as a mesh reinforced section was calculated using the assumed stress distribution at failure as shown below.

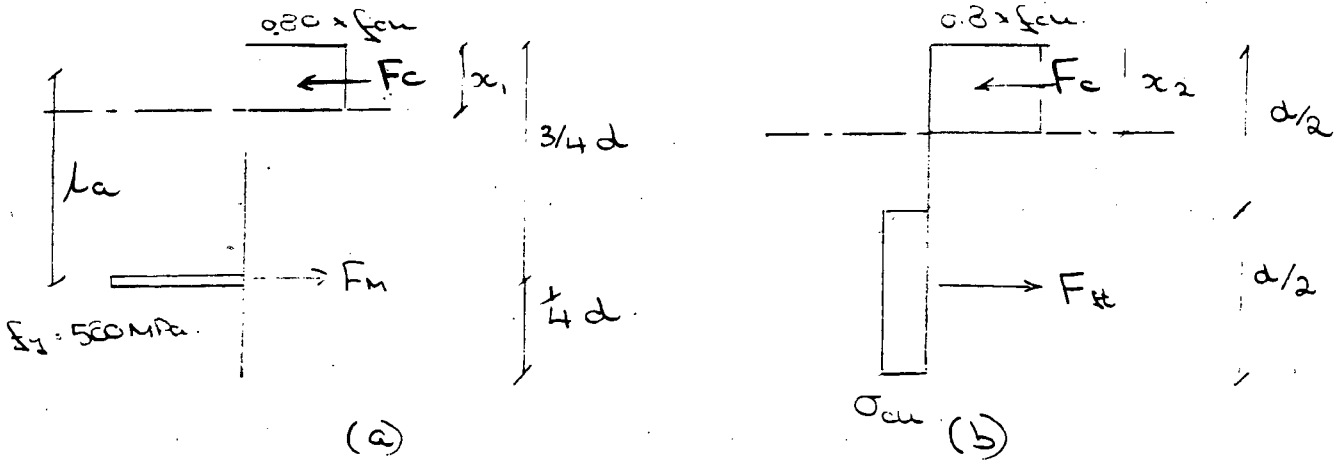

Fig G.1 Assumed stress distributions in (a) Mesh reinforced slab and (b) fibre reinforced slab.

The sections are analysed per metre length. The cross sectional area of the steel mesh over 1 metre is,

$$A_s = 1000/50 \times \left(\frac{3.15}{2}\right)^2 \times \pi.$$
$$= 156 mm^2$$

At ultimate state;

$$F_m = 500 \times 156 = 78,002 kN. \quad (G.1)$$

$$\therefore F_c = 0.80 \times f_{cu} \times 1000 \times x_1$$
$$= 0.80 \times 33.5 \times 1000 \times x_1 \quad (G2)$$

Since $F_m = F_c$ at ultimate,

$$x = 2.911 mm.$$

The ultimate moment of resistance of the most reinforced slab:

$$M_{MU} = F_M \times l_a$$
$$= 78{,}008 \times \left[60 - 15 - \left(\frac{2.9}{2}\right) \right] \times 10^{-3} \qquad (G.3)$$
$$= 3{,}397 \text{ kNm/unit length.}$$

Calculation of F_{ft}:

To calculate the force of the fibres in the tension zone, the ultimate strength of the composite in the tension zone needed to be determined.

The number of fibres crossing a crack of unit length for the 2-dimensional, partially reinforced section is;(89)

$$N = \frac{2}{\pi} \cdot \frac{V_f}{\pi r^2} \qquad (G.4)$$
$$= 4{,}824 \times 10^4 \cdot V_f \ m^{-2}$$

F_{ft} is thence calculated as the product of the number of fibres at the fracture surface (N), the average pullout length and the ultimate bond strength;

$$F_{ft} = N \times l_p \times \tau_{ULT} \times \pi D \qquad (G.5)$$

In a survey of the fractured prism surfaces of series E, the average pullout length (l_p) was determined as 23mm. The analysis of section 7 ..... yielded an ultimate bond strength of $\tau_{ULT} = 2{,}072$ MPa. for the partially-reinforced specimens. Substituting these values into equation (G.5);

$$F_{ft} = 4{,}824 \times 10^4 \times 2{,}072 \times 10^6 \times 0{,}023 \times \pi \times 0.71 \times 10^{-3} \cdot V_f$$
$$= 6{,}254 \times 10^6 \cdot V_f \ N.m^{-2}$$

From Figure I.1(b), at equilibrium of forces

$$F_c = F_{ft}. \qquad (G\ 6)$$

The average cube compressive stress was 33,5 MPa, thus:

$$0.8 \times 33.5 \times 10^6 \times 1.0 \times x_2 = 6,254 \times 10^6 V_f.$$

$$\therefore \quad x_2 = 0,233\ V_f.m^{-2}$$

The ultimate moment of resistance of the partially reinforced fibre-section is;

$$M_{fu} = F_{ft} \times l_a \qquad (G\ 7)$$

and for equal section strength;

$$G.7. = G.3 \qquad (G.8)$$

$$6,254 \times 10^6 V_f \times \left[60 - 15 - \left(\frac{0,233\ V_f}{2}\right)\right] = 3.397 \times 10^3\ Nm.$$

$$2,814 \times 10^5 V_f - 7,286 \times 10^6 V_f^2 = 3,397 \times 10^3\ Nm.$$

$$\therefore\ V_f^2 - 0,386\ V_f + 4,662 \times 10^{-3} = 0.$$

Solving the quadratic equation.

$$V_f = \frac{+0,386 \pm \sqrt{0,386^2 - 4 \times 4,662 \times 10^{-3}}}{2 \times 1}$$

$$= \frac{0,386 \pm 0,361}{2}$$

$$= 0,13735 \quad \text{or} \quad 0,01248$$

$\therefore$ Volume of fibre required to partially reinforce slab

$$= 1,25\% \longrightarrow$$

APPENDIX H

CALCULATION OF TOUGHNESS INDEXES FOR SFRC SPECIMENS

Beam type		Area up to first-crack Nmm^2	Area up to 1.9mm deflection Nmm^2	Toughness Index	
1.50% V_f					
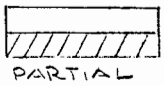 PARTIAL	1	550	4299	7.81	6.79
	2	825	5044	6.24	
	3	803	5070	6.32	
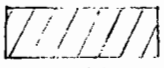 FULLY	1	413	5298	12.83	10.68
	2	525	5296	10.09	
	3	932	5777	9.13	
1.25% V_f					
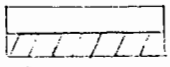 PARTIAL	1	-	-	-	5.98
	2	806	4702	5.84	
	3	840	5138	6.17	
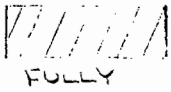 FULLY	1	825	5278	6.40	5.93
	2	1056	5798	7.37	
	3	1020	6188	5.91	

PARTIAL – PARTIALLY REINFORCED PRISMS
FULLY – FULLY REINFORCED PRISMS.

APPENDIX I

SLAB TESTING RESULTS

APPENDIX I.1

RECORDED LOAD-DEFLECTIONS FOR MESH REINFORCED SLABS UNDER STATIC LOADING

SLAB 1		SLAB 2		SLAB 3	
LOAD (KN)	DEFLECTION (mm)	LOAD (KN)	DEFLECTION (mm)	LOAD (KN)	DEFLECTION (mm)
0	0	0	0	0	0
1	0	1	0	1	0
2	0	2	0	2	0
3	0	3	0	3	0.082
4	0	4	0	4	0.232
5	0	5	0.002	5	0.396
6	0.014	6	0.008	6	0.647
7	0.033	7	0.028	7	0.876
8	0.136	8	0.142	8	1.229
9	0.413	9	0.388	9	2.100
10	0.790	10	0.888	10	2.945
11	1.670	11	1.688	11	3.565
12	3.680	12	3.338	12	4.475
14	6.395	13	4.563	13	5.075
16	11.98	14	5.813	14	5.735
18	16.87	15	8.438	16	8.585
20	26.57	17	13.888	18	13.935
22	34.9	19	18.438	20	25.135
24	44.92	21	27.788	22	38.545
26.6	>50mm	23	39.538	24	43.264
		25	49.86	26	> 50
		27	> 50	26.6	> 50
		28.4	> 50		

APPENDIX I.2

RECORDED LOAD-DEFLECTIONS FOR PARTIALLY SFRC SLABS UNDER STATIC LOADING

SLAB 1		SLAB 2		SLAB 3		SLAB 4	
LOAD (KN)	DEFLE. (mm)	LOAD (KN)	DEFL. (mm)	LOAD (KN)	DEFL. (mm)	LOAD (KN)	DEFL. (mm)
0	0	0	0	0	0	0	0
1	0	1	0	1	0	1	0
2	0.022	2	0.002	2	0.007	2	0.073
3	0.030	3	0.106	3	0.130	3	0.208
4	0.146	4	0.257	4	0.375	4	0.398
5	0.248	5	0.410	5	0.517	5	0.513
6	0.293	6	0.506	6	0.732	6	0.681
7	0.492	7	0.699	7	0.921	7	0.851
8	0.613	8	0.766	8	1.094	8	1.023
9	0.757	9	0.897	9	1.260	9	1.211
10	0.923	10	1.061	10	1.444	10	1.384
11	1.078	11	1.232	11	1.661	11	1.579
12	1.251	12	1.379	12	1.859	12	1.849
13	1.421	13	1.860	13	2.129	13	2.104
14	1.612	14	2.285	14	2.424	14	2.974
15	1.831	15	2.816	15	3.014	15	2.749
16	2.014	16	3.832	16	3.609	16	3.404
17	2.358	17	4.914	17	4.691	17	5.764
18	3.055	18	4.985	17.8	–	18	10.98
19.65	–	19	6.185			18.8	–
		19.8	–				

APPENDIX I.3

YIELD LINE ANALYSIS OF STATICALLY LOADED MESH REINFORCED SLAB

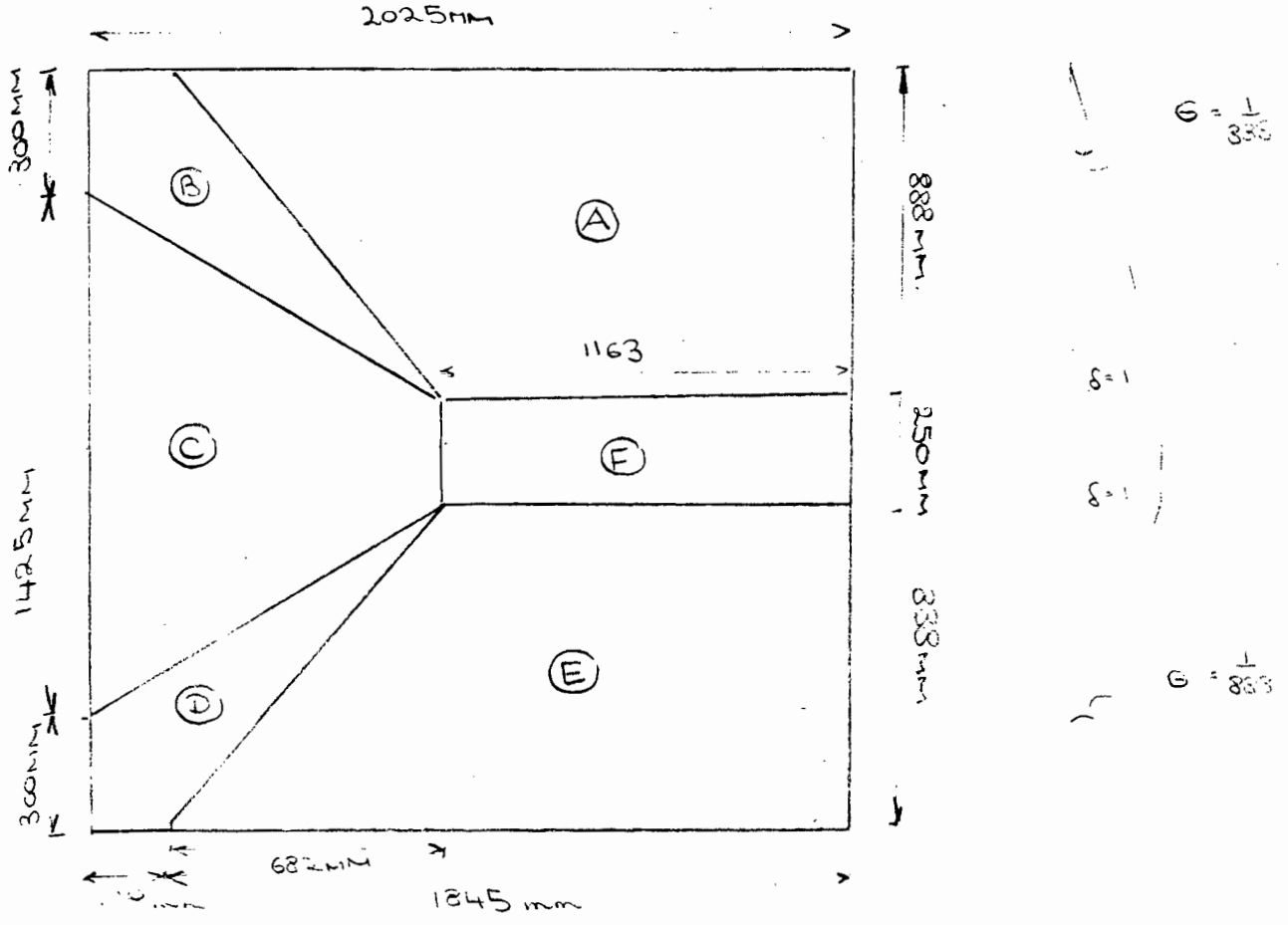

The rotations of panels (A) and (E) are simply $\epsilon_x = \frac{1}{338}$ and for panel (C) simply $\epsilon_y = \frac{1}{862}$.
The rotations ϵx and ϵy or panels (B) and (D) are calculated below;

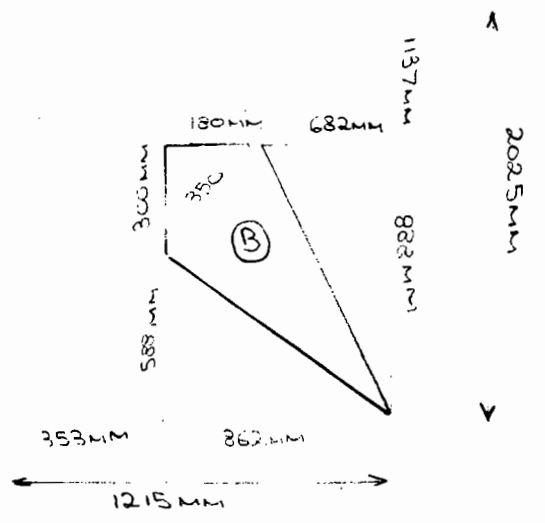

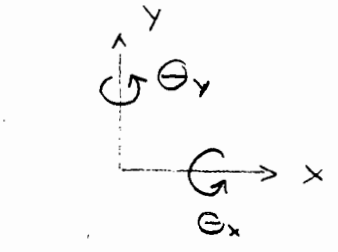

Thus $\Theta_x = \frac{1}{2025}$

$\Theta_Y = \frac{1}{1215}$

INTERNAL WORK

PANEL NO.	θ_x	θ_y	m_x	m_y	l_x	l_y	$m.\theta.l$
Ⓐ	1/888	0	m	m	1845	888	2,078m
Ⓑ	1/2025	1/1215			1544	1476	1,977m
Ⓒ	0	1/862			1724	1425	1,652m
Ⓓ	1/2025	1/1215			1544	1476	1,977m
Ⓔ	1/888	0			1845	888	2,078m
Ⓕ	0	0	v m	m	2326	250	0
						TOTAL	9.763m

EXTERNAL WORK

Ext. work = Area of panel × dead load × vertical displacement at centroid

Dead weight, w kN/m² = 248 kg/m² × 9.06 × 9.81 = 1.433 kN/m²

∴ Panel Ⓐ+Ⓔ $1.163 \times 0.888 \times 2 \times \frac{1}{3} + \frac{1}{2} \times 0.682 \times 0.888 \times \frac{1}{3}$ = 1.235×1.433

Ⓒ $0.250 \times 0.862 \times \frac{1}{3} + \frac{1}{2} \times 0.588 \times 0.862 \times 2 \times \frac{1}{3}$ = 0.2768×1.433

Ⓑ+Ⓓ $\frac{1}{2} \times 2 \times 0.350 \times 1.024 \times \frac{1}{3} - \frac{1}{2} \times 2 \times 0.350 \times 0.154 \times 0.0490$ = 0.1197×1.433

Ⓕ $1.163 \times 0.250 \times 1$ = 0.2908×1.433

2.7617 kN/m

+ work done by point load 27.2kN moving $\delta = 1$ = 2.7617 + 27.2

= 29.962 kNm/m

∴ Ultimate moment capacity per unit width length (m)

= External work ÷ internal work

= 29.962 / 9.763

= 3.065 kNm/m length →

YIELD LINE ANALYSIS OF STATICALLY LOADED PARTIALLY SFRC SLAB

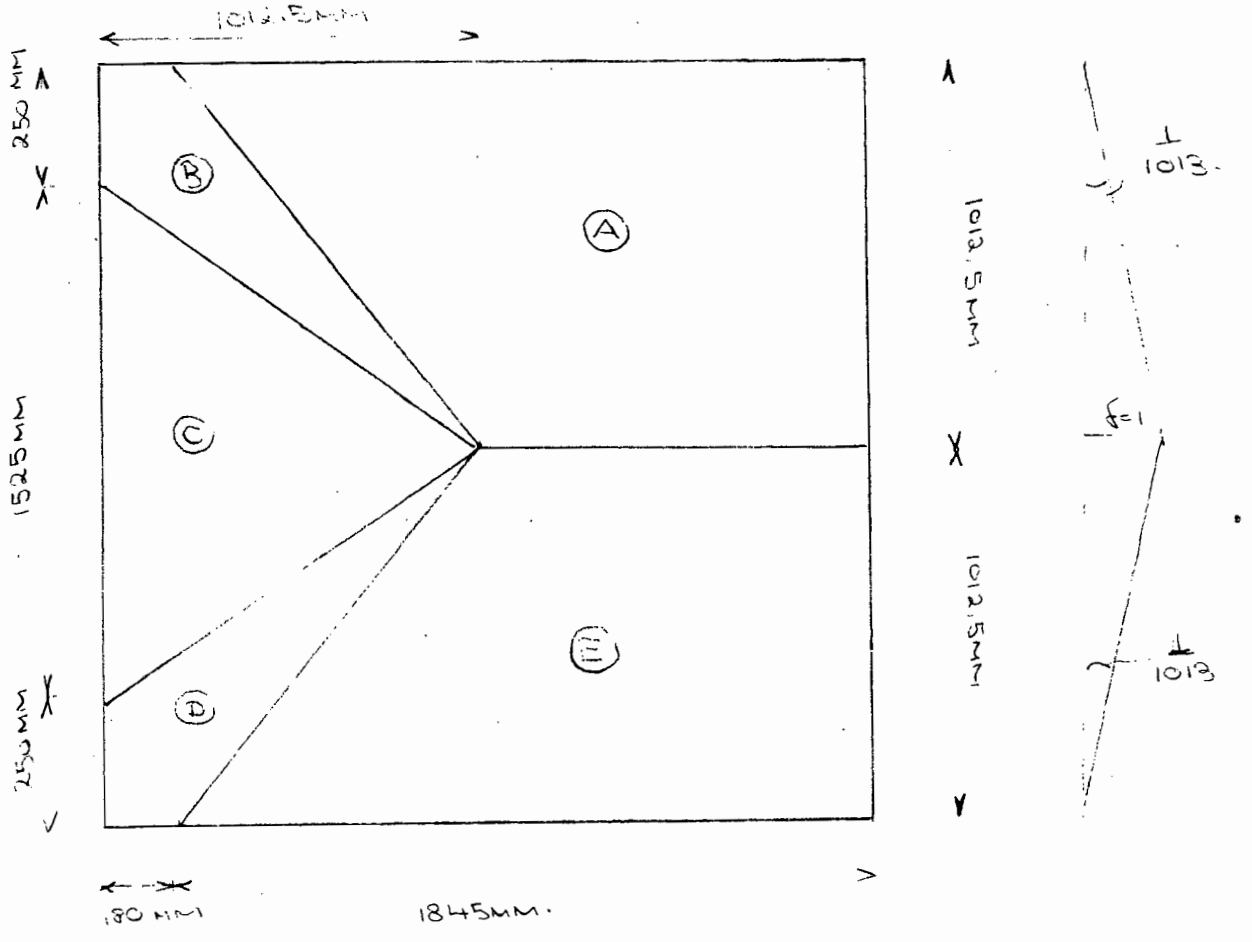

The rotations of panels (A) and (E) are multiple of $1/1012.5$ and of panel (C) equal to $1/1012.5$

The rotations of panels (B) and (D) are calculated twice:

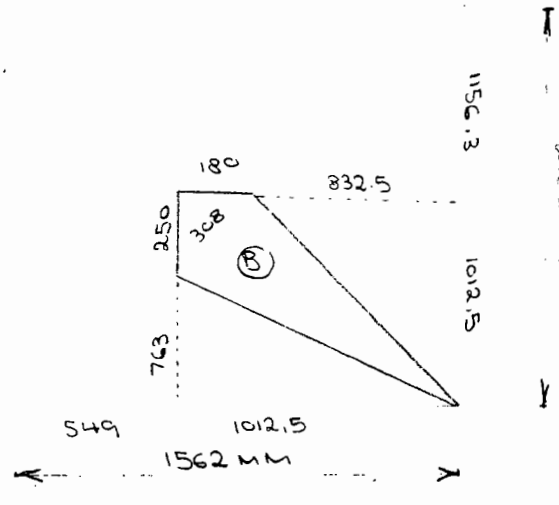

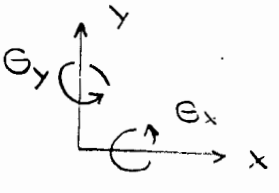

Thus

$$\Theta_x = \frac{1}{2168}$$

$$\Theta_y = \frac{1}{1562}$$

INTERNAL WORK

PANEL NO	θ_x	θ_y	$m_x = m_y = m$	l_x	l_y	$m.\theta.l$
A	$\frac{1}{1012.5}$	0	m	1845	1012.5	1.822 m
B	$\frac{1}{2168}$	$\frac{1}{1561.5}$		.845	1775	1.987 m
C	0	$\frac{1}{1012.5}$		2025	1525	1.5062 m
D	$\frac{1}{2168}$	$\frac{1}{1561.5}$		1845	1775	1.987 m
E	$\frac{1}{1012.5}$	0	m	1845	1012.5	1.822 m
				TOTAL		9.125 m

EXTERNAL WORK

External work = Area of panel × w × displ. at centroid + pt. load × 1.

$w = 2435\ kg/m^3 \times 9.8 \times 0.06m = 1.433\ kN/m^2$

∴ Panel (A) and (E) = $1,012.5 \times 1,012.5 \times \frac{1}{3} - 0.833 \times \frac{1}{2} \times 1,012.5 \times 2 \times \frac{1}{3}$ = 1.3063

(C) = $\frac{1}{2} \times 1,525 \times 1,012.5 \times \frac{1}{3}$ = 0.2573

(B) and (D) = $\frac{1}{2} \times 2 \times 3,03 \times 1,307 \times \frac{1}{3} - \frac{1}{2} \times 3,03 \times 1,146 \times 0.1030 \times 2$ = 0.1284

1,433 × 1,892

+ work done by load displacing by $\delta = 1$ = 19,012 × 1 = 19,0125

21,437

∴ Internal work = External work

$9.125m = 21,437$

$m = 21,437 / 9.125$

$= 2,349\ kNm/m$ length →

APPENDIX I.4

DEFLECTIONS OF MESH-REINFORCED SLAB UNDER IMPACT LOADING

Drop Height (m)	Permanent deflection			Total deflection		
	SLAB 1	SLAB 2	SLAB 3	SLAB 1	SLAB 2	SLAB 3
0.0	0.0	0.0	0.0	0.0	0.0	0.0
0.1	0.2	0.5	0.7	3.1	3.5	4.0
0.2	1.4	1.7	1.7	6.2	6.7	6.8
0.3	3.5	4.5	3.2	10.8	11.8	10.5
0.4	6.5	8.3	4.1	18.5	19.5	16.6
0.5	11.5	13.2	10.1	25.5	28.2	23.5
0.6	17.7	19.0	16.6	35.7	37.5	33.5
0.8	26.6	23.6	25.4	48.6	44.0	46.8
1.0	48.0	38.0	36.3	72.0	64.0	62.2
1.2	63.8	61.0	53.3	91.0	89.0	81.1
1.4			76.9			103.0
1.6			102.2			129.5

APPENDIX I.5

DEFLECTIONS OF PARTIALLY SFRC SLAB UNDER IMPACT LOADING

Drop Height (m)	Permanent deflection			Total deflection		
	SLAB 1	SLAB 2	SLAB 3	SLAB 1	SLAB 2	SLAB 3
0.0	0.0	0.0	0.0	0.0	0.0	0.0
0.1	0.4	0.3	0.5	3.7	2.9	3.2
0.2	0.8	0.5	0.9	5.2	4.4	5.1
0.3	2.2	1.9	2.4	7.3	6.1	8.3
0.4	5.0	3.6	6.5	11.6	8.4	13.0
0.5	15.1	7.5	15.6	19.8	13.6	21.7
0.6		22.8	42.4		25.4	42.3

APPENDIX J

ARCH TESTING RESULTS

J.1 Recorded load vs deflections for mesh-reinforced arches under static loading

J.2 Recorded load vs deflections for partially SFRC arches under static loading

J.3 Elastic and ultimate arch sectional analysis

J.4 Deflections of mesh-reinforced arch under impact loading

J.5 Deflections of partially SFRC arch under impact loading

APPENDIX J.1

RECORDED LOAD-DEFLECTIONS FOR MESH REINFORCED ARCHES UNDER STATIC LOADING

ARCH 1				ARCH 2			
LOAD (KN)	DEFL. (mm)	LOAD (KN)	DEFL. (mm)	LOAD (KN)	DEFL. (mm)	LOAD (KN)	DEFL (mm)
0	0	28	7,437	0	0	30	6,813
1	0,026	30	8,687	1	0,019	32	7,703
2	0,097	32	10,937	2	0,073	34	9,153
3	0,191	34	12,767	3	0.223	36	10,323
4	0,259	36	13,497	4	0,403	38	15,563
5	0.352	38	15,617	5	0,583	40	16,733
6	0.457	40	18,377	6	0,808	42	18,403
7	0.574	42	23,097	7	1,033	44	22,313
8	0.678	44	24,897	8	1,223	44,1	-
9	0.834	45.2	-	9	1,473		
10	1.001			10	1,713		
11	1.174			11	1,953		
12	1.344			12	2,153		
13	1.467			13	2,368		
14	1.672			14	2,561		
15	1.837			16	2,973		
16	2,007			18	3,140		
18	2,367			20	3,793		
20	3,097			22	4,243		
22	4,037			24	4,663		
24	4,921			26	5,233		
26	6,187			28	5,963		

APPENDIX J.2

RECORDED LOAD-DEFLECTIONS FOR PARTIALLY SFRC ARCHES UNDER STATIC LOADING

ARCH 1				ARCH 2			
LOAD (KN)	DEFL (mm)	LOAD (KN)	DEFL (mm)	LOAD (KN)	DEFL (mm)	LOAD (KN)	DEFL (mm)
0	0	24	3,578	0	0	26	4.762
1	0.004	26	4,423	1	0,001	28	5,667
2	0,042	28	6,083	2	0,029	30	6,873
3	0,081	30	8,593	3	0,086	32	8,502
4	0,160	31	9,338	4	0,166	34	10.372
5	0,261	32	10.103	5	0,247	36	11.932
6	0,362	33	10,873	6	0,346	38	13.792
7	0,481	34	11,603	7	0,452	40	16,262
8	0,593	35	12,363	8	0,599	41	18,252
9	0,682	36	13,343	9	0,711	42	19,332
10	0,852	37	14,313	10	0,869	43	21,347
11	1,003	38	15,653	11	0,976	44	23,172
12	1,145	39	17,343	12	1,106	44,5	26,252
13	1,255	40	18,993	13	1,231		
14	1,563	41	21,593	14	1,406		
15	1,579	42	-	15	1,539		
16	1,733	42,1	25,393	16	1,724		
17	1,859			17	1,833		
18	2,073			18	1,922		
19	2,258			20	2,349		
20	2,513			22	2,997		
22	3,008			24	3,822		

APPENDIX J.3

ELASTIC AND ULTIMATE ARCH SECTIONAL ANALYSIS

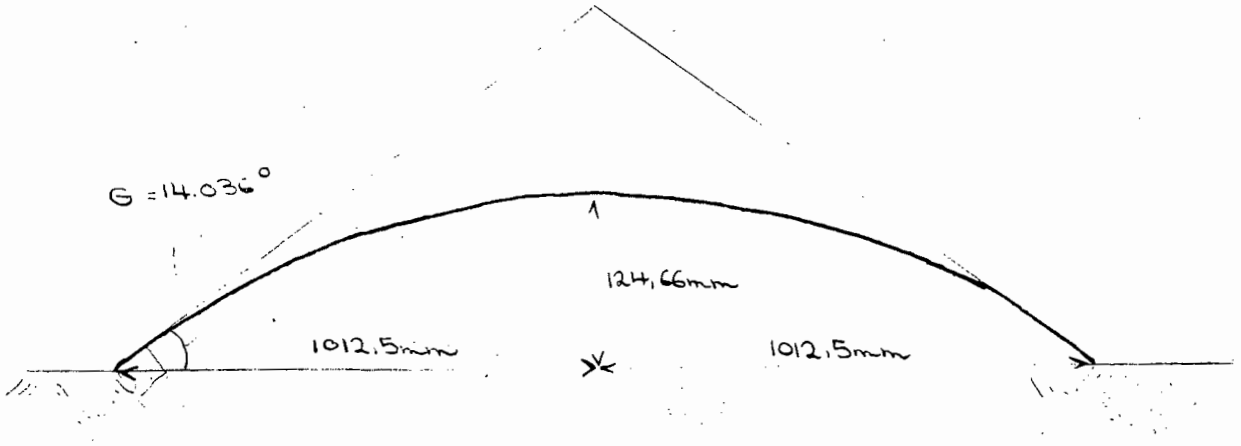

4050

R = 4174,66 mm

ARCH DIMENSIONS

θ = 14,036°

ANALYSIS OF ARCH

AVERAGE ULTIMATE LOAD CAPACITY = (45.2 + 44.1)/2
= 44.65 KN.

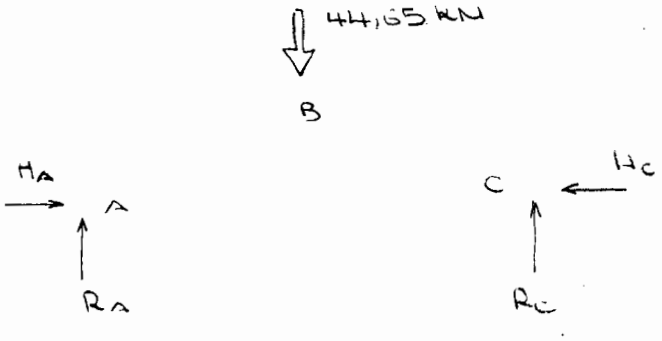

3 EQUILIBRIUM EQUATIONS
4 SUPPORT REACTIONS, ∴ 1 DEGREE OF INDETERMINANCY
- RELEASE H_C.

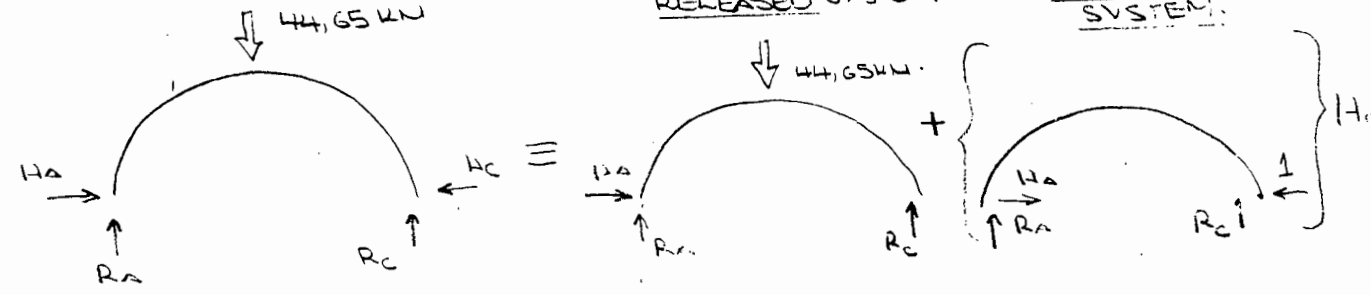

- Draw moment and axial force diagrams, and thence determine Hc. Since arch symmetrical, only need to plot half the diagram as the other side is a mirror image.
- (See next page for bending and axial force calculations)

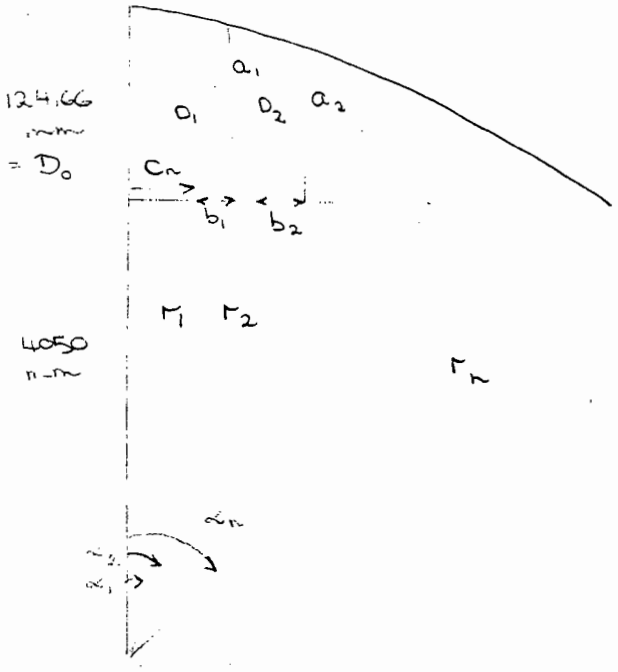

α_n	$M_n = 4050 \times \cos\alpha$	$D_n = 474.6 - r_n$	$a_n = D_n \times \cos\alpha$	$b_n = D_n \times \sin\alpha$	$C_n = 4050 \times \tan\alpha$	$x_n = b_n + C_n$	DISTANCE TO END (Z) $= 1012.5 - x_n$
0	4050	124.66	124.66	0 ✓	0 ✓	0	1012.5
2.339	4053.4	121.3	121.2	4.95	165.45	170.4	842.1
4.679	4063.5	111.1	110.8	9.06	331.5	340.5	671.9
7.018	4080.6	94.1	93.4	11.50	498.6	510.1	502.4
9.357	4104.6	70.0	69.1	11.39	667.4	678.8 ✓	333.7
11.697	4135.9	38.3	38 ✓	7.86	833.5	846.3	166.2
14.036	4174.7	0	0	0	1012.5 ✓	1012.5 ✓	0 ✓

RELEASED SYSTEM

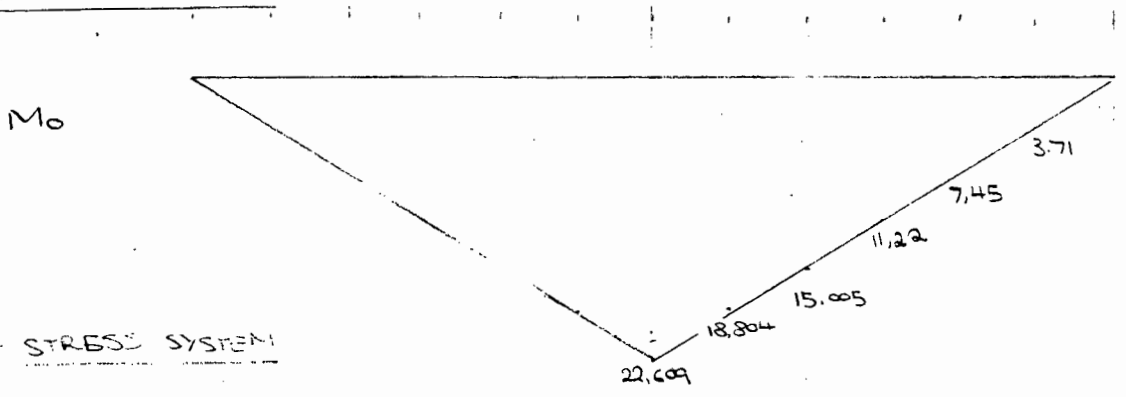

SELF-STRESS SYSTEM

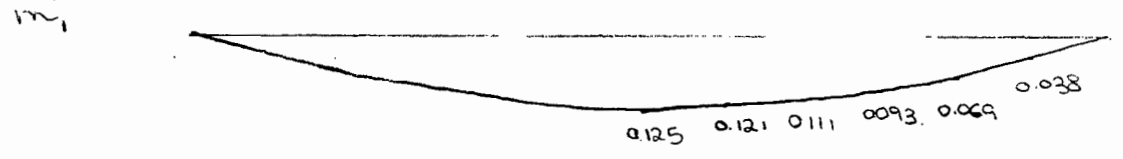

RELEASED SYSTEM

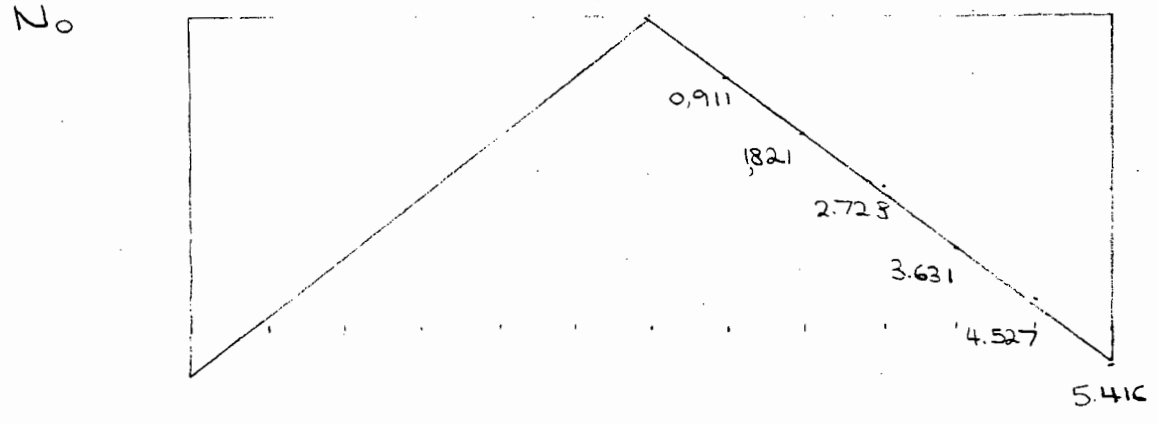

SELF STRESS SYSTEM

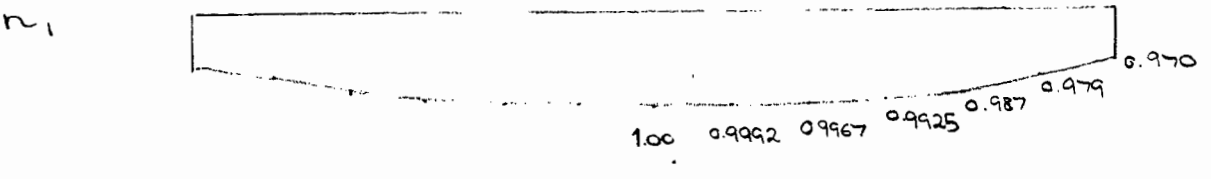

(N.B - DIAGRAMS NOT DRAWN TO SCALE)

From the principle of virtual work, $u_A = V_A = u_C = V_C = 0$

$$\therefore \delta_C = 0 = \int_0^{\text{ARC LENGTH}} m_1 K \, ds + \int_0^{\text{ARC LENGTH}} n' \varepsilon \, ds \qquad (.1)$$

where $K = M_0 + m_1 / EI$

$\varepsilon = N_0 + n_1 / EI$.

$$I = \frac{bd^3}{12} = \frac{2{,}100 \times 0{,}054^3}{12} = 2.7556 \times 10^{-5} \ m^4$$

$$A = b \times d = 2.100 \times 0.054 = 0.113 \ m^2$$

Substituting these values in equation (.1)

$$\delta_C = 0 = \int_0^{\text{ARC L.}} \left(\frac{m_1 M_0}{EI} + \frac{n_1^2 \cdot H_C}{EI} \right) ds + \int_0^{\text{ARC L.}} \left(\frac{n_1 N_0}{EA} + \frac{n_1^2 \cdot H_C}{EA} \right) ds$$

Rearranging the above equation and cancelling the common E:

$$H_C = -\int_0^{\text{ARC L.}} \frac{m_1 M_0 + n_1 N_0}{I} \, ds \Big/ \int_0^{\text{ARC L.}} \left(\frac{m_1^2}{I} + \frac{n_1^2}{A} \right) ds$$

Using Simpson's Rule:

$$H_C = -\Bigg[\tfrac{1}{3} \times \tfrac{1.0125}{6} \times \left(22.609 \times 0.125 + 4 \times 12.804 \times 0.121 + 2 \times 15.005 \times 0.111 + 4 \times 11.219 \times 0.093 + 2 \times 7.452 \times 0.069 + 4 \times 3.710 \times 0.038 \right) + \tfrac{1}{3} \times \tfrac{1.0125}{6} \times \left(4 \times 0.911 \times 0.9996 + 2 \times 1.821 \times 0.9967 + 4 \times 2.728 \times 0.9925 + 2 \times 3.631 \times 0.9867 + 4 \times 4.527 \times 0.9792 + 5.416 \times 0.9701 \right) \Bigg]$$

$$\Big/ \Bigg[\tfrac{1}{3} \times \tfrac{1.0125}{6} \times \left(0.125^2 + 4 \times 0.121^2 + 2 \times 0.111^2 + 4 \times 0.093^2 + 2 \times 0.069^2 + 4 \times 0.038^2 \right) + \left(1^2 + 4 \times 0.9996^2 + 2 \times 0.9967^2 + 4 \times 0.9925^2 + 2 \times 0.9867^2 + 4 \times 0.9792^2 + 0.9701^2 \right) \Bigg]$$

$$H_c = \left(\frac{21,024}{2.7556 \times 10^{-5}} + \frac{48.2535}{0,1134} \right) \Big/ \left(\frac{0.14873}{2.7556 \times 10^{-5}} + \frac{17.647}{0.1134} \right)$$

$\therefore H_c = 137,477 \text{ kN} \rightarrow$

Final bending moment diagram; $M = H_c \times a_n + V_c \times z_n$.

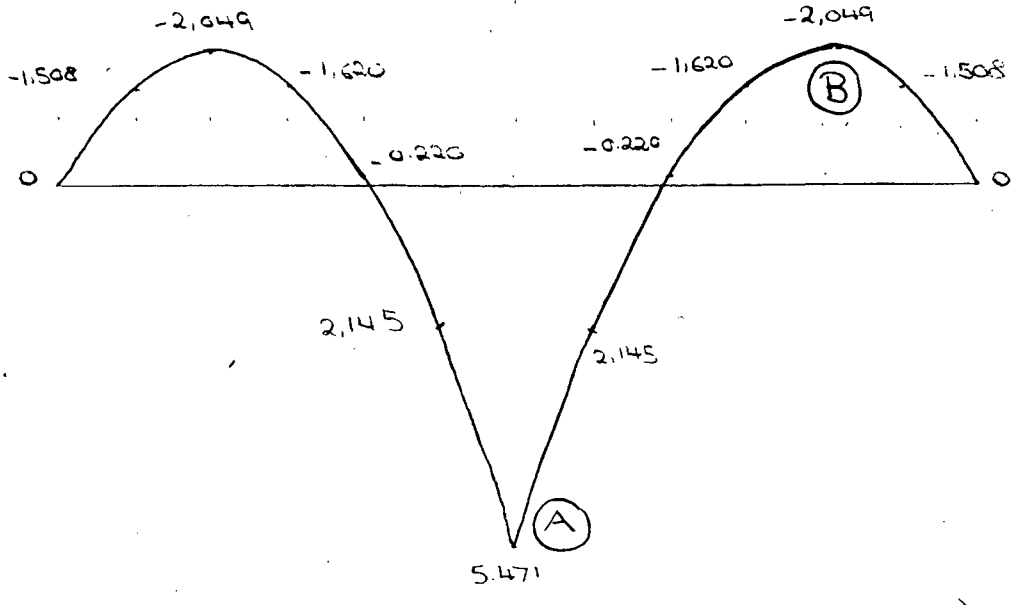

BENDING MOMENT DIAGRAM (KNm)

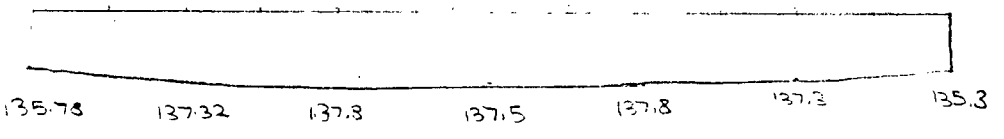

AXIAL FORCE DIAGRAM (KN)

CHECK STRESS DIAGRAM AT (A)

Using elastic analysis;

Axial stress (compressive) $= \frac{137,477 \times 10^3}{2100 \times 54} = -1,212 \text{ MPa}$

From bending, $\sigma_f = \frac{M \times y}{I} = \frac{5.471 \times 10^6 \times 27 \text{ mm}}{2.7556 \times 10^7 \text{ mm}} = 5.361 \text{ MPa}$

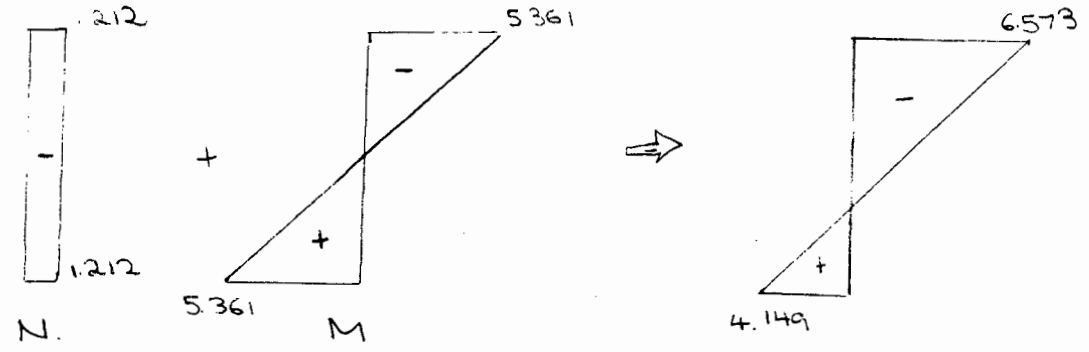

CHECK STRESSES AT (B)

$$\text{Axial stress} = \frac{137.32 \times 10^3}{2.00 \times 5\text{L}} = 1.211\text{MPa}.$$

$$\text{Bending stress} = \frac{2,049 \times 10^6 \times 27}{2.7556 \times 10^7} = 2,008\text{MPa}.$$

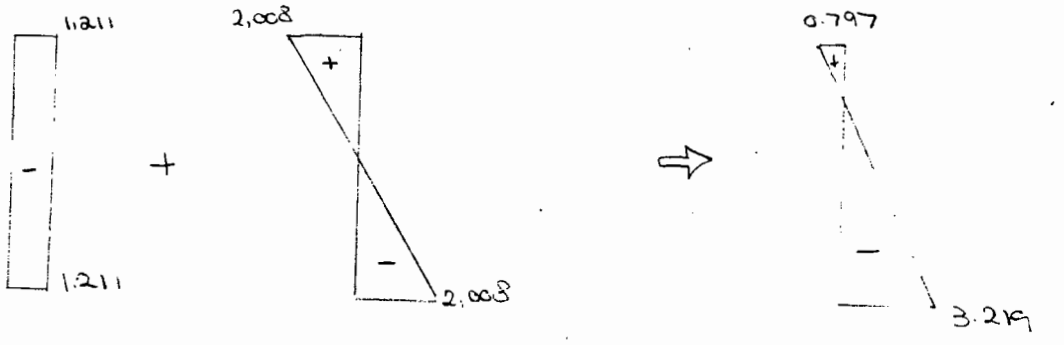

Failure of the arch is therefore likely, and actually did occur at (A)

ULTIMATE STATE ANALYSIS

The ultimate moment capacity of the arch is calculated as follows (for steel mesh yielding);

External axial force at point A = 137,477KN
(over a 2.1m length)

This force is resisted by the internal forces Fc and Fs.

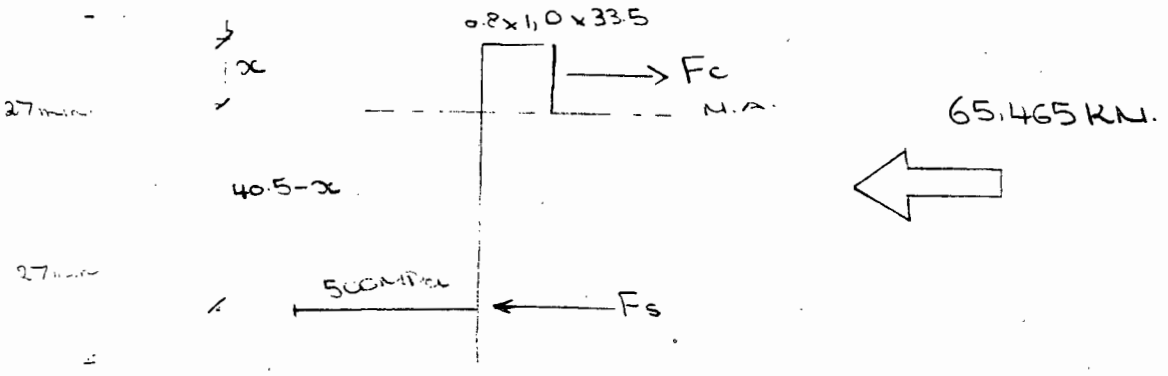

$F_s + F_c = 137.477\ KN$.

For the 2x2m steel mesh $F_s = 500\ MPa \times 156\ mm^2 \times 2 = 156.016\ KN$.

$\therefore (-156,016 \times 10^3 + 0.8 \times 33.5 \times 2100 \times x) = 137.477\ KN$

$56280\,x = 293.495\ KN$

$\therefore \quad x = 5.21\ mm$

The ultimate moment per metre length, M_u = $78,008\ KN \times 0.0135\ m + 143.465\ KN \times (0.027 - \frac{0.00521}{2})$

$= 4.554\ KNm/m.$

This is somewhat lower than the 5.471 KNm/m predicted by the elastic analysis. The bending moment diagram at ultimate is therefore similar to the elastic moment diagram with the redundance redistributed along the arch length

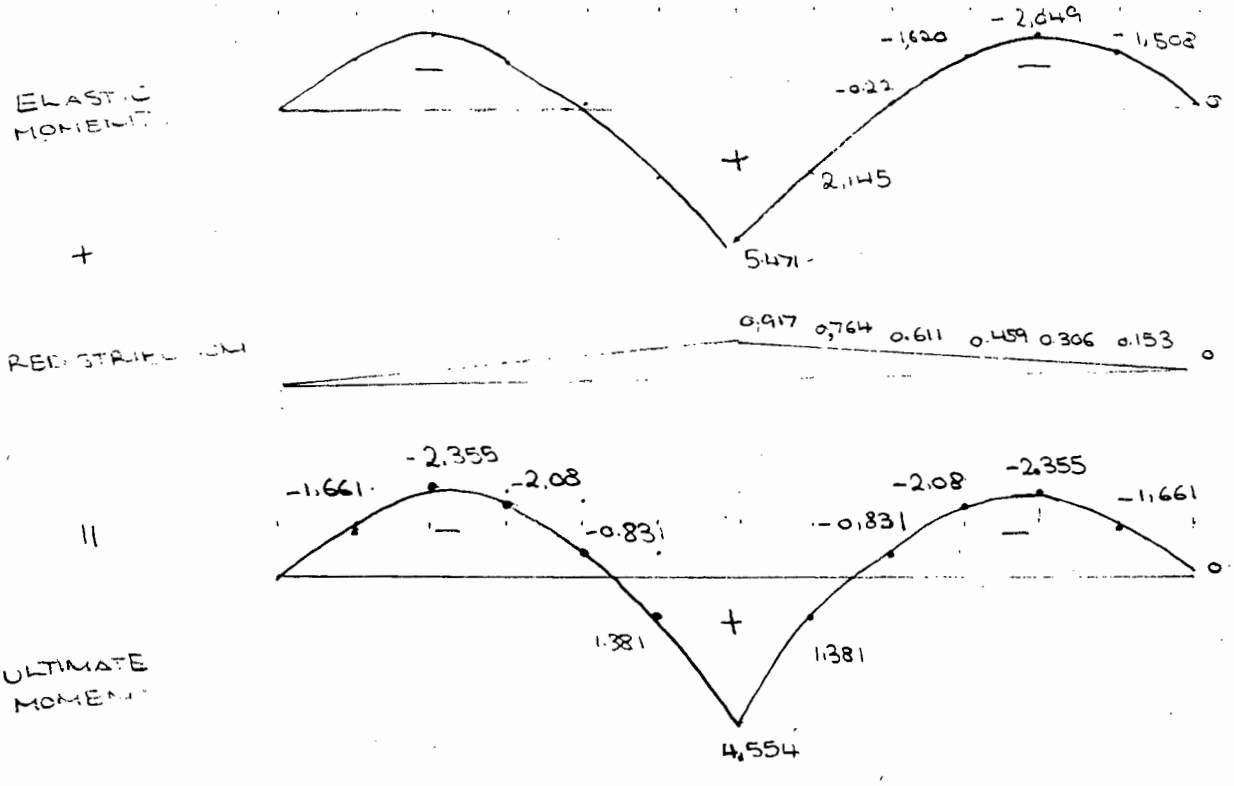

APPENDIX J.4

DEFLECTIONS OF MESH REINFORCED ARCHES
UNDER IMPACT LOADING

DROP HEIGHT (m)	PERMANENT DEFL. (mm)		TOTAL DEFLECTION (mm)	
	ARCH 1	ARCH 2	ARCH 1	ARCH 2
0.0	0.0	0.0	0.0	0.0
0.1	1.31	1.07	4.25	2.20
0.2	1.98	1.72	6.10	5.73
0.3	2.82	2.99	7.13	7.55
0.4	4.64	3.97	9.25	9.80
0.5	6.78	5.07	12.88	12.43
0.6	8.62	7.52	17.25	14.93
0.8	11.20	8.59	23.38	18.75
1.0	14.57	-	29.0	-
1.2	17.02	-	35.0	-

APPENDIX J.5

DEFLECTIONS OF PARTIALLY SFRC ARCHES
UNDER IMPACT LOADING

DROP HEIGHT (m)	PERMANENT DEFLECTION (mm)		TOTAL DEFLECTION (mm)	
	ARCH 1	ARCH 2	ARCH 1	ARCH 2
0.0	0.0	0.0	0.0	0.0
0.1	0.4	0.25	1.6	2.7
0.2	0.8	0.75	3.2	4.2
0.3	2.0	1.26	5.0	5.4
0.4	2.8	2.30	6.8	7.6
0.5	4.2	3.67	9.4	10.1
0.6	5.8	5.38	12.5	12.9
0.8	7.5	7.29	15.7	16.5
1.0	8.8	8.66	19.4	22.2